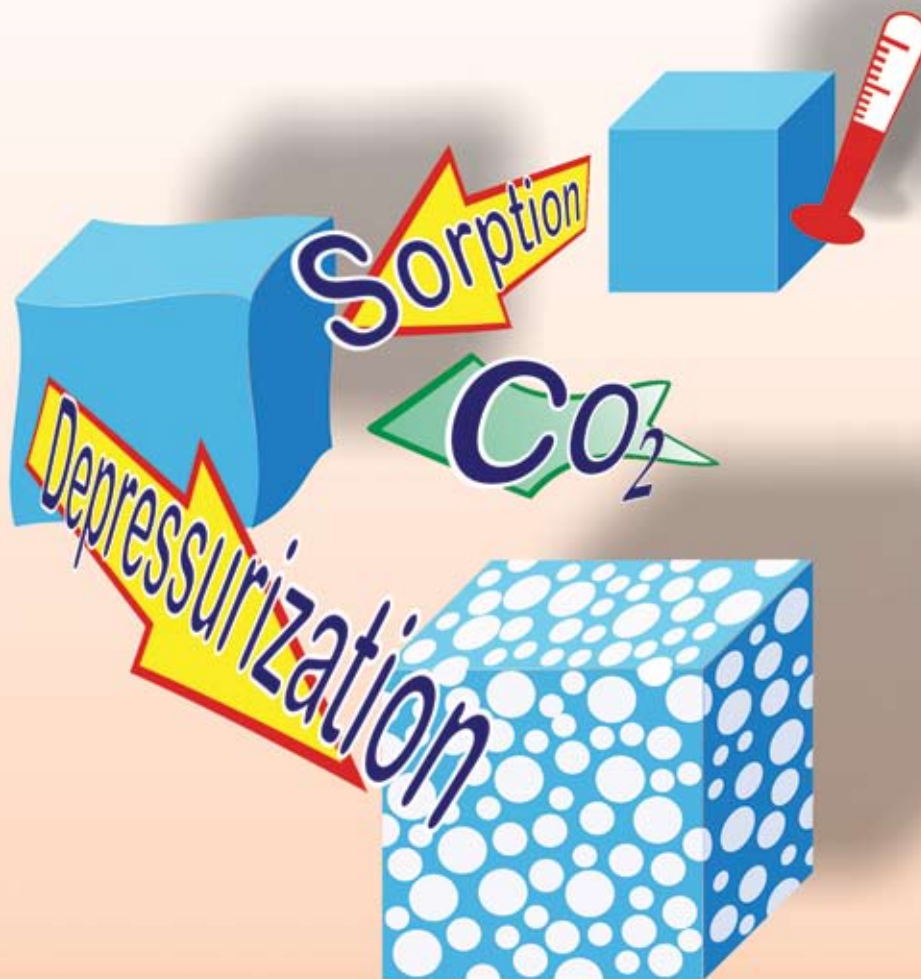


# Green Chemistry

Cutting-edge research for a greener sustainable future

[www.rsc.org/greenchem](http://www.rsc.org/greenchem)

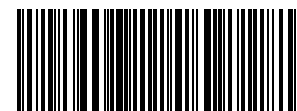
Volume 10 | Number 7 | July 2008 | Pages 721–812



ISSN 1463-9262

RSC Publishing

Jacobs *et al.*  
Sustainable polymer foaming using  
carbon dioxide  
Bhaskar *et al.*  
Debromination of flame retardant  
plastics with microwave irradiation



1463-9262(2008)10:7;1-B



# years of publishing!

## *Green Chemistry...*



- The most highly cited *Green Chemistry* journal, Impact factor = 4.192\*
- Fast publication, typically <90 days for full papers
- Full variety of research including reviews, communications, full papers and perspectives.

Celebrating 10 years of publishing, *Green Chemistry* offers the latest research that reduces the environmental impact of the chemical enterprise by developing alternative sustainable technologies, and provides a unique forum for the rapid publication of cutting-edge and innovative research for a greener, sustainable future

*...for a sustainable future!*

\* 2006 Thomson Scientific (ISI) Journal Citation Reports ®

# Green Chemistry

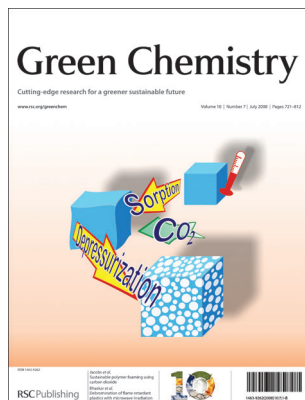
Cutting-edge research for a greener sustainable future

[www.rsc.org/greenchem](http://www.rsc.org/greenchem)

RSC Publishing is a not-for-profit publisher and a division of the Royal Society of Chemistry. Any surplus made is used to support charitable activities aimed at advancing the chemical sciences. Full details are available from [www.rsc.org](http://www.rsc.org)

## IN THIS ISSUE

ISSN 1463-9262 CODEN GRCHFJ 10(7) 721–812 (2008)



### Cover

See Jacobs *et al.*, pp. 731–738.  
A schematic representation of the polymer–CO<sub>2</sub> foaming process.

Image reproduced with permission from Leon Jacobs, from *Green Chem.*, 2008, **10**, 731.

## CHEMICAL TECHNOLOGY

### T49

Drawing together research highlights and news from all RSC publications, *Chemical Technology* provides a ‘snapshot’ of the latest applications and technological aspects of research across the chemical sciences, showcasing newsworthy articles and significant scientific advances.

## Chemical Technology

July 2008/Volume 5/Issue 7

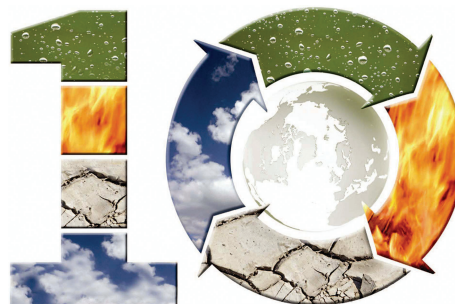
[www.rsc.org/chemicaltechnology](http://www.rsc.org/chemicaltechnology)

## EDITORIAL

### 730

#### Supercritical fluids in green chemistry

Walter Leitner and Martyn Poliakoff discuss the uses of supercritical fluids in green chemistry.



## EDITORIAL STAFF

**Editor**

Sarah Ruthven

**Assistant editor**

Sarah Dixon

**Publishing assistant**

Ruth Bircham

**Team leader, serials production**

Stephen Wilkes

**Technical editor**

Edward Morgan

**Production administration coordinator**

Sonya Spring

**Administration assistants**Clare Davies, Donna Fordham, Kirsty Lunnon,  
Julie Thompson**Publisher**

Emma Wilson

Green Chemistry (print: ISSN 1463-9262; electronic: ISSN 1463-9270) is published 12 times a year by the Royal Society of Chemistry, Thomas Graham House, Science Park, Milton Road, Cambridge, UK CB4 0WF.

All orders, with cheques made payable to the Royal Society of Chemistry, should be sent to RSC Distribution Services, c/o Portland Customer Services, Commerce Way, Colchester, Essex, UK CO2 8HP. Tel +44 (0) 1206 226050; E-mail sales@rscdistribution.org

2008 Annual (print + electronic) subscription price: £947; US\$1799. 2008 Annual (electronic) subscription price: £852; US\$1695. Customers in Canada will be subject to a surcharge to cover GST. Customers in the EU subscribing to the electronic version only will be charged VAT.

If you take an institutional subscription to any RSC journal you are entitled to free, site-wide web access to that journal. You can arrange access via Internet Protocol (IP) address at [www.rsc.org/ip](http://www.rsc.org/ip). Customers should make payments by cheque in sterling payable on a UK clearing bank or in US dollars payable on a US clearing bank. Periodicals postage paid at Rahway, NJ, USA and at additional mailing offices. Airfreight and mailing in the USA by Mercury Airfreight International Ltd., 365 Blair Road, Avenel, NJ 07001, USA.

US Postmaster: send address changes to Green Chemistry, c/o Mercury Airfreight International Ltd., 365 Blair Road, Avenel, NJ 07001. All despatches outside the UK by Consolidated Airfreight.

PRINTED IN THE UK

**Advertisement sales:** Tel +44 (0) 1223 432246; Fax +44 (0) 1223 426017; E-mail [advertising@rsc.org](mailto:advertising@rsc.org)

# Green Chemistry

Cutting-edge research for a greener sustainable future

[www.rsc.org/greenchem](http://www.rsc.org/greenchem)

Green Chemistry focuses on cutting-edge research that attempts to reduce the environmental impact of the chemical enterprise by developing a technology base that is inherently non-toxic to living things and the environment.

## EDITORIAL BOARD

**Chair**

Professor Martyn Poliakoff  
Nottingham, UK

**Scientific Editor**

Professor Walter Leitner  
RWTH-Aachen, Germany

**Associate Editors**

Professor C. J. Li  
McGill University, Canada

**Members**

Professor Paul Anastas  
Yale University, USA  
Professor Joan Brennecke  
University of Notre Dame, USA  
Professor Mike Green  
Sasol, South Africa  
Professor Buxing Han  
Chinese Academy of Sciences,  
China

Dr Alexei Lapkin  
Bath University, UK  
Professor Steven Ley  
Cambridge, UK  
Dr Janet Scott  
Unilever, UK  
Professor Tom Welton  
Imperial College, UK

## ADVISORY BOARD

James Clark, York, UK  
Avelino Corma, Universidad  
Politécnica de Valencia, Spain  
Mark Harmer, DuPont Central  
R&D, USA  
Herbert Hugl, Lanxess Fine  
Chemicals, Germany  
Roshan Jachuck,  
Clarkson University, USA  
Makato Misono, nite,  
Japan

Colin Raston,  
University of Western Australia,  
Australia  
Robin D. Rogers, Centre for Green  
Manufacturing, USA  
Kenneth Seddon, Queen's  
University, Belfast, UK  
Roger Sheldon, Delft University of  
Technology, The Netherlands  
Gary Sheldrake, Queen's  
University, Belfast, UK

Pietro Tundo, Università ca  
Foscari di Venezia, Italy

## INFORMATION FOR AUTHORS

Full details of how to submit material for publication in Green Chemistry are given in the Instructions for Authors (available from <http://www.rsc.org/authors>). Submissions should be sent via ReSource: <http://www.rsc.org/resource>.

Authors may reproduce/republish portions of their published contribution without seeking permission from the RSC, provided that any such republication is accompanied by an acknowledgement in the form: (Original citation) – Reproduced by permission of the Royal Society of Chemistry.

© The Royal Society of Chemistry 2008. Apart from fair dealing for the purposes of research or private study for non-commercial purposes, or criticism or review, as permitted under the Copyright, Designs and Patents Act 1988 and the Copyright and Related Rights Regulations 2003, this publication may only be reproduced, stored or transmitted, in any form or by any means, with the prior permission in writing of the Publishers or in the case of reprographic reproduction in accordance with the terms of licences issued by the Copyright Licensing Agency in the UK. US copyright law is applicable to users in the USA.

The Royal Society of Chemistry takes reasonable care in the preparation of this publication but does not accept liability for the consequences of any errors or omissions.

The paper used in this publication meets the requirements of ANSI/NISO Z39.48-1992 (Permanence of Paper).

Royal Society of Chemistry: Registered Charity No. 207890



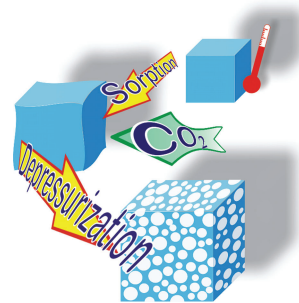
## CRITICAL REVIEW

731

**Sustainable polymer foaming using high pressure carbon dioxide: a review on fundamentals, processes and applications**

Leon J. M. Jacobs,\* Maartje F. Kemmere and Jos T. F. Keurentjes

Carbon dioxide has proven to be a more sustainable alternative as a blowing agent for the production of polymeric foams. Experimental parameters, such as the temperature and pressure at which the polymer is saturated with CO<sub>2</sub> and rate at which the pressure is released, controls the foam morphology



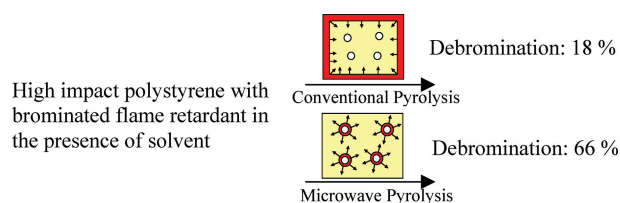
## COMMUNICATIONS

739

**Enhanced debromination of brominated flame retardant plastics under microwave irradiation**

Thallada Bhaskar,\* Asako Hosokawa, Akinori Muto, Yasunori Tsukahara, Tomohisa Yamauchi and Yuji Wada\*

A novel method for the debromination of high impact polystyrene with brominated flame retardant by microwave irradiation in the presence of triethylene glycol at 250 °C for 30 min was performed and achieved 85 wt% of debromination.

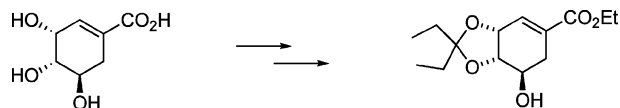


743

**Streamlined process for the esterification and ketalization of shikimic acid en route to the key precursor for oseltamivir phosphate (Tamiflu™)**

Robert Carr, Frank Ciccone, Richard Gabel, Martin Guinn, David Johnston, Jill Mastriona, Trevor Vandermeer and Michael Groaning\*

The chemistry described herein provides a novel means to eliminate the use of the noxious reagent thionyl chloride and streamlining of the process en route to Tamiflu™. This was accomplished by employing an *in situ* water scavenger to force the esterification to completion.



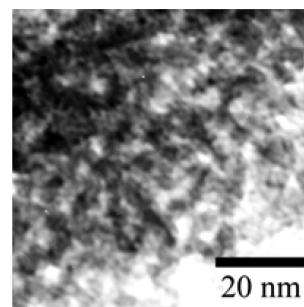
## PAPERS

746

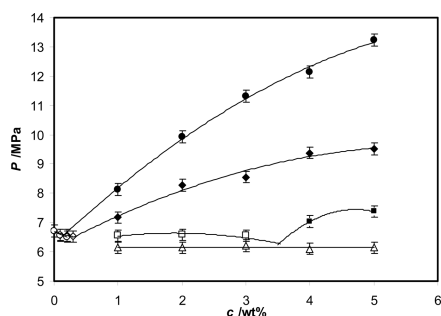
**Preparation of mesoporous polyoxometalate-tantalum pentoxide composite catalyst and its application for biodiesel production by esterification and transesterification**

Leilei Xu, Yuanhong Wang, Xia Yang, Xiaodan Yu, Yihang Guo\* and James H. Clark\*

A novel POM-containing environmentally friendly mesoporous composite, prepared by a one-step sol-gel-hydrothermal route, exhibits significantly high activity, selectivity, and stability towards biodiesel production under mild conditions.



756

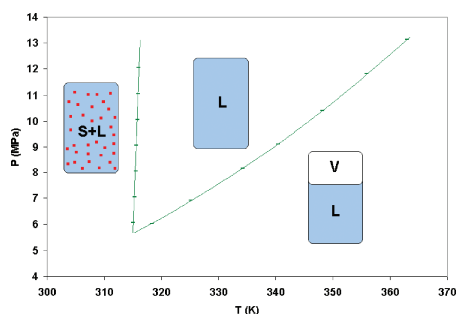


### Cellulose triacetate oligomers exhibit high solubility in dense CO<sub>2</sub>

Lei Hong,\* Matthew Fisher, Robert Enick\* and Eric Beckman

Cellulose triacetate oligomers were identified as highly CO<sub>2</sub>-soluble compounds that can be used as building-blocks for designing novel environmentally benign CO<sub>2</sub>-soluble surfactants and copolymers, significantly enhancing the role of CO<sub>2</sub> in green chemistry and engineering.

762

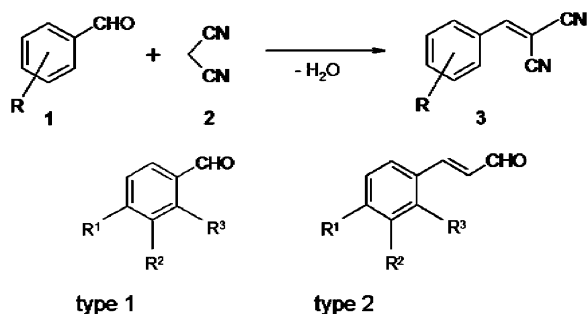


### Phase equilibria in ternary mixtures of the ionic liquid bmim[BF<sub>4</sub>], (*S*)-naproxen and CO<sub>2</sub> to determine optimum regions for green processing

Eliane Kühne, Sabrina Santarossa, Geert-Jan Witkamp and Cor J. Peters\*

Solid-liquid and liquid-vapour equilibria of the title system show that CO<sub>2</sub> influences the conditions for precipitation of (*S*)-naproxen in bmim[BF<sub>4</sub>] as well as the location and extension of the homogenous liquid phase region.

767

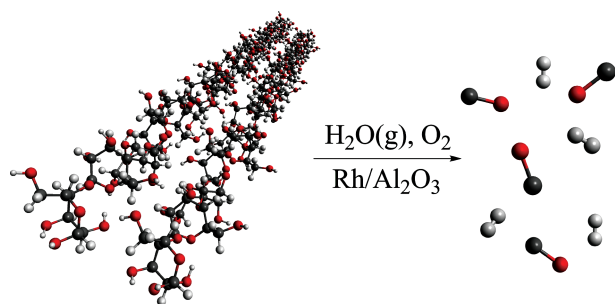


### Studies on the solvent-free and waste-free Knoevenagel condensation

Ronald Trotzki, Markus M. Hoffmann and Bernd Ondruschka\*

The mechanochemical reaction of malononitrile with various aldehydes was studied with the goal to achieve quantitative stoichiometric conversion of the reactants to their corresponding benzylidene-malononitriles in absence of any solvents and catalysts.

773



### Millisecond autothermal steam reforming of cellulose for synthetic biofuels by reactive flash volatilization

Joshua L. Colby, Paul J. Dauenhauer and Lanny D. Schmidt\*

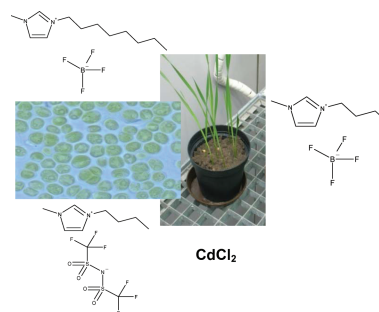
Integration of devolatilization, catalytic gas cleaning, and water-gas-shift of crystalline cellulose over a Rh-based heterogeneous catalyst permits conversion to synthesis gas for synthetic biofuels within a single, autothermal reactor at millisecond time-scales.

784

**Mixture effects and predictability of combination effects of imidazolium based ionic liquids as well as imidazolium based ionic liquids and cadmium on terrestrial plants (*Triticum aestivum*) and limnic green algae (*Scenedesmus vacuolatus*)**

Marianne Matzke,\* Stefan Stolte, Andrea Böschen and Juliane Filser

This study investigates the effects of three differently composed mixtures containing ionic liquids as well as ionic liquids and the heavy metal cadmium on limnic green algae and wheat.

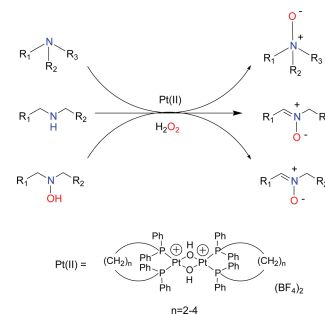


793

**Mild catalytic oxidation of secondary and tertiary amines to nitrones and *N*-oxides with H<sub>2</sub>O<sub>2</sub> mediated by Pt(II) catalysts**

Marco Colladon, Alessandro Scarso and Giorgio Strukul\*

Environmentally benign hydrogen peroxide oxidizes tertiary and secondary amines under mild conditions and with medium to excellent yields in the presence of bridging hydroxo complexes of Pt(II) as catalysts.

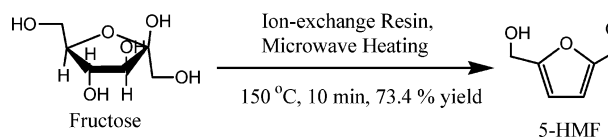


799

**Catalytic dehydration of fructose into 5-hydroxymethylfurfural by ion-exchange resin in mixed-aqueous system by microwave heating**

Xinhua Qi, Masaru Watanabe,\* Taku M. Aida and Richard Lee Smith, Jr.\*

Catalytic dehydration of fructose into 5-hydroxymethylfurfural was studied in acetone–water mixtures in the presence of a cation exchange resin catalyst.

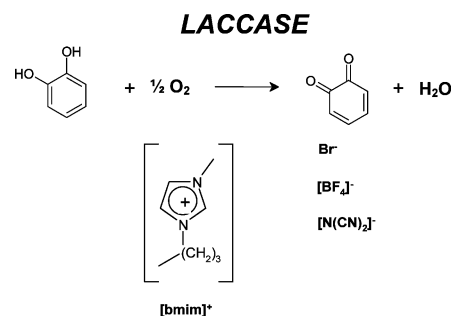


806

**Catalytic activity of laccases in aqueous solutions of ionic liquids**

Stepan Shipovskov, H. Q. Nimal Gunaratne, Kenneth R. Seddon and Gill Stephens\*

Laccase activity increases up to two-fold in mixtures of [bmim]Br or [bmim][N(CN)<sub>2</sub>] with water.



## AUTHOR INDEX

Aida, Taku M., 799  
 Beckman, Eric, 756  
 Bhaskar, Thallada, 739  
 Bösch, Andrea, 784  
 Carr, Robert, 743  
 Ciccone, Frank, 743  
 Clark, James H., 746  
 Colby, Joshua L., 773  
 Colladon, Marco, 793  
 Dauenhauer, Paul J., 773  
 Enick, Robert, 756  
 Filser, Juliane, 784  
 Fisher, Matthew, 756


Gabel, Richard, 743  
 Groaning, Michael, 743  
 Guinn, Martin, 743  
 Gunaratne, H. Q. Nimal, 806  
 Guo, Yihang, 746  
 Hoffmann, Markus M., 767  
 Hong, Lei, 756  
 Hosokawa, Asako, 739  
 Jacobs, Leon J. M., 731  
 Johnston, David, 743  
 Kemmere, Maartje F., 731  
 Keurentjes, Jos T. F., 731  
 Kühne, Eliane, 762

Mastriona, Jill, 743  
 Matzke, Marianne, 784  
 Muto, Akinori, 739  
 Ondruschka, Bernd, 767  
 Peters, Cor J., 762  
 Qi, Xinhua, 799  
 Santarossa, Sabrina, 762  
 Scarso, Alessandro, 793  
 Schmidt, Lanny D., 773  
 Seddon, Kenneth R., 806  
 Shipovskov, Stepan, 806  
 Smith, Jr., Richard Lee, 799  
 Stephens, Gill, 806

Stolte, Stefan, 784  
 Strukul, Giorgio, 793  
 Trotzki, Ronald, 767  
 Tsukahara, Yasunori, 739  
 Vandermeer, Trevor, 743  
 Wada, Yuji, 739  
 Wang, Yuanhong, 746  
 Watanabe, Masaru, 799  
 Witkamp, Geert-Jan, 762  
 Xu, Leilei, 746  
 Yamauchi, Tomohisa, 739  
 Yang, Xia, 746  
 Yu, Xiaodan, 746

## FREE E-MAIL ALERTS AND RSS FEEDS


Contents lists in advance of publication are available on the web *via* [www.rsc.org/greenchem](http://www.rsc.org/greenchem) – or take advantage of our free e-mail alerting service ([www.rsc.org/ej\\_alert](http://www.rsc.org/ej_alert)) to receive notification each time a new list becomes available.

 Try our RSS feeds for up-to-the-minute news of the latest research. By setting up RSS feeds, preferably using feed reader software, you can be alerted to the latest Advance Articles published on the RSC web site. Visit [www.rsc.org/publishing/technology/rss.asp](http://www.rsc.org/publishing/technology/rss.asp) for details.

## ADVANCE ARTICLES AND ELECTRONIC JOURNAL

Free site-wide access to Advance Articles and the electronic form of this journal is provided with a full-rate institutional subscription. See [www.rsc.org/ejs](http://www.rsc.org/ejs) for more information.

\* Indicates the author for correspondence: see article for details.

 Electronic supplementary information (ESI) is available *via* the online article (see <http://www.rsc.org/esi> for general information about ESI).

# ADDITIVES 2009

## Fuels and Lubricants for Energy Efficient and Sustainable Transport

York, UK, 27 - 30 April 2009

The sixth international conference on additives for automotive fuels and lubricants: their chemistry, mode of action and tribological performance.

- fuel and lubricant additives
- tribology and surface chemistry
- engine and transmission lubricants
- low environmental impact technology
- biofuels: the additive challenge

**Deadline for abstracts for oral presentation – 26 September 2008**  
**For a full list of speakers and how to submit an abstract please visit the website.**



Image courtesy of Lubrizol UK Ltd

RSC | Advancing the  
 Chemical Sciences

[www.rsc.org/Additives2009](http://www.rsc.org/Additives2009)

Registered Charity No. 207890

# Chemical Technology

Microfluidic device is designed to survive the extremes of space exploration

## Lab-on-a-chip looks for life on Mars

NASA scientists have developed a new microfluidic system that is tough enough to be used in outer space.

Peter Willis at the NASA Jet Propulsion Laboratory, Pasadena, US, and colleagues have created a lab-on-a-chip that they claim can survive the extremes of the European ExoMars rover mission scheduled for launch in 2013. The device could detect molecules essential for life, such as amino acids, they say.

It probably won't find any little green men but the ExoMars rover is designed to collect and analyse Martian mineral samples to look for evidence of life. The mission will take two years to reach Mars, with temperatures varying from minus to plus 50 degrees Celsius, so new materials are needed to survive these stresses.

Willis explains that the new system's strength results from its layers of glass and an elastomer called perfluoropolyether. 'It does not degrade when exposed to non-aqueous solvent nor do the



The ExoMars rover will collect and analyse Martian mineral samples for signs of life

elastomer-glass interfaces seal shut if left dormant for long periods of time, as typically happens with microfluidic valves,' he says. The team used the chip extensively at a range of temperatures and found that its performance was unaffected afterwards. The group now plan to check that the electrical characteristics of the devices do not change over time before working to make the system function unaided by humans.

As 2013 approaches, scientists can only speculate as to what the ExoMars rover will discover. As Jessica Malin, director of the Stanford Microfluidics Foundry, US, says: 'It will be exciting to see what scientific findings may result.' But with the help of his device, if there is evidence of life on Mars, past or present, Willis is confident that the ExoMars rover will find it.

Laura Howes

### Reference

P A Willis *et al*, *Lab Chip*, 2008, DOI: 10.1039/b804265a

## In this issue

### An eye for drug delivery

Refillable device dispenses medicine through a tube into the eye

### Glowing response to explosive detection

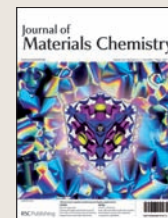
Fluorescent polymer identifies explosive particles

### Instant insight: Solar energy turns organic

Hiroshi Imahori and Tomokazu Umeyama explain why carbon nanotubes are promising candidates for organic solar cells

### Interview: Environmental impact

Jeff Tester talks to James Hodge about the importance of environmental science



The latest applications and technological aspects of research across the chemical sciences



# Application highlights

## Body odour indicates state of health

### Disease detection is skin deep

Scientists have used skin patches to investigate the biochemical profile of a person's body odour.

Information contained in skin odour may be used to diagnose, manage and assess diseases such as cancer, according to a team of scientists headed by Paul Thomas at Loughborough University, UK.

The team collected chemicals called volatile organic compounds (VOCs) from patients' skin using a patch made from a siloxane polymer. The group recovered the compounds adsorbed on the patch using thermal desorption, which uses heat to turn the VOCs into gases, and detected them using gas chromatography-mass spectrometry.

VOCs, the type of compound most likely to have an odour, are a beautiful area to research says co-worker Svetlana Riazanskaia from the University of Manchester, UK. 'Identifying specific VOCs could open a new non-invasive window into metabolic profiling of skin and illustrate how these profiles are altered in disease. At present, the



**The skin patch collects compounds from body odour. The presence of certain compounds could indicate disease.**

standard diagnostic tool for skin cancer is tissue biopsy, which is highly invasive, time-consuming and, most importantly, may be needless,' she says.

According to Ian Wilson, an expert in pharmaceutical analysis at AstraZeneca, Macclesfield, UK, VOCs can provide a great deal of important biochemical information about an individual's health. 'This is a very interesting innovation in the analysis of skin volatiles and may provide useful insights into a whole range of conditions,' he says.

'It has definite potential in both hospitals and doctor's offices,' comments Riazanskaia. 'It provides an opportunity for much earlier, easier and stress-free detection of biomarkers for human disorders. It also could be used in patients from whom it is difficult to collect blood, such as haemophiliacs or babies. This is too attractive to ignore.'

*Sarah Corcoran*

#### Reference

S Riazanskaia *et al*, *Analyst*, 2008, DOI: 10.1039/b802515k

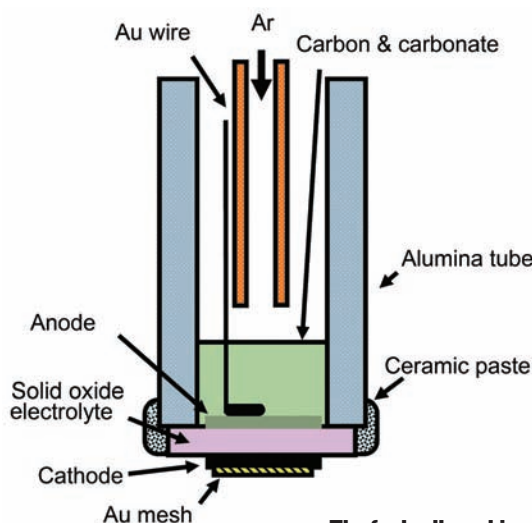
## Oxidation of carbon in molten electrolyte is key to enhanced performance

### Hybrid fuel cells show improved efficiency

UK scientists have discovered why combining two different fuel cell technologies can boost cell performance.

Direct carbon fuel cells run on solid carbon fuel and typically use solid oxide or molten carbonate electrolytes to transport ions between the electrodes. John Irvine at the University of St Andrews and colleagues made a hybrid direct carbon fuel cell containing both types of electrolyte. They found that the binary electrolyte system enhanced carbon oxidation because carbon was oxidised not only on the electrode surface but also in the carbon-electrolyte slurry.

Dianxue Cao, an expert in direct carbon fuel cells at Harbin Engineering University, China, is impressed by the findings. 'This significantly improves



understanding of the electrochemical oxidation of solid carbon in molten carbonates,' he says.

**The fuel cell combines two electrolytes to improve oxidation of the carbon fuel**

Solid carbon, which comes from various sources such as coal or plants, packs a lot of energy into a small volume, making it an attractive fuel. Irvine states that coal will be a major energy source in the future but, unless it can be converted into electricity more efficiently, will lead to an increase in carbon dioxide emissions. Fuel cells could be the answer, he says. 'Carbon fuel cells offer very high efficiency of conversion and, if implemented in the correct way, can yield two to three times the amount of energy for a given amount of coal compared to conventional thermal generation,' he explains.

*Madeline Chapman*

#### Reference

Y Nabaie *et al*, *Energy Environ. Sci.*, 2008, DOI:10.1039/b804785e

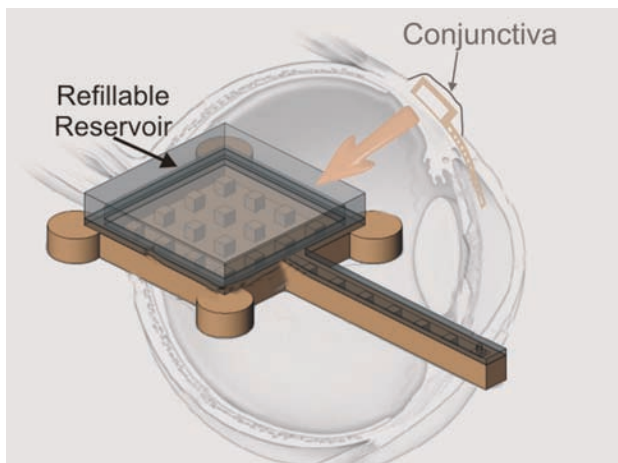
Refillable device dispenses medicine through a tube into the eye

## An eye for drug delivery

Patients with glaucoma and related eye diseases could soon be treated with a refillable drug delivery device, replacing the need for injections into the eyeball. Ellis Meng and colleagues at the University of Southern California, Los Angeles, US, have made a simple polymer device that attaches to the eye and delivers drugs to the site of disease via a flexible tube inserted into the side of the eye.

'This work came out of discussions with a retinal surgeon,' says Meng. 'He has days where patients line up to have injections into their eye because there's a lack of good drug delivery mechanisms for diseases that lead to blindness.'

The team showed their device, which is about one centimetre long, could be refilled repeatedly by piercing it using a syringe needle, without it developing a leak. Once attached to the eye, pressing the drug



reservoir dispenses the treatment through the delivery tube into the relevant part of the eye. Similar tubes are already used to drain excess fluid from the eyes of glaucoma patients, Meng adds.

**Pressing the refillable reservoir delivers drugs into the eye**

**Reference**  
R Lo *et al.*, *Lab Chip*, 2008, DOI: 10.1039/b804690e

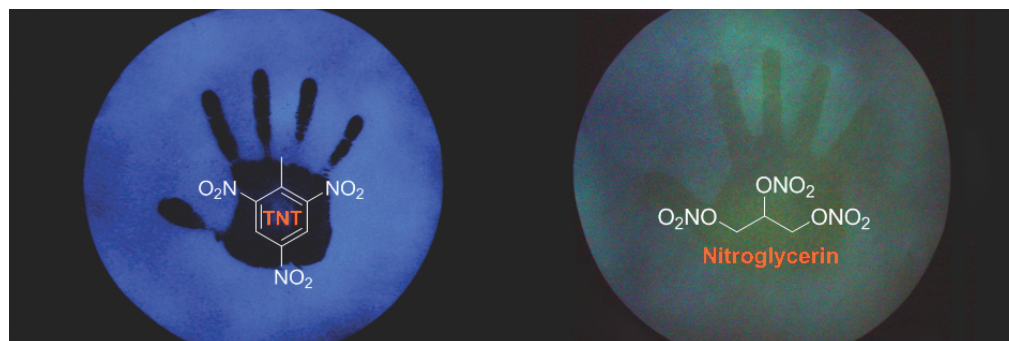
Susan Barker studies drug delivery devices for the eye at the University of East Anglia, Norwich, UK, and agrees that the device would be less invasive than current alternatives. 'This looks quite nice – the drug is effectively delivered into the side of the eye rather than an injection from the front. But manually dispensing the drug might not give a consistent dose and the device is quite large. Would the patient be able to feel it?'

Meng says she plans to address these issues. 'This prototype isn't optimally sized; it's our first go at proving the concept,' she explains. 'We're now building a next-generation device, which won't have square corners but will be rounded and contoured.' The next device will also be powered by a simple electrolysis pump to deliver accurate doses of the drug.

*James Mitchell Crow*

Fluorescent polymer identifies explosive particles

## Glowing response to explosive detection



Explosives can now be detected at picogram levels thanks to a polymer developed by scientists in the US.

William Trogler and his team at the University of California, San Diego, made a silafluorene-fluorene copolymer to identify nitrogen-containing explosives. It is the first of its kind to act as a switchable sensor with picogram detection limits.

Trogler's polymer can detect at much lower levels because, unlike

existing systems, it detects particles instead of explosive vapours. Trogler sprayed the polymer solution over the test area, let it dry then shined UV light on it. Spots of explosive quench the fluorescent polymer and turn blue.

The polymer is able to show the difference between nitrate esters, such as trinitroglycerin, and nitroaromatic explosives, such as TNT. Initially, polymer-treated spots of both compounds appear blue under UV light but after further

**Polymer-treated spots of explosive glow different colours under UV light depending on the type of explosive**

**Reference**  
J C Sanchez and W C Trogler, *J. Mater. Chem.*, 2008, DOI: 10.1039/b802623h

exposure, the trinitroglycerin spot fluoresces green–yellow while the TNT spot remains blue. This colour change is thought to be due to photooxidation of the fluorenyl groups of the polymer.

Trogler was surprised to find that adding a spirofluorene co-monomer gave the polymer a 100 per cent efficient conversion of UV light into fluorescence, describing this increase as dramatic. 'From a technology perspective, the most surprising thing was the ability to use photochemistry to attain a reasonably chemospecific turn-on sensor,' he says. The technology is now being produced commercially by RedXDefense, a security company based in the US, and has even been featured in an episode of the television program *CSI: Miami*.

The team are currently working on a similar system to detect peroxide-based explosives and say they hope to be able to investigate perchlorates and organic nitrates too. *Sylvia Pegg*

## High pressure cocrystals show unexpected properties

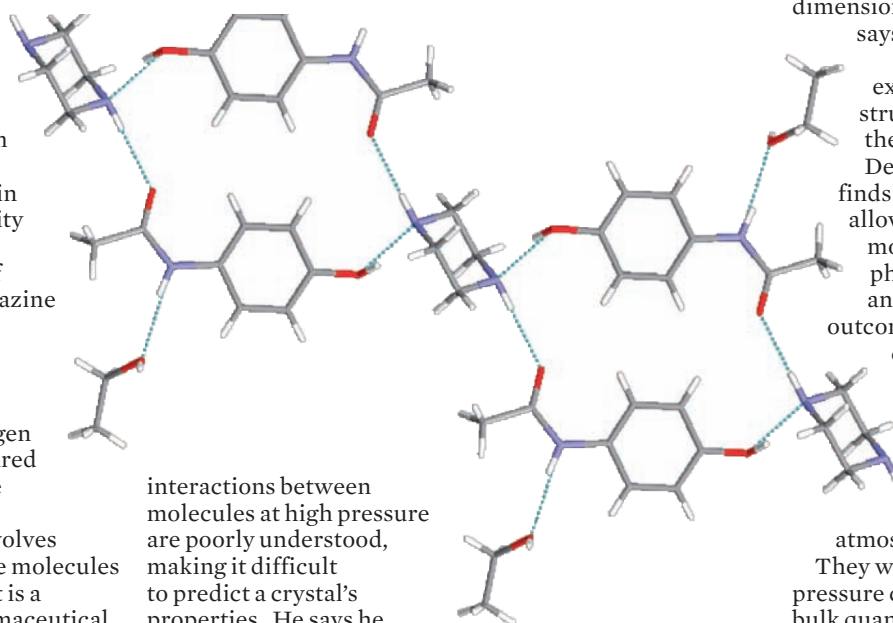
**Drugs under pressure**

The properties of drugs can be improved by using high pressure to make different crystalline forms, claim UK scientists.

Iain Oswald and Colin Pulham at the University of Edinburgh studied the cocrystallisation of paracetamol and piperazine under high pressure. They observed unexpected structural properties, such as unusually short hydrogen bonds, which disappeared when they reduced the pressure.

Cocrystallisation involves combining two or more molecules to form new crystals. It is a useful tool in the pharmaceutical industry because the new crystals can show improved properties over the individual crystals, such as solubility and stability. Until now, however, cocrystallisation of pharmaceuticals at high pressure has not been studied.

Oswald explains that



interactions between molecules at high pressure are poorly understood, making it difficult to predict a crystal's properties. He says he hopes that analysing the structures of cocrystals at high pressure will provide some insight. 'The method will not only increase our understanding of the organic solid state at pressure but it will also provide the cocrystal community with an extra

**Unusually short hydrogen bonds form between paracetamol and piperazine in the cocrystal**

dimension in materials discovery,' says Oswald.

Andrew Bond, an expert in solid state structure interactions at the University of Southern Denmark, Odense, finds the work exciting. 'It allows the forces between molecules in condensed phases to be perturbed and new crystallisation outcomes observed,' he commented.

Oswald and Pulham plan to investigate other cocrystals under pressure to find structures that are also stable at atmospheric pressure.

They will also use larger pressure chambers to produce bulk quantities of material. 'This will allow the industrial viability of crystals to be assessed under ambient conditions,' says Oswald. Harriet Brewerton

**Reference**

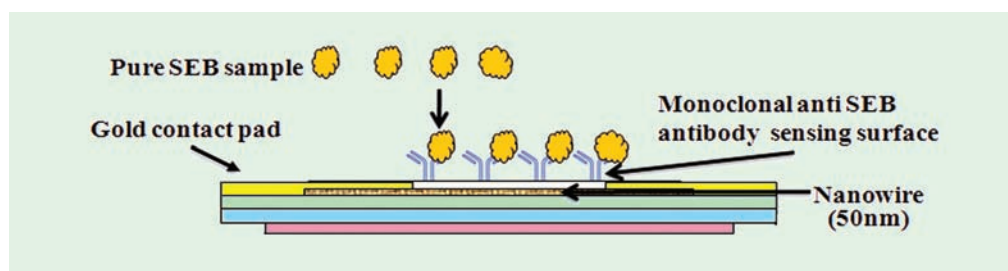
I D H Oswald, and C R Pulham, *Cryst. Eng. Comm.*, 2008, DOI: 10.1039/B805591B

## Biodetector could identify contaminated food

**Electronic sensor for bad bacteria**

Nanoscale transistors made from silicon nanowires can detect a bacterial toxin responsible for the most common form of food poisoning, claim US scientists.

Nirankar Mishra and his team at the University of Idaho, Post Falls, used nanolithography, a process that patterns nanometre-sized structures, to make silicon nanowires. They connected the ends of the wires to gold terminals to form a transistor. By coating the surface of the transistor with an antibody, the team were able to detect the toxin *Staphylococcus aureus* Enterotoxin B (SEB), which formed a complex with the antibody and altered the electric current through the transistor.



**The toxin forms a complex with the antibody coating on the surface of the transistor**

Mishra says he hopes that the transistors, known as field effect transistors, will one day be integrated into hand-held electronic devices for detecting different types of toxins. 'Research into nanodevices has enormous potential in the diagnostics world,' he says.

'Using field effect transistors for biodetection could enable highly sensitive and cost-effective devices to be produced.'

Katherine Davies

**Reference**

N M Mishra *et al*, *Lab Chip*, 2008, 8, 868 (DOI: 10.1039/b802036a)



## Interview

## Environmental impact

Jeff Tester talks to James Hodge about the importance of environmental science



### Jefferson Tester

Jefferson Tester is the H P Meissner Professor of Chemical Engineering at Massachusetts Institute of Technology, Cambridge, US. He is known for his work on various aspects of chemical and energy engineering. Jeff is on the editorial board of the RSC's new journal, *Energy & Environmental Science*.

#### Welcome to the editorial board of *Energy & Environmental Science (EES)*. Why is this journal going to be so important?

The interface between energy and environmental science is crucial as we move forward. The most interesting and important work is taking place at the intersection between several disciplines. *Green Chemistry* started for exactly the same reason – there was a lot of work going on that was very ‘interfacial’ and multi-disciplinary.

#### When you were a student, which inspiring environmental scientists did you look up to?

When I was studying for my PhD, there wasn't such an emphasis on global change as there is now. We concentrated on local issues associated with chemical effluents. I'm a chemical engineer – a lot of the formal training I had was to do with improving separations and improving yield and processes. Rachel Carson (and others like her) set us on a new path with respect to the influence of chemicals in the environment and how they can change ecosystems. Mario Molina and his co-workers did a lot of important work on CFCs and their effect on ozone depletion in the upper atmosphere but it took a long time for their enormous contribution to be recognised with a Nobel prize. The underlying research represents a great example of fundamental science with a specific application to sustainability – the kind we'd like to get into *EES* at an early stage.

#### How has environmental science (and the awareness of environmental issues) changed throughout the course of your career?

Certainly, science and engineering science have changed focus a lot; problems that we couldn't even imagine during the early part of my own professional life are now front-and-centre. Carbon capture, sequestration and storage of CO<sub>2</sub> in the ground and ocean are good examples of enabling technologies to allow us to make a transition to a more sustainable energy supply system. In the 1970s, the focus was on injecting CO<sub>2</sub> into oil reservoirs to increase production. It wasn't a climate change driven initiative.

Our view of resources in general has changed too. Now we're seeing serious efforts to build zero net energy buildings and commercial buildings that are much more sustainable in terms of indoor air quality, lower energy use with very efficient heating, air conditioning and lighting systems.

#### Do you feel that the US government is doing enough to support energy science?

In the past 20 years, energy science has been short-changed in America. Some may argue with this, but I know that in many areas – particularly fundamental research in earth sciences necessary for geothermal energy extraction – basic materials science for solar technology and fundamental research on wind and biomass energy have not been as active as they could be. Clearly, that's changing now though. The Department of Energy and the US Department of Agriculture are ‘re-tooling.’ Maybe by this time next year, an editorial will appear in *EES* to say that we're pleased to report there's a lot more governmental support for energy.

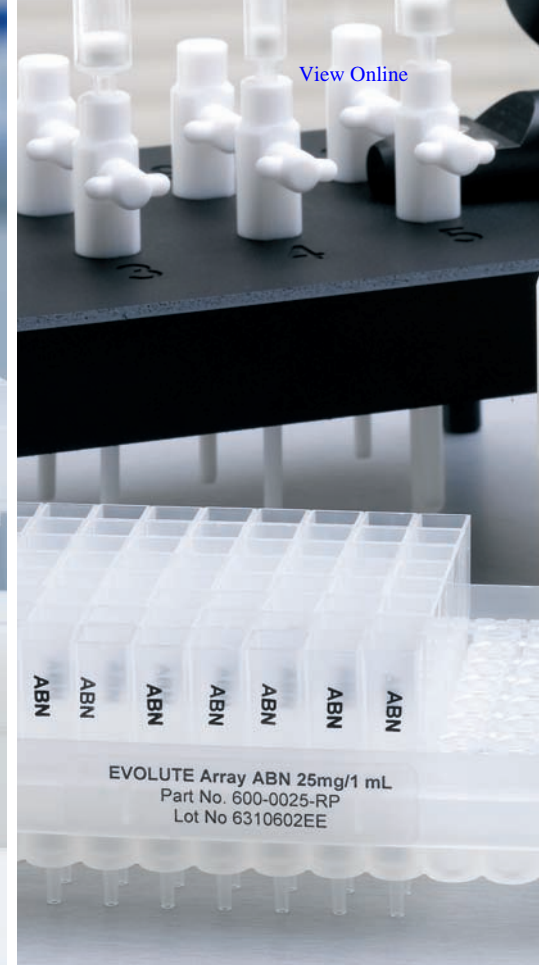
#### Are scientists doing enough to help governments to make those important decisions?

Well, in the US, the answer is clearly no. The scientific community needs to be much more involved in government to inform policy makers of the need to transform our energy system. Our country would benefit if more senators and representatives had formal scientific training.

More needs to be done but at least there has been a change of direction. For example, this past year, I and other scientists have been invited to testify to Congress on a number of energy issues. Some of us are sceptical whether this increased level of government interest in energy is being driven by fear of running out of oil rather than centred on a true commitment to long term sustainability.

#### Which chemical technologies show the most promise for the future in energy and environmental science?

Well, I'm working on hydrothermal transformative chemistry in high pressure water and CO<sub>2</sub>. Researchers are giving a lot of attention (and rightfully so) to doing biochemical transformations to make biofuels, but they tend to be extremely selective reactions. A lot of the available potential feedstocks are chemically complex mixtures like industrial, municipal and agricultural wastes. These are not amenable to straight biological transformation. I favour a two-fold approach: we could use hydrothermal methods to get partial chemical conversion and decomposition and then use biological techniques to operate on simpler molecules.



[View Online](#)

IST Sample Preparation • Bioanalysis • Clinical • Environmental • Forensic • Agrochemical • Food • Doping Control

## EVOLUTE® CX **NEW!**

### Mixed-mode selectivity, generic methodology and efficient extraction

EVOLUTE® CX mixed-mode resin-based SPE sorbent extracts a wide range of **basic drugs** from biological fluid samples. EVOLUTE CX removes matrix components such as proteins, salts, non-ionizable interferences and phospholipids, delivering cleaner extracts with reproducible recoveries for accurate quantitation.

## EVOLUTE® ABN

### Minimize matrix effects, reduce ion suppression and concentrate analytes of interest

EVOLUTE® ABN (Acid, Base, Neutral) is a water-wettable polymeric sorbent optimized for fast generic reversed phase SPE. Available in 30  $\mu\text{m}$  columns and 96-well plates for bioanalysis and **NEW 50  $\mu\text{m}$  columns** – ideally suited for environmental, food/agrochemical and industrial analysis as well as forensic and doping control applications.

Contact your local Biotage representative or visit [www.biotage.com](http://www.biotage.com) to request a **FREE** sample.

  
**Biotage**  
[www.biotage.com](http://www.biotage.com)



## Instant insight

# Solar energy turns organic

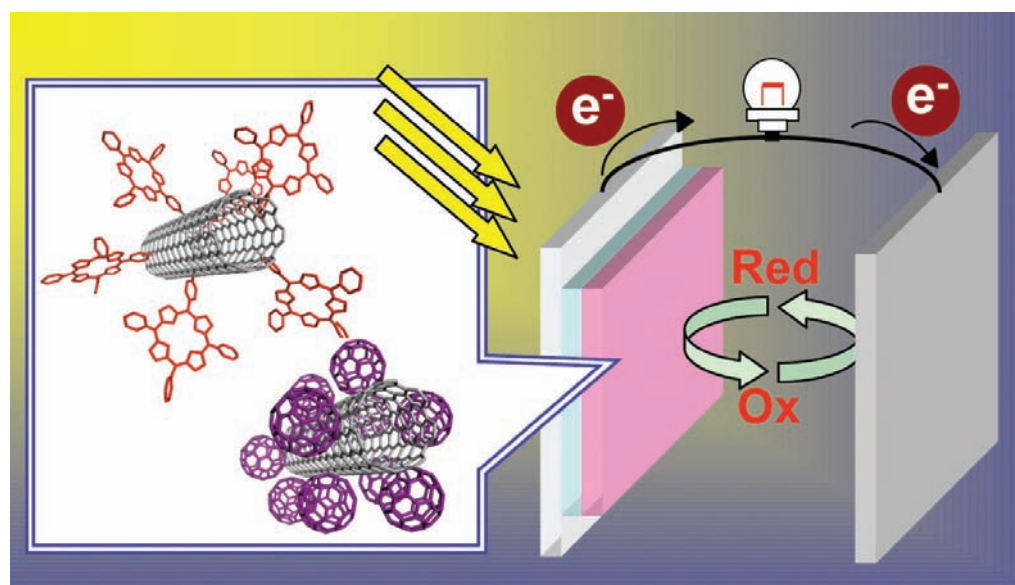
Hiroshi Imahori and Tomokazu Umeyama explain why carbon nanotubes are promising candidates for organic solar cells

Cheap and efficient conversion of solar energy into electricity could help combat global warming and the shortage of fossil fuels. However, the high production cost of electricity from silicon-based solar cells has limited the use of the technology. Low cost solar cells with high cell performance are highly desirable and organic solar cells could be the answer. They are easy to make from inexpensive organic materials and, unlike inorganic solar cells, are lightweight, flexible and colourful.

Light absorption by organic solar cells leads to an excitation state known as an exciton or electron-hole pair. The electrons and holes are separated from each other and carried through donor and acceptor molecules to the electrodes, generating a photocurrent.

This process of converting light directly into electricity is known as photovoltaics and it must be optimised for organic solar cells to be efficient. Much effort has been devoted to finding suitable donor and acceptor molecules and organising them on an electrode surface at the nanometre scale.

Fullerenes and their derivatives have been widely used as excellent acceptor molecules. More recently, carbon nanotubes (CNTs), which have a similar carbon-based structure, have attracted much attention. In contrast to the spherical shape of fullerenes, CNTs have a one dimensional, wire-like structure, which makes them better at forming electron- or hole-transporting highways in the cell. Their large surface area enhances the separation of the electron-hole pair and they show conductivity several times greater than that of conducting polymers. Also, CNTs



can act as both electron donors and acceptors depending on the redox properties of the other component in the cell. All of these features make CNTs promising candidates for charge separation and transport in organic solar cells.

A number of scientists have made photoelectrochemical devices or photovoltaic cells with CNT-modified electrodes. They have used a variety of methods, including layer-by-layer deposition and spray-coating, to organise the CNTs with suitable donor or acceptor molecules on electrode surfaces. At present, however, the energy conversion efficiency of CNT-modified electrodes has yet to reach the levels of high performance dye-sensitised solar cells – which use porous, nanocrystalline titanium dioxide electrodes sensitised with ruthenium dyes – or bulk heterojunction solar cells, which

**Carbon nanotubes' wire-like structures help them form charge-transporting highways in organic solar cells**

use conjugated polymers and functionalised fullerenes.

Currently, it is difficult to synthesise pure CNTs with a consistent, defect-free structure. To improve CNT-based solar cells, scientists may have to purify or sort out the CNTs with the best structure for charge transport. Alternatively, a fascinating approach is to use CNTs as nanoscaffolds for donor or acceptor molecules to construct charge-transporting highways.

The history of CNT-based organic solar cells is less than 10 years old. A great deal of work still has to be done to bring out their full potential for solar energy conversion.

Read Hiroshi Imahori and Tomokazu Umeyama's Feature Article 'Carbon Nanotube-Modified Electrodes for Solar Energy Conversion' in a forthcoming issue of *Energy & Environmental Science*.

**Reference**  
H Imahori and T Umeyama, *Energy Environ. Sci.*, 2008, DOI:10.1039/b805419n

# Essential elements

## Expanding the chemical sciences

RSC Publishing is set to increase its journal portfolio from 2009 following announcement of the launch of two new RSC journals. A press release on June 12th confirmed that two interdisciplinary titles, *Integrative Biology* and *Metallomics*, will both publish their first issue in January 2009.

*Integrative Biology* will provide a unique venue for research that leads to a greater understanding of biological processes and mechanisms. A highly interdisciplinary journal, it will focus on quantitative multi-scale biology using enabling technologies and tools to exploit the convergence of biology with physics, chemistry, engineering, imaging and informatics. The editorial board chair for this prestigious new journal will be Mina Bissell from Lawrence Berkeley National Laboratory, US.



*Metallomics* will cover the research fields related to metals in biological systems and is expected to be the core publication for the emerging metallomics community. *Metallomics* is receiving great attention as a new frontier of trace elements in biology and is expected to develop as an interdisciplinary science complementary to genomics and proteomics. Joseph Caruso of the University of Cincinnati/Agilent Technologies Metallomics Center of the Americas and a leading player in this emerging

field, will chair the editorial board of this timely new journal.

RSC Publishing boasts an accomplished record in launching new products. With *Integrative Biology* and *Metallomics* set to follow in the footsteps of success stories like *Soft Matter* and *Molecular BioSystems*, RSC Publishing again reinforces its position as a world-class scientific publisher.

From launch, the latest issues of both *Integrative Biology* and *Metallomics* will be made freely available to all readers via the website. Free institutional access to all issues of each journal published in 2009 and 2010 will be available following a simple registration process.

Watch [www.rsc.org/journals](http://www.rsc.org/journals) for all the latest news

## Molecules of Murder

This fascinating new book by John Emsley, due for publication in August 2008, is about infamous murderers and famous victims! It includes the stories of people such as Harold Shipman, Alexander Litvinenko, Adelaide Bartlett and Georgi Markov and takes the reader on a journey of discovery into the world of poisons. Few books on poisons analyse these crimes from the viewpoint of the poison itself, and doing so throws a new light on how the murders or attempted murders were carried out and ultimately how the perpetrators were uncovered and brought to justice. *Molecules of Murder* looks at how forensic chemists have developed cunning ways to detect minute traces of dangerous substances, and why some of these poisons are now being researched as possible life-savers!

John Emsley is a great science communicator. His entertaining books have contributed to the advancement of a positive awareness of science. In 2004 John was elected as an honorary member of The Society of Chemical Industry (SCI) in recognition of a lifetime of achievement and contributions to chemistry. He has written numerous popular science books and articles.

For more information on this exciting book and other forthcoming RSC Publishing titles please visit [www.rsc.org/books](http://www.rsc.org/books)

## Taking to the global stage

Scientists wanting to access the latest research linking all aspects of the chemical sciences relating to energy conversion and storage, alternative fuel technologies and environmental science have a new resource at their disposal.

The first Advance Articles for *Energy & Environmental Science*, the latest journal from RSC Publishing, are now available.

The publication of the journal's first issue is anticipated shortly, and will be freely available online.

Enthusiastically welcomed by the community, the first issue will demonstrate the range of subjects included in the scope: from new insights into photovoltaics to the synthesis of important new hydrogen

storage materials; from exciting new developments in hydrogen production from biomass to global climate change; from artificial photosynthesis to fuel cells; and from environmental catalysis to nanostructured materials for energy applications – they are all included.

Read the first articles on the website: [www.rsc.org/ees](http://www.rsc.org/ees)

*Chemical Technology* (ISSN:1744-1560) is published monthly by the Royal Society of Chemistry, Thomas Graham House, Science Park, Milton Road, Cambridge UK CB4 0WF. It is distributed free with *Chemical Communications*, *Journal of Materials Chemistry*, *The Analyst*, *Lab on a Chip*, *Journal of Atomic Absorption Spectrometry*, *Green Chemistry*, *CrystEngComm*, *Physical Chemistry Chemical Physics* and *Analytical Abstracts*. *Chemical Technology* can also be purchased separately. 2008 annual subscription rate: £199; US \$396. All orders accompanied by payment should be sent to Sales and Customer Services, RSC (address above). Tel +44 (0) 1223 432360, Fax +44 (0) 1223 426017 Email: [sales@rsc.org](mailto:sales@rsc.org)


**Editor:** Joanne Thomson  
**Deputy editor:** Michael Spencelayh  
**Associate editors:** Celia Clarke, Nina Notman  
**Interviews editor:** Elinor Richards  
**Web editors:** Nicola Convine, Michael Townsend, Debora Giovannelli  
**Essential elements:** Daniel Bradnam, Kathryn Lees, Valerie Simpson and Caroline Wain  
**Publishing assistant:** Ruth Bircham  
**Publisher:** Graham McCann

Apart from fair dealing for the purposes of research or private study for non-commercial purposes, or criticism or review, as permitted under the Copyright, Designs and Patents Act 1988 and the copyright and Related Rights Regulations 2003, this publication may only be reproduced, stored or transmitted, in any form or by any means, with the prior permission of the Publisher or in the case of reprographic reproduction in accordance with the terms of licences issued by the Copyright Licensing Agency in the UK. US copyright law is applicable to users in the USA.

The Royal Society of Chemistry takes reasonable care in the preparation of this publication but does not accept liability for the consequences of any errors or omissions.

Royal Society of Chemistry: Registered Charity No. 207890.

# RSC Publishing



# 2<sup>ND</sup> EUCHEMS CHEMISTRY CONGRESS

2008 SEPTEMBER 16 - 20  
TORINO, ITALY

## CHEMISTRY: THE GLOBAL SCIENCE

### PLENARY LECTURES BY

**Peter AGRE** (Baltimore, USA)  
**Avelino CORMA** (Valencia, Spain)  
**Jean M.J. FRÉCHET** (Berkeley, USA)  
**Robert H. GRUBBS** (Pasadena, USA)  
**Kyriacos C. NICOLAOU** (La Jolla, USA)  
**Martyn POLIAKOFF** (Nottingham, UK)  
**K. Barry SHARPLESS** (La Jolla, USA)

### KEYNOTE LECTURES BY

**Varinder AGGARWAL** (Bristol, UK)  
**Lucia BANCI** (Florence, IT)  
**Matthias BELLER** (Rostock, DE)  
**Richard CATLOW** (London, UK)  
**Ken CAULTON** (Bloomington, USA)  
**Fritz FRIMMEL** (Karlsruhe, DE)  
**Dante GATTESCHI** (Florence, IT)  
**Jana HAJŠLOVA** (Prague, CZ)  
**Dino MORAS** (Illkirch, FR)  
**Ulrich STIMMING** (Munich, DE)  
**Philip TAYLOR** (Geel, BE)  
**Jun-ichi YOSHIDA** (Kyoto, JP)

### SCIENTIFIC COMMITTEE

*Chair* **Hartmut MICHEL** (DE)  
*Co-chair* **Igor TKATCHENKO** (FR)

### ORGANISING COMMITTEE

*Chair* **Giovanni NATILE** (IT)  
*Co-chair* **Francesco DE ANGELIS** (IT)

### LOCAL ORGANISING COMMITTEE

*Chair* **Lorenza OPERTI** (IT)  
*Co-chair* **Salvatore COLUCCIA** (IT)

Special topic symposia:

### ADVANCES IN SYNTHESIS

- Organic Catalysis
- Radical Reactivity in Transition Metal Chemistry
- Reactions under Novel Conditions

### ADVANCES IN UNDERSTANDING

- Chemical Measurement Quality: Societal Impact
- Cutting Edge Chemistry with Computers
- Food Analysis: Pushing Detection Limits down to Nothing

### CHEMISTRY AND LIFE SCIENCES

- Biomolecular Interactions and Mechanisms
- Drug Targeting and Delivery
- Metal Homeostasis

### ENERGY AND INDUSTRY

- Biorefineries and Biotechnologies
- Energy Production & Storage
- New Trends for Agrochemicals

### ENVIRONMENT

- Greening Chemistry
- Greenhouse Gases
- Water Pollutants

### MATERIALS AND DEVICES

- Branched Polymers - Smart Functional Materials
- Nanomaterials
- Porous Materials



**ORGANISING SECRETARIAT**

**Centro Congressi Internazionale** s.r.l. - Corso Bramante 58/9 10126 Torino - I  
 tel +39 011.2446911 fax +39 011.2446900/44 - info@euchems-torino2008.it

[www.euchems-torino2008.it](http://www.euchems-torino2008.it)

\*EuChemS, the European Association for Chemical and Molecular Sciences incorporates  
 50 member societies which in total represent some  
 150.000 individual chemists in academia, industry and government in over  
 35 countries across Europe.



RSC | Advancing the  
Chemical Sciences

# Supercritical fluids in green chemistry

DOI: 10.1039/b809498p

The use of supercritical fluids is often highlighted as an important strategy within green chemistry to replace volatile organic compounds, VOCs, and to enable new, clean technologies. The now classic examples of natural product extraction have been practised in industry for more than twenty years on various scales.<sup>1</sup> In many of these cases, supercritical CO<sub>2</sub>, scCO<sub>2</sub>, penetrates into a solid substrate to remove a desired product or an unwanted component or impurity. In chemical reactions, scCO<sub>2</sub> is used as a solvent for reagents and/or catalysts to facilitate their intimate contact.<sup>2</sup> These and many more applications rely on the solvent power of scCO<sub>2</sub> and hence exploit in particular the liquid like properties of scCO<sub>2</sub>.

There are, however, also a number of application where the supercritical phase is used mainly because of its properties of a compressed gas phase. Among these applications are processes involving polymeric materials, where the sorption of the

compressed gas within the polymer matrix leads to a reduction in the temperatures of the glass transition or melting point. Possible applications of this basic phenomena are found in polymer processing, purification, or coating processes. If the gas phase is released very rapidly from the polymer matrix, foaming occurs allowing generation of polymer architectures and materials ranging from bulk to highly specialised products.

The review by Jacobs, Kemmere and Keurentjes in this issue of *Green Chemistry* (L. J. M. Jacobs, M. F. Kemmere and J. T. F. Keurentjes, *Green Chem.*, 2008, DOI: 10.1039/b801895b) provides an overview of the state of the art for this area of supercritical fluid research and application. It is interesting to note that the green chemistry aspect of these methods is in fact wider than the actual replacement of undesired VOCs by CO<sub>2</sub> within the process. The materials obtained can display favourable properties, such as

enhanced stability or insulation properties at reduced mass. New applications for biodegradable or bio-based polymers can be envisaged if porous materials can be accessed from them in a controlled manner.

In general, the integration of process and product design is an important target for green chemistry, although we have to admit that there is still some way to go before we can really talk about a “designer” process in this context. The 10th anniversary of the launch of this journal is certainly a timely opportunity to encourage further steps in that direction.

**Walter Leitner**  
**Martyn Poliakoff**

## References

- 1 P. G. Jessop and W. Leitner, in *Chemical Synthesis Using Supercritical Fluids*, VCH, Weinheim, 1999.
- 2 E. J. Beckman, *J. Supercrit. Fluids*, 2004, **28**, 121.



# Sustainable polymer foaming using high pressure carbon dioxide: a review on fundamentals, processes and applications

Leon J. M. Jacobs,\* Maartje F. Kemmere and Jos T. F. Keurentjes

Received 6th February 2008, Accepted 8th May 2008

First published as an Advance Article on the web 6th June 2008

DOI: 10.1039/b801895b

In recent years, carbon dioxide (CO<sub>2</sub>) has proven to be an environmentally friendly foaming agent for the production of polymeric foams. Until now, extrusion is used to scale-up the CO<sub>2</sub>-based foaming process. Once the production of large foamed blocks is also possible using the CO<sub>2</sub>-based foaming process, it has the potential to completely replace the currently used foam production process, thus making the world-wide foam production more sustainable. This review focuses on the polymer–CO<sub>2</sub>-foaming process, by first addressing the principles of the process, followed by an overview of papers on nucleation and cell growth of CO<sub>2</sub> in polymers. The last part will focus on application of the process for various purposes, including bulk polymer foaming, the production of bioscaffolds and polymer blends.

## 1. Introduction

The discovery of Bakelite<sup>1</sup> followed by the mass production of synthetic polymers a few decades later has had a major impact on today's society. By the end of the 20th century plastics had become one of the most important construction materials for consumer goods. The highly viscous nature of polymers brought about processing difficulties which led to the development of plasticization technology. From plasticizing agent to blowing agent is only a small step, and this resulted in the discovery and the large scale production of polymeric foams. Due to the increasing demand for light weight, insulating, shock and sound absorbing materials, the production and variety of polymeric foams has increased dramatically and has become a very important part of the annual polymer production.

One of the most commonly used production processes for polymeric foams is the so-called thermally induced phase separation (TIPS) process, where the foaming agent, which is dissolved in the polymer, induces a phase separation upon heating, followed by nucleation and cell growth. The foaming agent is usually a low boiling organic liquid, such as pentane and hydrochlorofluorocarbons (HCFCs), which is dissolved into the polymer at concentrations of about 7 wt%. Foaming *via* the TIPS process usually takes place in two steps. In the first step, polymer pellets with blowing agent are partly foamed with steam. These foamed pellets are then transferred into a mold and exposed to steam again, resulting in further foaming of the pellets. Due to the expansion, the pellets stick together and take the shape of the mold. This makes it relatively easy to produce large blocks of foamed material, which can then be cut into any shape. Furthermore, the density of the produced block can easily be controlled by the amount of partly foamed pellets added to the mold.

Process Development Group, Department of Chemical Engineering and Chemistry, Eindhoven University of Technology, P.O. Box 513, 5600 MB, Eindhoven, The Netherlands. E-mail: l.j.m.jacobs@tue.nl; Fax: +31 40 2446104; Tel: +31 40 2472884

A variation on the TIPS process is dissolving the polymer in a solvent at elevated temperatures, after which a temperature quench will induce a phase separation. Removal of the solvent results in the polymeric foam.<sup>2–4</sup> Next to the TIPS process, several other methods of preparing polymeric foams are available (Fig. 1). One of these methods involves foaming by means of a chemical foaming agent (CFA). The CFA is a thermally unstable component, which is added to the polymer. Upon heating the CFA decomposes into gaseous components, resulting in the desired foam. The gaseous CFA can also be formed by reaction of two polymeric components, which is the case in polyurethane (PUR) foams.<sup>5,6</sup>

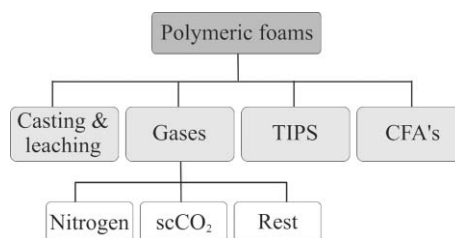


Fig. 1 Schematic overview of methods for preparing polymeric foams.

Polymeric foams can also be produced by casting and leaching. This method consists of dissolving the polymer in a highly volatile solvent and casting the solution into a mold containing a solid porogen. The porogen is usually a water soluble salt, such as NaCl or KCl, which is washed out after the solvent has evaporated, leaving a highly porous polymeric structure. The advantage of this method is that the pore size and morphology can be controlled by the size and distribution of the porogen and the amount added.<sup>7–9</sup>

The main problem with the above mentioned methods is, however, that they either lead to unwanted contaminations in the polymeric foams, such as residual solvents and salts, or lead to the emission of harmful substances, which cannot be recovered. For example, the European expandable polystyrene demand for 2002 was 3 million tons and is expected to grow to a demand of



approximately 3.7 million tons in 2010.<sup>10</sup> Since 7 wt% of blowing agent is used for foam production, this will result in an estimated emission of 256 thousand tons of low boiling organic liquids in 2010 in Europe alone. Problems concerning the environment and the need for environmentally benign foaming agents have triggered researchers to start working on this topic. Universities as well as industry are focusing their research on developing “greener” foaming processes using a non-toxic foaming agent. Despite the fact that companies have come up with the idea of an extrusion process using gases such as nitrogen and carbon dioxide as a blowing agent some time ago,<sup>11–14</sup> only in the early nineties were the first articles on foaming of polymers using gases published.<sup>15</sup> Although nitrogen can be used as a blowing agent in the polymer foaming process,<sup>16,17</sup> most publications on this topic address the foaming of polymers using carbon dioxide, because carbon dioxide also affects other polymer properties, thereby enhancing the processability of the polymer.<sup>18</sup> However, both nitrogen and carbon dioxide (CO<sub>2</sub>) are considered to be sustainable alternatives for the replacement of the currently used blowing agents.

Because the foaming of polymers using CO<sub>2</sub> has been a ‘hot topic’ and most probably will be for some time, here we review the most relevant literature on the polymer–CO<sub>2</sub>-foaming process. First, the principles of the polymer–CO<sub>2</sub>-foaming process are addressed, followed by a short overview of papers addressing the nucleation of CO<sub>2</sub> in polymers. Batch and continuous foaming processes will be discussed, after which the foamability of bio-based and synthetic polymers will be addressed. The last part of this review will focus on applications, such as bulk polymer foaming, bioscaffolds and polymer blends. Finally, conclusions and a future outlook will be given.

## 2. The CO<sub>2</sub>-foaming process

The CO<sub>2</sub>-based foaming process can roughly be divided into two steps. In the first step, the polymer is saturated with CO<sub>2</sub>, which is followed by an expansion step. Both steps, together with some important foaming parameters are schematically depicted in Fig. 2. During saturation of the polymer the glass transition temperature ( $T_g$ ) will decrease and the polymer is plasticized. This means that the  $T_g$  of the polymer decreases to a value below the temperature at which the polymer is saturated (*i.e.* the saturation temperature). The  $T_g$  is the temperature at which the polymer matrix becomes brittle upon cooling, or soft upon

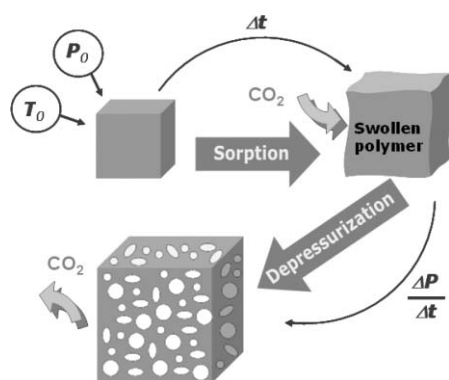


Fig. 2 Schematic representation of the CO<sub>2</sub>-foaming process.

heating. The state below  $T_g$  is called the glassy state and the state above  $T_g$  is called the rubbery state. Above  $T_g$ , polymers are capable of plastic deformation without fracture.<sup>19</sup> Furthermore, the polymer matrix will swell and the viscosity of the polymer decreases, allowing processing of the polymer–CO<sub>2</sub> mixture at lower temperatures. The diffusivity inside the polymer is also enhanced, enabling the use of CO<sub>2</sub> as a medium to add additives to the polymer matrix. The type of polymer, together with the applied pressure and temperature determine to a large extent the amount of CO<sub>2</sub> that can be dissolved in the polymer.

Once the polymer is saturated, a rapid decrease in pressure will induce a shift in the thermodynamic equilibrium, leading to an oversaturation of CO<sub>2</sub> in the polymer. However, this does not necessarily lead to nucleation and cell growth. If the temperature at which the polymer has been saturated is relatively low, the polymer can still be in the glassy state, because  $T_g$  has not been sufficiently depressed by the sorption of CO<sub>2</sub>. Therefore, phase separation and nucleation will only occur once the saturated sample is heated to a temperature above the glass transition temperature. This will lead to cell growth and the final formation of the polymeric foam. Below the glass transition temperature, foaming cannot occur, because the polymer matrix is too rigid. If the saturation temperature is high enough and the polymer–CO<sub>2</sub> mixture is in the rubbery state due to sufficient depression of  $T_g$ , phase separation and nucleation will occur instantaneously upon depressurization. Cell growth will stop once the polymer matrix returns to the glassy state, either due to a decrease in temperature or a decrease in the CO<sub>2</sub> concentration in the polymer and the polymer is no longer plasticized.

The gas phase can separate from the polymer phase by two mechanisms. If the pressure drop results in a metastable state, nucleation will be the dominant mechanism for foam formation. In the unstable state, spinodal decomposition will be the dominant mechanism.<sup>20</sup> This is schematically depicted in Fig. 3. Both mechanisms are diffusion driven, although the direction of diffusion is opposite. In spinodal decomposition, diffusion moves from low concentration to high concentration, due to a high driving force. This review, however, will focus on nucleation as the mechanism for polymer foaming since it is usually suggested as the dominant phase separation mechanism.

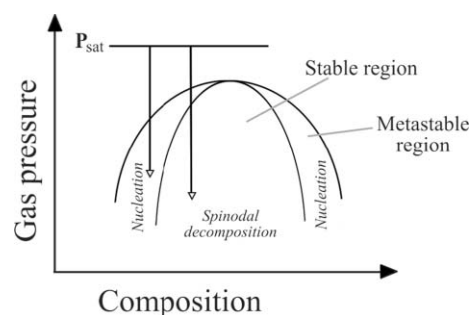


Fig. 3 Schematic phase diagram of the composition vs. the gas pressure.

## 3. Nucleation and cell growth

The classical nucleation theory is often used as a basis for modeling the nucleation process. The theory is based on the Gibbs free energy required to create a void in a liquid, resulting

in a critical bubble, which is in mechanical and thermodynamic equilibrium with the surrounding fluid.<sup>21,22</sup> However, the classical theory only holds for describing the boiling of low molecular-weight-liquids and does not apply to the nucleation of gases in viscous liquids such as polymers. For that reason, many extensions of the classical nucleation theory have been proposed, to include amongst others free volume effects and surface tension reduction due to the dissolved gases and additives,<sup>23,24</sup> polymer-solvent interactions and supersaturation of the blowing agent.<sup>25</sup> Colton *et al.*<sup>26</sup> have validated their adaptation of the theory with experiments, yielding a good qualitative description of nucleation behavior of microcellular bubbles in amorphous thermoplastic polymers.

Next to the modeling of nucleation, many theories have been published concerning cell growth in polymers. These models are mainly based on the diffusion-driven growth of a spherical bubble,<sup>27–29</sup> incorporating effects such as the dependencies on temperature and CO<sub>2</sub> concentration of the density, diffusivity and viscosity, respectively.<sup>30</sup> Leung *et al.*<sup>31</sup> have successfully developed a model to accurately describe the bubble growth of experimentally observed data for the polystyrene–CO<sub>2</sub> system.

Although numerous papers discuss either the nucleation behavior or cell growth, only few have tried to model both effects simultaneously. One of these models has been developed by Joshi *et al.*<sup>32</sup> As a base case for their model, parameters of the low density polyethylene–N<sub>2</sub> system have been used. However, only a numerical analysis has been performed without any experimental validation. More recently, Feng *et al.*<sup>33</sup> have integrated nucleation and cell growth models into a consistent theory, predicting the cell size distribution during the foaming process. Even though their results are in reasonable agreement with experimental data, the authors are very critical about their results and acknowledge the opportunities for further improvements.

The formation of nuclei in a viscous liquid followed by cell growth is a very complex mechanism, which is influenced by many parameters, such as temperature, viscosity, CO<sub>2</sub>-concentration, depressurization rate and pressure drop. Despite the significant research efforts, it will probably take a considerable time before the complete process is fully understood.

#### 4. Batch versus continuous

Polymeric foams can be produced batch-wise or continuously. For both processes the general foaming steps of Fig. 2 can be applied. The batch process is usually applied in the research and development field where new materials are foamed or the foaming behavior is studied. In order to make the foaming process economically feasible and possible on a larger scale, a continuous process based on extruders is commonly used. In general, the extrusion process consists of a mixing step, where the polymer is mixed with the additives and is pressurized with CO<sub>2</sub>. Due to sorption of CO<sub>2</sub>,  $T_g$  and viscosity will decrease, allowing processing of the polymer–CO<sub>2</sub> mixture at lower temperatures. This means that different zones in the extruder can be operated at different temperatures, making it possible to add or use temperature sensitive components or polymers. This could make the CO<sub>2</sub>-based foaming process applicable to bio-based polymers and/or additives. At the die of the extruder the

pressure is released and the polymer foam is produced. Several patents have claimed the process where an extruder is used in combination with a gas as a blowing agent.<sup>11,12</sup> Since the nineties, more and more patents claim specific parts of the extrusion foaming process, *e.g.* the way the gaseous blowing agent is added to the extruder,<sup>34,35</sup> the specific zones of the extruder,<sup>36</sup> as well as the dimensions of the die and pressure release zone.<sup>37</sup>

Next to patents claiming (parts of) the extrusion process, the extrusion process has also been investigated in academia. A division can be made between literature using the extruder as a means for mixing during the foaming process and literature optimizing and modeling the extruder and the extrusion process itself. In the former, only the processing conditions in the extruder are changed, such as saturation pressure and screw rotation speed<sup>38–43</sup> or the type and amount of additive added, such as carbon nanofibres<sup>44</sup> or nanoclays.<sup>45</sup>

The effect of the die geometry and temperature on the nucleation rate or the expansion ratio of the produced foams has also been investigated.<sup>46–48</sup> A proper die design plays a crucial role in improving the quality of the extruded foams, since the geometry of the die determines the pressure decay rate and absolute pressure drop, by which both cell density and cell morphology are dominantly affected.

Baldwin *et al.*<sup>49</sup> have developed generalized design models of nucleated solutions in an extruder. It approximates the pressure drop and flow rate experienced by a two-phase polymer/gas solution flow through a die channel, with the goal to capture the major physical attributes of the complicated flow and provide means of quickly estimating the required flow channel geometry and evaluating the feasibility of a flow channel design.

Additionally, Stephen *et al.*<sup>50</sup> have refined the model to incorporate more realistic features of gas nonideality and viscosity reduction.

## 5. Bulk polymer foaming

The main requirement of the CO<sub>2</sub>-foaming process is that a sufficient amount of CO<sub>2</sub> will dissolve in the polymer. This excludes the use of polymers such as cellulose and polyethylene, which have a very low affinity for CO<sub>2</sub>. Nevertheless, a full range of polymers is still available that can be used in this process, including polystyrene, poly(methyl methacrylate) and biopolymers such as poly(lactic-co-glycolic). The properties of the polymer determine to a large extent the properties of the foam and, therefore, the field of application: for insulation purposes different requirements are needed as compared to biomedical applications. For the latter, bio-based polymers are preferably used, as these polymers are generally biocompatible and/or biodegradable.

### 5.1 Micro- and macrocellular foams

Polymeric foams can be divided into two groups: microcellular foams (MCFs) and macrocellular foams. The latter have typical cell sizes of 50  $\mu\text{m}$  or larger and are mainly used as insulation and packaging materials, due to their relatively poor mechanical properties. MCFs have a typical cell size of 0.1–10  $\mu\text{m}$  and cell densities ranging from 10<sup>9</sup>–10<sup>15</sup> cells cm<sup>-3</sup>. The main idea for producing these materials has been materials savings, by creating

voids without compromising material properties too much. This has been accomplished by keeping the cell size below a critical size, smaller than the pre-existing flaws in the polymeric matrix. In that way the cells would act as crazing initiation sites and toughen the material. Suh *et al.*<sup>51,52</sup> were one of the first to produce MCFs in the early 1980s, followed by other publications on this topic in the late 1980s and after.<sup>26,53,54</sup> Initially, MCFs were the main subject studied in the literature, produced by saturating a polymeric sample at room temperature with a gas at a certain pressure, followed by heating to a temperature above the glass transition temperature. The latter induces nucleation and gives the polymer matrix the flexibility needed for cell growth.<sup>55,56</sup> In the early 1990s, Goel and Beckman<sup>57,58</sup> were one of the first to describe the pressure quench method for producing MCFs, which is similar to the procedure described in paragraph 2. Both procedures are now used to produce microcellular as well as macrocellular foams.

Based upon the results published in the literature,<sup>53,57,59–66</sup> several general conclusions about the polymer foaming process can be drawn. These conclusions have been illustrated with experimental results, in which poly(styrene-co-methyl methacrylate) (SMMA) has been foamed at different temperatures, pressures and depressurization rates.<sup>66</sup> The results can be found in Fig. 4, 5 and 7. For both foaming methods, the number of nuclei that will be formed upon fast depressurization increases with increasing saturation pressure. Fig. 4 clearly shows that the cell size decreases with increasing pressure resulting in more cells per unit volume. For the pressure quench method, it can be generalized that a higher saturation temperature results in larger cells and an overall lower bulk density, as can be seen in Fig. 5. The polymer matrix will be less rigid at higher temperatures, resulting in less resistance to cell growth. Furthermore, the time available for cell growth is also longer at higher temperatures, since vitrification of the polymer matrix will occur at a later stage. This is schematically depicted in Fig. 6. A decrease in depressurization rate also has an effect on polymer foaming. As this rate decreases, the degree of oversaturation per unit time decreases as well and fewer nuclei will be formed. Therefore, more time is available for diffusion of CO<sub>2</sub> from the polymer

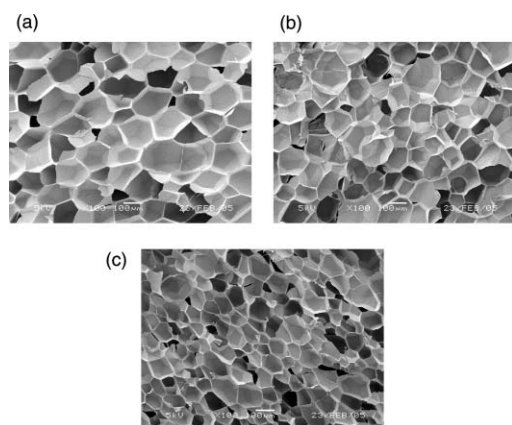


**Fig. 4** A sequence of SEM pictures (100×) of SMMA foamed at 119 °C and (A) 100 bar, (B) 150 bar and (C) 175 bar, where a decrease in cell size with increasing pressure is clearly visible. These results are typically obtained for both the pressure quench foaming method and the foaming method induced by an increase in temperature.

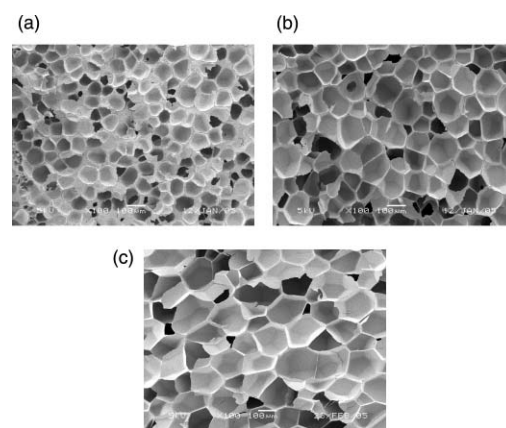


**Fig. 5** A sequence of SEM pictures (100×) of SMMA foamed at 100 bar and (A) 93 °C, (B) 110 °C and (C) 119 °C, where an increase in cell size with increasing temperature is clearly visible. These results are typically obtained for both the pressure quench foaming method and the foaming method induced by an increase in temperature.

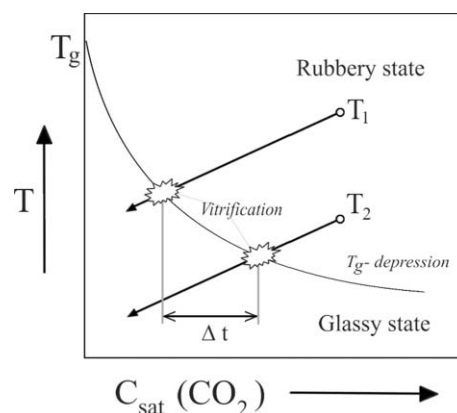


**Fig. 6** Schematic representation of the decrease in foaming time at lower temperatures of saturation.

matrix into the cells, which results in larger cells. Fig. 7 clearly illustrates the effect of a decreasing depressurization rate on the cell size. If depressurization occurs in two steps, a foam with a bimodal cell size distribution will be produced. The first

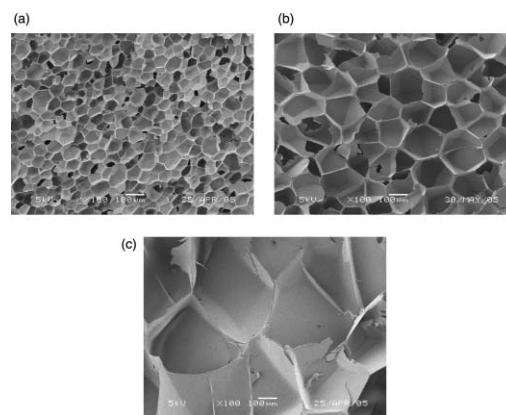


**Fig. 7** A sequence of SEM pictures (100×) of SMMA foamed at 119 °C, 200 bar and (A) < 1 s, (B) 35 s and (C) 230 s. These figures clearly show the effect of decreasing depressurization rate, which results in an increase in cell size.



step will induce nucleation and some cell growth. The second depressurization step results in secondary nucleation and further growth of the primary nucleated cells. The secondary nuclei have less time to grow and will therefore be smaller. An example of such a foam is given in Fig. 8.

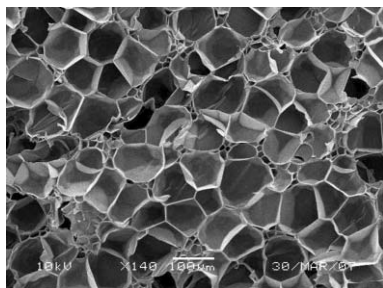


**Fig. 8** A typical bimodal cell size distribution which can be obtained when depressurization of the foaming process occurs in two steps.

Molecular weight and polydispersity do not appear to have a significant effect on the foam morphology.<sup>67</sup> However, the presence of even a few percent of low molecular weight compounds will increase the cell size and decrease the nucleation density in microcellular foaming processes. The effect of the low molecular compound cannot be explained by the classical nucleation theory. It is suggested that spinodal decomposition causes this effect.

In almost all CO<sub>2</sub> foaming literature the formation of a skin at the surface of the foamed sample is described. The main reason for skin formation is the rapid diffusion of CO<sub>2</sub> from the surface of the sample upon depressurization. Especially in the foaming of thin films, where the surface/thickness ratio is unfavorable, the skin can be relatively thick. To overcome this problem, Siripurapu *et al.*<sup>68</sup> have proposed to confine the polymeric film between two CO<sub>2</sub>-impermeable surfaces, so CO<sub>2</sub> can only escape through the film edges. This resulted in polymeric films with very thin skins (approximately 1 cell diameter thick), or even without any skin, making them interesting materials for application in molecular separation processes, biotechnology and microelectronics.

## 5.2 Nanocomposite foams

One of the problems with polymeric foams for the use as a construction material is that the mechanical strength decreases as the cell size increases. By introducing nanoparticles in the polymeric matrix, not only can the mechanical properties of nanocomposite foams be enhanced, but also the physical properties, such as the fire resistance of the polymer. One of the most widely used particles is montmorillonite (MMT) clay, but also carbon nanofibres (CNF), spherical silica particles, nanocrystals, gold and other metal nanoparticles can be used.<sup>69–73</sup> Because of the small dimension of the nanoparticles, they are especially beneficial for reinforcing cell walls of the foams, since the thickness of the cell walls is in the micron and submicron range.

Lee *et al.*<sup>74</sup> have shown that PS foamed with CO<sub>2</sub> containing 1 wt% of CNF increased the tensile modulus by 28%, as compared to neat PS foams with a similar density of 0.6 g cm<sup>-3</sup>. The tensile modulus of PS foams with 5 wt% of CNF increased by 45% to a

value of 1.07 GPa, which is close to that of bulk PS (1.26 GPa). The compression modulus of both the CNF foams was even higher than the compression modulus of bulk PS.

Another advantage of the nanoparticles is that they act as very effective heterogeneous nucleation sites. The lowered energy barrier for nucleation in combination with a high nucleant density can result in a high nucleation rate and therefore a high cell density with a small cell size, which makes these nanocomposite materials especially suited for the production of microcellular foams.<sup>75</sup> Furthermore, the obtained cell size distribution is much more homogeneous. Zhai *et al.*<sup>76</sup> have produced polycarbonate (PC) foams with nano-silica particle content ranging from 1 to 9 wt% and have found that the homogeneity of the foams increased with an increasing amount of nano-silica particles. PC foams with 1 wt% of nano-silica particles had a cell size ranging from 0.2–1.5 µm which means a dramatic increase in homogeneity, as compared to the cell size range of neat PC foams (from 0.7 µm up to 6 µm). The cell size distribution of the PC foams with 9 wt% nano-silica particles is even narrower: 0.1–0.8 µm.

A new trend in polymer composite foaming is the addition of so called molecular composites to the polymeric matrix. Contrary to the addition of nanoparticles, rigid-rod polymers are dispersed on the molecular level, so the polymeric matrix is directly reinforced with the rigid-rod chains. An example of such a rigid-rod polymer is polybenzimidazole (PBI). However, miscibility of PBI with other polymers can be an issue. Sulfonated and aminated polysulfone (PSF), polyphenylsulfone (PPSF) and carboxylated polysulfone (C-PSF) have been reported to form miscible blends with PBI. Furthermore, these composites have been successfully foamed with CO<sub>2</sub>.<sup>77–79</sup> The reason why it is interesting to foam composites with rigid-rod polymers is that there are no defects in a single molecular chain. Therefore, these molecular ‘fibers’ can possibly act as reinforcements of the struts and walls of polymeric foams, which could greatly improve the compression modulus and strength of the foam. Furthermore, most rigid-rod polymers also have very good thermostability. The combination of mechanical strength and improved thermal properties would make these type of nanocomposite foams suitable for a full range of high-tech applications in, for example, military and commercial aircraft.

## 6. Bioscaffolds

Porous biodegradable polymer matrices have received increasing attention because of their potential application within the field of tissue engineering and guided tissue regeneration. These materials can act as a temporary support for *in vitro* cell growth and can encourage cellular growth *in vivo*. As the cells grow, the support of the matrix is no longer needed and over time, the polymer matrix degrades into chemically benign components, which are not harmful to the surrounding cells. One of the most commonly used biopolymers is poly(lactic-co-glycolic) acid (PLGA), because it biodegrades into lactic and glycolic acid, which are relatively harmless to the growing cells. Furthermore, its use in other *in vivo* applications, such as resorbable sutures, has been approved by the Food and Drug Administration.<sup>80</sup> Also, the degradation rate of PLGA can be controlled by varying the ratio of its co-monomers, lactic acid and glycolic

acid. Several techniques have been reported to produce porous PLGA, such as casting and leaching, fiber waving and phase separation.<sup>81–84</sup> Although scaffolds with high porosity and large cells have been produced, the main drawback of these methods that they use organic solvents in the fabrication process, which can remain in the polymer after processing. These substances may be harmful to the cells and can inactivate many biologically active compounds (*e.g.* growth factors).

To overcome this problem, CO<sub>2</sub> has been used in order to produce porous bioscaffolds. Singh *et al.*<sup>85</sup> have studied the generation of 85/15 PLGA foams for biomedical applications at temperatures up to 40 °C and CO<sub>2</sub>-pressures ranging from 100 to 200 bar. The obtained porosity was 89% with a pore size ranging from 30 to 100 μm. Mooney *et al.*<sup>86</sup> obtained higher porosities of approx. 97% for 50/50 PLGA foamed at ambient temperatures and 55 bar. These results are confirmed by Sheridan *et al.*<sup>87</sup> who have found similar results at similar saturation temperatures and pressures. A patent by De Ponti *et al.*<sup>88</sup> also describes the foaming of PLGA using scCO<sub>2</sub>. In general, it appears that milder process conditions are favorable for a high porosity.

Due to the fact that scaffolds have very large pores, mercury intrusion porosimetry (MIP) is generally regarded as an unsuitable method for scaffold characterization. SEM and micro-CT images yield results for the pore size and pore size distribution. Fig. 9 shows an example of a micro-CT image of a poly(ethyl methacrylate)/tetrahydrofurfuryl methacrylate (PEMA/THFMA) scaffold produced with CO<sub>2</sub>.<sup>89</sup> MIP, however, can be used to measure the pore apertures and permeability of scaffolds.

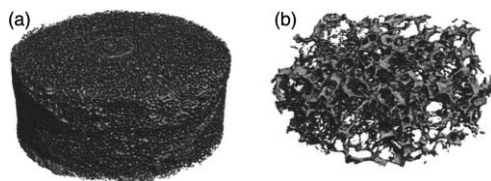


**Fig. 9** Micro-CT image of scaffolds processed at (a) rapid depressurization; and (b) very slow depressurization. This figure is taken from Barry *et al.*<sup>89</sup> and has been reproduced with kind permission of Springer Science and Business Media.

Teng *et al.*<sup>90</sup> have combined the CO<sub>2</sub>-foaming process with salt leaching in order to increase the porosity and interconnectivity of poly(D,L)lactic acid (PDLA)/hydroxyapatite (HA) scaffolds. PDLA/HA composite and NaCl have been mixed in a heated mold after which the mixture is foamed with CO<sub>2</sub> and the salt is washed out.

Next to the previously described polymers, PEMA/THFMA,<sup>91,92</sup> poly(isoprene-co-styrene)/THFMA<sup>91</sup> and polycaprolactone (PCL)<sup>62</sup> also have also been successfully foamed using CO<sub>2</sub> and have a high potential to be used as bioscaffolds.

## 7. Polymer blends

So far, the foaming of only one type of polymer, with or without a non-polymeric additive has been discussed. In these cases, CO<sub>2</sub> dissolves only in the polymeric phase and the additive acts as sites for heterogeneous nucleation. It is also possible to mix two types of polymers and use CO<sub>2</sub> to foam the blends. The

difference in solubility and diffusivity of CO<sub>2</sub> in both polymer phases provides an additional means to influence the foam morphology. Of course, the ratio of the blend and the degree of mixing will have an effect on the morphology of the foam as well. Han *et al.*<sup>70</sup> have demonstrated the latter. Well-mixed and poorly mixed PS/9 wt% PMMA blends were foamed with CO<sub>2</sub>. The well-mixed blends were rather homogeneous, whereas the poorly mixed blends clearly showed a dominant small cell phase and larger cells spread as stripes through the foamed sample. Interestingly enough, the smaller cells are formed in the PS phase and the larger cells in the PMMA phase. These results are opposite of what would be expected based upon the results of foaming experiments of both pure polymers, where foamed PMMA in general forms smaller cells as compared to foamed PS at similar conditions. These opposite results have been attributed to the diffusion of CO<sub>2</sub> from the PMMA phase to the PS phase. As a result, the CO<sub>2</sub> concentration in the PMMA phase decreases, which leads to a lower degree of oversaturation in this phase, resulting in fewer nuclei and larger cells.

Related to the situation of poorly mixed blends is the case of blending non-miscible polymers. Foaming of these “blends” can result in remarkable foam morphologies. Taki *et al.*<sup>93</sup> have produced foams with a bimodal cell size distribution of the “blends” of polyethylene glycol (PEG) and PS, where the PEG particles are dispersed in a PS matrix. Due to a higher diffusivity and solubility of CO<sub>2</sub> in the PEG-phase, nucleation and cell growth are faster in this phase. Furthermore, cell coalescence occurs more easily in the PEG-phase, resulting in a bimodal cell size distribution in the produced foams, with cells ranging from 40 μm to 500 μm dispersed in cells of less than 20 μm (see Fig. 10). The mechanism of this type of cell formation is schematically depicted in Fig. 11. Similarly to the results described by Han *et al.*,<sup>70</sup> the cell size in the PS phase is also smaller than the cell size in neat PS, foamed at similar conditions. In this case, however, the smaller cell size is attributed to the faster growing PEG cells, which cause a depletion of CO<sub>2</sub> in the PS-phase. Due to this decrease in CO<sub>2</sub> concentration in the PS phase, the plasticization effect of CO<sub>2</sub> becomes less. Therefore, the PS-matrix vitrifies which results in a suppression of cell growth and, hence, a smaller cell size.

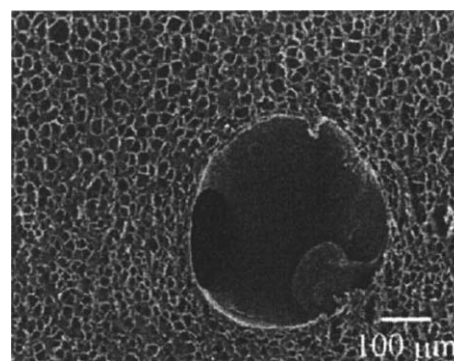


**Fig. 10** Cellular structure of a PEG/PS blend foam, prepared at 110 °C and 100 bar. This figure is taken from Taki *et al.*<sup>93</sup> and has been reproduced with kind permission of John Wiley & Sons, Inc.

Because of the immiscibility of PS and PEG, the resulting foam morphology is largely dependent on the initial dispersion



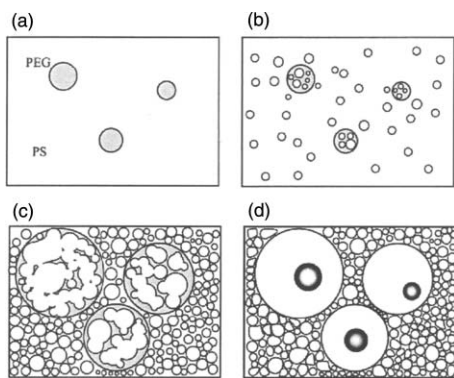


**Fig. 11** Schematic diagram of the formation of the bimodal cellular structure observed in Fig. 10: (a) initial state, (b) bubble nucleation and growth, (c) bubble coalescence and (d) particle formation. This figure is taken from Taki *et al.*<sup>93</sup> and has been reproduced with kind permission of John Wiley & Sons, Inc.

of PEG in the PS-matrix. This provides an extra means of controlling the resulting foam morphology. For example, a better and more homogeneous dispersion of smaller PEG particles will lead to a homogeneous bimodal cell structure, which can result in an open cellular structure, due to the fact that the cell walls between separate PEG cells will rupture once these cells come into contact. Furthermore, dispersing PEG as “fibers” in the polymer matrix can result in the formation of open channels, which provide a whole new range of applications for these materials.

## 8. Conclusion and outlook

As demonstrated in this review, the foaming of polymers using  $\text{scCO}_2$  has been a topic of interest for many years and most probably will be for many years to come. In the early years, patents and research focused mainly on how to produce the foam itself. Later on, research shifted towards understanding and controlling the foaming process followed by an interest into the foaming of biocompatible or biodegradable polymers for the use as bioscaffolds. Recently, more papers on the production of microcellular nanocomposite foams have been published because of the high potential of these composite foams as high-tech, light weight and strong construction materials.

Empirically, the foaming process can be described quite well. The influence of different parameters, such as pressure, temperature and depressurization rate, are well known for many polymers. However, the theory behind polymer foaming is rather complex. Despite many efforts to modify classical nucleation and crystallization theories to include polymer–gas properties and interactions, these theories still fail to give an accurate description of nucleation experiments. Moreover, nucleation and cell growth are modeled separately in many studies, even though in the polymer foaming process both nucleation and growth are fully integrated and can occur simultaneously. Research on this topic will need to continue for many years to come to deliver accurate and predictive models that describe nucleation and cell growth. Such a model will provide the tools to really predict and control the polymer foaming process. This will help in evaluating polymers for their foamability without having to test all foaming

parameters experimentally, making the choice of a polymer for a specific application much easier.

So far, the only way to scale-up the  $\text{CO}_2$ -based foaming process is by means of extrusion. Some companies are already using an extruder based foaming process, where  $\text{CO}_2$  is used as a blowing agent (*e.g.* Styrodur<sup>®</sup>, extruded polystyrene (XPS) produced by BASF). One of the drawbacks of the extrusion process is that is not (yet) possible to produce large blocks of foamed material. Furthermore, the minimum foam density that can be obtained by extrusion is much higher ( $> 30 \text{ kg m}^{-3}$ ) as compared to the minimum densities that can be obtained using the TIPS process ( $\sim 10 \text{ kg m}^{-3}$ ). This makes the extruded foams too expensive for packaging purposes. Once very low density foams can also be produced using the  $\text{CO}_2$ -based foaming process, it has the potential to completely replace the TIPS process, thus making the world-wide foam production more environmentally friendly.

## References

- 1 L. H. Baekeland, *GB Pat.*, 190821566, 1909.
- 2 P. Schaaf, B. Lotz and J. C. Wittmann, *Polymer*, 1978, **28**, 193.
- 3 H. Ogawa, A. Ito, K. Taki and M. Ohshima, *J. Appl. Polym. Sci.*, 2007, **106**, 2825.
- 4 W. H. Hou and T. B. Lloyd, *J. Appl. Polym. Sci.*, 1992, **45**, 1783.
- 5 *Handbook of Polymer Foams*, Rapra Technology Limited, 2004.
- 6 *The Polyurethanes Book*, Wiley, New York, 2003.
- 7 L. Draghi, S. Resta, M. G. Pirozzolo and M. C. Tanzi, *J. Mater. Sci.: Mater. Med.*, 2005, **16**, 1093.
- 8 Q. Zhou, Y. Gong and C. Gao, *J. Appl. Polym. Sci.*, 2005, **98**, 1373.
- 9 Z. Ma, C. Gao, Y. Gong and J. Shen, *J. Biomed. Mater. Res. Part B: Appl. Biomater.*, 2003, **67B**, 610.
- 10 The European Manufacturers of Expanded Polystyrene, 2008, <http://www.eumaps.org>.
- 11 Foster Grant Co. Inc., *GB Pat.*, 912888, 1962.
- 12 Union Carbide Corporation, *GB Pat.*, 1517219, 1975.
- 13 R. H. Hansen, Western Electric Company, Inc., *GB Pat.*, 1060412, 1967.
- 14 S. Baxter Samuel and G. J. Harold, Monsanto Chemicals Limited, *GB Pat.*, 1034120, 1966.
- 15 S. K. Goel and E. J. Beckman, *Cell. Polym.*, 1993, **12**, 251.
- 16 Sumarno, T. Sunada, Y. Sato, S. Takishima and H. Masuoka, *Polym. Eng. Sci.*, 2000, **40**, 1510.
- 17 J. W. S. Lee and C. B. Park, *Macromol. Mater. Eng.*, 2006, **291**, 1233.
- 18 S. G. Kazarian, *Polym. Sci., Ser. C.*, 2000, **42**, 78–101.
- 19 M. P. Stevens, *Polymer Chemistry*, Oxford University Press, New York, 1990, pp80–85.
- 20 S. T. Lee, in *Polymeric foams: mechanisms and materials*, ed. S. T. Lee and N. S. Ramesh, CRC Press, New York, 2004, ch. 1, pp. 1.
- 21 R. Cole, in *Advances in Heat Transfer*, ed. J. P. Hartnett and T. F. Irvine, Jr., Academic Press, London, 1974, vol. 10, pp. 85–166.
- 22 A. W. Hodgson, *Adv. Colloid Interface Sci.*, 1984, **21**, 303.
- 23 J. G. Lee and R. W. Flumerfelt, *J. Colloid Interface Sci.*, 1996, **184**, 335.
- 24 J. S. Colton and N. P. Suh, *Polym. Eng. Sci.*, 1987, **27**, 485.
- 25 J. H. Han and C. D. Han, *J. Polym. Sci., Part B: Polym. Phys.*, 1990, **28**, 743.
- 26 J. S. Colton and N. P. Suh, *Polym. Eng. Sci.*, 1987, **27**, 493.
- 27 A. Arefmanesh and S. G. Advani, *Rheol. Acta*, 1991, **30**, 274.
- 28 D. C. Venerus and N. Yala, *AICHE J.*, 1997, **43**, 2948.
- 29 D. C. Venerus, N. Yala and B. Bernstein, *J. Non-Newtonian Fluid Mech.*, 1998, **75**, 55.
- 30 S. K. Goel and E. J. Beckman, *AICHE J.*, 1995, **41**, 357–367.
- 31 S. N. Leung, C. B. Park, D. Xu, H. Li and R. G. Fenton, *Ind. Eng. Chem. Res.*, 2006, **45**, 7823.
- 32 K. Joshi, J. G. Lee, M. A. Shafi and R. W. Flumerfelt, *Polym. Eng. Sci.*, 1998, **67**, 1353–1368.
- 33 J. J. Feng and C. A. Bertelo, *J. Rheol.*, 2004, **48**, 439.
- 34 B. Klane and G. Schaefer, *EU Pat.*, 0486957, 1992.

- 35 M. Walter, O. Pfannschmidt and T. Schröder, *DE Pat.*, 19853021, 2000.
- 36 C. Borer, U. G. Naef, B. A. Culbert and F. Innerebner, *DE Pat.*, 98-19800166, 1998.
- 37 R. Eiben, W. Ebeling, H. M. Sulzbach and R. Reiner, *US Pat.*, 5883143, 1999.
- 38 X. Han, K. W. Koelling, D. L. Tomasko and L. J. Lee, *Polym. Eng. Sci.*, 2002, **42**, 2094.
- 39 S. Siripurapu, Y. J. Gaya, J. R. Royera, J. M. DeSimonea, R. J. Spontaka and S. A. Khan, *Polymer*, 2002, **43**, 5511.
- 40 M. Lee, C. Tzoganakis and C. B. Park, *Polym. Eng. Sci.*, 1998, **38**, 1112.
- 41 E. Di Maio, G. Mensitieri, S. Iannace, L. Nicolais, W. Li and R. W. Flumerfelt, *Polym. Eng. Sci.*, 2005, **45**, 432.
- 42 J. Reigner, R. Gendron and M. F. Champagne, *Cell. Polym.*, 2007, **26**, 83.
- 43 C. B. Park, A. H. Behraves and R. D. Venter, *Polym. Eng. Sci.*, 1998, **38**, 1812.
- 44 J. Shen, X. Han and L. J. Lee, *J. Cell. Plast.*, 2006, **42**, 105.
- 45 X. Han, C. Zeng, L. J. Lee, K. W. Koelling and D. L. Tomasko, *Polym. Eng. Sci.*, 2003, **43**, 1261.
- 46 C. B. Park, D. F. Baldwin and N. P. Suh, *Polym. Eng. Sci.*, 1995, **35**, 432–440.
- 47 S. Alavi and S. S. H. Rizvi, *Int. J. Food Prop.*, 2005, **8**, 23.
- 48 J. W. S. Lee, K. Wang and C. B. Park, *Ind. Eng. Chem. Res.*, 2005, **44**, 92.
- 49 D. F. Baldwin, C. B. Park and N. P. Suh, *Polym. Eng. Sci.*, 1998, **38**, 674.
- 50 C. Stephen, S. N. Bhattacharya, A. A. Khan and C. Stephen, *Polym. Eng. Sci.*, 2006, **46**, 751.
- 51 N. P. Suh, *Macromol. Symp.*, 2003, **201**, 187.
- 52 H. Sun, in *Innovation in polymer processing: moulding*, ed. J. F. Stevenson, Hanser Gardner Publications, New York, 1996, ch. 3, pp. 93.
- 53 B. Krause, R. Mettinkhof, N. F. A. van der Vegt and M. Wessling, *Macromolecules*, 2001, **34**, 874.
- 54 V. Kumar and N. P. Suh, *Polym. Eng. Sci.*, 1990, **30**, 1323.
- 55 V. Kumar and J. E. Weller, *Int. Polym. Process.*, 1993, **8**, 73.
- 56 M. Wessling, Z. Borneman, T. Van Den Boomgaard and C. A. Smolders, *J. Appl. Polym. Sci.*, 1994, **53**, 1497.
- 57 S. K. Goel and E. J. Beckman, *Polym. Eng. Sci.*, 1994, **34**, 1137–1147.
- 58 S. K. Goel and E. J. Beckman, *Polym. Eng. Sci.*, 1994, **34**, 1148–1156.
- 59 K. A. Arora, A. J. Lesser and T. J. McCarthy, *Macromolecules*, 1998, **31**, 4614.
- 60 M. T. Liang and C. M. Wang, *Ind. Eng. Chem. Res.*, 2000, **39**, 4622.
- 61 J. Wang, X. Cheng, X. Zheng and M. Yuan, *J. He, J. Polym. Sci. Part B: Polym. Phys.*, 2003, **41**, 368.
- 62 Q. Xu, X. Ren, Y. Chang, J. Wang, L. Yu and K. Dean, *J. Appl. Polym. Sci.*, 2004, **94**, 593.
- 63 M. A. Jacobs, M. F. Kemmere and J. T. F. Keurentjes, *Polymer*, 2004, **45**, 7539.
- 64 E. Reverchon and S. Cardea, *J. Supercrit. Fluids*, 2007, **40**, 144.
- 65 P. A. M. Lips, I. W. Velthoen, P. J. Dijkstra, M. Wessling and J. Feijen, *Polymer*, 2005, **46**, 9396.
- 66 L. J. M. Jacobs, K. C. H. Danen, M. F. Kemmere and J. T. F. Keurentjes, *Polymer*, 2007, **48**, 3771.
- 67 C. M. Stafford, T. P. Russell and T. J. McCarthy, *Macromolecules*, 1999, **32**, 7610.
- 68 S. Siripurapu, J. M. DeSimone, S. A. Khan and R. J. Spontak, *Adv. Mater.*, 2004, **16**, 989.
- 69 C. Zeng, X. Han, L. J. Lee, K. W. Koelling and D. L. Tomasko, *Adv. Mater.*, 2003, **15**, 1743.
- 70 X. Han, J. Shen, H. Huang, D. L. Tomasko and L. J. Lee, *Polym. Eng. Sci.*, 2007, **47**, 103.
- 71 Y. Di, S. Iannace, E. Di Maio and L. Nicolais, *J. Polym. Sci., Part B: Polym. Phys.*, 2005, **43**, 689.
- 72 Y. Ema, M. Ikeya and M. Okamoto, *Polymer*, 2006, **47**, 5350.
- 73 Y. Fujimoto, S. S. Ray, M. Okamoto, A. Ogami, K. Yamada and K. Ueda, *Macromol. Rapid Commun.*, 2003, **24**, 457.
- 74 L. J. Lee, C. Zeng, X. Cao, X. Han, J. Shen and G. Xu, *Compos. Sci. Technol.*, 2005, **65**, 2344.
- 75 X. Han, L. J. Lee and D. L. Tomasko, *Aust. J. Chem.*, 2005, **58**, 492.
- 76 W. Zhai, J. Yu, L. Wu, W. Ma and J. He, *Polymer*, 2006, **47**, 7580.
- 77 H. Sun, J. E. Mark, S. C. Tan, N. Venkatasubramanian, M. D. Houtz, S. T. Tan, F. E. Arnold and C. Y.-C. Lee, *J. Macromol. Sci., Pure Appl. Chem.*, 2004, **41**, 981.
- 78 H. Sun, J. E. Mark, S. C. Tan, N. Venkatasubramanian, M. D. Houtz, F. E. Arnold, Ch. and Y.-C. Lee, *Polymer*, 2005, **46**, 6623.
- 79 C. S. Wang, I. J. Goldfarb and T. E. Helminiak, *Polymer*, 1988, **29**, 825.
- 80 H. Tai, V. K. Popov, K. M. Shakesheff and S. M. Howdle, *Biochem. Soc. Trans.*, 2007, **35**, 516.
- 81 A. G. Mikos, G. Sarakinos, S. M. Leite, J. P. Vacanti and R. Langer, *Biomaterials*, 1993, **14**, 323–30.
- 82 H. Lo, M. S. Ponticello and K. W. Leong, *Tissue Eng.*, 1995, **1**, 15–28.
- 83 S. Nunes, *Trends Polym. Sci.*, 1997, **5**, 187–92.
- 84 R. Bansil and G. Liao, *Trends Polym. Sci.*, 1997, **5**, 146–54.
- 85 L. Singh, V. Kumar and B. D. Ratner, *Biomaterials*, 2004, **25**, 2611.
- 86 D. J. Mooney, D. F. Baldwin, N. P. Suh, J. P. Vacanti and R. Langer, *Biomaterials*, 1996, **17**, 1417.
- 87 M. H. Sheridan, L. D. Shea, M. C. Peters and D. J. Mooney, *J. Controlled Release*, 2000, **64**, 91.
- 88 R. De Ponti, R. Torricelli, A. Martini and E. Lardini, *WO Pat.*, 9109073.
- 89 J. J. A. Barry, M. M. C. G. Silva, S. H. Cartmell, R. E. Gulberg, C. A. Scotchford and S. M. Howdle, *J. Mater. Sci.: Mater. Med.*, 2006, **41**, 4197.
- 90 X. Teng, J. Ren and S. Gu, *J. Biomed. Mater. Res. Part B: Appl. Biomed.*, 2007, **81B**, 185.
- 91 J. J. A. Barry, H. S. Gidda, C. A. Scotchford and S. M. Howdle, *Biomaterials*, 2004, **25**, 3559.
- 92 J. J. A. Barry, M. M. C. G. Silva, V. K. Popov, K. M. Shakesheff and S. M. Howdle, *Philos. Trans. R. Soc. London, Ser. A*, 2006, **364**, 249.
- 93 K. Taki, K. Nitta, S. I. Kihara and M. Ohshima, *J. Appl. Polym. Sci.*, 2005, **97**, 1899.

# Enhanced debromination of brominated flame retardant plastics under microwave irradiation

Thallada Bhaskar,<sup>\*a</sup> Asako Hosokawa,<sup>b</sup> Akinori Muto,<sup>b</sup> Yasunori Tsukahara,<sup>c</sup> Tomohisa Yamauchi<sup>c</sup> and Yuji Wada<sup>\*d</sup>

Received 30th April 2008, Accepted 28th May 2008

First published as an Advance Article on the web 10th June 2008

DOI: 10.1039/b807370h

Microwave irradiation of high impact polystyrene (HIPS-Br) containing brominated flame retardant *i.e.*, decabromodiphenyl ether (DDO) or decabromodiphenyl ethane (DDE) was performed using aqueous and organic solvents for the removal of bromine. The microwave irradiation of HIPS-Br with triethylene glycol (TEG; 20 ml) at 250 °C for 30 min was found to be suitable condition for the removal of bromine (85 wt%) from the plastic, enabling recovery of the bromine free plastics.

## Introduction

Plastics are among the best 'fruits' of the chemical industry and are used extensively in our daily life. As these materials are not biodegradable, the development of viable recycling technologies for plastic waste materials is becoming increasingly important. Municipal and industrial plastic wastes are predominantly treated in three ways: landfill, incineration (energy recovery by incineration) and material recycling. Each of these methods has disadvantages. Landfill treatment is undesirable due to poor bio-degradability of plastics and other environmental problems; and incineration is unacceptable due to the possibility of toxic emissions<sup>1</sup> and loss of the energy accumulated in plastic during the preparation and the valuable organic materials. True material recycling (the conversion of scrap polymer into new products) is a preferable method of treatment but the recycled plastic products often cost more than virgin plastic<sup>2</sup> and the secondary plastics have less market value.

Plastics from waste from electrical and electronic equipment (WEEE), such as high impact polystyrene (HIPS-Br) and acrylonitrile-butadiene-styrene (ABS), used for more than half of the plastic housing in domestic electrical and electronic appliances plastic,<sup>3</sup> generally contain flame-retardants as an additive to avoid inflammation. Pyrolysis or feedstock recycling appears to be gaining increased attention, as the chemical

value of the polymer is completely lost through incineration. However, treatment of WEEE is considered to present substantially more environmental problems than is the case with municipal waste plastics, because WEEE can contain polybrominated biphenyls, polybrominated diphenyloxides or tetrabromobisphenol-A, which can be converted into dioxine or furane by the treatment. Thus, it poses a great challenge<sup>4,5</sup> for effective recycling methods which are environmentally and economically sustainable.

There has been a plethora of research works on the decomposition and recycling of flame retardant plastics by several processes.<sup>6-12</sup> In recent years, Bhaskar *et al.* have reported the development of catalyst/sorbent for the removal of bromine in the pyrolysis of the brominated flame retardant mixed plastics. However, during this process the bromine was found to be still present in liquid, solid and gaseous products. Li *et al.*<sup>13</sup> reported the debromination of decabrominated diphenyl ether by resin bound iron nanoparticles and showed that the debromination was step-wise, less brominated congeners were produced with increasing reaction time up to 10 days. Extensive investigations on hydrodehalogenation of different halogenated compounds over Ni-catalysts<sup>14,15</sup> and Pd<sup>16</sup> supported catalysts have been carried out.

Microwave induced pyrolysis processes are relatively new and were initially developed by Tech-En Ltd., Hainault, UK.<sup>17</sup> The process involves mixing of plastic-containing wastes, which are known to have very high transparencies to microwaves, with a highly microwave-absorbing material, such as particulate carbon.<sup>18</sup> Yoshiyama *et al.*<sup>19</sup> reported the microwave induced dechlorination of poly(vinyl chloride). In the present investigation, we report for the first time the microwave induced debromination of high impact polystyrene containing two different types of flame retardants, decabromodiphenyl ether (DDO) and decabromodiphenyl ethane (DDE), immersed in aqueous and organic solvents. The plastic samples also contained antimony trioxide, which is generally added as a synergist.

## Results and discussion

The microwave induced debromination of high impact polystyrene containing brominated flame retardant was performed in the presence of aqueous, *i.e.* H<sub>2</sub>O and KOH, and organic solvents, such as ethylene glycol (EG), triethylene glycol (TEG). The detailed information of the contents in the plastics samples is presented in Table 1. Microwave irradiation with aqueous solvents at 100 °C showed debromination of less than

<sup>a</sup>Catalytic Conversion Process Division (CCPD), Indian Institute of Petroleum (IIP), Dehradun, 248005, India. E-mail: tbhaskar@iip.res.in; Fax: +91-135-266-0202; Tel: +91-135-266-0145

<sup>b</sup>Department of Applied Chemistry, Graduate School of Natural Science and Technology, Okayama University, Okayama, 700-8530, Japan

<sup>c</sup>Department of Material and Life Science, Graduate School of Engineering, Osaka University, 2-1 Yamada-oka, Suita, Osaka, 565-0871, Japan

<sup>d</sup>Department of Applied Chemistry, Graduate School of Science and Engineering, Tokyo Institute of Technology, 2-12-1 O-okayama, Meguro, Tokyo, 152-8552, Japan. E-mail: yuji-w@apc.titech.ac.jp

**Table 1** Compositional analysis of HIPS-Br samples

Sample code	Breakdown of sample (wt%)		
HIPS-DDO-Sb(5)	HIPS	82	Br: 10.8
	DDO	13	
	Sb <sub>2</sub> O <sub>3</sub>	5	
HIPS-DDO-Sb(0)	HIPS	87	Br: 10.8
	DDO	13	
	Sb <sub>2</sub> O <sub>3</sub>	0	
HIPS-DDE-Sb(5)	HIPS	82	Br: 10.7
	DDE	13	
	Sb <sub>2</sub> O <sub>3</sub>	5	
HIPS-DDE-Sb(0)	HIPS	87	Br: 10.7
	DDE	13	
	Sb <sub>2</sub> O <sub>3</sub>	0	

1 wt% from the plastic samples used in the present study. Microwave irradiation with EG (b.p. 197.6 °C) and TEG (b.p. 285 °C) was performed at different conditions, such as reaction temperature, irradiation time and volume of solvent, in order to find the optimized conditions for debromination. Microwave irradiation of the plastic samples with EG at room temp., 100, 150 and 197 °C for 10 min did not show significant debromination. Similarly, microwave irradiation of the plastic samples with TEG at room temp., 150 °C for 10 min showed no debromination. However, microwave irradiation at 250 °C for 10 min induced the successful debromination (Table 2).

In order to see the effect of microwave irradiation, the comparison with the conventional fixed bed pyrolysis with electrical heating was performed at 250 °C for 10 min in the presence of TEG. The rate of heating for the microwave irradiation and conventional pyrolysis was kept same (*ca.* 25 °C min<sup>-1</sup>). The results of the effects of microwave irradiation and conventional pyrolysis on the debromination are tabulated in Table 2. The debromination exceeded 60 wt% under microwave irradiation independent of which sample was used, while it stayed between 39–50 wt% for conventional pyrolysis (Table 2). This clear enhancement in the debromination content should be attributed to the effect of microwave irradiation.

The conditions of the debromination under microwave irradiation studied in this investigation were provided in Table 3. Temperature, irradiation time and the amount of TEG were varied in the debromination experiments under microwave irradiation. The high amount TEG (40 ml) at lower reaction times (10 min) indicated that the debromination was around 62–66 wt% in all the four samples studied. Under identical reaction conditions,

**Table 2** Effect of microwave irradiation and conventional pyrolysis for the debromination of brominated high impact polystyrenes. Solvent: TEG; 20 ml, temp: 250 °C, time: 10 min

Sample	Debromination	
	Conventional pyrolysis (wt%)	Microwave irradiation (wt%)
HIPS-DDO-Sb(5)	39	62
HIPS-DDO-Sb(0)	35	62
HIPS-DDE-Sb(5)	18	66
HIPS-DDE-Sb(0)	50	64

**Table 3** Effect of microwave irradiation time and amount TEG solvent on debromination of HIPS-DDO-Sb(5)

Sample no.	Temp/°C	Irradiation time/min	TEG/ml	Debromination (wt%)
1	250	10	20	62
2	250	30	20	85
3	250	60	20	83
4	285	10	20	78
5	285	30	20	84
6	250	10	40	62

there is no significant increase in debromination with the increase of reaction temperature from 250 °C to 285 °C (Table 3). The maximum debromination achieved was 85 wt% at 250 °C, 30 min reaction time, 20 mL TEG for HIPS-DDO-Sb(5) and HIPS-DDO-Sb(0), and the debromination was 80 wt% for HIPS-DDE-Sb(5) and HIPS-DDE-Sb(0) under identical conditions.

There are various types of flame retardant extraction methods reported in the literature. Wang *et al.*,<sup>6</sup> reported the extraction of flame retardants (triphenyl phosphate) in electronic printed circuit boards by supercritical carbon dioxide. Up to 90% of extraction efficiency was obtained at an extraction temperature of 343 K and a pressure of 25 MPa. Gamse and Marr<sup>7</sup> measured the extraction behaviour of HBCD and TBBA from polybutyleneterephthalate with supercritical carbon dioxide. The extraction yields achieved were up to 100% at 50 MPa and 373 K. Gardette *et al.*<sup>20</sup> studied flame retarded PP, and reported that from the IR spectrum modifications, the fire retardant is decomposed throughout by UV irradiation, which can be attributed to photolytic reactions including the formation of free radicals. In particular, the formation of bromine radicals is expected. It involves in a first step a homolytic cleavage of the C–Br bond, leading to the formation of reactive bromine radicals that can induce a hydrogen abstraction on the polymeric backbone. Antos and Sedlar<sup>21</sup> reported that the photochemical (300–400 nm) decomposition of decabromodiphenyl ether induced by light is a radical process leading to the formation of HBr provided there is a hydrogen donor (RH) in the system. The stepwise debromination of the aromatic ring takes place, giving rise to lower brominated diphenyl ethers with a number of by-products. However, in the present investigation we could not find any such products in the liquid (solvent).

Jakab *et al.*,<sup>8</sup> reported that the presence of Sb<sub>2</sub>O<sub>3</sub> reduces the thermal stability (*ca.* 50 °C) of the samples, indicating that Sb<sub>2</sub>O<sub>3</sub> initiated the decomposition of the flame retardants and PS. It was established that the brominated additives themselves do not change the decomposition temperature of polystyrene (PS). Nevertheless, the majority of PS decomposes at a higher temperature. The two brominated flame retardants decompose by different pathways. The scission of C–C bonds, resulting in the formation of bromotoluenes, is the most important reaction of DDO additives. In contrast, DDE decomposes by an intermolecular ring closure pathway producing brominated dibenzofurans (DBF).

Hydrothermal treatment of HIPS-Br plastics showed that the presence of poly(propylene) promoted the debromination due to the availability of tertiary hydrogen from poly(propylene).<sup>22</sup> In the present investigation, the glycol acted as a source of



hydrogen for the facilitation of debromination reaction. The reaction conditions in the microwave irradiation are not severe and there is no possibility of formation of dioxins under the reaction conditions. The physical form of the plastic samples was intact after the microwave irradiation. Gas chromatography equipped with an atomic emission detector (GC-AED) was used for the analysis of bromine compounds present in the solvent after the microwave irradiation (Fig. 1). It is clear from Fig. 1 that there is a single (major) bromine compound and very small concentration of various other brominated compounds observed from both DDE-Sb(5) and DDO-Sb(5) containing samples. These results support the quantitative analysis of bromine content remaining in the plastic samples after the microwave irradiation. Due to the analytical limitations, we could not perform quantitative analysis of bromine compounds observed from the GC-AED analysis. The above results show that the microwave irradiation of brominated flame-retardant containing polystyrene samples did not produce the wide range of brominated hydrocarbons. In the case of conventional pyrolysis of HIPS-Br samples,<sup>23</sup> the wide range of brominated hydrocarbons and congeners of polybrominated diphenyl ether were observed in liquid products and the bromine is also found in residue and gaseous products in the form of HBr.

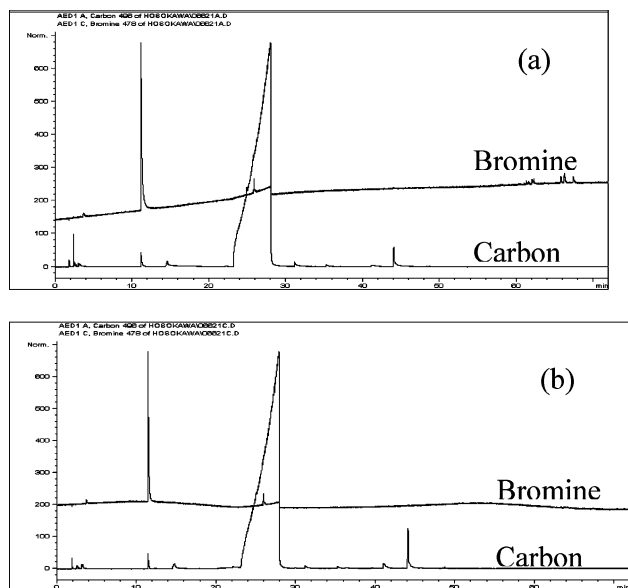


**Fig. 1** GC-AED analysis of TEG solvent after reaction at 250 °C for 10 min, TEG 20 ml: (a) HIPS-DDO-Sb(5), (b) HIPS-DDE-Sb(5).

## Experimental

### Materials

Commercially available high impact polystyrene (Br-HIPS) was used in the present investigation. High impact polystyrene (HIPS) containing decabromodiphenyl ether (DDO) flame retardant with  $\text{Sb}_2\text{O}_3$  (5 wt%) is abbreviated as HIPS-DDO-Sb(5) and without  $\text{Sb}_2\text{O}_3$  as HIPS-DDO-Sb(0). In a similar way, high impact polystyrene (HIPS) containing decabromodiphenyl ethane (DDE) flame retardant with  $\text{Sb}_2\text{O}_3$  (5 wt%) is abbreviated as HIPS-DDE-Sb(5) and DDE without  $\text{Sb}_2\text{O}_3$  as HIPS-DDE-

Sb(0). All the above HIPS-Br sample contains approximately 1–2 wt% of (poly)butadiene.

### Experimental procedure

Microwave induced debromination was performed in a  $\mu$ -reactor (2.45 GHz, 40–770 W) from Shikoku-Keisoku Instruments, Japan. Samples (2 × 2 mm) can be heated at the adjusted temperatures under the automatically controlled output of microwaves. Ion exchanged water and potassium hydroxide (KOH; 1 M) solutions were used as aqueous solvents. Ethylene glycol (EG) and triethylene glycol (TEG) were used as organic solvents. EG and TEG were obtained from TCI, Japan and used as received.

Briefly, the required amount of aqueous and organic solvent and 1 g of plastics sample were placed in a 100 ml two-necked round-bottom flask. The water condenser and thermocouple (from a thermocouple guide) were inserted into the flask. The polymer/solvent suspension was stirred during the microwave treatment. The experimental procedure for the pyrolysis of plastics samples can be found elsewhere.<sup>24</sup>

### Analysis procedure

The bromine content present in the plastic samples after the microwave-induced debromination was performed using a combustion flask followed by ion chromatographic analysis. In brief, a small portion (about 8–10 mg) of microwave treated plastic sample was combusted with  $\text{O}_2$  in a pyrex flask, containing a pair of electric wires, a Pt sample pan held by the panholder and a Pt filament for firing the sample. The combustion products were absorbed in about 40 ml water containing  $\text{H}_2\text{O}_2$  (0.3 ml) and subsequently analyzed by ion chromatography.

## Conclusions

An enhancement in the debromination of flame retardant containing plastics by microwave irradiation has been demonstrated. This new method should provide a new methodology for recycling of waste plastics from electrical and electronic equipment. Microwave irradiation is a simple but effective method to remove the major portion of bromine content from solid plastics before they are converted into basic petrochemicals or fuels.

## Acknowledgements

The authors would express their thanks to Professor Yusaku Sakata (Emeritus), Okayama University for his having led to collaboration among the authors in this work.

## References

- 1 F. Rodriguez, *Principles of Polymer Systems*, Hemisphere, Washington, DC, 3rd edn, 1989, p. 241.
- 2 M. Lee, *Chem. Brit.*, 1995, 7, 515.
- 3 L. Tange, *Technical workshop report on sustainable management for plastics with bromine in Tokyo*, 1999.
- 4 T. Ida, M. Nakanishi and K. Goto, *Polym. Sci., Polym. Chem. Ed.*, 1974, 12, 737.
- 5 W. Christmann, D. Kasioko, K. D. Kloppel, H. Partocht and W. Rotard, *Chemosphere.*, 1989, 19, 387.

- 6 H. Wang, M. Hirahara, M. Goto and T. Hirose, *J. Supercrit. Fluids*, 2004, **29**, 251.
- 7 T. Gamse and R. Marr, Removal of flame retardants from electronic waste by supercritical CO<sub>2</sub> extraction, *Proceedings of the Second International Meeting on High Pressure Chemical Engineering*, Hamburg, 2001.
- 8 E. Jakab, Md., A. Uddin, Y. Sakata and T. Bhaskar, *J. Anal. Appl. Pyrolysis*, 2003, **68–69**, 83.
- 9 W. J. Hall and P. T. Williams, *J. Anal. Appl. Pyrolysis*, 2006, **77**, 75.
- 10 M. Blazso and Z. Czegeny, *J. Chromatogr. A*, 2006, **1130**, 91.
- 11 M. Blazso, *J. Anal. Appl. Pyrolysis*, 2005, **74**, 344.
- 12 M. Blazso, Z. Czegeny and C. Csoma, *J. Anal. Appl. Pyrolysis*, 2002, **64**, 249.
- 13 A. Li, C. Tai, Z. Zhao, Y. Wang, Q. Zhang, G. Jiang and J. Hu, *Environ. Sci. Technol.*, 2007, **41**, 6841–6846.
- 14 K. V. Murthy, P. M. Patterson, G. Jacobs, B. H. Davis and M. A. Keane, *J. Catal.*, 2004, **223**, 74–85.
- 15 K. V. Murthy, P. M. Patterson and M. A. Keane, *J. Mol. Catal. A: Chem.*, 2005, **225**, 149–160.
- 16 M. A. Aramendia, V. Borau, I. M. Garcia, C. Jimenez, J. M. Marinas and F. J. Urbano, *Appl. Catal., B*, 1999, **20**, 101–110.
- 17 C. Lulow-Palafox and H. A. Chase, *Chem. Eng.*, 2001, **717**, 28–29.
- 18 C. Lulow-Palafox and H. A. Chase, *Ind. Eng. Chem. Res.*, 2001, **40**, 4749.
- 19 T. Yoshiyama and Y. Takeuchi, *Jpn. Pat.* H07-157776, 1995.
- 20 J. L. Gardette, C. Sinturer and J. Lemaire, *Polym. Degrad. Stab.*, 1999, **64**, 411–417.
- 21 K. Antos and J. Sedlar, *Polym. Degrad. Stab.*, 2005, **90**, 180–187.
- 22 Md. A. Uddin, T. Bhaskar, T. Kusaba, K. Hamano, A. Muto and Y. Sakata, *Green Chem.*, 2003, **5**, 260.
- 23 T. Bhaskar, W. J. Hall, N. M. M. Mitan, A. Muto, P. T. Williams and Y. Sakata, *Polym. Degrad. Stab.*, 2007, **92**, 211.
- 24 T. Bhaskar, K. Murai, M. Brebu, T. Matsui, Md. A. Uddin, A. Muto and Y. Sakata, *Green Chem.*, 2002, **4**, 603.

# Streamlined process for the esterification and ketalization of shikimic acid en route to the key precursor for oseltamivir phosphate (Tamiflu™)

Robert Carr,<sup>a</sup> Frank Ciccone,<sup>b</sup> Richard Gabel,<sup>b</sup> Martin Guinn,<sup>†b</sup> David Johnston,<sup>b</sup> Jill Mastriona,<sup>b</sup> Trevor Vandermeer<sup>‡b</sup> and Michael Groaning<sup>\*§b</sup>

Received 29th January 2008, Accepted 7th May 2008

First published as an Advance Article on the web 21st May 2008

DOI: 10.1039/b801582a

In an effort to streamline the current process for the key precursor en route to Tamiflu™ (oseltamivir phosphate), the ketalization reaction was re-evaluated for areas of improvement. Removal of thionyl chloride was a priority from a EH & S and operational perspective. Finally, the reduction of solvents and telescoping steps would improve throughput and minimize waste streams.

## Introduction

With an increasing demand for Tamiflu™ (oseltamivir phosphate) (**1** in Fig. 1),<sup>1</sup> analysis of its synthesis has received a large amount of attention from both academia and industry. Our efforts in this arena focused on the manufacturing process of a key precursor ((1*S*,5*R*,6*S*)-ethyl 5-(pentan-3-yloxy)-7-oxabicyclo[4.1.0]hept-3-ene-3-carboxylate) (**2** in Fig. 1). The initial goal was established by a comparative health risk analysis which was performed. This provided a quantitative method to identify key reagents and steps that needed to be addressed. Removal of thionyl chloride from the current process was the first priority. A relative risk indicator for solvents/liquid reagents at 25 °C was used to compare reagents (vapor hazard ratio: VHR).<sup>2</sup> It is calculated as the following ratio: saturation vapor concentration of a solvent or liquid reagent *versus* occupational exposure limit (OEL). The higher the VHR, the more likely the solvent/reagent will become airborne in the workplace and cause a potential health risk. The VHR describes how many times a vapor saturated air volume has to be diluted by the same volume so that the occupational exposure limit is not exceeded. This method provides a better indicator of risk that vapor pressure alone cannot. For example, a compound that has minimal vapor pressure with an extremely low OEL, could be significantly more hazardous than a compound that has moderate vapor pressure and a moderately low OEL.

Comparison of thionyl chloride to hydrochloric acid demonstrates the increased risks associated with its use. Hydrochloric

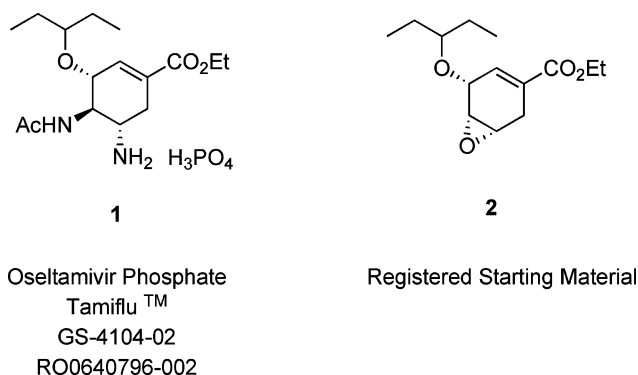


Fig. 1 Oseltamivir phosphate and registered starting material.

acid is moderately toxic with an LC<sub>50</sub> of 3124 ppm h<sup>-1</sup> and a VHR of 73 026. Thionyl chloride is toxic with an LC<sub>50</sub> of 500 ppm h<sup>-1</sup> and a VHR of 155 064. Additionally, thionyl chloride reacts quite violently with water with the evolution of the green house gases sulfur dioxide and hydrochloric acid. The evolution of these gases necessitates the use of a separate scrubber unit which renders this a more vessel intensive process with a superfluous waste stream.

Thionyl chloride was originally implemented as an *in situ* means to generate anhydrous hydrochloric acid which was necessary for >99% reaction completion. This same effect could be realized using other means to generate an anhydrous acidic environment. In an effort to streamline the whole process of this starting material, we revisited the direct ketalization route. Entry to the sequence of synthetic steps to this precursor could begin with shikimic acid or quinic acid. At the beginning of the technical development, both routes were necessary as the purity of shikimic acid was unpredictable. The direct ketalization route using 3-pentanone was abandoned early on as the intermediate purification *via* crystallization of a highly crystalline acetamide was necessary to achieve the requisite for overall purity.<sup>3</sup> The overall yield was reduced 20% if the current telescoping process was employed (Scheme 1).

Over the past 5–10 years there has been a consistent improvement in the shikimic acid quality available from fermentation.

Herein, we report an improved process for esterifying shikimic acid and subsequent formation of the pentylidene ketal with the ultimate goal of developing a streamlined environmentally friendly process.<sup>4</sup>

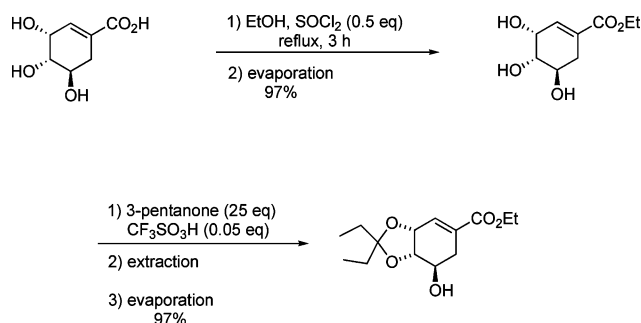
<sup>a</sup>Roche Carolina, 6173 East Old Marion Highway, Florence, SC, 29506, USA

<sup>b</sup>Roche Colorado Corporation, 2075 North 55th Street, Boulder, CO, 80301, USA. E-mail: MGroaning@endocyte.com

<sup>†</sup> Current address: Wyeth Research, 401 N. Middletown Rd., Pearl River, NY, 10965, USA.

<sup>‡</sup> Current address: New England Controls, 9 Oxford Road, Mansfield, MA, 02048, USA.

<sup>§</sup> Current address: Endocyte, Inc., 3000 Kent Avenue, Suite A1-100, West Lafayette, IN, 47906, USA.

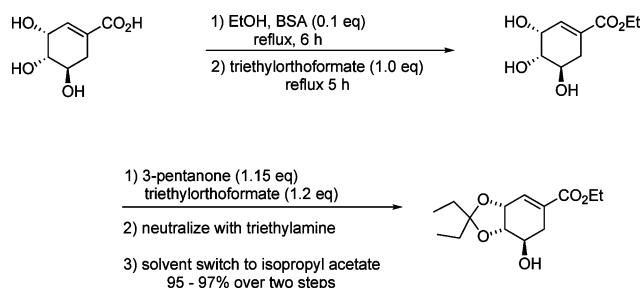


**Scheme 1** Original synthesis of (3*aR*,7*R*,7*aS*)-ethyl 2,2-diethyl-7-hydroxy-3*a*,6,7,7*a*-tetrahydrobenzo[*d*][1,3]dioxole-5-carboxylate **5** from shikimic acid **3**.

## Results and discussion

During our initial Fischer esterification studies of shikimic acid, we screened typical organic acids: *p*-toluenesulfonic acid (PTSA), benzenesulfonic acid (BSA) and heterogeneous conditions such as Dowex resin. We investigated benzenesulfonic acid more carefully as it is commercially available as a solid or as a solution.

It was determined that moderate amounts of water in the reaction mixture were detrimental with a plateau of 97% conversion being achieved even under the most anhydrous conditions.<sup>5</sup> The liberation of water during the Fischer Esterification reaction was enough to stop the reaction from proceeding beyond 97% unless a water scavenger was added. Use of 95% ethanol resulted in a plateau at 85–88% conversion, with the decreased conversion being attributed to the presence of additional water. Increasing the molar equivalents of anhydrous benzenesulfonic acid added could allow the acid catalyst to act as an internal water scavenger but had deleterious effects on the following transformation due to the acid sensitivity of 3-pentanone.<sup>6</sup> Use of technical grade benzenesulfonic acid (~80%) afforded the same conversion and purity as the more expensive 99+% grade. The remaining 20% of technical grade BSA is sulfuric acid which is used to produce the reagent. In order to solve the problem of incomplete conversion, a search for another water scavenger was initiated. It was discovered that the orthoformates would serve as an adequate water scavenger. Under the acidic conditions, any liberated water would react with the triethylorthoformate to produce ethanol and ethyl formate. Introduction of triethylorthoformate increased the conversion to >99% (Scheme 2).



**Scheme 2** Alternative synthesis of (3*aR*,7*R*,7*aS*)-ethyl 2,2-diethyl-7-hydroxy-3*a*,6,7,7*a*-tetrahydrobenzo[*d*][1,3]dioxole-5-carboxylate **5** from shikimic acid **3**.

Initially, the ester was isolated and taken into the next step as a melt of the ester and benzenesulfonic acid (10 mol%). Subsequently, the solution was taken into the ketalization step without isolation. The original route using 3-pentanone was an inefficient process requiring 25 equivalents of reagent. It was envisaged that transketalization from the 3,3-diethoxypentane could be a viable alternative and resources were focused on this route.

3,3-Diethoxypentane is not commercially available but could be generated as an ethanol solution by using a modification of the method described by Fife.<sup>7,8</sup> Originally, it was intended that the reagent would be produced in a separate vessel and transferred into the ethanol solution of the ethyl ester of shikimic acid. Generation of the reagent *in situ* afforded the added advantage of telescoping the first two transformations in an elegant sequence.

With the introduction of triethylorthoformate in the esterification step as a water scavenger, it seemed obvious to combine the first two steps. In the end, production of the hydroxy pentylidene ester in a two step, one pot reaction was possible with excellent yield and subsequent high purity at the epoxide (**2**) (Scheme 2).<sup>9</sup>

In summary, a streamlined process was developed to eliminate the use of thionyl chloride and shorten the overall process by employing a direct ketalization strategy.

## References

- S. Abrecht, M. C. Federspiel, H. Estermann, R. Fischer, M. Karpf, H.-J. Mair, T. Oberhauser, G. Rimmler, R. Trussardi and U. Zutter, *Chimia*, 2007, **61**, 93.
- W. Popendorf, *Am. Ind. Hyg. Assoc. J.*, 1984, **45**, 10.
- M. Federspiel, R. Fischer, M. Hennig, H.-J. Mair, T. Oberhauser, G. Rimmler, T. Albiez, J. Bruhin, H. Estermann, C. Gandert, V. Göckel, S. Götzö, U. Hoffmann, G. Huber, G. Janatsch, S. Lauper, O. Röckel-Stäbler, R. Trussardi and A. G. Zwahlen, *Org. Process Res. Dev.*, 1999, **3**, 266.
- R. Gabel, M. D. Groaning, D. A. Johnston, *Epoxide, intermediate in the Tamiflu™ synthesis*, WO 2007/074091, July 5, 2007.
- For a review of the kinetic model used in esterification reactions see: R. Rönneck, T. Salmi, A. Vuori, H. Haario, J. Lehtonen, A. Sundqvist and E. Tirronen, *Chem. Eng. Sci.*, 1997, **52**, 3369.
- Initial studies revealed that 3-pentanone was sensitive to acid mediated condensation and polymerization.
- T. H. Fife and L. Hagopian, *J. Org. Chem.*, 1966, **31**, 1772.
- Method: to a 500 ml round bottomed flask was added triethylorthoformate (96 ml, 574 mmol) followed by 3-pentanone (61 ml, 574 mmol) and ethanol (34 ml, 574 mmol). To this solution was added benzenesulfonic acid (182 mg, 0.2 mol%). The solution was stirred at room temperature for 3 h. This colourless solution is ready for use in the ketalization step.
- (3*R*,4*R*,5*S*)-ethyl 4-acetamido-5-amino-3-(pentan-3-yloxy)cyclohex-1-enecarboxylate**. To a 500 ml jacketed 3-neck flask fitted with a mechanical stirrer, reflux condenser and thermometer was added shikimic acid (287 mmole), SDA 2B-3 ethanol (150 ml) and 80% benzenesulfonic acid solution in ethanol (29 mmole). Using a bath set at 90–95 °C, the slurry was heated to reflux for 5 h. The reaction was cooled slightly and triethylorthoformate (287 mmole) was added and reflux was continued for an additional 5 h (shikimic acid <1%). The solution was cooled to 25 °C and triethylorthoformate (344 mmole) and 3-pentanone (330 mmole) was added. The reaction was stirred for *ca.* 30 min and reaction completion was analyzed (ester < 1%). The reaction mixture was neutralized with triethylamine (35 mmole) to a pH of ~8. Using a bath temperature of 35 °C, ethanol was distilled under vacuum. Isopropyl acetate (150 ml) was charged and the solvent distilled. Isopropyl acetate (150 ml) was charged to give



a solution of the hydroxy pentylidene ester (5). The solution can be taken on to the next step without further purification. **FOR CHARACTERIZATION:** the solution was stripped to dryness and recrystallized from heptane. (96.2% yield over two steps) mp = 60–62 °C. <sup>1</sup>H NMR (500 MHz, CDCl<sub>3</sub>) δ 0.89 (t, *J* = 7.5 Hz, 3H), 0.93 (t, *J* = 7.5 Hz, 3H), 1.30 (t, *J* = 7.0 Hz, 3H), 1.67 (m, 4H), 2.28 (br.

m, 1H), 2.79 (dd, *J* = 17.0, 4.5 Hz, 2H), 3.92 (m, 1H), 4.12 (q, *J* = 7.0 Hz, 2H), 4.23 (dd, *J* = 14.0, 7.0 Hz, 1H), 4.77 (m, 1H), 6.93 (m, 1H); <sup>13</sup>C NMR (125 MHz, CDCl<sub>3</sub>) δ 8.14, 8.78, 14.39, 29.36, 29.54, 29.91, 61.28, 69.17, 72.47, 78.08, 113.87, 130.65, 134.27, 166.40; IR (neat) 3285, 2981, 2942, 1702, 1276, 1108 cm<sup>-1</sup>; HRFABMS found *m/z* (M + Na<sup>+</sup>) 293.1520, calcd. for C<sub>14</sub>H<sub>22</sub>O<sub>5</sub>Na (293.1365).

# Preparation of mesoporous polyoxometalate-tantalum pentoxide composite catalyst and its application for biodiesel production by esterification and transesterification

Leilei Xu,<sup>a</sup> Yuanhong Wang,<sup>a</sup> Xia Yang,<sup>a</sup> Xiaodan Yu,<sup>a</sup> Yihang Guo<sup>\*a</sup> and James H. Clark<sup>\*b</sup>

Received 25th February 2008, Accepted 8th May 2008

First published as an Advance Article on the web 11th June 2008

DOI: 10.1039/b803220c

Mesoporous polyoxometalate-tantalum pentoxide composite catalyst,  $H_3PW_{12}O_{40}/Ta_2O_5$ , with  $H_3PW_{12}O_{40}$  loading from 3.6 to 20.1% was prepared by a one-step sol-gel-hydrothermal route in the presence of a triblock copolymer surfactant. Bulk and surface sensitive probe testing results indicated that the primary Keggin structure remained intact after formation of the composite, and strong interaction between the Keggin unit and  $Ta_2O_5$  framework existed in the composite. Additionally, the composite exhibited larger and well-distributed three-dimensionally interconnected pores (3.9–5.0 nm), larger BET surface area (106.0–126.9  $m^2 g^{-1}$ ), high porosity (0.44–1.37  $cm^3 g^{-1}$ ), and homogeneous dispersion of the Keggin unit throughout the composite. As an environmentally friendly solid acid catalyst, the catalytic performance of the  $H_3PW_{12}O_{40}/Ta_2O_5$  was evaluated in the esterification of lauric acid and myristic acid, the transesterification of tripalmitin as well as the direct use of soybean oil for biodiesel production. Regardless of the presence of free fatty acids, the  $H_3PW_{12}O_{40}/Ta_2O_5$  composite showed high reactivity and selectivity towards simultaneous esterification and transesterification under mild conditions. The catalyst can be recovered, reactivated and reused several times.

## Introduction

Biodiesel is an alternative fuel candidate composed of a mixture of  $C_{12}$ – $C_{22}$  monoalkyl esters of fatty acids based on ASTM D6751 standards.<sup>1–5</sup> It has similar physical properties to petrodiesel but unique advantages including being renewable, biodegradable, non-toxic and low emissions.<sup>5</sup> It can be manufactured from vegetable oils, animal fat, and even from recycled oils from the food industry. Standard biodiesel production involves the catalytic transesterification of long- or branched-chain triglycerides with short-chain alcohols.<sup>5</sup> The conventional catalysts for this reaction are homogeneous strong bases such as alkali metal hydroxides and alkoxides.<sup>2,6–8</sup> These catalysts are highly efficient and of low cost. However, they suffer from many drawbacks including sensitivity to moisture and free fatty acid (FFA). Both of these components may induce saponification under alkaline conditions, which not only consumes the catalyst, but also causes the formation of emulsions. Thus, it is difficult to recover and purify biodiesel.<sup>9</sup> Accordingly, dehydrated vegetable oil with less than 0.5 wt% FFAs, an anhydrous alkali catalyst, and anhydrous alcohol are necessary for commercially viable alkali-catalyzed production systems. This requirement is likely to be a significant limitation to the use of low-cost

feedstocks.<sup>10</sup> As a result, biodiesel production by these routes is still not cost-competitive with petrodiesel. Use of solid base catalysts, such as some zeolites,<sup>11</sup> alkali earth oxides,<sup>12–16</sup> and hydrotalcites,<sup>17–19</sup> offer several process advantages for transesterification reactions. However, FFAs in vegetable oils still interfere with the transesterification process catalyzed by solid base catalysts.

Transesterification catalyzed by an acid catalyst has the important advantage with respect to base catalysts that it is not strongly affected by the presence of FFAs in the feedstock. In fact, acid catalysts can catalyze both esterification and transesterification simultaneously.<sup>10</sup> To date, acid-catalyzed biodiesel production has been largely ignored, mainly due to its low efficiency. Higher pressure has been applied to increase the reaction temperature for improving the yield of monoester,<sup>2,20–22</sup> but at the expense of higher process costs and side reactions. Homogeneous acid catalysts such as sulfuric acid, hydrofluoric acid, and *p*-toluenesulfonic acid can also lead to serious contamination problems. Therefore, the development of robust and stable solid acids with strong Brønsted acid sites to be used as catalysts for biodiesel production is required both for green chemistry and economic viability. So far, some heterogeneous acid catalysts, including zeolites,<sup>23</sup> ion-exchange resins,<sup>2</sup> mixed metal oxides like sulfated zirconia,<sup>24</sup> and a sugar-based catalyst,<sup>1</sup> have been reported to exhibit reactivity for biodiesel production. However, catalysts with small pores, such as zeolites, are not suitable for biodiesel production because of the diffusion limitation of molecules having long alkyl chains.<sup>25,26</sup> Ion-exchange resins are active strong acids, but they have a low thermal stability and deactivate after 2 to 5 h.<sup>2,23,27</sup> In the

<sup>a</sup>School of Chemistry, Northeast Normal University, Changchun, P. R. China 130024. E-mail: guoyh@nenu.edu.cn; Fax: +86 431 85098705; Tel: +86 431 85098705

<sup>b</sup>Green Chemistry Centre, Department of Chemistry, University of York, Heslington, York, UK YO10 5DD. E-mail: jhc1@york.ac.uk; Fax: +44 1904 434550; Tel: +44 1904 432559

case of sulfated zirconia, catalyst stability can be decreased due to the blocking of the small pores by larger product molecules and coke formation.<sup>2,28</sup> Besides these solid acids, the uses of strongly acidic Keggin-type polyoxometalates (POMs), especially 12-tungstophosphoric acid ( $\text{H}_3\text{PW}_{12}\text{O}_{40}$ ), have attracted much attention for biodiesel synthesis.<sup>29</sup>  $\text{H}_3\text{PW}_{12}\text{O}_{40}$  is catalytically effective to both esterification and transesterification reactions, but they can act homogeneously and their small surface area ( $<10 \text{ m}^2 \text{ g}^{-1}$ )<sup>30</sup> hinders accessibility to the strong acidic sites, thereby limiting catalytic activity. To eliminate both of the problems, heterogeneous POMs such as Keggin type salts ( $\text{Cs}_x\text{H}_{3-x}\text{PW}_{12}\text{O}_{40}$ )<sup>31,32</sup> and supported POMs<sup>20</sup> have been developed and tested for biodiesel synthesis.  $\text{Cs}_x\text{H}_{3-x}\text{PW}_{12}\text{O}_{40}$  with  $x = 2.0\text{--}2.3$  exhibit high esterification as well as transesterification activity, but they suffer from separation problems due to the formation of colloidal suspension in polar media.<sup>31,33</sup> The supported POM, *e.g.*, MCM-41-supported POM prepared by a post-synthesis grafting method showed good activity at  $110^\circ\text{C}$  in the esterification of acetic acid and 1-butanol in the gas phase.<sup>34</sup> However, the catalyst suffers from several drawbacks including poor control over POM loading, POM leaching, and the lack of structural homogeneity. All of these lead to reduced activity of the immobilized POMs.

Our current work focuses on the design and preparation of more active, selective, and catalytically stable POM-containing composite catalysts for both esterification and transesterification conditions. The POM selected is  $\text{H}_3\text{PW}_{12}\text{O}_{40}$ , while  $\text{Ta}_2\text{O}_5$ , formed *via* hydrolysis and condensation of  $\text{TaCl}_5$ , is used as the support.  $\text{Ta}_2\text{O}_5$  has been shown to have catalytic activities in acid-catalyzed reactions such as the esterification of methacrylic acid with methanol, the alkylation of benzene with ethane, or the isomerization of 1-butene;<sup>35–37</sup>  $\text{Ta}^{5+}$  (1.50, 0.064 nm) and  $\text{W}^{6+}$  (1.70, 0.060 nm) have well-matched electronegativity and ionic radius. Thus, some of the W atoms may substitute for Ta atoms and form W–O–Ta bonds at the surface of the  $\text{Ta}_2\text{O}_5$ . This strong interaction between the Keggin unit and  $\text{Ta}_2\text{O}_5$  support are expected to enhance the stability of the composite catalyst.

We have used a one step sol–gel co-condensation-templating-hydrothermal route for catalyst preparation. Such a procedure is appropriate for the preparation of high-surface-area composite catalysts with unique surface properties, such as three-dimensional interconnected mesopore system of large pores, high pore volume, and homogeneous dispersion of the Keggin units. These characteristics along with controllable  $\text{H}_3\text{PW}_{12}\text{O}_{40}$  loading should benefit the materials suitability for biodiesel synthesis.

The structure, morphology, and surface physicochemical properties of as-prepared composites were well characterized by FT-IR,  $^{31}\text{P}$  MAS NMR, Raman scattering spectroscopy, XPS, XRD, nitrogen gas porosimetry, and TEM. Subsequently, their acid catalytic activity, selectivity, and stability were evaluated under mild conditions (atmosphere refluxing): in the esterification of lauric acid with ethanol; the transesterification of tripalmitin with methanol; the simultaneous esterification of myristic acid and transesterification of tripalmitin with methanol; and the direct use of soybean oil for the preparation of biodiesel. The influences of key reaction parameters such as the molar ratios of lauric acid/tripalmitin to alcohol and catalyst loading were also studied.

## Experimental

### Reagents

$\text{H}_3\text{PW}_{12}\text{O}_{40}\cdot x\text{H}_2\text{O}$  and P123 ( $M = 5800$ ) were purchased from Aldrich. Tantalum pentachloride ( $\text{TaCl}_5$ , 99%), lauric acid (97.5%), ethyl laurate (98%), and methyl palmitate (97%) were purchased from ABCR. Tripalmitin (99%) was purchased from Tokyo Kasei Kogyo Co. Ltd. Soybean oil is commercially available. All chemicals were used without further purification.

### Catalyst preparation

In a typical preparation of  $\text{H}_3\text{PW}_{12}\text{O}_{40}/\text{Ta}_2\text{O}_5$ ,  $\text{TaCl}_5$  was dissolved in P123/ethanol solution. After vigorous stirring the mixture for 1 h at room temperature, an aqueous  $\text{H}_3\text{PW}_{12}\text{O}_{40}$  solution was added dropwise to the above mixture, and the resulting sol was stirred at room temperature for 1 h. The molar ratio of  $\text{H}_3\text{PW}_{12}\text{O}_{40} : \text{P123} : \text{TaCl}_5 : \text{ethanol} = (0.0029\text{--}0.019) : 0.026 : 1 : 100$ . The clear sol obtained was aged at  $45^\circ\text{C}$  for 24 h, and then subjected to hydrothermal treatment at  $80^\circ\text{C}$  for 48 h at a heating ramp of  $2^\circ\text{C min}^{-1}$ . The hydrogel formed was cooled to room temperature and then dehydrated slowly at  $45^\circ\text{C}$  in vacuum until complete gel particulate was formed. The gel particulate was further dried in vacuum at 60 and  $80^\circ\text{C}$ , respectively. Removal of P123 was performed by boiling ethanol extraction for 3 h, and then the product was separated by centrifugation and dried in vacuum at  $45^\circ\text{C}$  for 24 h. The above procedure was repeated three times to ensure most of the P123 was removed from the product. The final product is denoted as  $\text{H}_3\text{PW}_{12}\text{O}_{40}/\text{Ta}_2\text{O}_5\text{-}x$ , where  $x$  represents  $\text{H}_3\text{PW}_{12}\text{O}_{40}$  loading (wt%) in the composite. Herein,  $x = 3.6, 10.8, 15.1$  and  $20.1\%$ , respectively, determined by a Leeman Prodigy Spec ICP-AES.

Pure  $\text{Ta}_2\text{O}_5$  was prepared by using the above method in the absence of  $\text{H}_3\text{PW}_{12}\text{O}_{40}$ .  $\text{H}_3\text{PW}_{12}\text{O}_{40}/\text{SBA-15-10.9}$  and  $\text{H}_3\text{PW}_{12}\text{O}_{40}/\text{Ta}_2\text{O}_5\text{-9.9-D}$  were prepared according to our previous methods.<sup>38,39,40</sup>

### Catalyst characterization

FT-IR spectra were recorded on a Nicolet Magna 560 IR spectrophotometer. Raman scattering spectra were recorded on a Jobin-Yvon HR 800 instrument with an  $\text{Ar}^+$  laser source of 488 nm wavelength in a macroscopic configuration.  $^{31}\text{P}$  MAS NMR spectra were obtained on a Varian Unity-400 NMR spectrometer. Low- and wide-angle XRD patterns of the composites were obtained on a D/max-2200 VPC diffractometer using  $\text{CuK}\alpha$  radiation. XPS was performed on a VG-ADES 400 instrument with  $\text{Mg K}\alpha$ -ADES source at a residual gas pressure of below  $10^{-8}$  Pa. TEM images were obtained on a JEOL JEM-2010 transmission electron microscope at an accelerating voltage of 200 kV. Nitrogen porosimetry was performed on a Micromeritics ASAP 2010 instrument. Surface areas were calculated using the BET equation. Pore size distributions were calculated using the BJH model based on nitrogen desorption isotherms.

### Testing of the catalysts

The catalysts were dried for 2 h at  $150^\circ\text{C}$  in vacuum before the catalytic tests.

All reactions were carried out in a round bottomed glass flask (25 ml) fitted with a water cooled condenser. For each reaction, 50 mg (2% w/w) of air-exposed catalyst was added, and the reaction was performed at reflux in air. Esterification was performed at 78 °C with different lauric acid to ethanol molar ratios (1 : 1 to 1 : 9) and constant reaction volume (2.5 ml). Transesterification was performed at 65 °C with tripalmitin to methanol molar ratio of 1 : 15 to 1 : 120 and constant reaction volume (2.5 ml). Simultaneous esterification and transesterification was performed *via* stirring the mixture of myristic acid (0.6 mmol), tripalmitin (0.6 mmol), and methanol (45 mmol) at 65 °C. Soybean oil transesterification reaction was performed *via* stirring the mixture of myristic acid (0.6 mmol), soybean oil (0.6 mmol), and methanol (45 mmol) at 65 °C. The samples were withdrawn periodically and then centrifuged for determination of the concentrations of the produced monoesters in the resulting solution on a Shimadzu GC-14C gas chromatograph fitted with a 1 Rtx-1 capillary column (film thickness, 1 μm; i.d., 0.25 mm; length, 30 m) and flame ionization detector. The product distribution in esterification reaction system was analyzed by a GC-6890N/MS-5975 GC-MS, while the product distribution in transesterification reaction system was analyzed on an Applied Biosystem LC (C<sub>8</sub> column)-Q-Trap triple quadrupole MS equipped with an ESI source.

The performance of the catalysts was characterized quantitatively by the yields of monoesters (% *Y*) and reaction turnover frequencies (TOFs, min<sup>-1</sup>) obtained at the selected conditions. *Y* was calculated as follows:  $Y = (M_D/M_T) \times 100$ , where *M<sub>D</sub>* is the number of moles of monoesters produced (ethyl laurate, methyl palmitate, or methyl myristate), and *M<sub>T</sub>* is the number of moles of monoesters expected. TOF was calculated as the number of moles of the monoester yielded in a period of reaction time (*τ*) per mole of H<sub>3</sub>PW<sub>12</sub>O<sub>40</sub> (*M<sub>HPW</sub>*):  $TOF = M_D/M_{HPW}\tau$ . The monoesters yielded over pure Ta<sub>2</sub>O<sub>5</sub> have been subtracted when TOFs of H<sub>3</sub>PW<sub>12</sub>O<sub>40</sub>/Ta<sub>2</sub>O<sub>5</sub> composites were calculated.

## Results and discussion

### Catalyst characterization

**Compositional and structural information.** The determined H<sub>3</sub>PW<sub>12</sub>O<sub>40</sub> loadings in as-prepared H<sub>3</sub>PW<sub>12</sub>O<sub>40</sub>/Ta<sub>2</sub>O<sub>5</sub> composites were as expected, implying that the preparation method employed can effectively inhibit the loss of the Keggin unit during the template extraction process.

Structure integrity of the Keggin unit and the interaction between the Keggin unit and Ta<sub>2</sub>O<sub>5</sub> support in the H<sub>3</sub>PW<sub>12</sub>O<sub>40</sub>/Ta<sub>2</sub>O<sub>5</sub> composites were studied by spectroscopic methods, including FT-IR, Raman, and <sup>31</sup>P MAS NMR coupled with surface sensitive XPS. Fig. 1 shows FT-IR spectra of the parent H<sub>3</sub>PW<sub>12</sub>O<sub>40</sub> and H<sub>3</sub>PW<sub>12</sub>O<sub>40</sub>/Ta<sub>2</sub>O<sub>5</sub> composites. Compared with the parent H<sub>3</sub>PW<sub>12</sub>O<sub>40</sub>, the characteristic vibrational frequencies related to the Keggin unit for the four tested H<sub>3</sub>PW<sub>12</sub>O<sub>40</sub>/Ta<sub>2</sub>O<sub>5</sub> were unchanged. These vibrational frequencies are 1080, 983, 893 and 800 cm<sup>-1</sup>, respectively, attributed to stretching vibration modes of P–O, W=O, and W–O–W bonds of the Keggin unit.<sup>41</sup> However, the peak intensities decreased after introduction of the Keggin unit into the Ta<sub>2</sub>O<sub>5</sub> framework.

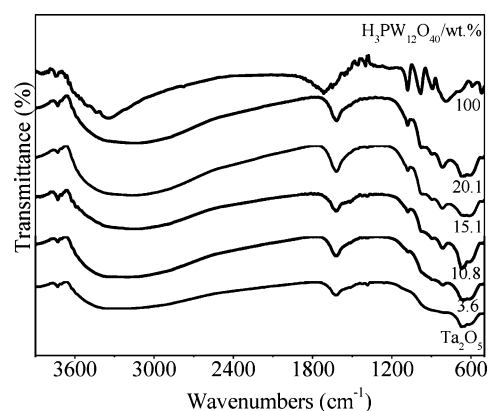


**Fig. 1** FTIR spectra of H<sub>3</sub>PW<sub>12</sub>O<sub>40</sub>/Ta<sub>2</sub>O<sub>5</sub> series as a function of H<sub>3</sub>PW<sub>12</sub>O<sub>40</sub> loading. Comparative spectrum of pure Ta<sub>2</sub>O<sub>5</sub> is also shown.

Additional structural information relating to the presence of Keggin units in the composite is obtained from Raman spectroscopy. Fig. 2 depicts the spectra under ambient conditions of parent H<sub>3</sub>PW<sub>12</sub>O<sub>40</sub>, pure Ta<sub>2</sub>O<sub>5</sub>, and H<sub>3</sub>PW<sub>12</sub>O<sub>40</sub>/Ta<sub>2</sub>O<sub>5</sub>-20.1. The bands characteristic of the W–O–W symmetric and asymmetric stretches of pure H<sub>3</sub>PW<sub>12</sub>O<sub>40</sub> were found at 533, 886 and 926 cm<sup>-1</sup>, and intense bands characteristic of terminal W=O stretches were situated at 977 and 1001 cm<sup>-1</sup>. The Raman spectrum of H<sub>3</sub>PW<sub>12</sub>O<sub>40</sub>/Ta<sub>2</sub>O<sub>5</sub>-20.1 resembles that of pure H<sub>3</sub>PW<sub>12</sub>O<sub>40</sub> with bands of 926 (W–O–W stretches) and 1001 cm<sup>-1</sup> (W=O stretches). The spectra are similar to that of silica supported H<sub>3</sub>PW<sub>12</sub>O<sub>40</sub> composites.<sup>41</sup> The bands at 660 cm<sup>-1</sup> for pure Ta<sub>2</sub>O<sub>5</sub> and 684 cm<sup>-1</sup> for H<sub>3</sub>PW<sub>12</sub>O<sub>40</sub>/Ta<sub>2</sub>O<sub>5</sub> are assigned to Ta–O vibration modes.<sup>35,42</sup>

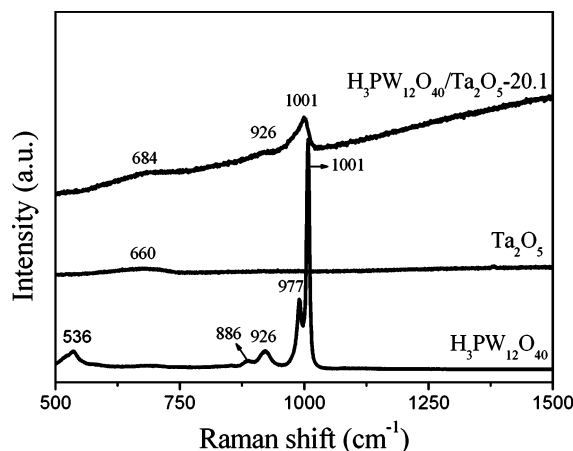


**Fig. 2** Raman spectra of pure Ta<sub>2</sub>O<sub>5</sub>, starting H<sub>3</sub>PW<sub>12</sub>O<sub>40</sub>, and H<sub>3</sub>PW<sub>12</sub>O<sub>40</sub>/Ta<sub>2</sub>O<sub>5</sub>-20.1 composite.

<sup>31</sup>P MAS NMR spectra strongly support the above results, with characteristic a P chemical shift (*δ*) of –14.2, and –17.1 ppm, respectively, for as-prepared H<sub>3</sub>PW<sub>12</sub>O<sub>40</sub>/Ta<sub>2</sub>O<sub>5</sub>-10.8 composite (Fig. 3a). The stronger peak at –14.2 ppm originates from the PO<sub>4</sub> unit within the bulk H<sub>3</sub>PW<sub>12</sub>O<sub>40</sub> environment.<sup>31</sup> While the weaker peak at *δ* = –17.1 ppm may originate from the PO<sub>4</sub> unit within H<sub>3</sub>PW<sub>12</sub>O<sub>40</sub> located near the Ta<sub>2</sub>O<sub>5</sub> surface. The chemical shift value is different for the latter due to perturbations by the Ta<sub>2</sub>O<sub>5</sub> support. The same result was obtained for the H<sub>3</sub>PW<sub>12</sub>O<sub>40</sub>/Ta<sub>2</sub>O<sub>5</sub>-9.9-D sample (Fig. 3b).



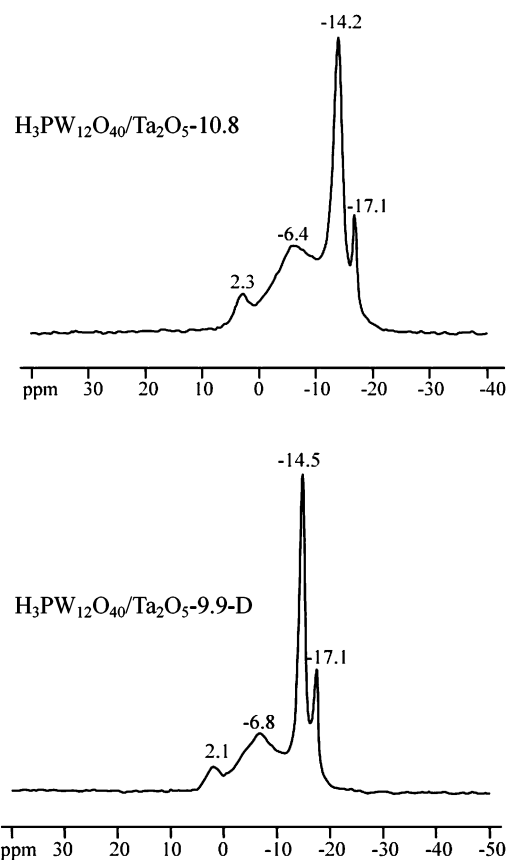


Fig. 3  $^{31}\text{P}$  MAS NMR spectra of  $\text{H}_3\text{PW}_{12}\text{O}_{40}/\text{Ta}_2\text{O}_5$  composites.

Thus it is inferred that the distortion of the Keggin cage at the interface of two components occurred due to the strong interaction between the Keggin unit and  $\text{Ta}_2\text{O}_5$ .

The nature of the surface species was explored by surface spectroscopy (XPS). Evaluation of the surface tungsten, oxygen, and tantalum environments were followed (Fig. 4). The resulting W 4f and Ta 4f XPS spectra are characteristic of high oxidation state tungsten and tantalum environment. Additionally, compared with parent  $\text{H}_3\text{PW}_{12}\text{O}_{40}$ , the binding energy (BE) of W 4f, O 1s and Ta 4f all had a slight shift to low values after incorporation of the Keggin unit into  $\text{Ta}_2\text{O}_5$  support. Higher  $\text{H}_3\text{PW}_{12}\text{O}_{40}$  loading resulted in lower BE (Table 1).

Together the spectroscopy data suggest that the primary Keggin structure remained intact after formation of the  $\text{H}_3\text{PW}_{12}\text{O}_{40}/\text{Ta}_2\text{O}_5$  composites. At the same time, strong interactions between the Keggin unit and  $\text{Ta}_2\text{O}_5$  support resulted in decreased IR intensities and changes in the Raman bands due to W=O, W–O–W and P–O bonds (molecular symmetry within the  $\text{H}_3\text{PW}_{12}\text{O}_{40}$  cluster was broken near the interface). Considering the very similar electronegativity and ionic radius of  $\text{Ta}^{5+}$  and  $\text{W}^{6+}$ , and the work reported by other groups,<sup>33,43</sup> we tentatively infer that the terminal W=O groups within the Keggin units coordinate to the surface  $\equiv\text{Ta}-\text{OH}$  groups within  $\text{Ta}_2\text{O}_5$  via Ta–O–W bonds and form  $(\equiv\text{TaOH}_2)_n^+[\text{H}_{3-n}\text{PW}_{12}\text{O}_{40}]^{n-}$  species at the interface.

**Mesostructure, morphology and porosity.** The low-angle XRD patterns of as-prepared  $\text{Ta}_2\text{O}_5$  and four  $\text{H}_3\text{PW}_{12}\text{O}_{40}/\text{Ta}_2\text{O}_5$  composites are shown in Fig. 5A. In the range of  $0.93$ – $1.17^\circ$ ,

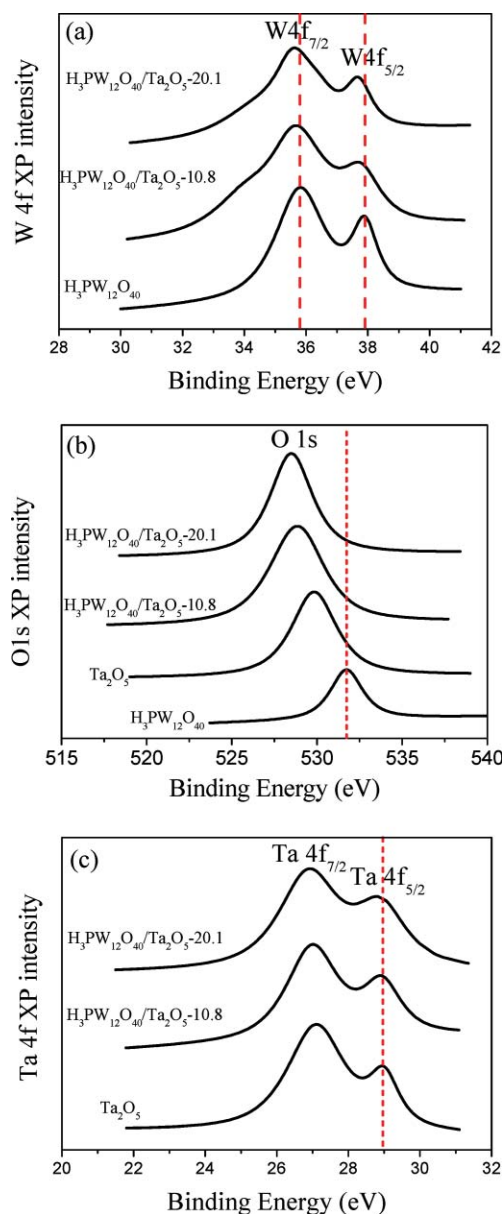
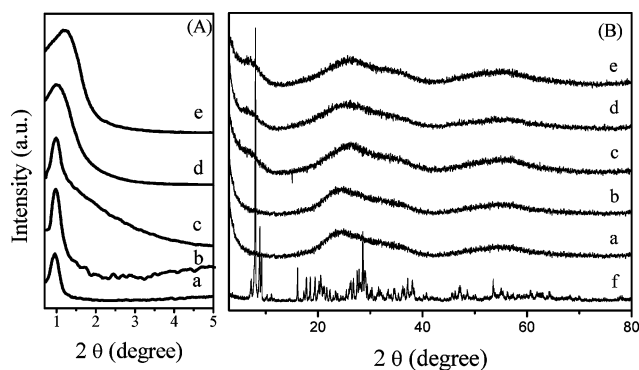


Fig. 4 High-resolution XPS spectra of  $\text{H}_3\text{PW}_{12}\text{O}_{40}/\text{Ta}_2\text{O}_5$  composites in the W 4f (a), O 1s (b), and Ta 4f (c) binding energy regions.

there is a broader reflection peak (100) for all tested samples. This is in good agreement with the materials prepared by using a neutral template, indicative of a wormhole-like unordered mesoporous structure.<sup>44,45</sup> Additionally, by increasing  $\text{H}_3\text{PW}_{12}\text{O}_{40}$  loading from 3.6 to 20.1%, the peak (100) shifts to higher  $2\theta$  values slightly (Table 2), at the same time, the peak becomes broader accompanied by decreased diffraction intensity. The phenomenon has been reported earlier by other researchers and is attributed to the filling of the host mesopores by materials that scatter X-rays.<sup>46</sup> This leads to increased phase cancellation between X-rays scattered from the walls and the pore regions, and thus reduces the intensities of XRD peaks.<sup>47</sup> Fig. 5B shows the wide-angle XRD patterns of  $\text{H}_3\text{PW}_{12}\text{O}_{40}/\text{Ta}_2\text{O}_5$  materials with respect to the starting  $\text{H}_3\text{PW}_{12}\text{O}_{40}$  and  $\text{Ta}_2\text{O}_5$  matrix. Upon loading the  $\text{H}_3\text{PW}_{12}\text{O}_{40}$  up to 20.1%, the reflection patterns corresponding to  $\text{H}_3\text{PW}_{12}\text{O}_{40}$  were still not found. The two broad

**Table 1** Binding energy (eV) of Ta 4f, W 4f, and O 1s of the starting  $H_3PW_{12}O_{40}$ ,  $Ta_2O_5$ , and  $H_3PW_{12}O_{40}/Ta_2O_5$  composites

Sample	Ta 4f		W 4f		O 1s
	4 $f_{7/2}$	4 $f_{5/2}$	4 $f_{7/2}$	4 $f_{5/2}$	
$Ta_2O_5$ (found)	27.1	28.9	—	—	529.8
$Ta_2O_5$ (expected)	27.1	29.0	—	—	531.1
$H_3PW_{12}O_{40}$ (found)	—	—	35.8	37.9	531.6
$H_3PW_{12}O_{40}$ (expected)	—	—	35.8	37.9	531.8
$H_3PW_{12}O_{40}/Ta_2O_5$ -10.8	27.0	28.9	35.7	37.7	528.8
$H_3PW_{12}O_{40}/Ta_2O_5$ -20.1	26.9	28.8	35.6	37.6	528.5

**Fig. 5** Low-angle (A) and wide-angle (B) XRD patterns of  $H_3PW_{12}O_{40}/Ta_2O_5$  composites,  $H_3PW_{12}O_{40}$  and  $Ta_2O_5$  are shown for comparison. (a) Pure  $Ta_2O_5$ , (b)  $H_3PW_{12}O_{40}/Ta_2O_5$ -3.6, (c)  $H_3PW_{12}O_{40}/Ta_2O_5$ -10.8, (d)  $H_3PW_{12}O_{40}/Ta_2O_5$ -15.1 (e)  $H_3PW_{12}O_{40}/Ta_2O_5$ -20.1 and (f)  $H_3PW_{12}O_{40}$ .**Table 2** Structural and textural information of different mesoporous materials

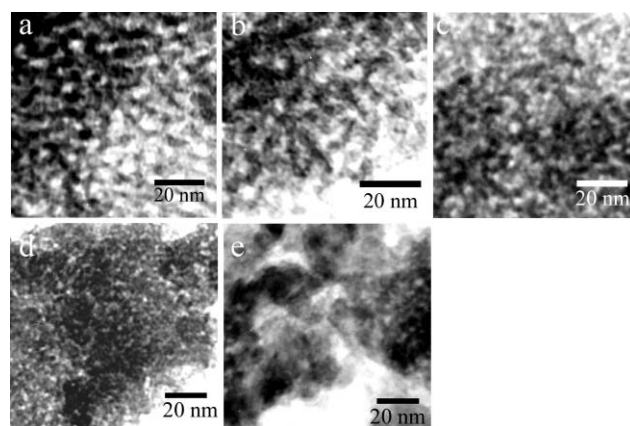
Catalyst	$2\theta/^\circ$	$S_{BET}/m^2 g^{-1}$	$D_p^a/nm$	$V_p^b/cm^3 g^{-1}$
$Ta_2O_5$	0.93	135.8	3.6	1.32
$H_3PW_{12}O_{40}/Ta_2O_5$ -3.6	0.95	126.9	3.9	1.37
$H_3PW_{12}O_{40}/Ta_2O_5$ -10.8	0.96	117.8	5.0	0.81
$H_3PW_{12}O_{40}/Ta_2O_5$ -15.1	0.98	114.7	4.4	0.80
$H_3PW_{12}O_{40}/Ta_2O_5$ -20.1	1.17	106.0	3.9	0.44
$H_3PW_{12}O_{40}/Ta_2O_5$ -D-9.9	—	167.3	1.2/2.5	0.029/0.017
$H_3PW_{12}O_{40}/SBA$ -15-10.9	0.97	727.8	6.3	1.41

<sup>a</sup> Average pore diameter estimated from BJH desorption determination.

<sup>b</sup> Maximum pore volume at a single point estimated from BJH desorption cumulative volume of pores.

peaks situated at *ca.* 25 and 55° originated from amorphous  $Ta_2O_5$ . Therefore, it is confirmed that the Keggin units are homogeneously dispersed throughout as-prepared composites.

TEM images of as-prepared  $H_3PW_{12}O_{40}/Ta_2O_5$  are shown in Fig. 6. For comparison, as-prepared  $Ta_2O_5$  and  $H_3PW_{12}O_{40}/Ta_2O_5$ -9.9-D are also shown. Samples prepared in the presence of P123 exhibited a three-dimensionally interconnected pore-network structure with high porosity and well-distributed pores (Fig. 6a–d). The results are in agreement with those of low-angle XRD, implying that the pores are contained within single particles. Increasing  $H_3PW_{12}O_{40}$  loading from 3.6 to 20.1% enhances the disorder of the pores with decreased porosity. The result suggests the blockage of part of the pores of  $Ta_2O_5$  matrix by the introduction of large Keggin units into the  $Ta_2O_5$  support. The morphology of  $H_3PW_{12}O_{40}/Ta_2O_5$ -9.9-D (Fig. 6e) is different from that of the above samples obtained by

**Fig. 6** TEM images of pure  $Ta_2O_5$  (a),  $H_3PW_{12}O_{40}/Ta_2O_5$ -3.6 (b),  $H_3PW_{12}O_{40}/Ta_2O_5$ -10.8 (c),  $H_3PW_{12}O_{40}/Ta_2O_5$ -20.1 (d), and  $H_3PW_{12}O_{40}/Ta_2O_5$ -D-9.9 (e) composites.

using a neutral template, showing obvious aggregation among particles with low porosity and uneven pore size distribution. This result implies that the pores of  $H_3PW_{12}O_{40}/Ta_2O_5$ -9.9-D occur as voids among the particles.

The overall mesoporosity of as-prepared  $Ta_2O_5$  and  $H_3PW_{12}O_{40}/Ta_2O_5$  was examined by nitrogen gas porosimetry, and the results are shown in Fig. 7 and Table 2. All of the isotherms for the tested materials are Type IV with H2-type hysteresis (Fig. 7a), which is an indicator of the three-dimensionally interconnected porous structure of the samples.<sup>44,45</sup> The narrow pore size distribution of the tested samples (Fig. 7b) implies that the pores within the  $Ta_2O_5$  support and  $H_3PW_{12}O_{40}/Ta_2O_5$  composites are uniform. Also the Keggin units are homogeneously distributed across the sol-gel co-condensed materials. From Table 2, it can be seen that BET surface areas and pore volumes of the  $H_3PW_{12}O_{40}/Ta_2O_5$  composites decreased gradually with increasing  $H_3PW_{12}O_{40}$  loading from 3.6 to 20.1%. However, the BET surface area of the composite increased greatly compared with the starting  $H_3PW_{12}O_{40}$ . The average pore diameter of the composites is in the range of 3.9 to 5.0 nm, a little higher than  $Ta_2O_5$  support. The above results lead us to assume that the Keggin units are located inside the pores of  $Ta_2O_5$  network through interaction with it. Therefore, the pores of  $H_3PW_{12}O_{40}/Ta_2O_5$  were enlarged. On increasing  $H_3PW_{12}O_{40}$  loading from 3.6 to 10.8%, the pore diameter increases from 3.9 to 5.0 nm, suggesting that the blockage of the pores of  $Ta_2O_5$  matrix do not occur. Further increases in the  $H_3PW_{12}O_{40}$  loading to 15.1 or 20.1% leads to further decreases in the pore diameter of the composites, implying partial blockage of the

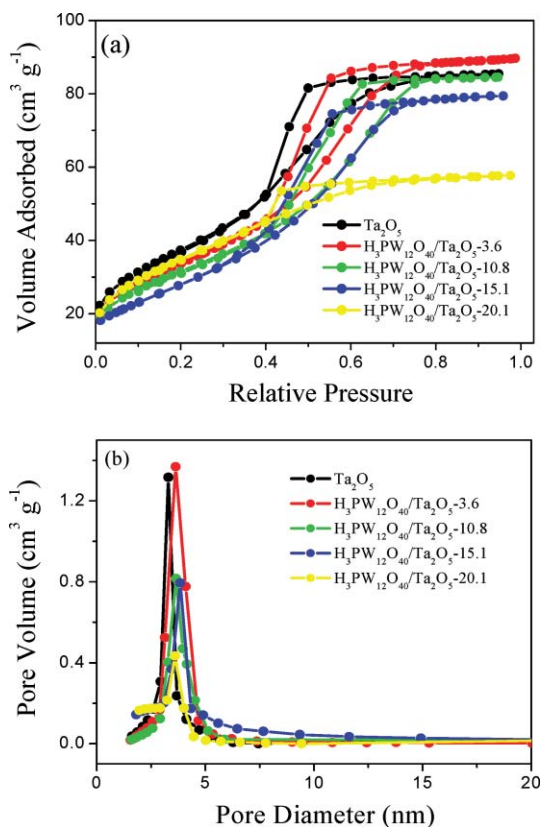


**Fig. 7** Nitrogen adsorption–desorption isotherms (a) and pore size distribution profiles (b) of mesoporous  $\text{Ta}_2\text{O}_5$  and  $\text{H}_3\text{PW}_{12}\text{O}_{40}/\text{Ta}_2\text{O}_5$  composites.

pores. The above results are consistent with those of the TEM and XRD, indicating that as-prepared mesoporous materials are tailored by nonionic templates. The textural properties of as-prepared  $\text{H}_3\text{PW}_{12}\text{O}_{40}/\text{Ta}_2\text{O}_5$  are superior to those of our previous reported  $\text{H}_3\text{PW}_{12}\text{O}_{40}/\text{Ta}_2\text{O}_5$ -9.9-D.<sup>40</sup> The BET surface area of  $\text{H}_3\text{PW}_{12}\text{O}_{40}/\text{Ta}_2\text{O}_5$ -9.9-D is  $167.3 \text{ m}^2 \text{ g}^{-1}$ , but its pore size distribution is uneven with average pore size of 1.2 and 2.5 nm, respectively. The pore volumes, 0.029 and  $0.017 \text{ cm}^3 \text{ g}^{-1}$ , respectively, for micropores and mesopores, are extremely low. In the absence of the structure directing reagent, micro- and mesopores of the  $\text{H}_3\text{PW}_{12}\text{O}_{40}/\text{Ta}_2\text{O}_5$ -9.9-D were formed due to finer and larger intra-aggregated among particles, respectively. The above results suggest that P123 indeed acts as a structure directing function.

### Testing of the catalysts

The insoluble nature of the  $\text{H}_3\text{PW}_{12}\text{O}_{40}/\text{Ta}_2\text{O}_5$  composite in polar media makes this catalyst attractive for applications in both esterification and transesterification reactions, which are pertinent to biodiesel production. Therefore, the catalytic performance of as-prepared  $\text{H}_3\text{PW}_{12}\text{O}_{40}/\text{Ta}_2\text{O}_5$  was evaluated in the esterification of lauric acid (a major saturated fatty acid found in coconut oil) and the transesterification of tripalmitin (a natural constituent of palm oil), separately. Afterwards, the catalytic behaviors of the  $\text{H}_3\text{PW}_{12}\text{O}_{40}/\text{Ta}_2\text{O}_5$  were further screened for the simultaneous esterification of myristic acid (main FA found in nutmeg butter) and transesterification of

tripalmitin reactions. At the same time, a comparative study was made using bulk  $\text{H}_3\text{PW}_{12}\text{O}_{40}$ ,  $\text{Ta}_2\text{O}_5$ ,  $\text{H}_3\text{PW}_{12}\text{O}_{40}/\text{SBA-15-10.9}$ , and  $\text{H}_3\text{PW}_{12}\text{O}_{40}/\text{Ta}_2\text{O}_5$ -D-9.9, respectively. Finally,  $\text{H}_3\text{PW}_{12}\text{O}_{40}/\text{Ta}_2\text{O}_5$  was tested *via* direct use of soybean oil for the preparation of biodiesel.

**Esterification of lauric acid and transesterification of tripalmitin.** The selectivity of both reactions was evaluated firstly over the  $\text{H}_3\text{PW}_{12}\text{O}_{40}/\text{Ta}_2\text{O}_5$ -10.8. For lauric acid esterification with ethanol, the selectivity to ethyl laurate is close to 100% (by GC-MS). For the transesterification of tripalmitin with methanol, the intermediates, including methyl palmitate, dipalmitin and monopalmitin, were identified by LC-MS. The results suggest that the transesterification reaction catalyzed by the  $\text{H}_3\text{PW}_{12}\text{O}_{40}/\text{Ta}_2\text{O}_5$  is stepwise. The result is in agreement with other work.<sup>20,24</sup> At a methanol to tripalmitin molar ratio of 90 : 1 and 2% w/w  $\text{H}_3\text{PW}_{12}\text{O}_{40}/\text{Ta}_2\text{O}_5$ -10.8 loading, the conversion of tripalmitin to di- and mono-palmitin is complete in 2 h. Moreover, the concentrations of di- and mono-palmitin in the systems decreased as the yield of methyl palmitate increased up to 10 h.

The molar ratio of alcohol to lauric acid or tripalmitin is one of the most important factors to affect the ester yield. Theoretically, the esterification of 1 mole of fatty acid requires 1 mole of alcohol, while the transesterification of 1 mole of triglyceride needs 3 moles of alcohol. Since both reactions are reversible, the excess of alcohol can shift the equilibrium in the direction of ester formation. Fig. 8a shows the influence of ethanol to lauric acid molar ratio on laurate yield using  $\text{H}_3\text{PW}_{12}\text{O}_{40}/\text{Ta}_2\text{O}_5$ -10.8 as a catalyst. On changing the molar ratio of ethanol to lauric acid from 1 : 1 to 7 : 1 with a constant total volume, the yield of laurate increased from 12.7 to 100% after 3 h. Fig. 8b shows the influence of methanol to tripalmitin molar ratio on the yield of methyl palmitate using  $\text{H}_3\text{PW}_{12}\text{O}_{40}/\text{Ta}_2\text{O}_5$ -20.1 as a catalyst. The yield of methyl palmitate increased from 3.3 to 28.4% on increasing the methanol to tripalmitin molar ratio from 15 : 1 to 90 : 1 after 6 h. At 120 : 1 the ester yield was reduced. The above results suggest that much more alcohol is needed for the transesterification than the esterification reaction so as to improve the rate of the reaction. This is due to the stepwise nature of the transesterification reaction. The effect of  $\text{H}_3\text{PW}_{12}\text{O}_{40}$  loading on the yield of ester during esterification of lauric acid and transesterification of tripalmitin was studied. Fig. 9 shows the resultant ethyl laurate and methyl palmitate yields over the  $\text{H}_3\text{PW}_{12}\text{O}_{40}/\text{Ta}_2\text{O}_5$  composites with different  $\text{H}_3\text{PW}_{12}\text{O}_{40}$  loadings. Pure  $\text{Ta}_2\text{O}_5$  is active towards both reactions. By using  $\text{Ta}_2\text{O}_5$  as a catalyst (2% w/w), the yield of ethyl laurate reached 40.2% after 3 h with an ethanol to acid molar ratio of 3 : 1. The yield of methyl palmitate reached 37.3% after the transesterification reaction ran for 10 h and methanol to tripalmitin molar ratio of 90 : 1. The four tested  $\text{H}_3\text{PW}_{12}\text{O}_{40}/\text{Ta}_2\text{O}_5$  composites all exhibited higher catalytic activity on the two reactions compared with pure  $\text{Ta}_2\text{O}_5$  under the same conditions.  $\text{H}_3\text{PW}_{12}\text{O}_{40}/\text{Ta}_2\text{O}_5$ -10.8 is the most active among the tested catalysts with the yield of ethyl laurate and methyl palmitate reaching 65.6 and 66.2%, respectively, under the selected conditions. Results from the comparative studies are shown in Table 3.

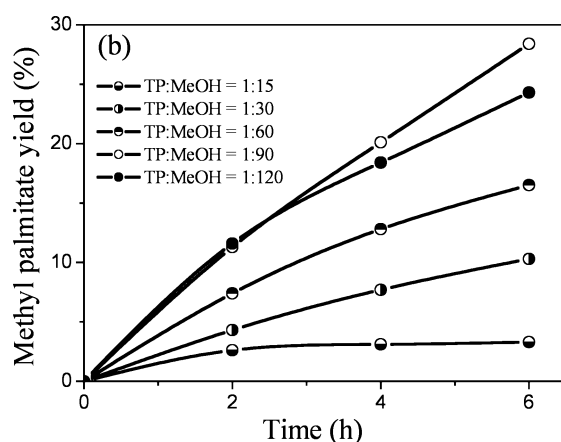
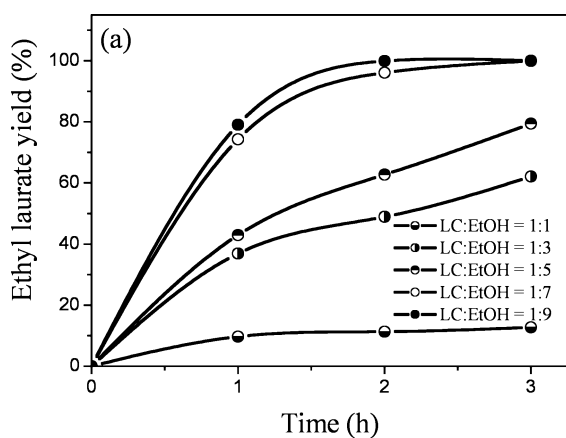


**Fig. 8** (a) Influence of the molar ratio of lauric acid (LC) to ethanol (EtOH) on the yield of ethyl laurate.  $\text{H}_3\text{PW}_{12}\text{O}_{40}/\text{Ta}_2\text{O}_5$ -10.8 (2% w/w); 78 °C. (b) Influence of the molar ratio of tripalmitin (TP) to methanol (MeOH) on the yield of methyl palmitate.  $\text{H}_3\text{PW}_{12}\text{O}_{40}/\text{Ta}_2\text{O}_5$ -20.1 (2% w/w); 65 °C.

**Simultaneous esterification of myristic acid and transesterification of tripalmitin.** The presence of high concentrations of FFAs in low-cost lipid feedstock may have adverse effects on the catalyst activity. A good solid acid catalyst must be able to carry out both esterification and transesterification simultaneously. Having demonstrated mesoporous  $\text{H}_3\text{PW}_{12}\text{O}_{40}/\text{Ta}_2\text{O}_5$  composites were active in both esterification and transesterification, we conducted a one-pot reaction with the  $\text{H}_3\text{PW}_{12}\text{O}_{40}/\text{Ta}_2\text{O}_5$ -10.8

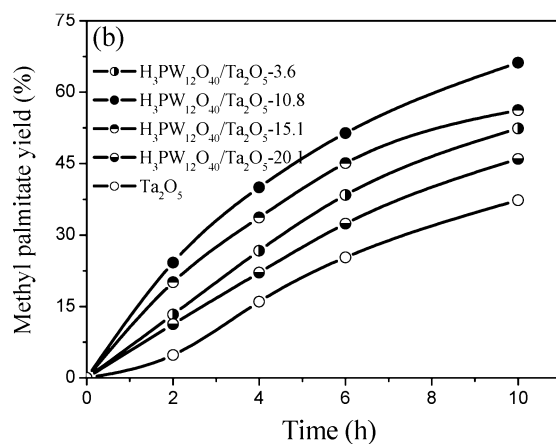
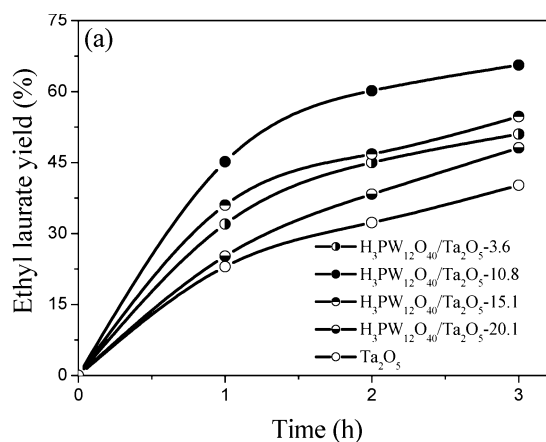


**Fig. 9** Time courses of esterification of lauric acid with ethanol (a, 78 °C, LC : EtOH = 1 : 3) and transesterification of tripalmitin with methanol (b, 65 °C, TP : MeOH = 1 : 90) catalyzed over the mesoporous  $\text{H}_3\text{PW}_{12}\text{O}_{40}/\text{Ta}_2\text{O}_5$  composites with various  $\text{H}_3\text{PW}_{12}\text{O}_{40}$  loadings.

catalyst to determine whether both esterification and transesterification reactions could be undertaken simultaneously.

The influence of free fatty acid level on the yield of monoester was studied by adding 20 wt% of myristic acid to a tripalmitin transesterification system. The simultaneous esterification and transesterification reactions were performed at 65 °C, a molar ratio of myristic acid : tripalmitin : methanol of 1 : 1 : 90, and a 2% w/w catalyst loading. After 6 h, the yield of methyl myristate reached 100%, while the yield of methyl palmitate was 50.7%.

**Table 3** Comparison of the yield and TOF for various catalysts (2% w/w) in esterification of lauric acid and transesterification of tripalmitin reactions

Catalyst	Ethyl laurate yield (%) <sup>a</sup>	TOF <sub>E</sub> /min <sup>-1b</sup>	Methyl palmitate yield (%) <sup>c</sup>	TOF <sub>T</sub> /min <sup>-1d</sup>
$\text{H}_3\text{PW}_{12}\text{O}_{40}/\text{Ta}_2\text{O}_5$ -3.6	51.0	7.07	38.4	1.19
$\text{H}_3\text{PW}_{12}\text{O}_{40}/\text{Ta}_2\text{O}_5$ -10.8	65.6	5.58	51.4	0.79
$\text{H}_3\text{PW}_{12}\text{O}_{40}/\text{Ta}_2\text{O}_5$ -15.1	54.7	2.26	45.1	0.43
$\text{H}_3\text{PW}_{12}\text{O}_{40}/\text{Ta}_2\text{O}_5$ -20.1	48.1	0.94	35.4	0.17
$\text{H}_3\text{PW}_{12}\text{O}_{40}/\text{Ta}_2\text{O}_5$ -D-9.9	24.2	3.42	17.3	0.37
$\text{H}_3\text{PW}_{12}\text{O}_{40}/\text{SBA}$ -15-10.9	20.0	4.32	9.8	0.29
$\text{H}_3\text{PW}_{12}\text{O}_{40}$	68.4	1.62	48.1	0.16
$\text{Ta}_2\text{O}_5$	40.2	—	25.3	—
$\text{Ta}_2\text{O}_5$ -D	9.8	—	6.3	—

<sup>a</sup> Temperature 78 °C; ethanol to lauric acid molar ratio 3 : 1; 3 h. <sup>b</sup> TOF of esterification reaction. <sup>c</sup> Temperature 65 °C; methanol to tripalmitin molar ratio 90 : 1; 6 h. <sup>d</sup> TOF of transesterification reaction.



**Table 4** Reaction of soybean oil esterification and transesterification with methanol catalyzed over mesoporous  $\text{H}_3\text{PW}_{12}\text{O}_{40}/\text{Ta}_2\text{O}_5$ 

Catalyst	Esterification yield (%) <sup>a,b</sup>	Transesterification yield (%) <sup>b</sup>		
		Methyl palmitin	Methyl oleate	Methyl linoleate
$\text{H}_3\text{PW}_{12}\text{O}_{40}/\text{Ta}_2\text{O}_5$ -3.6	> 99%	23.1	18.9	28.3
$\text{H}_3\text{PW}_{12}\text{O}_{40}/\text{Ta}_2\text{O}_5$ -10.8	> 99%	24.9	20.5	30.4
$\text{H}_3\text{PW}_{12}\text{O}_{40}/\text{Ta}_2\text{O}_5$ -15.1	> 99%	18.5	15.6	22.6
$\text{H}_3\text{PW}_{12}\text{O}_{40}/\text{Ta}_2\text{O}_5$ -20.1	> 99%	7.9	6.2	9.3

<sup>a</sup> 20 wt% myristic acid in soybean oil. <sup>b</sup> Temperature 65 °C; methanol to soybean oil molar ratio 90 : 1; 24 h.

Under the same conditions, the yield of methyl palmitate was 51.4% for a single transesterification of tripalmitin. The result indicates that the acid catalytic activity of the  $\text{H}_3\text{PW}_{12}\text{O}_{40}/\text{Ta}_2\text{O}_5$  composite in transesterifications is little affected by the presence of free FFA. This performance makes the  $\text{H}_3\text{PW}_{12}\text{O}_{40}/\text{Ta}_2\text{O}_5$  an ideal catalyst for biodiesel production.

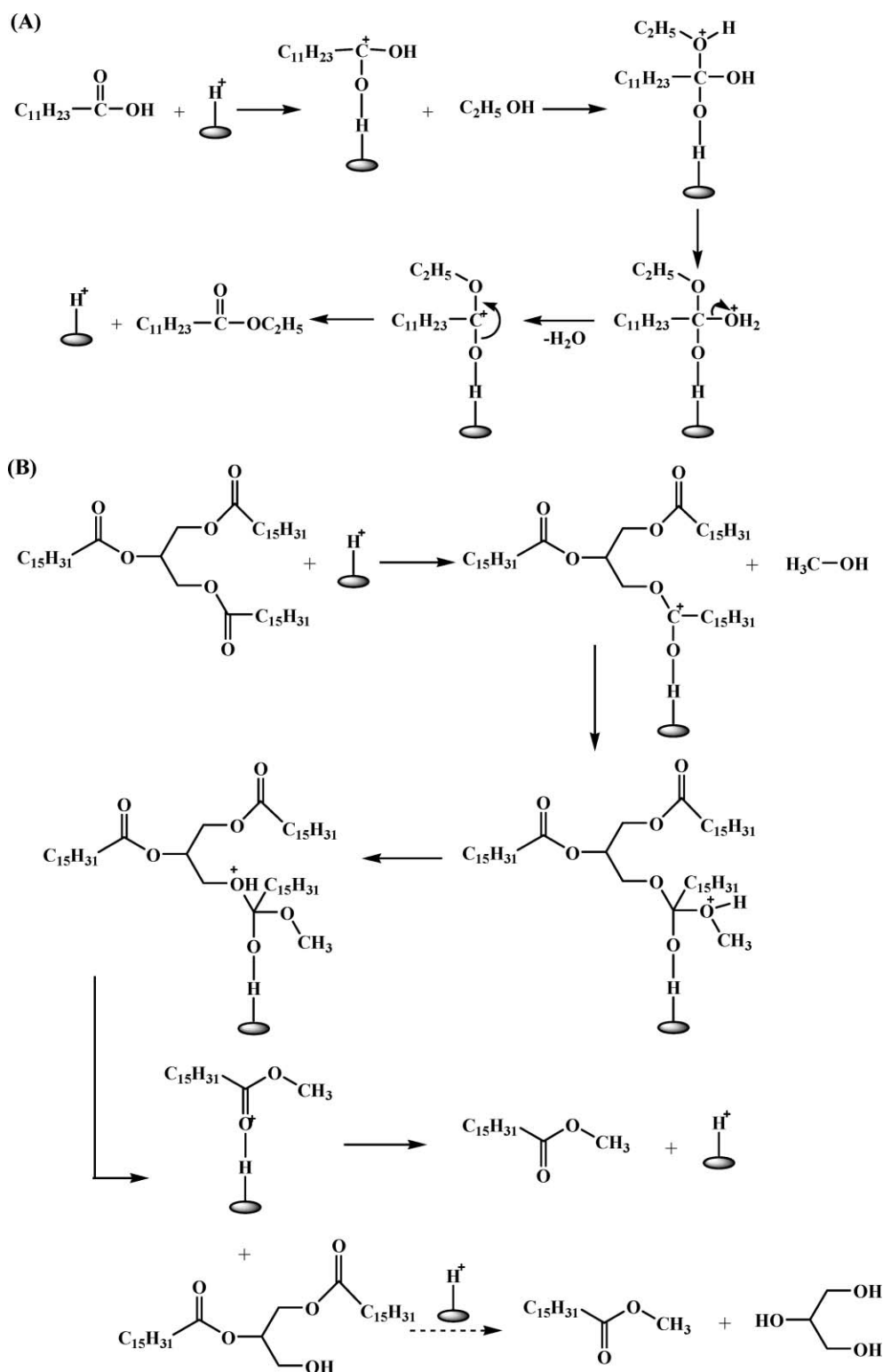
**Preparation of biodiesel from soybean oil.** Considering practical applications of as-prepared  $\text{H}_3\text{PW}_{12}\text{O}_{40}/\text{Ta}_2\text{O}_5$  composites, direct use of soybean oil for the preparation of biodiesel is tested. Soybean oil mainly consists of three kinds of triglyceride, oleic, palmitic and linoleic triglyceride, and their total content exceeds 75%, as analyzed by GC-MS. In the soybean oil transesterification reaction, the catalyst performance was characterized by the yield of methyl palmitin, methyl oleate and methyl linoleate, respectively. From the results shown in Table 4, it can be seen  $\text{H}_3\text{PW}_{12}\text{O}_{40}/\text{Ta}_2\text{O}_5$ -10.8 and  $\text{H}_3\text{PW}_{12}\text{O}_{40}/\text{Ta}_2\text{O}_5$ -20.1 still demonstrated the highest and the lowest catalytic activity, respectively, towards the transesterification reaction of soybean oil. In addition, under given experimental conditions, esterification of myristic acid catalyzed over each of the tested  $\text{H}_3\text{PW}_{12}\text{O}_{40}/\text{Ta}_2\text{O}_5$  is complete.

**Mechanism consideration.** The reaction mechanism of esterification and transesterification catalyzed by mesoporous  $\text{H}_3\text{PW}_{12}\text{O}_{40}/\text{Ta}_2\text{O}_5$  composite is shown in Scheme 1. Both reactions take place between acid/triglyceride and ethanol/methanol adsorbed on acidic sites of the catalyst surface. The protonation of the carbonyl oxygen of free fatty acid or monoglyceride with the acidic site of the catalyst forms a carbocation. The nucleophilic attack of alcohol to the carbocation produces a tetrahedral intermediate. Finally, proton migration and breakdown of the intermediate occurs. The transesterification mechanism can be extended to bi- and mono-glyceride and give one mole of ester in each step. Also, as shown in Scheme 1, the catalyst is regenerated after the esterification and transesterification.

**Catalyst recycling.** To evaluate the reusability and regeneration of as-prepared  $\text{H}_3\text{PW}_{12}\text{O}_{40}/\text{Ta}_2\text{O}_5$ , the simultaneous esterification of myristic acid and transesterification of tripalmitin reactions catalyzed by the  $\text{H}_3\text{PW}_{12}\text{O}_{40}/\text{Ta}_2\text{O}_5$ -10.8 were repeated five times. After the reaction, the catalyst was removed by hot filtration. The catalyst-free reaction solution was analyzed by ICP-AES to estimate the drop of  $\text{H}_3\text{PW}_{12}\text{O}_{40}$ . As expected, P and W were hardly detected in this solution, implying high stability of as-prepared  $\text{H}_3\text{PW}_{12}\text{O}_{40}/\text{Ta}_2\text{O}_5$ . The recovered catalyst was

used for the second and third runs under the same conditions, and the methyl myristate yield decreased to 88.9 and 66.1%, respectively. At the same time, the yield of methyl palmitate is 46.3 and 33.8%, respectively. However, we still did not detect P and W in the catalyst-free reaction solutions. Therefore, we regenerated the catalyst by hot ethanol and hexane washing overnight, and then calcined the catalyst at 300 °C in vacuum. The reactivated catalyst was used in the fourth and fifth catalytic runs. The methyl myristate yield obtained was 96.6 and 94.9%, respectively. And the yield of methyl palmitate is 49.1 and 48.2%, respectively. The above results imply that the decreased activity of  $\text{H}_3\text{PW}_{12}\text{O}_{40}/\text{Ta}_2\text{O}_5$ -10.8 is mainly due to surface adsorption of the catalyst with polar (e.g. methanol or glycerol) or non-polar (e.g. methyl myristate or methyl palmitate) compounds. A similar result has also been reported elsewhere.<sup>20</sup> The catalyst recycling tests also further confirmed the strong interaction existed between the Keggin unit and  $\text{Ta}_2\text{O}_5$  support: an especially important property for the supported POM catalyst.

Based on the above catalytic test results and physicochemical properties of the tested catalysts, the reasons behind the higher activity of as-prepared mesoporous  $\text{H}_3\text{PW}_{12}\text{O}_{40}/\text{Ta}_2\text{O}_5$  composites towards both esterification and transesterification reactions can be deduced. Firstly, stronger Brønsted acid sites in mesoporous  $\text{H}_3\text{PW}_{12}\text{O}_{40}/\text{Ta}_2\text{O}_5$  composites ensure the reactions proceed at an acceptable rate. After incorporation of the Keggin unit into  $\text{Ta}_2\text{O}_5$  support, ( $\equiv\text{TaOH}_2$ )<sub>n</sub><sup>+</sup>[ $\text{H}_3\text{-nPW}_{12}\text{O}_{40}$ ]<sub>n</sub><sup>-</sup> species were formed at the surface of the composite catalyst via Ta–O–W bonds. Consequently, electron transfer from the terminal oxygen atoms within W=O groups to  $\text{Ta}_2\text{O}_5$  may occur, leading to charging of the composite surface, which could promote the release of protons and increase the Brønsted acidity of the composite. Additionally, the strong interaction of the Keggin unit and  $\text{Ta}_2\text{O}_5$  support may lead to lower proton releasing energy and resulting in an increase of the Brønsted acidity of the catalyst. This coincides with the XPS results (Fig. 4) showing that the BE of W 4f, O 1s, and Ta 4f all had a slight shift to low values after incorporation of the Keggin unit into the  $\text{Ta}_2\text{O}_5$  support. A similar explanation has been reported for titania supported  $\text{H}_3\text{PW}_{12}\text{O}_{40}$  composite.<sup>48</sup> Secondly, as-prepared  $\text{H}_3\text{PW}_{12}\text{O}_{40}/\text{Ta}_2\text{O}_5$  composites exhibit unique surface textural properties, including larger interconnected pore structure with high porosity, uniform pore size distribution and homogeneous dispersion of the Keggin unit throughout the composite, which has played an important role in improving the catalytic activity. A larger interconnected pore structure and uniform pore size distribution would minimize diffusion problems of molecules having long alkyl chains, while homogeneous dispersion of active site can increase the accessibility to their acid sites, and high porosity of the composite may give rise to a higher population of available acid sites. All of these characteristics ensure as-prepared mesoporous  $\text{H}_3\text{PW}_{12}\text{O}_{40}/\text{Ta}_2\text{O}_5$  composites give significantly high reactivity in esterification and transesterification reactions compared with  $\text{H}_3\text{PW}_{12}\text{O}_{40}/\text{Ta}_2\text{O}_5$  prepared without a neutral template ( $\text{H}_3\text{PW}_{12}\text{O}_{40}/\text{Ta}_2\text{O}_5$ -D-9.9). Among the four tested mesoporous  $\text{H}_3\text{PW}_{12}\text{O}_{40}/\text{Ta}_2\text{O}_5$  composites,  $\text{H}_3\text{PW}_{12}\text{O}_{40}/\text{Ta}_2\text{O}_5$ -10.8 and  $\text{H}_3\text{PW}_{12}\text{O}_{40}/\text{Ta}_2\text{O}_5$ -20.1 demonstrated the highest and the lowest catalytic activity, respectively, towards both reactions. This is due to the fact that higher  $\text{H}_3\text{PW}_{12}\text{O}_{40}$  loading (above 10.8%) resulted in the



**Scheme 1** Esterification of lauric acid (A) and transesterification of tripalmitin (B) catalyzed over the  $\text{H}_3\text{PW}_{12}\text{O}_{40}/\text{Ta}_2\text{O}_5$  composite.

blockage of part of the pores of  $\text{Ta}_2\text{O}_5$  matrix thereby decreasing the porosity of the composite (Table 1).

Finally, it should be emphasized that contribution of Brønsted acidity is more important for the catalytic activity compared to surface physicochemical properties of POM-

containing composite catalysts. The conclusion is supported by the testing results of mesoporous  $\text{H}_3\text{PW}_{12}\text{O}_{40}/\text{Ta}_2\text{O}_5$ -10.8 and  $\text{H}_3\text{PW}_{12}\text{O}_{40}/\text{SiO}_2$ -10.9, where the latter was prepared with the same route of the  $\text{H}_3\text{PW}_{12}\text{O}_{40}/\text{Ta}_2\text{O}_5$ . At the same  $\text{H}_3\text{PW}_{12}\text{O}_{40}$  loading, the  $\text{H}_3\text{PW}_{12}\text{O}_{40}/\text{SiO}_2$ -10.9 showed a much

lower catalytic activity with respect to the  $\text{H}_3\text{PW}_{12}\text{O}_{40}/\text{Ta}_2\text{O}_5$ -10.8 (Table 3). However, the  $\text{H}_3\text{PW}_{12}\text{O}_{40}/\text{SiO}_2$ -10.9 had a much larger BET surface area ( $727.8 \text{ m}^2 \text{ g}^{-1}$ ), pore diameter (6.3 nm) and pore volume ( $0.92 \text{ cm}^3 \text{ g}^{-1}$ ).<sup>39</sup> A lower catalytic activity of the  $\text{H}_3\text{PW}_{12}\text{O}_{40}/\text{SiO}_2$ -10.9 is attributed to its weaker Brønsted acid sites. For a silica-supported  $\text{H}_3\text{PW}_{12}\text{O}_{40}$  composite, it is impossible to form W–O–Si bond due to mismatching of the electronegativity and ionic radius of  $\text{W}^{6+}$  and  $\text{Si}^{4+}$  (1.8, 0.026 nm). Thus, the ability of proton release is weaker than that of  $\text{Ta}_2\text{O}_5$ -supported  $\text{H}_3\text{PW}_{12}\text{O}_{40}$  composite.

## Conclusions

The present work demonstrated a novel POM-containing environmentally friendly solid acid composite catalyst,  $\text{H}_3\text{PW}_{12}\text{O}_{40}/\text{Ta}_2\text{O}_5$ . The composite exhibited significantly high catalytic activity, selectivity and stability towards biodiesel production under mild conditions. The excellent catalytic performance of the as-prepared composite catalyst is mainly attributed to stronger acid sites of the composites than homogeneous  $\text{H}_3\text{PW}_{12}\text{O}_{40}$  or  $\text{Ta}_2\text{O}_5$  owing to the strong interaction of Keggin units and surface hydroxyl groups of  $\text{Ta}_2\text{O}_5$ ; additionally, the unique surface physicochemical properties of the composite, including larger three-dimensionally interconnected pore, larger BET surface area, high porosity, uniform pore diameter and homogeneous dispersion of the Keggin unit throughout the composite, played an important role in this enhanced catalytic activity.

## Acknowledgements

This work is supported by the Program of New Century Excellent Talents in University (NCET-04-0311), the Key Project of Chinese Ministry of Education (No. 308008), the Program for Changjiang Scholars and Innovative Research Team in University, and Analysis and Testing Foundation of Northeast Normal University.

## References

- M. Zong, Z. Duan, W. Lou, T. J. Smith and H. Wu, *Green Chem.*, 2007, **5**, 434.
- A. A. Kiss, A. C. Dimian and G. Rothenberg, *Adv. Synth. Catal.*, 2006, **348**, 75.
- M. J. Haas, K. M. Scott, T. L. Alleman and R. L. McCormick, *Energy Fuels*, 2001, **15**, 1207.
- A. K. Agarwal and L. M. Das, *Trans. ASME*, 2001, **123**, 440.
- E. Lotero, Y. Liu, D. E. Lopez, K. Suwannakarn, D. A. Bruce and J. G. Goodwin, Jr., *Ind. Eng. Chem. Res.*, 2005, **44**, 5353.
- L. Bournay, D. Casanave, B. Delfort, G. Hillion and J. A. Chodorge, *Catal. Today*, 2005, **106**, 190.
- A. J. Kinney and T. E. Clemente, *Fuel Process. Technol.*, 2005, **86**, 1137.
- M. L. Granados, M. D. Zafra Poves, D. M. Alonso, R. Mariscal, F. C. Galisteo, R. Moreno-Tost, J. Santamaría and J. L. G. Fierro, *Appl. Catal., B*, 2007, **73**, 317.
- N. A. Zafropoulos, H. L. Ngo, T. A. Foglia, E. T. Samulski and W. Lin, *Chem. Commun.*, 2007, 3670.
- S. Al-Zuhair, *Biofuels, Bioprod. Bioref.*, 2007, **1**, 57.
- G. J. Suppes, M. A. Dasari, E. J. Doskocil, P. J. Mankidy and M. J. Goff, *Appl. Catal., A*, 2004, **257**, 213.
- H. Fukuda, A. Kondo and H. Noda, *J. Biosci. Bioeng.*, 2001, **92**(5), 405.
- C. R. V. Reddy, R. Oshel and J. G. Verkade, *Energy Fuels*, 2006, **20**, 1310.
- W. Xie and X. Huang, *Catal. Lett.*, 2006, **107**, 53.
- G. Arzamendi, I. Campo, E. Arguiñarena, M. Sánchez, M. Montes and L. M. Gandía, *Chem. Eng. J.*, 2007, **134**, 123.
- M. L. Granados, M. D. Zafra Poves, D. Martín Alonso, R. Mariscal, F. Cabello Galisteo, R. Moreno-Tost, J. Santamaría and J. L. G. Fierro, *Appl. Catal., B*, 2007, **73**, 317.
- H. J. Kim, B. S. Kang, M. J. Kim, Y. M. Park, D. K. Kim, J. S. Lee and K. Y. Lee, *Catal. Today*, 2004, **315**, 93.
- T. Ebiura, T. Echizen, A. Ishikawa, K. Murai and T. Baba, *Appl. Catal., A*, 2005, **283**, 111.
- M. Di Serio, M. Cozzolino, M. Giordano, R. Patrono and E. Santacesaria, *Ind. Eng. Chem. Res.*, 2007, **46**, 6379–6384.
- M. G. Kulkarni, R. Gopinath, L. C. Meher and A. K. Dalai, *Green Chem.*, 2006, **8**, 1056.
- Isa K. Mbaraka, D. R. Radu, V. S.-Y. Lin and B. H. Shanks, *J. Catal.*, 2003, **219**, 329.
- Isa K. Mbaraka and B. H. Shanks, *J. Catal.*, 2005, **229**, 365.
- T. Okuhara, *Chem. Rev.*, 2002, **102**, 3641.
- D. E. Lopez, K. Suwannakarn, D. A. Bruce and J. G. Goodwin Jr., *J. Catal.*, 2007, **247**, 43.
- W. M. Van Rhijn, D. E. De Vos, B. F. Sels, W. D. Bossaert and P. A. Jacobs, *Chem. Commun.*, 1998, 317.
- M. A. Harmer, W. E. Farneth and Q. Sun, *Adv. Mater.*, 1998, **10**, 1255.
- M. A. Harmer and Q. Sun, *Appl. Catal., A*, 2001, **221**, 45.
- G. D. Yadav and J. J. Nair, *Microporous Mesoporous Mater.*, 1999, **33**, 1.
- P. Morin, B. Hamad, G. Sapaly, M. G. Carneiro Rocha, P. G. Pries deOliveira, W. A. Gonzalez, E. Andrade Sales and N. Essayem, *Appl. Catal., A*, 2007, **330**, 69.
- I. V. Kozhevnikov, *Appl. Catal., A*, 2003, **256**, 3.
- K. Narasimharao, D. R. Brown, A. F. Lee, A. D. Newman, P. F. Siril, S. J. Tavener and K. Wilson, *J. Catal.*, 2007, **248**, 226.
- F. Chai, F. Cao, F. Zhai, Y. Chen, X. Wang and Z. Su, *Adv. Synth. Catal.*, 2007, **349**, 1057.
- P. M. Rao, A. Wolfson, S. Kababya, S. Vega and M. V. Landau, *J. Catal.*, 2005, **232**, 210.
- M. J. Verhoeft, P. J. Kooyman, J. A. Peters and H. van Bekkum, *Microporous Mesoporous Mater.*, 1999, **27**, 365.
- B. Samaranch, P. R. Piscina, G. Clet, M. Houalla, P. Gélin and N. Homs, *Chem. Mater.*, 2007, **19**, 1445.
- T. Ushikubo and K. Wada, *Appl. Catal.*, 1990, **67**, 25.
- E. Garrone, R. Chiappetta, G. Spoto, P. Uglienzo, A. Zecchina and E. Fajula, *Proceedings from the Ninth International Zeolite Conference*, 1993, vol II, p. 267.
- Y. Guo, K. Li and J. H. Clark, *Green Chem.*, 2007, **9**, 839.
- Y. Guo, K. Li, X. Yu and J. H. Clark, *Appl. Catal., B*, DOI: 10.1016/j.apcatb.2007.12.020.
- S. Jiang, Y. Guo, C. Wang, X. Qu and L. Li, *J. Colloid Interface Sci.*, 2007, **208**, 208.
- A. D. Newman, A. F. Lee, K. Wilson and N. A. Young, *Catal. Lett.*, 2005, **102**, 45.
- Y. Chen, J. L. G. Fierro, T. Tanaka and I. E. Wachs, *J. Phys. Chem. B*, 2003, **107**, 5243.
- E. Lopez-Salinas, J. G. H. -Cortez, I. Schifter, E. Torres-Garcia, J. Navarrete, A. Gutierrez-Carrillo, T. Lopez, P. P. Lottici and D. Bersani, *Appl. Catal., A*, 2000, **193**, 215.
- B. Lee, T. Yamashita, D. Lu, Junko N. Kondo and K. Domen, *Chem. Mater.*, 2002, **14**, 867.
- S.-S. Kim, T. R. Pauly and T. J. Pinnavaia, *Chem. Commun.*, 2000, 835.
- L. Li, Q. Wu, Y. Guo and C. Hu, *Microporous Mesoporous Mater.*, 2005, **87**, 1.
- D. Kumar and C. C. Landry, *Microporous Mesoporous Mater.*, 2007, **98**, 309.
- S. M. Kumbar, *J. Mol. Catal. A: Chem.*, 2006, **256**, 324.

# Cellulose triacetate oligomers exhibit high solubility in dense CO<sub>2</sub>†

Lei Hong,<sup>\*a,b</sup> Matthew Fisher,<sup>b</sup> Robert Enick<sup>\*b,c</sup> and Eric Beckman<sup>b</sup>

Received 16th January 2008, Accepted 9th May 2008

First published as an Advance Article on the web 12th June 2008

DOI: 10.1039/b800812d

Cellulose triacetate (CTA) is CO<sub>2</sub>-insoluble primarily due to its crystallinity, but oligomers of CTA have been shown to be highly CO<sub>2</sub>-soluble. These oligomers were generated *via* the pivalolysis of high molecular weight CTA. The resultant mixture of oligomers was fractionated with organic solvents, and the CO<sub>2</sub>-solubility of the each fraction was determined at 300 K. The fluid phase behavior of mixtures containing CO<sub>2</sub> and oligo-CTA composed of one to four per-acetylated monosaccharide repeat units was determined over the 0.1–5 wt% oligo-CTA range. In this concentration range, only bubble points were observed for the monomer. Both bubble points and dew points were observed for the dimer, trimer and tetramer. At a concentration of 5 wt% of oligo-CTA, two-phase pressures of 6.14, 7.38, 9.51 and 13.24 MPa were measured for the monomer, dimer, trimer and tetramer, respectively.

## Introduction

The inexpensive, non-toxic, non-flammable nature of supercritical carbon dioxide (scCO<sub>2</sub>) has led to the exploration of its use in many processes of both laboratory and industrial scale in order to replace hazardous organic solvents. Numerous successful applications of scCO<sub>2</sub> have been found in the areas of supercritical fluid extraction,<sup>1–5</sup> supercritical fluid chromatography,<sup>6,7</sup> reaction engineering,<sup>8–10</sup> injection modeling and extrusion,<sup>11</sup> particle formation,<sup>12–14</sup> electronic chip manufacturing,<sup>15,16</sup> dry cleaning,<sup>17</sup> sand binder,<sup>18</sup> and polymerization.<sup>19,20</sup> A significant technical barrier to the use of CO<sub>2</sub> in even more applications is the low solubility of many high molecular weight and/or polar compounds in this feeble solvent, and the limited availability of inexpensive CO<sub>2</sub>-philic ligands that can be used to enhance the solubility of compounds in scCO<sub>2</sub>. For example, many biologically derived materials are highly polar and thus exhibit very low solubility in liquid and supercritical CO<sub>2</sub>. Although highly CO<sub>2</sub>-philic moieties, such as polyfluoroacrylates and polyfluoroethers, have been used to generate CO<sub>2</sub>-soluble compounds, the inherent disadvantages of the fluororous materials include high cost and poor environmental degradability. Therefore, it is highly desirable to discover lower cost environmentally benign compounds that have the potential to be incorporated as the CO<sub>2</sub>-philic segments of CO<sub>2</sub>-soluble surfactants, dispersants, chelating agents and co-polymers.

Raveendran and Wallen suggested that acetylation of polyhydroxyls, such as carbohydrates, is an excellent method for

making these compounds highly CO<sub>2</sub>-philic.<sup>21,22</sup> Although CO<sub>2</sub> has a zero dipole moment, it is a charge-separated molecule with a non-zero bond dipole moment, which results in a significant quadrupole moment.<sup>23–25</sup> The solvation power of CO<sub>2</sub> is attributed to this large quadrupole moment. The quadrupolar charge separation results in a partial positive charge on the carbon and partial negative charges on the electronegative oxygens, therefore CO<sub>2</sub> can act as a Lewis acid and a Lewis base, as shown in Fig. 1.<sup>21,26,27</sup> This interaction provided approximately 0.5 kcal mol<sup>-1</sup> additional stabilization energy.<sup>28</sup>

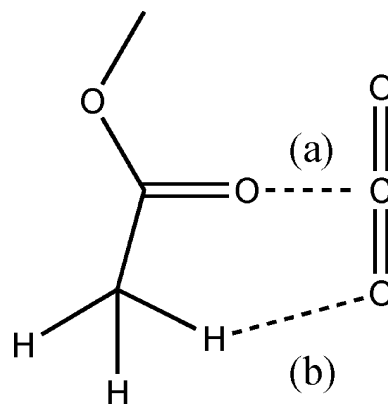


**Fig. 1** Schematic diagram of interactions between CO<sub>2</sub> and CO<sub>2</sub>-philic group, (a) CO<sub>2</sub> as a Lewis acid (C=O...C<sub>CO<sub>2</sub></sub>); (b) CO<sub>2</sub> acts as a Lewis base (C–H...O<sub>CO<sub>2</sub></sub>).

Our *ab initio* molecular simulation studies demonstrated that the ether or ester oxygens in the side chain are as important as the carbonyl oxygens in facilitating CO<sub>2</sub>-philicity.<sup>29</sup> Three different optimized binding modes were identified through optimizations, as shown in Fig. 2, in which isopropyl acetate (IPA) was used to model a single poly(vinyl acetate) repeat unit. The large red spheres, large grey spheres and small white spheres represent oxygen atoms, carbon atoms and hydrogen atoms, respectively. The dashed lines denote the interaction points between two

<sup>a</sup>Department of Chemistry, University of Pittsburgh, 613 Chevron Science Center, 219 Parkman Avenue, Pittsburgh, PA, 15260, USA

<sup>b</sup>Department of Chemical and Petroleum Engineering, University of Pittsburgh, 1249 Benedum Hall, Pittsburgh, PA, 15261, USA

<sup>c</sup>US DOE NETL IAES Resident Fellow, 626 Cochran Mill Rd., Pittsburgh, PA, 15236-0940, United States

† Electronic supplementary information (ESI) available: Fig. A. MALDI spectrum of pivalolysis products of CTA after 48 hours. See DOI: 10.1039/b800812d



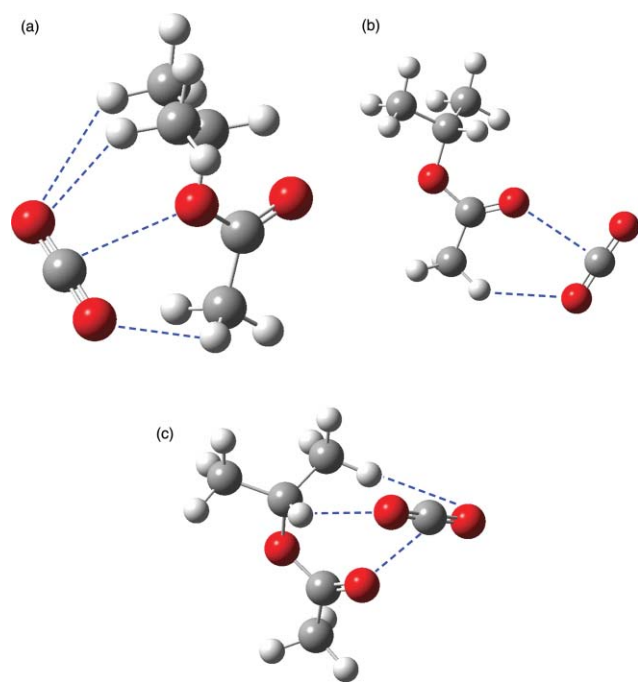


**Fig. 2** Favorable binding geometries for the isopropyl acetate (IPA)/CO<sub>2</sub> complex through *ab initio* calculations; (a) is ether oxygen/CO<sub>2</sub> binding; (b) and (c) are carbonyl oxygen/CO<sub>2</sub> binding.<sup>29</sup>

molecules. The interaction energies are  $-14.8 \text{ kJ mol}^{-1}$  for ether oxygen binding shown in Fig. 2(a), and  $-14.2$  and  $-15.9 \text{ kJ mol}^{-1}$ , for the carbonyl oxygen binding shown in Fig. 2b and 2c, respectively.

As one of the most common biologically produced materials, saccharides are not only found in starch, glycogen and cellulose, but also used in a number of industrial applications, such as fibers, films, adhesives, thickeners, gellants, emulsifiers, drug delivery agents and delivery systems of many commercial products. Saccharides are usually classified by the number of saccharide units they contain, such as mono-, di-, tri-, tetra-, oligo- and polysaccharides. Produced from biological compounds, saccharides are generally renewable, non-toxic and biodegradable. A preliminary study has found that some acetylated mono- and di-saccharides exhibited remarkably high solubility in CO<sub>2</sub>. The combination of the environmentally friendly features of saccharides and CO<sub>2</sub> will promisingly open numerous doors in designing processes based on green chemistry and engineering.<sup>30</sup>

Raveendran and Wallen studied the solubility of three sugar acetates in liquid and supercritical CO<sub>2</sub>.  $\beta$ -forms of 1,2,3,4,6-pentacetyl-D-glucose (BGLU) melted in CO<sub>2</sub> at about 55.9 bar and 296 K. This melting point depression reflects the strong affinity between the solvent CO<sub>2</sub> and the solute BGLU.  $\alpha$ -forms of 1,2,3,4,6-pentacetyl-D-glucose (AGLU) exhibited a lower deliquescence point than that of BGLU by approximate 6–7 bar, while the third sugar, 1,2,3,4,6-pentacetyl  $\beta$ -D-galactose (BGAL), does not exhibit this behavior. All of the per-acetylated sugar derivatives completely dissolve in liquid and supercritical CO<sub>2</sub> at a high concentration up to 30 wt% under a relatively mild pressure ( $<11 \text{ MPa}$ ).<sup>22</sup>

Our group has studied the phase behavior of various per-acetylated sugar derivatives in CO<sub>2</sub>. The solubility of  $\beta$ -D-galactose pentaacetate in CO<sub>2</sub> was measured at 298 and 313 K, which showed very low bubble points, e.g. 6.34 MPa at 298 K and 5 wt%.<sup>31</sup> A series of peracetylated cyclodextrins (per-acetylated  $\alpha$ -,  $\beta$ -, and  $\gamma$ -cyclodextrin) exhibited high solubility in dense CO<sub>2</sub>. The two phase boundaries of the CO<sub>2</sub>-peracetylated cyclodextrins, below and above the CO<sub>2</sub> critical temperature, were very flat at cyclodextrin concentrations greater than 15 wt%. All these results suggested that the per-acetylated cyclodextrins are highly accessible for favorable Lewis acid:Lewis base interactions with CO<sub>2</sub>.<sup>32</sup> Our group also determined the global phase behavior for a binary mixture of the CO<sub>2</sub>-philic solid  $\beta$ -D-maltose octaacetate (MOA) with carbon dioxide. MOA is a representative compound for acetylated CO<sub>2</sub>-philic compounds that exhibit melting point depression and high solubility in dense CO<sub>2</sub>. In the global pressure vs. temperature phase behavior, a distinguishing feature of this system was the long three-phase VL<sub>1</sub>L<sub>2</sub> line that extends over a range of more than 20 K.<sup>33</sup>

Given the extraordinary solubility of many per-acetylated monosaccharides, disaccharides and cyclodextrins in CO<sub>2</sub>, one might expect that a polymer based on a repeat unit of per-acetylated saccharides, cellulose triacetate, would exhibit a high degree of solubility in CO<sub>2</sub>. Although cellulose triacetate (CTA) ( $M_w = \sim 103\,000 \text{ g mol}^{-1}$ ), a commercially available polysaccharide, can be plasticized in the presence of dense CO<sub>2</sub> as evidenced by a slight softening of the CTA pellets and an increase in their transparency, this per-acetylated polysaccharide was observed to be insoluble in CO<sub>2</sub> over the 298–448 K temperature range at pressures up to 52 MPa.<sup>31</sup> This insolubility may be attributed to the high crystallinity of the high molecular weight CTA, although the very high molecular weight of the CTA may also contribute to its poor solubility in CO<sub>2</sub>.

Having established that per-acetylated monosaccharides (see Fig. 3a),<sup>31</sup> and disaccharides (see Fig. 3b)<sup>33</sup> can exhibit very high solubility in CO<sub>2</sub> while CTA is completely CO<sub>2</sub>-insoluble, we propose that CTA oligomers are promising candidates for inexpensive and environmentally benign compounds with high CO<sub>2</sub>-solubility. The objective of this work was to determine the CO<sub>2</sub> solubility of CTA oligomers, as shown in Fig. 3. If oligo-CTA is CO<sub>2</sub>-soluble, it may serve as a potential CO<sub>2</sub>-philic compound or as the CO<sub>2</sub>-philic portion of amphiphilic compounds designed for enhancing CO<sub>2</sub> as an alternative solvent to common organic solvents. In this study, the isothermal phase behavior of several oligo-CTA + CO<sub>2</sub> mixtures was studied at 300 K.

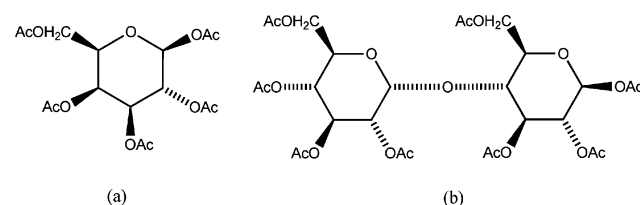


**Fig. 3** A per-acetylated monosaccharide and disaccharide, where  $\text{Ac} = \text{—C(=O)—CH}_3$ , (a)  $\beta$ -D-galactose pentaacetate; (b)  $\beta$ -D-maltose octaacetate (MOA).

**Table 1** Phase equilibrium data for CTA oligomers + CO<sub>2</sub> binary system at 300 K<sup>a</sup>

Oligomer wt% in solution	Monomer	Dimer	Trimer	Tetramer
0.1	—	—	6.52 (B.P.)	6.56 (B.P.)
0.2	—	—	6.56 (B.P.)	6.52 (B.P.)
0.3	—	—	6.58 (B.P.)	—
1	6.14 (B.P.) <sup>b</sup>	6.55 (B.P.)	7.17 (D.P.) <sup>c</sup>	8.14 (D.P.)
2	6.14 (B.P.)	6.58 (B.P.)	8.27 (D.P.)	9.93 (D.P.)
3	6.21 (B.P.)	6.55 (B.P.)	8.55 (D.P.)	11.31 (D.P.)
4	6.10 (B.P.)	7.03 (D.P.)	9.38 (D.P.)	12.13 (D.P.)
5	6.14 (B.P.)	7.38 (D.P.)	9.51 (D.P.)	13.24 (D.P.)

<sup>a</sup> CO<sub>2</sub> vapor pressure at 300K: 6.71 MPa.<sup>35</sup> <sup>b</sup> B.P.: VL bubble point.  
<sup>c</sup> D.P.: L<sub>1</sub>L<sub>2</sub> dew point.

## Results and discussion

The bubble point and dew point data for the four binary mixtures are listed in Table 1 and illustrated in Fig. 4. For the CO<sub>2</sub> + monomer system, only bubble points were observed. A three-phase VL<sub>2</sub>S equilibrium line was identified while a VL<sub>1</sub>L<sub>2</sub> equilibrium line was not observed. The general nature of the corresponding pressure–composition (*P*–*x*) diagram for such systems is illustrated in Fig. 5, the *P*–*x* diagram for solid-supercritical fluid system depicted by McHugh and Krukonic.<sup>34</sup> The small box labeled A within Fig. 5 qualitatively represents the region where the bubble point loci were measured.

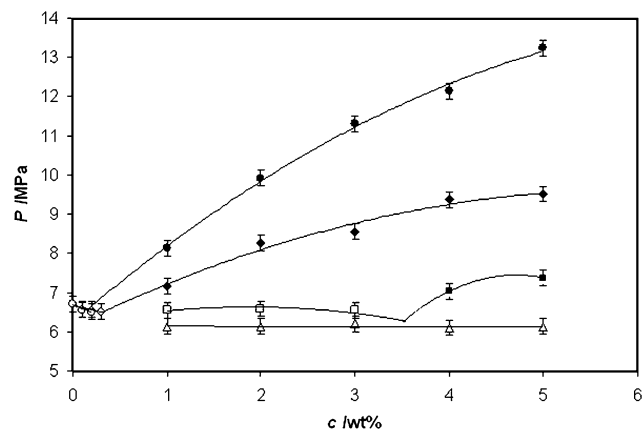


**Fig. 4** Pressure–composition diagram for CO<sub>2</sub> + CTA oligomer system at 300 K.  $\Delta$  represents the monomer's VL bubble point;  $\square$  and  $\blacksquare$  represent the dimer's VL<sub>1</sub> bubble point and L<sub>1</sub>L<sub>2</sub> dew point, respectively;  $\diamond$  and  $\blacklozenge$  represent the trimer's VL<sub>1</sub> bubble point and L<sub>1</sub>L<sub>2</sub> dew point, respectively;  $\circ$  and  $\bullet$  represent the tetramer's VL<sub>1</sub> bubble point and L<sub>1</sub>L<sub>2</sub> dew point, respectively.

The phase behavior of the CO<sub>2</sub> + CTA dimer, CO<sub>2</sub> + trimer, and CO<sub>2</sub> + tetramer systems are consistent with the novel type of phase behavior for solids that melt and dissolve in dense CO<sub>2</sub>.<sup>33</sup> These diagrams are characterized by two three-phase equilibrium lines, VL<sub>1</sub>L<sub>2</sub> and VL<sub>2</sub>S, as shown in Fig. 6. The observation of melting point depression was identified by VL<sub>1</sub>L<sub>2</sub> equilibrium. (L<sub>1</sub> is the CO<sub>2</sub>-rich liquid, L<sub>2</sub> is the CTA-rich liquid.) Both VL<sub>1</sub>L<sub>2</sub> and VL<sub>2</sub>S equilibria were observed in the

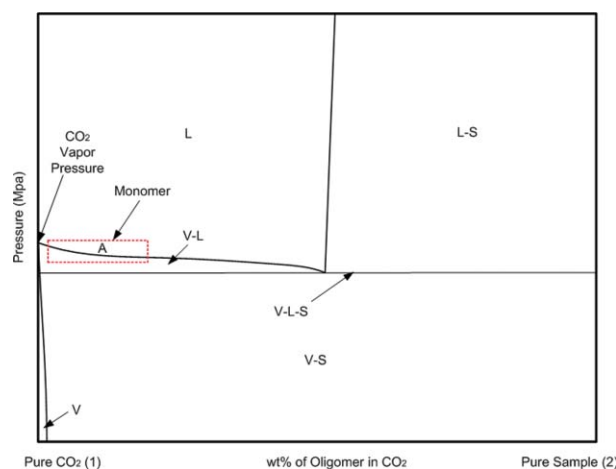


**Fig. 5** General pressure–composition (*P*–*x*) phase diagram for classic sub/supercritical CO<sub>2</sub> + heavy solid system.<sup>34</sup>

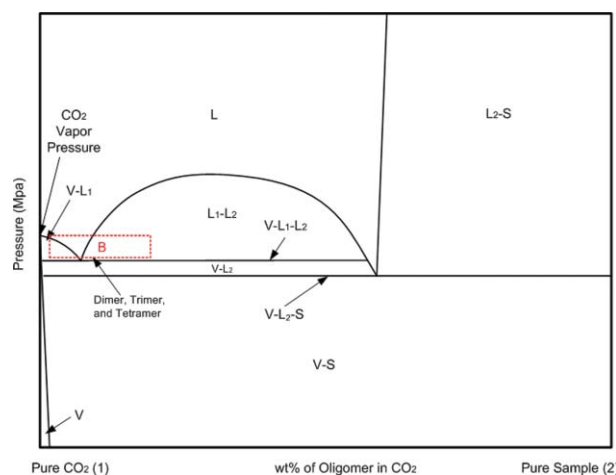


**Fig. 6** General pressure–composition (*P*–*x*) phase diagram for the subcritical CO<sub>2</sub> + CO<sub>2</sub>-philic solid system.<sup>33</sup>

binary mixtures of CO<sub>2</sub> with either the CTA dimer, trimer or tetramer. The dotted-line box “B” within Fig. 6 qualitatively represents the region where the data was collected for the CO<sub>2</sub> + dimer/trimer/tetramer systems. Note that the VL<sub>1</sub> region became smaller as the molecular weight of the oligomer increases from the dimer to the tetramer. Table 2 shows the three phase equilibrium pressure values for all the CO<sub>2</sub> + CTA oligomer mixtures. It is noted that the bubble point pressures in Table 1 are close to the VL<sub>1</sub>L<sub>2</sub> three equilibrium pressures. This is attributed to the small size of VL<sub>1</sub> region and the experimental uncertainty associated with the pressure measurements.

Table 3 lists the solubility data at 5wt% in CO<sub>2</sub> obtained in this work and those of per-acetylated polysaccharides reported

**Table 2** Three phase equilibrium data of all the oligomers at 300 K

	VL <sub>1</sub> L <sub>2</sub> /MPa	VLS/MPa
Monomer	—	5.24
Dimer	6.55	5.07
Trimer	6.58	3.65
Tetramer	6.41	4.48

**Table 3** The miscibility pressures of per-acetylated polysaccharides at the concentration of 5wt% in CO<sub>2</sub> at 298–300 K

Name	MW	# of saccharide rings	Two-phase equil. <i>P</i> at 5 wt% (MPa)	Exp. temp/K	Ref.
CTA monomer	497	1	6.14	300	This work
β-D-Galactose pentaacetate (GPA)	390	1	7.39	298	31
CTA dimer	785	2	7.38	300	This work
β-D-Maltose octaacetate (MOA)	679	2	6.89	298	33
CTA trimer	1073	3	9.51	300	This work
CTA tetramer	1361	4	13.24	300	This work
α-Cyclodextrin octadecaacetate (6-PACD)	1729	6	28	298	32
β-Cyclodextrin heneicosacetate (7-PACD)	2017	7	28.2	298	32
γ-Cyclodextrin tetracosacetate (8-PACD)	2305	8	31	298	32

in the literature, which include galactose pentaacetate, maltose octaacetate, and per-acetylated cyclodextrins. Generally, the miscibility pressures exhibit an increasing trend with increasing number of saccharide rings. The branched pivalate structure leads to a larger molecular weight for CTA oligomers compared to the per-acetylated mono- and disaccharides that have same number of saccharide rings. With one saccharide ring, the CTA monomer exhibited slightly higher solubility compared to that of β-D-galactose pentaacetate. However, the CTA dimer exhibited a slightly lower miscibility than its two-ring per-acetylated analog β-D-maltose octaacetate (MOA) at 5 wt%. At this point, we are unable to provide a convincing explanation for this effect, in that we expected the per-acetylated saccharides to be more CO<sub>2</sub>-soluble than the saccharides with the acetyl groups and *t*-butyl groups for all oligomers.<sup>21,36–38</sup> Perhaps the *tert*-butyl groups reduce the intra-molecular interaction among the CTA monomers, resulting in a lower cohesive energy and consequently higher solubility than β-D-galactose pentaacetate.

Ardnt *et al.* reported many new reactions based on those CTA oligomers.<sup>39</sup> The reactions, although they are not in common use, will offer numerous opportunities for designing and synthesizing novel environmentally acceptable CO<sub>2</sub> soluble materials which will significantly enhance the role of CO<sub>2</sub> as a green alternative to the common organic solvents.

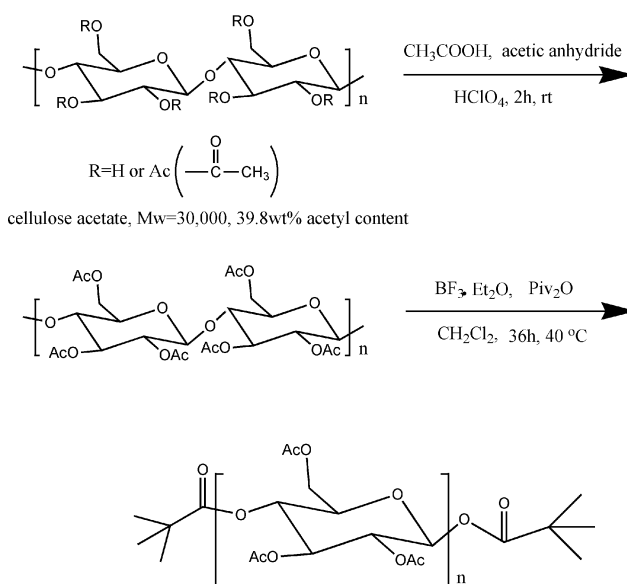
## Experimental

### Materials

Cellulose acetate (39.8 wt% acetyl content, average  $M_n = 30\,000$  (GPC)), anhydrous dichloromethane, boron trifluoride diethyl etherate, and pivalic anhydride were obtained from Aldrich. Acetic acid, perchloric acid, sodium bicarbonate, and silica gel (60–200 mesh) were purchased from J. T. Baker. Acetic anhydride and cyclohexane were obtained from Fisher Scientific. Ethyl acetate was purchased from EMD Chemicals Inc. All the chemicals were used as received without further processing.

### Synthesis of cellulose triacetate (CTA) oligomers

Cellulose acetate was first fully acetylated to form cellulose triacetate. We then employed a recently reported CTA degradation method, pivaloylysis, as shown in Fig. 7,<sup>39</sup> to prepare CTA oligomers. The technique avoids the presence of aggressive acid catalysts widely used in the conventional degradation methods for polysaccharides. Those methods bring severe impacts on

**Fig. 7** Pivaloylysis of cellulose triacetate<sup>39</sup> MW = 288*n* + 186.

environment and lead to more or less undesired degradation products. Pivaloylysis offers a great opportunity to attain short-chain polysaccharides in a milder and efficient way. The products can be easily obtained by common separation methods such as column chromatography and preparative liquid chromatography. More importantly, the pivaloylysis products would have pivalate as the end group rather than a CO<sub>2</sub>-phobic hydroxyl end group.

Cellulose acetate (Aldrich) was first fully acetylated in acetic acid, acetic anhydride and perchloric acid. After washing with sodium hydrogen carbonate solution and pure water alternately, the dried 2,3,6-tri-*O*-acetyl-cellulose was degraded in dichloromethane using pivalic anhydride and boron trifluoride diethyl etherate. The reaction was ended after 48 hours and the oligomeric products were separated by column chromatography using the mixture solvent of cyclohexane and ethyl acetate as the eluent system. Mono-, di-, tri- and tetra- acetylated saccharides were obtained *via* a previously described solvent extraction technique.<sup>40</sup> MALDI-TOF (PerSeptive Voyager STR MS, Center for Molecular Analysis (CMA), Carnegie Mellon University) was performed on the fractions to verify the molecular weight, and therefore number of saccharide rings, in each fraction. As

**Table 4** Melting points of the CTA oligomers

CTA oligomers	Monomer	Dimer	Trimer	Tetramer
Melting Point/°C	63–64	170–173	190–191	206–208

shown in the ESI,<sup>†</sup> although the MW of the oligo-CTA is ( $288n + 186$ ) by calculation, the measured MW values ( $288n + 209$ ) are slightly higher because of the presence of the sodium ion (MW = 23) introduced by the characterization technique. The major peak of the MALDI results for the monomer, dimer, trimer and tetramer agreed with the expected values of 497, 785, 1073 and 1361, respectively. The melting points of the oligomers were measured by a melting point apparatus (Electrothermal<sup>®</sup>) and are listed in Table 4.

### Phase behavior measurement

The phase behavior of the CO<sub>2</sub> + oligo-CTA systems was studied using a non-sampling technique involving isothermal compression and expansion of binary mixtures of known overall composition. Described in detail elsewhere in the literature are the techniques used to obtain dew point and cloud point curves, critical points and three-phase loci for mixtures of CO<sub>2</sub> and polymers<sup>41</sup> or small compounds.<sup>33,42</sup> The pressures for two-phase boundaries were measured three times, with a reproducibility of  $\pm 0.2$  MPa. Three-phase pressures were also recorded three times, with a reproducibility of  $\pm 0.1$  MPa.

### Conclusions

The CO<sub>2</sub>-solubility of CTA oligomers prepared by pivaloyl-ysis was examined. Oligomers with one to four repeat units were fractionated and characterized. Each of these oligomers exhibited remarkably high CO<sub>2</sub> solubility. As expected, as the number of repeat units increased, the pressure required to attain miscibility over the 0.1–5 wt% concentration range also increased. For the CO<sub>2</sub> + dimer, CO<sub>2</sub> + trimer and CO<sub>2</sub> + tetramer systems, the phase diagrams are characterized by VL<sub>1</sub>L<sub>2</sub> and VLS equilibrium lines that are associated with binary systems of CO<sub>2</sub> and CO<sub>2</sub>-philic solids.<sup>33</sup> Cellulose triacetate oligomers may therefore constitute a new group of CO<sub>2</sub>-philic compounds suitable for the design of CO<sub>2</sub>-soluble compounds.

### Acknowledgements

The authors would like to thank the U.S. Environmental Protection Agency Grant EPA-RD-83150401-1 for providing the financial support for this research. US DOE NETL (DE-PS26-04NT15450-0) also supported this project. Many thanks also go to Dr Karl Johnson and Dr Yang Wang. The authors appreciate the kindness of Dr Relich and Dr Pyplo Organisch-Chemisches Institut, Westfälische Wilhelms-Universität Münster, Germany. The authors would also like to acknowledge Dr Mark Bier and Mr Eric Lanni from Carnegie Mellon University for their help in the MALDI experiments.

### References

- 1 E. J. Beckman., *Chem. Commun.*, 2004, (17), 1885–1888.
- 2 S. Stavrouliou and C. Panayiotou, *Chem. Biochem. Eng. Q.*, 2005, **19**(4), 373–381.
- 3 P. Zacchi, J. Daghero, P. Jaeger and R. Eggers, *Braz. J. Chem. Eng.*, 2006, **23**(1), 105–110.
- 4 D. Mongkholkhajornsilp, S. Douglas, P. L. Douglas, A. Elkamel, W. Teppaitoon and S. Pongamphai, *J. Food Eng.*, 2005, **71**(4), 331–340.
- 5 A. Yazdi and D. E. J. Beckman, *Ind. Eng. Chem. Res.*, 1996, **35**, 3644–3642.
- 6 E. Lesellier, C. West and A. Tchaplá, *J. Chromatogr., A*, 2003, **1018**(2), 225–232.
- 7 G. Terflöth, *J. Chromatogr., A*, 2001, **906**(1–2), 301–307.
- 8 R. Glaser and J. Weitkamp, *Ind. Eng. Chem. Res.*, 2003, **42**(25), 6294–6302.
- 9 E. J. Beckman, *Environ. Sci. Technol.*, 2003, **37**(23), 5289–5296.
- 10 P. G. Jessop, T. Ikariya and R. Noyori, *Chem. Rev.*, 1999, **99**, 475–493.
- 11 G. Verreck, A. Decorte, K. Heymans, J. Adriaensen, D. Cleeren, A. Jacobs, D. H. Liu, D. Tomasko, A. Arien, J. Peeters, P. Rombaut, G. Van Den Mooter and M. E. Brewster, *Eur. J. Pharm. Sci.*, 2005, **26**(3–4), 349–358.
- 12 L. Hong, J. Z. Guo, Y. Gao and W. K. Yuan, *Ind. Eng. Chem. Res.*, 2000, **39**(12), 4882–4887.
- 13 R. Thakur and R. B. Gupta, *Ind. Eng. Chem. Res.*, 2005, **44**(19), 7380–7387.
- 14 A. Blasig, C. Shi, R. M. Enick and M. C. Thies, *Ind. Eng. Chem. Res.*, 2002, **41**, 4976–4983.
- 15 R. A. Pai, R. Humayun, M. T. Schulberg, A. Sengupta, J. N. Sun and J. J. Watkins, *Science*, 2004, **303**(5657), 507–510.
- 16 J. M. Blackburn, D. P. Long, A. Cabanas and J. J. Watkins, *Science*, 2001, **294**(5540), 141–145.
- 17 J. M. DeSimone, T. Romack, D. E. Betts and J. B. McClain, Cleaning process using carbon dioxide as a solvent and employing molecularly engineered surfactants, *U. S. Pat.* 5 783 082, 1998.
- 18 L. Hong, E. Fidler, R. Enick and R. Marentis, *J. Supercrit. Fluids*, 2008, **44**(1), 1–7.
- 19 J. M. DeSimone, E. E. Maury, Y. Z. Menciloglu, J. B. McClain, T. J. Romack and J. R. Combes, *Science*, 1994, **265**(15), 356–359.
- 20 T. S. Ahmed, J. M. DeSimone and G. W. Roberts, *Macromolecules*, 2006, **39**(1), 15–18.
- 21 P. Raveendran and S. L. Wallen, *J. Am. Chem. Soc.*, 2002, **124**(42), 12590–12599.
- 22 P. Raveendran and S. L. Wallen, *J. Am. Chem. Soc.*, 2002, **124**(25), 7274–7275.
- 23 M. R. Nelson and R. F. Borkman, *J. Phys. Chem. A*, 1998, **102**(40), 7860–7863.
- 24 S. G. Kazarian, M. F. Vincent, F. V. Bright, C. L. Liotta and C. A. Eckert, *J. Am. Chem. Soc.*, 1996, **118**(7), 1729–1736.
- 25 J. C. Meredith, K. P. Johnston, J. M. Seminario, S. G. Kazarian and C. A. Eckert, *J. Phys. Chem.*, 1996, **100**, 10837–10848.
- 26 T. Tsukahara, Y. Kayaki, T. Ikariya and Y. Ikeda, *Angew. Chem., Int. Ed.*, 2004, **43**, 3719–3722.
- 27 B. Chandrika, L. K. Schnackenberg, P. Raveendran and S. L. Wallen, *Chem.–Eur. J.*, 2005, **11**, 6266–6271.
- 28 M. A. Blatchford, P. Raveendran and S. L. Wallen, *J. Am. Chem. Soc.*, 2002, **124**, 14818–14819.
- 29 S. Kilic, S. Michalick, Y. Wang, J. K. Johnson, R. M. Enick and E. J. Beckman, *Macromolecules*, 2007, **40**, 1332–1341.
- 30 <http://www.polysaccharidecenter.com/>.
- 31 V. K. Potluri, J. Xu, R. M. Enick, E. J. Beckman and A. D. Hamilton, *Org. Lett.*, 2002, **4**(14), 2333–2335.
- 32 V. K. Potluri, A. D. Hamilton, C. F. Karanikas, S. E. Bane, J. Xu, E. J. Beckman and R. M. Enick, *Fluid Phase Equilib.*, 2003, **211**(2), 211–217.
- 33 L. Hong, M. C. Thies and R. M. Enick, *J. Supercrit. Fluids*, 2005, **34**, 11–16.
- 34 M. A. McHugh, V. J. Krukoni, *Supercritical Fluid Extraction, Principle and Practice*, 2nd edn, Butterworth-Heinemann, Boston, 1994.
- 35 <http://webbook.nist.gov/chemistry/fluid/>.
- 36 P. Raveendran, Y. Ikushima and S. L. Wallen, *Acc. Chem. Res.*, 2005, **38**, 478–485.



- 
- 37 P. Raveendran and S. L. Wallen, *J. Phys. Chem. B*, 2003, **107**(6), 1473–1477.
- 38 B. Baradie, M. S. Shoichet, Z. H. Shen, M. A. McHugh, L. Hong, Y. Wang, J. K. Johnson, E. J. Beckman and R. M. Enick, *Macromolecules*, 2004, **37**(20), 7799–7807.
- 39 P. Arndt, K. Bockholt, R. Gerdes, S. Huschens, J. Pyplo, H. Redlich and K. Samm, *Cellulose*, 2003, **10**(1), 75–83.
- 40 P. Arndt, R. Gerdes, S. Huschens, J. Pyplo-Schnieders and H. Redlich, *Cellulose*, 2005, **12**(3), 317–326.
- 41 Z. Shen, M. A. McHugh, J. Xu, J. Belardi, S. Kilic, A. Mesiano, S. Bane, C. Karnikas, E. J. Beckman and R. M. Enick, *Polymer*, 2003, **44**(5), 1491–1498.
- 42 R. M. Enick, E. J. Beckman, A. Yazdi, V. J. Krukonis, H. Schone-mann and J. Howell, *J. Supercrit. Fluids*, 1998, **13**, 121–126.

# Phase equilibria in ternary mixtures of the ionic liquid bmim[BF<sub>4</sub>], (*S*)-naproxen and CO<sub>2</sub> to determine optimum regions for green processing

Eliane Kühne,<sup>a,c</sup> Sabrina Santarossa,<sup>b</sup> Geert-Jan Witkamp<sup>c</sup> and Cor J. Peters<sup>\*a,c</sup>

Received 21st January 2008, Accepted 9th April 2008

First published as an Advance Article on the web 13th May 2008

DOI: 10.1039/b801068d

In order to optimize reaction and separation processes, knowledge of the phase behaviour of the system is of fundamental importance. In this contribution we present the solid–liquid and liquid–vapour equilibria of the ternary system 1-butyl-3-methylimidazolium tetrafluoroborate + (*S*)-naproxen + carbon dioxide. Five different samples were studied, with CO<sub>2</sub> concentrations ranging from 10 to 50 mol%, and pressure and temperature conditions of 1 to 14 MPa, and 310 to 370 K, respectively. It is shown that the amount of CO<sub>2</sub> influences not only the location of the homogeneous liquid phase region, but also the extension of the region in which it occurs. Based on the collected experimental data, optimum pressure and temperature conditions can be selected for the precipitation of (*S*)-naproxen from the ionic liquid in order to improve the efficiency of the separation.

## Introduction

The increasing concern regarding the environment is directing scientists' attention to novel processes based on greener technologies. The quest for atom-efficient synthesis, benign solvents, and sustainable technology combined in highly efficient synthesis–extraction processes is of interest for all types of industry. Particularly, pharmaceutical companies are facing substantial challenges to replace their troublesome processes to more environmentally-friendly ones. For instance, the syntheses of drugs quite often are based on multi-step reactions involving large amounts of organic solvents and generating undesirable by-products as well. The E-factor developed by R. A. Sheldon<sup>1</sup> shows that pharmaceutical companies are the ones producing the most waste, from 25 to 100 kg of waste per kg of product. Part of this waste is the release of volatile organic solvents into the atmosphere.

To reduce the amount of volatile organic solvents (VOSs) used in industry, ionic liquids are emerging as an attractive alternative in synthesis and extraction processes. Ionic liquids are calling attention due to their notable properties like their negligible vapour pressure, the possibility of designing the ionic liquid according to one's need, their non-flammability, large *liquidus* range and high thermal stability, to mention only a few.<sup>2</sup>

Besides ionic liquids, supercritical fluids are also good candidates for replacing VOSs. Among the most studied super-

critical fluids is carbon dioxide: it is cheap, easily available, non-flammable, non-toxic and has mild critical pressure and temperature ( $T_c = 304.25$  K and  $P_c = 7.38$  MPa).<sup>3</sup>

Consequently, it is not surprising that there is an increasing interest in environmentally-benign processes based simultaneously on ionic liquids and supercritical carbon dioxide (scCO<sub>2</sub>). An article published by Blanchard *et al.*<sup>4</sup> is one of the landmarks that showed scientists how profitable a process based on ionic liquids and CO<sub>2</sub> could be. It was shown that when scCO<sub>2</sub> is used to extract compounds from the ionic liquid medium, no detectable amount of ionic liquid will be present in the supercritical phase, *i.e.*, the finally extracted product will be free of any contamination of both the ionic liquid and scCO<sub>2</sub>. Moreover, it is known that ionic liquids can be used as an excellent reaction medium or even act as immobilized catalysts. Furthermore, carbon dioxide can be used to control the number of fluid phases of a system, as well as acting as a solvent to extract the product from the ionic liquid rich phase.

Based on a phenomenon discussed by Gauter *et al.*,<sup>5,6</sup> Scurto *et al.*<sup>7</sup> found that CO<sub>2</sub> could be used to change the miscibility of an ionic liquid with organic solvents. An application of the miscibility switch phenomenon is that reactions can be carried out in a single phase and products can be extracted from the heterogeneous system.

Recently, Kroon *et al.*<sup>8</sup> showed that it is possible to perform reactions in ionic liquids and extract the products with very high purity using supercritical carbon dioxide. This combined approach offers unique advantages: there is no solvent release into the atmosphere, both the ionic liquid and CO<sub>2</sub> can be recycled during the process, recovery of the product is easily done by simply decreasing the pressure and the product is obtained without any contamination by the solvent and/or the catalyst.

This significant finding encouraged various groups to investigate in more detail systems with carbon dioxide and ionic

<sup>a</sup>Delft University of Technology – Faculty of Applied Sciences (DelftChemTech), Laboratory of Physical Chemistry and Molecular Thermodynamics, Julianalaan 136, 2628, BL, Delft, The Netherlands. E-mail: c.j.peters@tudelft.nl

<sup>b</sup>University of Trieste – Department of Chemical, Environmental and Raw Materials Engineering of the University of Trieste (DICAMP), Piazzale Europa 1, 34127, Trieste, Italy

<sup>c</sup>Delft University of Technology – Faculty of Mechanical, Maritime and Materials Engineering, Laboratory for Process Equipment, Leeghwaterstraat 44, 2628, CA, Delft, The Netherlands

liquids as the major constituents, both experimentally and theoretically.<sup>9–11</sup>

In order to replace an existing synthesis of pharmaceutical compounds by an ionic liquid–CO<sub>2</sub> based process, knowledge of the phase behaviour is of crucial importance. This is especially the case when there is an interest in applying the miscibility switch phenomenon, as identification of the location of homogeneous and heterogeneous regions is necessary to select optimum pressure and temperature conditions for the process.

Therefore, in this study we present the phase behaviour of ternary mixtures of 1-butyl-3-methylimidazolium tetrafluoroborate (bmim[BF<sub>4</sub>]), (*S*)-naproxen (Fig. 1) and carbon dioxide. This work is the initial part of a more complex and extensive study which includes the complete synthesis followed by extraction of the product from the ionic liquid medium. Based on the experimental data obtained in this work, the pressure and temperature conditions can be selected for optimum efficiency of extraction of the solute by precipitation from the ionic liquid phase.

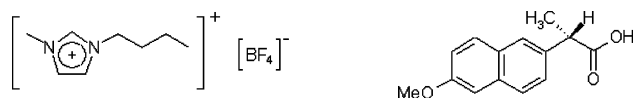


**Fig. 1** Molecular structure of the ionic liquid bmim[BF<sub>4</sub>] and the solute (*S*)-naproxen.

(*S*)-(+)-2-(6-Methoxy-2-naphthyl)propionic acid (in this article referred to as (*S*)-naproxen) is a widely used non-steroidal anti-inflammatory drug (NS-AID). Recent research suggests that some NS-AIDs can be also used for cancer prevention,<sup>12</sup> which might increase its production. Therefore, improving the synthesis of this compound will not only contribute to the benefit of health conditions of our society, but also offers enormous advantages for environmental protection.

## Experimental

### Materials

The following chemicals were used in this work:

—bmim[BF<sub>4</sub>]: 1-Butyl-3-methylimidazolium tetrafluoroborate was synthesized in our facilities according to a known procedure.<sup>13</sup> Water content was determined by Karl–Fischer analysis to be as high as 350 ppm, and the ionic liquid was stored in a desiccator under vacuum conditions with phosphorous pentoxide.

—Carbon dioxide: carbon dioxide was purchased from Hoek-Loos B.V., with 99.995% purity.

—(*S*)-Naproxen: the solute (*S*)-naproxen (CAS number: 22204-53-1, melting point = 427.6 K<sup>15</sup>) was purchased from TCI Europe nv with minimum purity of 99%, and used as received.

### Equipment

Solid–liquid and liquid–vapour boundaries were measured by a synthetic method with the Cailletet apparatus. In this apparatus phase changes can be observed visually. Operational temperatures are from 278 to 368 K, and pressure is limited to a maximum of 14.0 MPa.

This equipment basically consists of a thick-walled Pyrex glass-tube closed at one end, where a sample of known overall composition is confined. A stainless steel ball moved up and down by two reciprocating magnets to stir the sample. The open end of the tube is mounted into an autoclave, where mercury is used as a sealing fluid to the sample, as well as pressure transmitting fluid from a pressure generating system. The Cailletet tube is surrounded by a heat-transferring fluid, which circulates in a glass jacket. The thermostat liquid (water) ensures that during measurements, the temperature of the sample is constant at a desired value. The platinum resistance thermometer is mounted close to the top of the Cailletet tube and the temperature is measured with a maximum error of  $\pm 0.02$  K.

After setting the temperature, pressure is varied by means of a dead weight pressure gauge until the last crystal (for solid–liquid equilibria) or the last bubble (for liquid–vapour equilibria) disappears. The accuracy of the pressure measurements is  $\pm 0.03\%$  of the reading.

A scheme of the Cailletet apparatus with the Cailletet tube is depicted in Fig. 2.

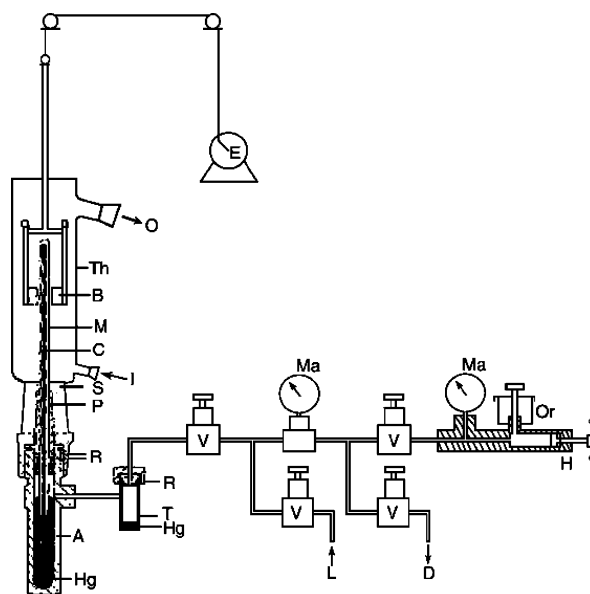


**Fig. 2** The Cailletet apparatus. Legend: A, autoclave; B, magnets; C, capillary glass tube; D, drain; E, motor; H, rotating hand pump; Hg, mercury; I, thermostat liquid in; L, line to dead weight pressure gauge; M, mixture being investigated; Ma, manometers; O, thermostat liquid out; Or, hydraulic oil reservoir; P, closing plug; R, Viton-O-rings; S, silicone rubber stopper; T, mercury trap; Th, glass thermostat; V, valve.

### Sample preparation

To prepare the sample, a known amount of bmim[BF<sub>4</sub>] was inserted into the Cailletet tube with a micro-syringe. (*S*)-Naproxen was then added to the ionic liquid inside the tube in the form of pellets, aiming a constant composition of 5 mol% relative to the ionic liquid.

The tube containing bmim[BF<sub>4</sub>] and (*S*)-naproxen was then connected to the equipment in which degassing of the mixture is carried out, ensuring that no other gas was present in the sample.

Even in small amounts, presence of other gasses could lead to significant errors during the measurements.

After degassing of the sample, carbon dioxide was added volumetrically to the tube according to a desired concentration.

The tube, now containing the three components, was sealed with mercury and mounted into the Cailletet equipment. Pressure and temperature measurements were taken for each phase transition, respecting the limitations of the equipment, *i.e.* up to 14 MPa for the pressure and temperatures between 310 and 370 K.

This procedure was repeated for five samples in a concentration range of CO<sub>2</sub> in the ternary system varying from 10 to 50 mol%.

## Results and discussions

Experimental data collected for solid–liquid and liquid–vapour transitions in the ternary system bmim[BF<sub>4</sub>] + (*S*)-naproxen + CO<sub>2</sub> are given in Table 1. As mentioned in the previous section, the concentration of the solid solute was kept at an approximate concentration of 5 mol% in bmim[BF<sub>4</sub>] at a carbon dioxide-free basis. The CO<sub>2</sub> concentration in the ternary system varied from

10 to 50 mol%, respecting the pressure limitations of the Cailletet apparatus.

The location of the homogeneous liquid (L) region, the heterogeneous solid-liquid (S + L) and liquid–vapour regions (L + V) are represented in Fig. 3. This Figure applies for the sample of the ternary system with 39.98 mol% of CO<sub>2</sub>.

To facilitate interpretation and allow comparison of the effect of increase in CO<sub>2</sub> concentration in each sample, Fig. 4 illustrates the data comprised in Table 1 in a pressure *versus* temperature diagram.

From this Figure, it is possible to notice that a concurrent effect arises from the increase of the carbon dioxide molar fraction in the system. As expected, the higher the concentration of CO<sub>2</sub> in the ternary system, the higher the pressure needed to completely dissolve it in the mixture bmim[BF<sub>4</sub>] + (*S*)-naproxen. This effect results in a shift of the L + V boundaries up to higher pressures. Earlier investigations from our group showed similar behaviour for CO<sub>2</sub> solubility in a ternary system with other organic compounds.<sup>13</sup>

By adding CO<sub>2</sub> to the ternary system the solid–liquid boundary shifts to lower temperatures. In this case, the higher the concentration of CO<sub>2</sub>, the lower is the temperature needed

**Table 1** Experimental data for solid–liquid and liquid–vapour boundaries in the ternary system bmim[BF<sub>4</sub>] + (*S*)-naproxen + CO<sub>2</sub>.  $x_{\text{CO}_2}$ : molar fraction of CO<sub>2</sub> in the ternary system;  $x_{(\text{S})\text{-nap CO}_2\text{-free}}$ : molar fraction of (*S*)-naproxen in bmim[BF<sub>4</sub>]

$x_{\text{CO}_2}$	$x_{(\text{S})\text{-nap CO}_2\text{-free}}^a$	Transition	$P/\text{MPa}$	$T/\text{K}$	$P/\text{MPa}$	$T/\text{K}$
0.1071	0.0495	L + V → L	1.233	328.28	1.773	353.24
			1.327	333.32	1.892	358.24
			1.432	338.30	2.012	363.29
			1.543	343.28	2.133	368.30
			1.658	348.27		
		S + L → L	1.398	321.91	5.899	320.62
			2.398	321.62	7.400	320.86
			3.898	321.07	10.899	320.74
			4.899	320.80	11.899	320.88
0.2048	0.0520	L + V → L	2.238	317.80	3.985	354.89
			2.691	328.53	4.185	358.57
			3.051	336.27	4.501	364.52
			3.419	343.90	4.691	367.86
			3.686	349.11		
		S + L → L	2.356	317.52	4.057	317.86
			3.057	317.62	5.056	317.86
0.3093	0.0497	L + V → L	3.965	319.24	6.810	351.70
			4.450	325.10	7.525	358.79
			5.175	333.77	8.055	363.9
			5.815	340.84	8.559	368.68
			6.055	317.18	9.053	317.36
		S + L → L	4.055	316.72	8.053	317.34
			6.055	317.30	10.053	317.49
			7.055	317.31		
0.3998	0.0554	L + V → L	6.019	318.33	10.411	348.14
			6.919	325.18	11.803	355.9
			8.156	334.19	13.139	362.94
			9.111	340.38		
			10.055	315.11	10.053	315.88
		S + L → L	7.055	315.34	11.054	315.99
			8.055	315.58	12.055	316.09
			9.055	315.64		
0.5045	0.0486	L + V → L	9.052	313.01	12.052	313.41
			10.052	313.24	13.052	313.63
			11.052	313.35		
		S + L → L	8.503	313.37	13.363	326.53
			10.072	318.36		

<sup>a</sup> Because the addition of solid was done separately for each sample, it was not possible to keep the ratio (*S*)-naproxen : bmim[BF<sub>4</sub>] constant at 5.0% for all the samples.



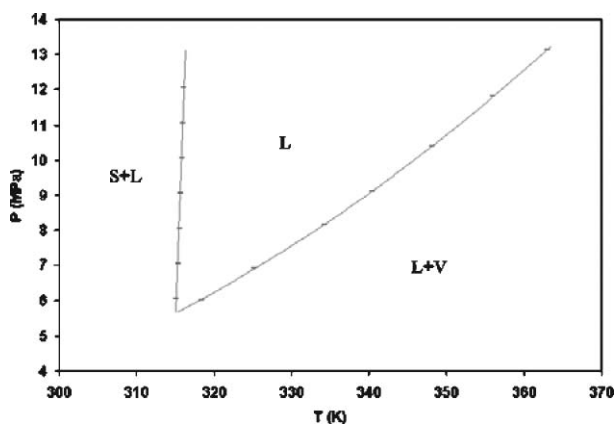


**Fig. 3** Phase diagram for the ternary system  $\text{bmim}[\text{BF}_4] + (S)\text{-naproxen} + \text{CO}_2$ , with a mol fraction of 0.3998  $\text{CO}_2$ . See Table 1 for the numerical values of the experimental data.

to dissolve the solid and to obtain a homogeneous liquid phase.

The combination of both effects as described above, caused the homogeneous L region to shift to higher pressures for higher concentrations of carbon dioxide. Although the shift of the S + L boundary to lower temperatures results in milder temperature conditions to obtain an homogeneous phase and therefore increase the temperature range in which it is found, the effect of  $\text{CO}_2$  concentration is more pronounced for L + V boundaries, resulting in a shrink of the homogeneous L phase in

† There is a considerable scattering in data measured for 10 mol%  $\text{CO}_2$ . This scatter can be explained by the troublesome measurement of solid-liquid boundaries. The visualization of complete disappearance of the solid phase is problematic, especially when the solid phase is present as very fine, disperse particles. For low concentrations of carbon dioxide, the co-solvent effect is less pronounced and the visualization of very fine particles becomes impossible, leading, therefore, to errors.

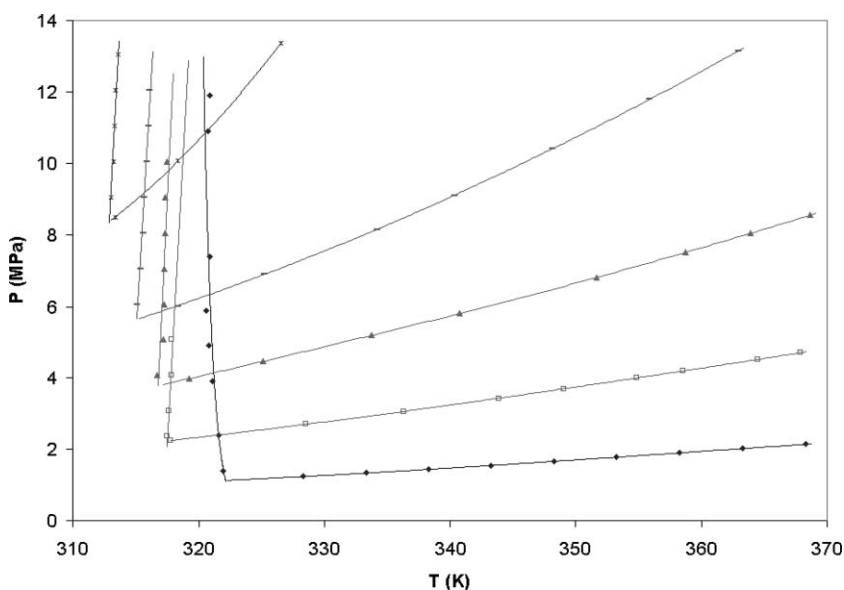


**Fig. 4** Phase diagram for the ternary system  $\text{bmim}[\text{BF}_4] + (S)\text{-naproxen} + \text{CO}_2$ . Isopleths for S + L and L + V boundaries are shown for different concentrations of carbon dioxide. Legend: 10.71 mol%  $\text{CO}_2$  (diamonds), 20.48 mol%  $\text{CO}_2$  (open squares), 30.93 mol%  $\text{CO}_2$  (triangles), 39.98 mol%  $\text{CO}_2$  (dashes) and 50.45 mol%  $\text{CO}_2$  (stars)†

the pressure and temperature range of our study. Therefore, it is expected that at a certain concentration of carbon dioxide higher than 50 mol%, the homogeneous liquid phase will completely disappear. Unfortunately, this effect could not be detected by our experiments due to pressure limitations of the equipment.

In order to demonstrate the effect of  $\text{CO}_2$  concentration on the solubility of (S)-naproxen in  $\text{bmim}[\text{BF}_4]$ , Fig. 5 illustrates the precipitation temperature as a function of the molar fraction of  $\text{CO}_2$  present in the ternary system. To collect data for Fig. 5, the data for each of the S + L boundaries from Table 1 were fitted to a third-degree polynomial curve.

From Fig. 5, the co-solvency effect of supercritical carbon dioxide in the system can be observed: the higher the  $\text{CO}_2$ -concentration, the lower the temperature required to completely

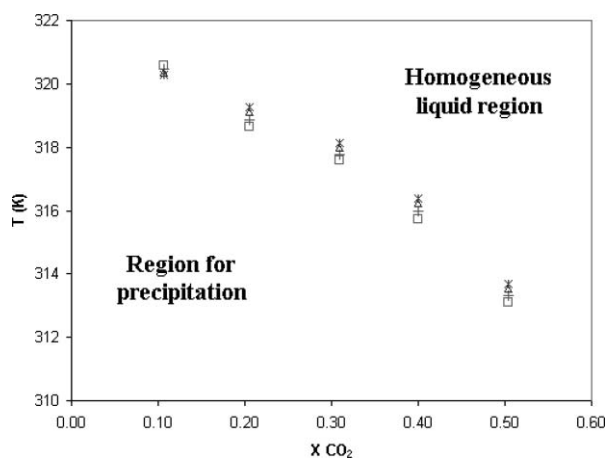


**Fig. 5** Isobars for precipitation of (S)-naproxen in  $\text{bmim}[\text{BF}_4]$  as function of  $\text{CO}_2$  composition in the system. Data was obtained by linear fit of S + L boundaries in Fig. 4. Pressures are 9.5 MPa (squares), 11.0 MPa (crosses), 12.5 MPa (triangles) and 13.5 MPa (stars).

dissolve a fixed amount of (*S*)-naproxen in bmim[BF<sub>4</sub>]<sup>‡</sup>. However, on the other hand it is expected that the isobars will show a minimum for the precipitation temperature at a certain concentration of CO<sub>2</sub>, and with increasing CO<sub>2</sub> concentration, carbon dioxide gradually will start to act as an anti-solvent for (*S*)-naproxen in the ionic liquid, *i.e.*, higher temperatures will be required to completely dissolve (*S*)-naproxen in bmim[BF<sub>4</sub>] with increasing CO<sub>2</sub> composition. This effect was already shown by Shariati *et al.*<sup>14</sup> for a ternary system based on carbon dioxide + 1-propanol + salicylic acid. From this work it became apparent that a change of behaviour of CO<sub>2</sub> from co- to anti-solvent usually occurs at CO<sub>2</sub> mole fractions of about 0.6.

Because higher pressures are necessary to dissolve carbon dioxide in ionic liquids than in some of the most common organic solvents, it was not possible to work in this contribution with concentrations of carbon dioxide above 50 mol%. Therefore, the anti-solvent effect—which is expected to occur above 60 mol% of CO<sub>2</sub>—could not be detected in our system due to pressure limitations.

One additional interesting phenomenon is observed in Fig. 5: for a concentration of 10 mol% of CO<sub>2</sub>, the lowest precipitation temperature is found for the highest pressure (13.5 MPa). For all the other four concentrations of CO<sub>2</sub>, the higher the pressure, the slightly higher the temperature required to precipitate the solid. This effect might have to be ascribed to the scattering of the data for the concentration of 10 mol%, as explained elsewhere in the text.

When separation of (*S*)-naproxen from the ionic liquid is required, supercritical CO<sub>2</sub> extraction is not viable due to the low solubility of (*S*)-naproxen in supercritical CO<sub>2</sub>.<sup>16,17</sup> Although the phase diagrams presented in this work show that CO<sub>2</sub> can be used to precipitate (*S*)-naproxen from bmim[BF<sub>4</sub>], further isolation of the product from the ionic liquid is still a problem to overcome, as been pointed out in other recent studies of anti-solvent crystallization of organic compounds from ionic liquids using carbon dioxide.<sup>8,18</sup>

## Conclusions

In this work the phase behaviour of the ternary system bmim[BF<sub>4</sub>] + (*S*)-naproxen + CO<sub>2</sub> is presented for five different molar fractions of carbon dioxide. It is shown that by adding carbon dioxide to a solution of bmim[BF<sub>4</sub>] and (*S*)-naproxen, the solute (at first poorly soluble in the ionic liquid at normal pressure and temperature conditions) can be completely dissolved by increasing the pressure of the system. Therefore, the amount of dissolved carbon dioxide can be used to switch the

miscibility of the solid solute in the system, allowing the selection of the most convenient operational conditions for reactions (one homogeneous phase) or separations (heterogeneous solid + liquid phase).

From our results it can be seen that an increase of the CO<sub>2</sub> concentration influences the location of the homogeneous liquid phase region as this region shifts rapidly with the CO<sub>2</sub> concentration to higher pressures. This is clearly demonstrated in Fig. 4 where the L + V boundaries shift up to higher pressures, whereas the S + L boundaries are shifted to lower temperatures. As a final result of both effects, the extension of the homogeneous liquid phase is reduced, limiting the pressure and temperature conditions in which one phase is present. Although due to experimental limitations the change of co-solvency into anti-solvency effect with increasing CO<sub>2</sub> concentration in the system could not be observed, it may be expected to occur also in this system.

## Notes

- 1 R. A. Sheldon, *Pure Appl. Chem.*, 2000, **72**(7), 1233–1246.
- 2 P. Wasserscheid and T. Welton, *Ionic Liquids in Synthesis*, 1st edn, Wiley-VCH.
- 3 P. G. Jessop and W. Leitner, *Chemical Synthesis Using Supercritical Fluids*, 1st edn, Wiley-VCH.
- 4 L. A. Blanchard, D. Hâncu, E. J. Beckman and J. F. Brennecke, *Nature*, 1999, **399**, 28–29.
- 5 C. J. Peters and K. Guter, *Chem. Rev.*, 1999, **99**, 419–431.
- 6 K. Guter, C. J. Peters, A. L. Scheidgen and G. M. Schneider, *Fluid Phase Equilib.*, 2000, **171**(1–2), 127–149.
- 7 A. M. Scurto, S. N. V. K. Aki and J. F. Brennecke, *J. Am. Chem. Soc.*, 2002, **124**(35), 10276–10277.
- 8 M. C. Kroon, J. v. Spronsen, C. J. Peters, R. A. Sheldon and G. J. Witkamp, *Green Chem.*, 2006, **8**, 246–249.
- 9 S. Lee, Y. J. Zhang, J. Y. Piao, H. Yoon, C. E. Song, J. H. Choi and J. Hong, *Chem. Commun.*, 2003, **20**, 2624–2625.
- 10 Y. Qin and J. M. Prausnitz, *Ind. Eng. Chem. Res.*, 2006, **45**, 5518–5523.
- 11 Y. S. Kim, W. Y. Choi, J. H. Jang, K.-P. Yoo and C. S. Lee, *Fluid Phase Equilib.*, 2005, **228–229**, 439–445.
- 12 Cornelia M. Ulrich, Jeannette Bigler and John D. Potter, *Nat. Rev. Cancer*, 2006, **6**, 130–140.
- 13 E. Kühne, C. J. Peters, J. v. Spronsen and G. J. Witkamp, *Green Chem.*, 2006, **8**, 287–291.
- 14 A. Shariati and C. J. Peters, *J. Supercrit. Fluids*, 2002, **23**, 195–208.
- 15 C. P. Mora and F. Martínez, *Phys. Chem. Liquids*, 2006, **44**(5), 585–596.
- 16 D. Suleiman, L. A. Estévez, J. C. Pulido, J. E. García and C. Mojica, *J. Chem. Eng. Data*, 2005, **50**(4), 1234–1241.
- 17 S. S. T. Ting, D. L. Tomasko, N. R. Foster and S. J. Macnaughton, *Ind. Eng. Chem. Res.*, 1993, **32**(7), 1471–1481.
- 18 M. C. Kroon, V. A. Toussaint, A. Shariati, L. J. Florusse, J. v. Spronsen, G. J. Witkamp and C. J. Peters, *Green Chem.*, 2008, **10**, 333–336.

<sup>‡</sup> At room temperature and atmospheric pressure, the solubility of (*S*)-naproxen in pure bmim[BF<sub>4</sub>] is lower than 5 mol%, *i.e.*, only a solid-liquid equilibrium is found at the composition studied in this work.

# Studies on the solvent-free and waste-free Knoevenagel condensation

Ronald Trotzki,<sup>a</sup> Markus M. Hoffmann<sup>b</sup> and Bernd Ondruschka<sup>\*a</sup>

Received 30th January 2008, Accepted 16th April 2008

First published as an Advance Article on the web 16th May 2008

DOI: 10.1039/b801661e

The mechanochemical reaction of malononitrile with various aldehydes was studied with the goal to achieve quantitative stoichiometric conversion of the reactants to their corresponding benzylidene-malononitriles in absence of any solvents and catalysts. Besides already known reactions in the solid state, reactions with liquid aldehydes were also attempted. These reactions were carried out in vibration and planetary ball mills as well as, for comparison, in a melt under microwave irradiation. A successful quantitative conversion depended strongly on the choice of the aldehyde, precluding a generalization of the reaction scheme. Furthermore, the results obtained from the various approaches for non-classical heating (ball mills, microwaves) were compared.

## Introduction

There has been a long standing desire in preparative chemistry to avoid waste, to substitute benign chemicals for toxic ones and to use solvent-less reactions. However, improving the energy efficiency of chemical reactions has found much less consideration although the importance of this aspect can be expected to increase considerably given the continuing price increases on the worldwide energy markets. In this regard, there has been an increased interest in an almost forgotten approach to chemical synthesis: mechanochemistry (or often also referred to as tribochemistry), where a number of publications concerning “reactive milling” have appeared in recent years. While mechanochemical processes have played a continued, albeit minor role in inorganic chemistry, they have found essentially no consideration in organic chemistry. It was not until the 1990s that mechanochemical organic reactions on support materials were reported such as, for example, the conversion of aromatic compounds on silica gel and alumina,<sup>1</sup> the halogenation of olefins with HX-silica-gel<sup>2</sup> as well as the oxidation of organic compounds on Al<sub>2</sub>O<sub>3</sub>-KMnO<sub>4</sub>.<sup>3</sup> However, these mechanochemical reactions were often carried out under undefined conditions. Specifically, commercial mills were not used,<sup>2,3</sup> but the components were milled by hand.<sup>1</sup> In many cases the use of quantitative support materials did not achieve quantitative conversion.

Since 2000, the groups of Toda<sup>4</sup> and Kaupp<sup>5</sup> have reported comprehensive work on the stoichiometric conversion of organic compounds in solid-state reactions. The advantages of solvent-less synthesis have thereby been convincingly described.<sup>6,7</sup> Stoichiometric reactions with quantitative yields to the desired final product, carried out in absence of a support material and

a catalyst make the usual work-up step of product isolation unnecessary. Any possible condensation side products like water for example can be easily removed by drying. Thus, it is principally possible to work without solvents and to completely avoid wastes. A multitude of substitution and addition reactions as well as elimination reactions can be carried out with this approach.<sup>5</sup> Reactions can be carried out between a gas and a solid<sup>8</sup> as well as between two solids.<sup>9</sup> As a direct-crystallization process, the latter does not even require any input of external energy.<sup>10</sup> Furthermore, stoichiometric conversion of solids can also be carried out in a melt.<sup>11</sup> The subsequent removal of the frozen product melt usually necessitates the use of solvents, making the chemical synthesis “solvent-free” but not “solvent-less”. However, the resulting solid from a mechanochemical reaction can also be removed from the mill container by mechanical means. For the reader interested to learn more about using mechanochemistry for organic synthesis we refer to the recent review article by Rodríguez *et al.*<sup>12</sup>

In this study we focus on the Knoevenagel reaction, a reaction which has been known just as long (1898) as mechanochemistry.<sup>13,14</sup> The Knoevenagel reaction is a particularly desirable candidate for achieving a quantitative stoichiometric conversion, because the classic conversion of the reactants is conducted under reflux in a mixture of glacial acetic acid and benzene (under separation of water), pyridine and piperidine or methanol and piperidine.<sup>15</sup> The yields are between 50 to maximum 90% necessitating a tedious work-up to obtain the pure product. The group of Kaupp has conducted quantitative stoichiometric Knoevenagel condensation reactions of aldehydes with various methylene components mechanochemically as well as in the melt.<sup>11</sup> Because their work showed only results for a limited number of quantitatively converted aldehydes, there is the open question, can the underlying reaction scheme be generalized to a wider range of aromatic aldehydes under their reaction conditions. To answer this question, ten substituted aldehydes were mechanochemically reacted with malononitrile. Malononitrile was chosen because it is the most reactive methylene component. Kaupp's group carried out reactions with malononitrile only in a melt, heating for one hour

<sup>a</sup>Institute for Technical Chemistry and Environmental Chemistry, Friedrich-Schiller-University, Lessingstr. 12, Jena, Germany.  
E-mail: Bernd.Ondruschka@uni-jena.de; Fax: +49 (0) 3641 948402;  
Tel: +49 (0) 3641 948400

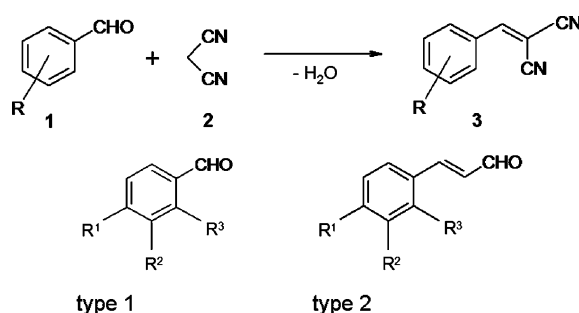
<sup>b</sup>Department of Chemistry, State University of New York College at Brockport, Brockport, USA

under vacuum at 150 °C.<sup>11</sup> Therefore, it was necessary to conduct for comparison the reactions with the chosen aldehydes also in the melt. The melt reactions were also carried out at 150 °C, but under microwave irradiation at ambient pressure. A main motivation for choosing microwave irradiation was the realization that the generated water could condense in colder zones, outside of the microwave irradiated area, and would thus be removed from the chemical equilibrium. Additionally, we have compared using a mill vs. a microwave, two non-classical methods of heating.

## Experimental

### Synthesis details

Ten substituted aldehydes (solid as well as liquid) of type 1 and type 2 were used in the Knoevenagel condensation with malononitrile, as indicated in Scheme 1 and Table 1.



Scheme 1

The stoichiometric reaction mixtures each containing one of the aldehydes listed in Table 1 were generally converted under defined reaction conditions solvent-less and in absence of any catalysts or water absorbing drying agents. The mixtures were reacted in three systems: a monomodal microwave reactor, a vibration ball mill (VM), and a planetary ball mill (PM).

The reactants were directly weighed into the reaction vessel. Since the reaction vessels of the mills exceeded the capacity of the analytical balance, external weighing dishes were used for experiments with the mills. Coarse-grained or crystalline components were ground with a mortar and pestle. The aldehydes **1a**, **1f**, **1h** and **1j** were freshly distilled. All other aldehydes as well as **2** were used as received (Aldrich, Germany) and were of purity >98%.

Table 1 Substituents of the aldehydes used

RCHO	R <sup>1</sup>	R <sup>2</sup>	R <sup>3</sup>	Mp/°C <sup>a</sup>
<b>1a</b>	H	H	H	-26
<b>1b</b>	NO <sub>2</sub>	H	H	104–106
<b>1c</b>	(CH <sub>3</sub> ) <sub>2</sub> N	H	H	71–73
<b>1d</b>	OH	OCH <sub>3</sub>	H	82
<b>1e</b>	H	OCH <sub>3</sub>	OCH <sub>3</sub>	48–52
<b>1f<sup>b</sup></b>	H	H	H	-9
<b>1g</b>	Cl	H	H	44–47
<b>1h</b>	H	H	Cl	9–11
<b>1i</b>	OH	H	H	112–116
<b>1j</b>	H	H	OH	1–2

<sup>a</sup> Melting points were taken from the literature of the chemical supplier (Aldrich). <sup>b</sup> Aldehyde **1f** is of type 2, all others are of type 1.

When weighing the liquid aldehydes, the measuring dishes and eye-dropper were weighed again to determine the delivered amounts of substance by weight difference. Any additionally needed aldehyde was then added drop-wise to the reaction vessels in increments of 20 to 25 mg, depending on density. To establish truly stoichiometric amounts of reactant, the impurity levels were considered in calculating the needed mass amounts. As a microwave system the model Discover, from company CEM, USA, was used with the typical program settings: 1 h/100 W/150 °C. Depending on the behavior of the reaction some microwave programming was modified. A 50 mL round flask with Claisen stillhead (for temperature sensor and pressure balance) was used as a reaction vessel. The Schlenk-curvature of the flask was meant to collect the condensing water from the reaction in the colder zones above the melt. The regulation of power for the microwave irradiation was achieved through a fiber-optic sensor placed directly into the reaction mixture.

The two mills used were the vibration mill MM 301 from company Retsch GmbH, Germany, with 25 mL stainless steel reaction vessels and 5 stainless steel balls of 1.0 cm diameter, and the planetary mill Pulverisette 7 from company Fritsch, Germany, with 45 mL stainless steel reaction vessels and 5 stainless steel balls of 1.5 cm diameter. Unless stated otherwise, the amounts of each reactants were 20 mmol for the PM and 10 mmol for the VM. Each reaction using microwave, VM or PM was repeated, usually with essentially identical results. Additional experiments were conducted if yield deviations were greater than 5%.<sup>†</sup>

### Measurement and analysis details

A meter of brand Energy Check 3000 from company Voltcraft, Germany, was used to measure line power consumption.

<sup>†</sup> **Benzylidene-malononitrile (3a)** <sup>1</sup>H-NMR (DMSO-*d*<sub>6</sub>) δ = 8.53 (s, 1H), 7.92 (d, 2H), 7.64 (m, 3H); <sup>13</sup>C-NMR (DMSO-*d*<sub>6</sub>) δ = 161.46, 134.26, 131.19, 130.39 (2C), 129.41 (2C), 114.08, 113.09, 81.50. **4-Nitrobenzylidene-malononitrile (3b)** <sup>1</sup>H-NMR (DMSO-*d*<sub>6</sub>) δ = 8.70 (s, 1H), 8.39 (d, 2H), 8.14 (d, 2H); <sup>13</sup>C-NMR (DMSO-*d*<sub>6</sub>) δ = 159.25, 149.67, 136.63, 131.40 (2C), 124.33 (2C), 113.56, 112.46, 85.90. **4-Dimethylaminobenzylidene-malononitrile (3c)** <sup>1</sup>H-NMR (DMSO-*d*<sub>6</sub>) δ = 8.03 (s, 1H), 7.81 (d, 2H), 6.84 (d, 2H), 3.09 (s, 6H); <sup>13</sup>C-NMR (DMSO-*d*<sub>6</sub>) δ = 158.80, 154.28, 133.53 (2C), 118.69, 116.19, 115.46, 111.74 (2C), 80.62, 39.91. **4-Hydroxy-3-methoxybenzylidene-malononitrile (3d)** <sup>1</sup>H-NMR (DMSO-*d*<sub>6</sub>) δ = 10.65 (s<sub>broad</sub>, OH), 8.24 (s, 1H), 7.62 (s, 1H), 7.47 (d, 1H), 6.98 (d, 1H), 3.79 (s, 3H); <sup>13</sup>C-NMR (DMSO-*d*<sub>6</sub>) δ = 160.55, 153.85, 147.88, 127.65, 123.05, 116.13, 115.07, 114.31, 113.14, 74.97, 55.54. **2,3-Dimethoxybenzylidene-malononitrile (3e)** <sup>1</sup>H-NMR (DMSO-*d*<sub>6</sub>) δ = 8.49 (s, 1H), 7.57 (d, 1H), 7.37 (d, 1H), 7.26 (d, 1H), 3.86 (s, 3H), 3.84 (s, 3H); <sup>13</sup>C-NMR (DMSO-*d*<sub>6</sub>) δ = 156.45, 152.63, 148.94, 125.04, 124.70, 119.38, 118.94, 114.30, 113.15, 82.97, 61.71, 56.19. **2-(3-Phenyl-allylidene)-malononitrile (3f)** <sup>1</sup>H-NMR (DMSO-*d*<sub>6</sub>) δ = 8.29 (s, 1H), 8.23 (s, 1H), 7.72 (d, 2H), 7.47 (s, 1H), 7.45 (m, 3H); <sup>13</sup>C-NMR (DMSO-*d*<sub>6</sub>) δ = 161.78, 150.83, 133.84, 131.52, 128.97 (2C), 128.87 (2C), 122.27, 113.87, 111.88, 80.70. **4-Chlorobenzylidene-malononitrile (3g)** <sup>1</sup>H-NMR (DMSO-*d*<sub>6</sub>) δ = 8.52 (s, 1H), 7.92 (d, 2H), 7.71 (d, 2H); <sup>13</sup>C-NMR (DMSO-*d*<sub>6</sub>) δ = 159.94, 138.87, 131.96 (2C), 129.90, 129.54 (2C), 113.86, 112.82, 82.08. **2-Chlorobenzylidene-malononitrile (3h)** <sup>1</sup>H-NMR (DMSO-*d*<sub>6</sub>) δ = 8.63 (s, 1H), 7.98 (d, 1H), 7.66 (s, 1H), 7.59 (dd, 2H); <sup>13</sup>C-NMR (DMSO-*d*<sub>6</sub>) δ = 157.31, 134.19, 133.59, 129.70, 129.16, 128.94, 127.32, 112.76, 111.69, 85.92. **4-Hydroxybenzylidene-malononitrile (3i)** <sup>1</sup>H-NMR (DMSO-*d*<sub>6</sub>) δ = 10.42 (s<sub>broad</sub>, OH), 8.26 (s, 1H), 7.84 (d, 2H), 6.96 (d, 2H); <sup>13</sup>C-NMR (DMSO-*d*<sub>6</sub>) δ = 163.92, 160.43, 133.82 (2C), 122.72, 116.59 (2C), 115.04, 114.14, 75.02.



The benzylidene-malononitriles obtained (**3a–3i**) were characterized structurally with  $^1\text{H}$ - and  $^{13}\text{C}$ -NMR in DMSO- $d_6$  on a Bruker A 200 (200 MHz).

The GC examinations were carried out on Hewlett-Packard instruments (FID: series 5890, Mass-selective detector series 5972) using columns HP 5 (30 m, ID  $0.32 \times 0.25$  mm). Temperature program: 3 min isotherm at  $50^\circ\text{C}$ , followed by a temperature ramp of  $8\text{ K min}^{-1}$  to  $320^\circ\text{C}$ . The detector temperature was set to  $300^\circ\text{C}$  and the column inlet pressure was entered as 0.7 bar (10 psi), the split-valve setting was 150 : 1. The entire reaction mixture was dissolved in 2 mL solvent per mmol substance, and  $1\ \mu\text{L}$  of the obtained solution was injected. The retention times of the target products were between 15–25 min. For accurate product yield determination using GC it is important to dissolve the entire final reaction mixture because variations in results were obtained for samples of the reaction mixture taken from the reaction vessel wall, as opposed to the center of the reaction vessel. Such deviations can occur when a reactant sinters at the beginning of the grinding process and adheres to the reaction vessel. Appropriate solvents were THF, DMSO (**3d**, **3e**, **3j**) or DMF (**3c**). It is also important to conduct GC analysis immediately after completion of the conversion since the reaction mixture may continue to react in the solid phase as well as dissolved in the solvent. Yields reported in the literature are mostly based on NMR signal intensities, and it is often not certain how soon after completion of the experiment yields were analyzed. Due to the rather low signal strength, determining yields from NMR measurements are also much less accurate and precise than determining yields by GC, especially for yields  $>97\%$ . These experimental aspects, in evaluating accurate product yields, may explain why some of the yields reported here deviate from values previously reported in the literature.

Other experimental details pertaining to the interpretation and discussion of the results are provided.

## Results and discussion

The Knoevenagel reactions were first studied under microwave irradiation in the melt, where for each reaction a stoichiometric mixture of 20 mmol of each reactant was irradiated for 1 h at  $150^\circ\text{C}$  and ambient pressure using a power setting of 100 W. Nearly quantitative conversions with yields of 95% or higher were obtained only in three cases. As can be seen in Table 2, the yields of the desired products were in some cases even lower than the conversions due to the presence of not further characterized side products.

The reaction of some aldehydes with malononitrile proceeded differently than expected. Aldehyde **1a** condensed under default conditions as an azeotropic mixture with the liberated reaction water outside of the reaction zone, thereby becoming a limiting reagent in the reaction mixture. The yields measured with GC were correspondingly lower. Thus, the synthesis of **3a** was repeated at a lower power setting of 80 W at a set temperature of only  $120^\circ\text{C}$ . However, these reaction conditions proved to be too mild for a successful conversion. After a few seconds of irradiation of reaction mixtures **1i** and **1j** a vigorously exothermic reaction ( $>220^\circ\text{C}$ ) was observed in each case. The mixtures still reacted uncontrollably when conditions were set

**Table 2** Knoevenagel reactions by microwave-assisted melts of aldehydes with malononitrile

RCHO	MW-condition	Conversion <b>1</b> (%) <sup>a</sup>	Yield <b>3</b> (%) <sup>a</sup>
<b>1a</b>	1 h/ $150^\circ\text{C}$ /100 W	83	83
<b>1a</b>	1 h/ $120^\circ\text{C}$ /80 W	12	12
<b>1b</b>	1 h/ $150^\circ\text{C}$ /100 W	95	95
<b>1b</b>	1 h/ $120^\circ\text{C}$ /80 W	91	91
<b>1c</b>	1 h/ $150^\circ\text{C}$ /100 W	43	40
<b>1d</b>	1 h/ $150^\circ\text{C}$ /100 W	97	91
<b>1e</b>	1 h/ $150^\circ\text{C}$ /100 W	92	92
<b>1f</b>	1 h/ $150^\circ\text{C}$ /100 W	95	84
<b>1g</b>	1 h/ $150^\circ\text{C}$ /100 W	97	96
<b>1h</b>	1 h/ $150^\circ\text{C}$ /100 W	98	95
<b>1i</b> <sup>b</sup>	1 h/ $150^\circ\text{C}$ /100 W	—	—
<b>1i</b> <sup>b</sup>	1 h/ $100^\circ\text{C}$ /80 W	—	—
<b>1j</b> <sup>b</sup>	1 h/ $150^\circ\text{C}$ /100 W	—	—
<b>1j</b> <sup>b</sup>	1 h/ $100^\circ\text{C}$ /80 W	—	—

<sup>a</sup> Obtained from GC analysis. <sup>b</sup> No useful material obtained due to uncontrolled reaction.

to  $80\text{ W}/100^\circ\text{C}$ . The resulting solids of red brown to black colors were only slightly soluble or completely insoluble in all common solvents, and a characterization of the products was not pursued. Since Kaupp reports a quantitative reaction for at least **1i**,<sup>11</sup> the condensation reactions of aldehydes **1i** and **1j** were attempted according to procedures from the literature using a conventional pre-heated oil bath at  $150^\circ\text{C}$  and application of vacuum. The obtained yield of **1i** was 92%. However, the liquid reaction mixture with **1j** again reacted vigorously and uncontrollably after an induction period of 35 min resulting in the same insoluble solid substance previously observed under microwave irradiation. Apparently, this aldehyde cannot be used for a thermal conversion. Furthermore, side products were observed for **1c**, **1d**, **1f**, **1g**, and **1h**, whereas **1c** converted only partially. None of the aldehydes in Table 2 were quantitatively converted into the targeted product.

The next series of experiments concern Knoevenagel reactions by mechanochemical conversion using the VM. In consideration of the physical dimension constraints of the reaction vessel of the VM, the stoichiometric reaction mixtures were 10 mmol of each reactant. The reaction vessel of the VM was of screw-type, and it was possible to cool the VM with liquid nitrogen, which would appear to be advantageous. Cooling with liquid nitrogen ensures that aldehydes which are liquid at room temperature also undergo solid–solid reactions with malononitrile. Also, the generated water side product should crystallize out, which should shift the chemical equilibrium towards the product side. A blind test with sodium chloride revealed that after cooling with liquid nitrogen the reaction vessel of the VM reheated to room temperature after 10 min of operation, at maximum setting of 30 Hz due to frictional heating during the grinding process. Thus, for a first series of measurements, the reaction mixtures were cooled with liquid nitrogen before milling with the VM. As one can see from Table 3, while the yield for **3b** was 99%, the yields were much lower for the other entries, 5% for example for **3a**. Thus, freezing with liquid nitrogen did not offer any improvement for reactions with the liquid aldehydes.

Besides pure mechanical effects and the associated heating of the system, mechanochemical activation for example through the formation of triboplasma<sup>16</sup> needs to be considered during

**Table 3** Knoevenagel reactions of aldehydes with malononitrile using a vibration mill (10 min/30 Hz)

RCHO	Yield <b>3</b> (%)
<b>1a</b>	5
<b>1b</b>	99
<b>1c</b>	2
<b>1d</b>	5
<b>1e</b>	2
<b>1f</b>	13
<b>1g</b>	7
<b>1h</b>	15
<b>1i</b>	51
<b>1j</b>	23

the milling process. Therefore, the default settings were changed for additional experiments with the VM. The reaction time was increased to 60 min without any cooling. No additional experiments were pursued for **1b** since a quantitative yield was already obtained. While the reactions with **1d**, **1e**, and **1f** proceeded incident-free, a massive leakage of fluid out of the hand tightened reaction vessel occurred during the reactions with **1a** and **1c**. Their remains inside the reaction vessel were nevertheless also analyzed by GC. The results from these experiments are shown in Table 4.

Only the conversion of **1e** and perhaps **1f** resulted in a satisfactory yield. The wax-like solid obtained after VM grinding of **1d** converted after 24 h on its own into a deep yellow solid. GC analysis of this product revealed an increased yield in **3d** from the initial 2% to 89%, which apparently resulted from a direct crystallization. Thus, the presence of small amounts of **3d** obtained from the milling process seems to have initiated the subsequent conversion to the target product. The observed leakage during the reaction of **1a** and **1c** probably resulted from the heating of the reaction vessel to 70–90 °C, causing the thermally expanding cap of the vessel (larger diameter) to lose its seal. In fact, the initially at room temperature tightly screwed-on cap could be rotated another 1/8 turn after completion of the milling. In spite of the leakage, a quantitative conversion of **1a** to **3a** was indicated. In fact, the pure product **3a** has a melting point of 83 °C (as per supplier, Aldrich, Germany), and must have been a liquid under the conditions of the milling process. Likewise, the eutectic mixture of **1c**, malononitrile and **3c** were also in the liquid phase under the experimental conditions and leaked out of the VM as well. That the also liquid reactant **1f** did not leak out can be explained by a fast reaction in the early stages of the grinding process. In response to the overall unsatisfactory results obtained with the VM no further experiments were pursued using this mill. In particular, reactions with **1g** and **1h** were not

**Table 4** Knoevenagel reactions of aldehydes with malononitrile with vibration mill (60 min/30 Hz)

RCHO	Yield <b>3</b> (%)
<b>1a</b>	>99 <sup>a</sup>
<b>1c</b>	71 <sup>a</sup>
<b>1d</b>	2 <sup>b</sup>
<b>1e</b>	98 <sup>b</sup>
<b>1f</b>	93 <sup>b</sup>

<sup>a</sup> Portions of reaction mixture leaked out of reaction vessel. <sup>b</sup> Compact mixture of solids.

attempted because of safety concerns if these were to leak out of the VM during the reaction.

With respect to the PM, its reaction vessel is closed by an external compression seal which prevents any leakage. To determine the optimized experimental parameters for carrying out the reaction studies, several preliminary experiments were conducted first with the rather reactive aldehyde **1b**. The amount of aldehyde as well as the grinding time and rotational speed were varied. The optimal settings were then, also, applied for the conversion of the slowly reacting aldehydes. From the results of these tests, shown in Table 5, it was decided to use 20 mmol of starting aldehyde and to grind for 60 min.

To further investigate the effect of the setting for rotational speed two complete series of duplicate experiments were carried out at, respectively, 400 and 800 revolutions per minute (rpm). The temperature inside the reaction vessel was determined immediately upon completion of the experiment using an IR-Sensor. The temperatures for the experiments at 400 rpm were always less than 30 °C, but were 50–60 °C after grinding with 800 rpm. Blind tests at the same settings with comparable amounts of sodium chloride resulted in higher temperatures, 35 and 70 °C, respectively. Although, especially without knowledge of heat capacities, this blind test is only a crude experiment. It appears that the overall process of mixing of the reactants and the ensuing reaction for the Knoevenagel reactions studied here is endothermic, absorbing some of the heat that is generated by the grinding. When comparing the yields from the experiments listed in Tables 6 and 7 one can see that with the exception of **1d** all aldehydes reacted to give higher yields with increasing temperature, indicating that thermal activation is necessary. This observation is in keeping with the previously discussed results in Tables 3 and 4. Only **1b** is so reactive that it reacts quickly even at low temperatures.

**Table 5** Preliminary Knoevenagel reactions of aldehydes with malononitrile with the planetary mill

RCHO	(mmol)	Condition	Yield <b>3</b> (%)
<b>1b</b>	10	10 min/800 rpm	55
<b>1b</b>	20	10 min/800 rpm	99
<b>1b</b>	20	10 min/400 rpm	79
<b>1b</b>	20	60 min/400 rpm	99
<b>1d</b>	20	10 min/800 rpm	0
<b>1d</b>	20	60 min/400 rpm	2

**Table 6** Knoevenagel results with the PM at 400 rpm, 1 h

RCHO	Yield <b>3</b> (%)	
	Immediately after grinding	Grinding + 24 h under N <sub>2</sub>
<b>1a</b>	31	99
<b>1b</b>	99	—
<b>1c</b>	2	71
<b>1d</b>	2	89
<b>1e</b>	6	6
<b>1f</b>	9	21
<b>1g</b>	10	76
<b>1h</b>	30	99
<b>1i</b>	77	95
<b>1j</b>	21	60

**Table 7** Knoevenagel results with the PM at 800 rpm, 1 h

RCHO	Yield <b>3</b> (%)	Yield <b>3</b> (%)
	Immediately after grinding	Grinding + 24 h under N <sub>2</sub>
<b>1a</b>	97	99
<b>1b</b>	—	—
<b>1c</b>	69	78
<b>1d</b>	5	91
<b>1e</b>	94	96
<b>1f</b>	95	95
<b>1g</b>	>99	—
<b>1h</b>	>99	—
<b>1i</b>	96	>99
<b>1j</b>	59	77

Interestingly, as already noted in the early stages of our studies, the pre-reacted reaction mixtures were observed to continue to convert in many cases into the desired product after completion of the milling process when left to stand at room temperature. Two series of independent reaction experiments were conducted for each utilized rpm setting (400 rpm, 800 rpm), to investigate this behavior quantitatively. In one series, the entire reaction mixture was immediately dissolved for GC analysis upon completion after grinding. In the other series, a portion of the reaction mixture after grinding was left for 24 h under a nitrogen atmosphere to minimize possible autoxidation, and the products were then dissolved and immediately analyzed by GC. The results are summarized in Tables 6 and 7 and show that in some instances quantitative yields can be obtained, depending on the reactivity of the aldehyde. An intensive investigation is under way to further explore the phenomenon of an inductive effect, including experiments in solution phase. These findings are beyond the scope of this article and will be separately published.

The continued reaction of these reaction mixtures is most likely due to direct crystallization, which has been described for other solid–solid reactions in the literature.<sup>10</sup> Because a direct crystallization can at times be initiated by the presence of the target product, as was the case for the experiments listed in Tables 6 and 7, it remains to be seen if the same effect can occur in absence of any target product. Therefore, the most reactive aldehydes **1a**, **1b**, **1h** and **1i** as well as, for comparison, the slowly reacting aldehydes **1c**, **1d** and **1j** were mixed by brief shaking in 10 mmol stoichiometric amounts with malononitrile and left standing for 24 h under nitrogen at room temperature. The yields obtained by GC analysis are summarized in Table 8.

The liquid reaction mixtures with **1a** and **1h** did not react as much as expected. Interestingly, the solid mixture with **1d** reacted

**Table 8** Direct crystallization results for the Knoevenagel reaction

RCHO	Yield <b>3</b> (%)
<b>1a</b>	13
<b>1b</b>	92
<b>1h</b> (THF)	98
<b>1c</b>	0
<b>1d</b>	7
<b>1h</b>	18
<b>1i</b>	95
<b>1j</b>	0

only to a yield of 7%, even though a yield of 89% was observed in the presence of an initial 2% of target product. Apparently, small amounts of target material are sufficient to initiate the direct crystallization process. The incomplete reactions with **1b** and **1i** are due to insufficient mixing of the reactants. To confirm this explanation, a reaction mixture with **1b** was first dissolved in THF and the solvent was then quickly removed, again by evaporation under vacuum. After standing for 24 h the yield in **3b** was 98%. Homogenization of the mixture is obviously a necessary condition to achieve quantitative conversion. The reaction mixtures are also immediately homogenized during the initial stages of the mechanochemical conversion.

Although there are few reports which describe attempting the Knoevenagel reaction with malononitrile under mechanochemical conditions, our findings can be further discussed with regard to some of the observations made in these previous studies.<sup>11,17</sup> Kaupp *et al.* observed that the mechanochemical reaction of the aldehydes **1a**, **1b**, **1g**, and **1i** did not proceed with malononitrile at room temperature, which supports the finding that thermal activation is generally necessary. Wada and Suzuki used calcite and fluorite as the catalyst for Knoevenagel condensation of various aldehydes with malononitrile and methyl cyanoacetate. They observed that the reaction proceeded to high yields when the mineral reagent was mechanically crushed to 1–3 mm pieces prior to use, but no reaction occurred when fine powder was used. They explained this observation with the speculation that the “newborn solid surface should be highly activated with the naked ionic species *in-situ* generated”. However, it appears more likely that the added minerals did not act as a catalyst but merely served as additional grinding stones during milling of the reactants. When mineral powder was used instead, the reaction mixtures became effectively diluted and the grinding less effective explaining the unsuccessful conversions. Unfortunately, the authors did not report experiments without the use of the mineral agents nor did they vary their amount.

It is also instructive to discuss the reactivity of the various aldehydes. It was possible to convert the aldehydes **1b**, **1g** and **1h** quantitatively as well as **1a** and **1i** nearly quantitatively to their corresponding benzylidene-malononitriles under optimum experimental conditions. Aldehyde **1j** was the exception. At first, **1j** does react with malononitrile to the desired target product. However, in parallel to the Knoevenagel reaction, the hydroxyl group in the *ortho*-position in the product further reacts with the neighboring nitrile group to form a ring, which under elimination of hydrocyanic acid leads to benzofuran-2-carbonitrile. This, at first, unknown side product was eventually detected by GC-MS analysis. This intramolecular ring formation of the *ortho*-substituent with the side chain nitrile proceeds in time in the isolated solid as well as in solution and results in a quantitative degradation of **3j**. The unexpected vigor at which **1i** and **1j** reacted in the melt under microwave irradiation prevented the control of the reaction temperature under these conditions. For these reactions it was not possible to achieve yields greater than 98%. Rather, the formation of side products was often observed. These side products were not found during the mechanochemical conversion. Since the mechanochemical conversion of **1i** and **1j** were most successful at internally generated temperatures of 50–90 °C, it appears that the formation of side products requires larger thermal

activation at temperatures above these temperatures. Indeed, the temperature of the melt was 150 °C.

A comparison of energy consumption using the different methods of conducting Knoevenagel condensation is also instructive. The total power consumption was directly measured with a line power consumption meter when carrying out the reaction using the microwave system, the VM or the PM. The total line power consumption of the microwave system running for one hour at 100 W of microwave irradiation (including a 10 min ventilation time) is 130 kWh. The power consumption of the milling systems at the same reaction time is only 0.4 and 0.2 kWh for the VM at 30 Hz cycle time and the PM at 800 rpm, respectively. The corresponding power consumption on a molar basis of reactant for one hour reaction time is thus 6.5 kW mmol<sup>-1</sup> for the microwave system, 0.04 kW mmol<sup>-1</sup> for the VM and 0.01 kW mmol<sup>-1</sup> for the PM.

## Conclusions

The combined results from this study show that a generalization of the reaction scheme for the quantitative stoichiometric conversion of aromatic aldehydes with malononitrile cannot be made. The success of a quantitative Knoevenagel reaction depends both on the choice of the aldehyde and on the choice of how the necessary activation energy is introduced into the reaction mixture. For example, under mechanochemical conversion 4-nitro-benzaldehyde (**1b**) reacts quantitatively already under mild conditions, while vanillin (**1d**) reacts barely at all and salicylic aldehyde (**1j**) reacts only partially but forms instable products. Furthermore, it was observed that partially converted reaction mixtures often continue to convert, to significantly increased yields through direct crystallization. For the more reactive aldehydes the yields may even be quantitative within 24 h and proceed without introducing any external energy into the reaction mixture. It is necessary though that the reaction mixture is completely homogenized. It was also noticed that the temperature within the reaction vessel significantly affected the degree of conversion. In general, the reactions in this study converted quantitatively at temperatures between 50–90 °C, at least for the more reactive aldehydes. The chemical conversions are thus not due to pure mechanochemical effects. Rather, the reactions are initiated through the heat generated through friction during the grinding process, which then enables the reaction of the homogenized mixture to proceed. This explains why only unsatisfactory conversions were obtained with the PM at 400 rpm, where the temperature within the reaction vessel never exceeded 30 °C.

While the PM with its leak-tight closure system could be used for all of the studied reactions, the screw-type closure of the VM would lose its seal at higher temperatures and any

liquid reaction mixture or product would leak out. The VM can still be used without any problems for reaction mixtures and resulting products that remain solid throughout the course of the reaction.

For mechanochemical conversions, the sintered product can be easily and essentially completely retrieved without the use of solvents. The loss in substance is about 1% in mass. Thus the synthesis is solvent-less. In contrast, solvents were necessary to retrieve the products from reactions in the melt under microwave irradiation, which overall did not result in quantitative yields under the conditions studied and often included the formation of side products. The one hour usage of the microwave system also required 6.5 kW mmol<sup>-1</sup> of energy, significantly more than the VM and PM milling systems which required only 0.04 and 0.01 kW mmol<sup>-1</sup>, respectively.

More investigations are under way to elucidate the effect of continued reaction without the addition of external energy, and the results will be reported in due course.

## Acknowledgements

This study was supported by the Fonds der chemischen Industrie. MMH acknowledges support from the American Chemical Society (PRF 46578-UFS) and SUNY Brockport for a sabbatical leave at FSU Jena, Germany. We thank J. Emory Morris for proofreading the manuscript.

## References

- 1 L. D. Field, S. Sternhell and H. V. Wilton, *Tetrahedron*, 1997, **53**, 4051.
- 2 H. Sohmiya, T. Kimura, M. Fujita and T. Ando, *Tetrahedron*, 1998, **54**, 13737.
- 3 M. Nüchter, B. Ondruschka and R. Trotzki, *J. Prakt. Chem./Chem.-Ztg.*, 2000, **342**, 720.
- 4 K. Tanaka and F. Toda, *Chem. Rev.*, 2000, **100**, 1025.
- 5 G. Kaupp, *Top. Curr. Chem.*, 2005, **254**, 95.
- 6 J. O. Metzger, *Angew. Chem.*, 1998, **110**, 3145.
- 7 M. Epple, *Chem.-Ing.-Tech.*, 1999, **71**, 35.
- 8 G. Kaupp and A. Herrmann, *J. Prakt. Chem./Chem.-Ztg.*, 1997, **339**, 256.
- 9 G. Kaupp, J. Schmeyers, A. Kuse and A. Atfeh, *Angew. Chem.*, 1999, **111**, 3073.
- 10 G. Kaupp, *CrystEngComm*, 2006, **8**, 794.
- 11 G. Kaupp, M. R. Naimi-Jamal and J. Schmeyers, *Tetrahedron*, 2003, **59**, 3753.
- 12 B. Rodríguez, A. Bruckmann, T. Rantanen and C. Bolm, *Adv. Synth. Catal.*, 2007, **349**, 2213.
- 13 M. Carey Lea, *Philos. Mag.*, 1882, **34**, 46.
- 14 W. Ostwald, C. Drucker, *Handbuch der allgemeinen Chemie*, Akademische Verlagsgesellschaft m. b. H., Leipzig, Germany, 1919.
- 15 *Organikum, Organisch-Chemisches GrundPraktikum*, Wiley-VCH, Weinheim, Germany, 21st edn, 1998, 527f.
- 16 G. Heinicke, *Tribochemistry*, Akademie-Verlag, Berlin, Germany, 1984.
- 17 S. Wada and H. Suzuki, *Tetrahedron Lett.*, 2003, **44**, 399.



# Millisecond autothermal steam reforming of cellulose for synthetic biofuels by reactive flash volatilization†

Joshua L. Colby, Paul J. Dauenhauer and Lanny D. Schmidt\*

Received 19th March 2008, Accepted 25th April 2008

First published as an Advance Article on the web 2nd June 2008

DOI: 10.1039/b804691c

Three biomass-to-liquid process steps (volatilization of cellulose, tar-cleaning of organic products, and water-gas-shift of the gaseous effluent) have been integrated into a single autothermal catalytic reactor for the production of high quality synthesis gas at millisecond residence times ( $\sim 30$  ms). Particles of cellulose ( $\sim 300$   $\mu\text{m}$ ) were directly impinged upon the hot, catalytic bed of Rh–Ce/ $\gamma$ - $\text{Al}_2\text{O}_3$  catalyst on 1.3 mm  $\alpha$ - $\text{Al}_2\text{O}_3$  spheres in the presence of  $\text{O}_2$ ,  $\text{N}_2$ , and steam in a continuous flow fixed-bed reactor at 500–1100 °C. Complete conversion to gases was observed for all experimental parameters including  $\text{N}_2/\text{O}_2$ , S/C, the total flow rate of cellulose, and the fuel-to-oxygen ratio (C/O). The addition of steam increased the selectivity to  $\text{H}_2$  and decreased the selectivity to CO in agreement with water-gas-shift equilibrium. Optimal conditions produced a clean gaseous effluent which exhibited  $\sim 80\%$  selectivity to  $\text{H}_2$  at a synthesis gas ratio of  $\text{H}_2/\text{CO} = 2.3$  with no dilution from  $\text{N}_2$  at a fuel efficiency of  $\sim 75\%$ . Carbon-free processing was explained by relating the domain of experimental parameters to the thermodynamic prediction for the formation of solid carbon,  $\text{C}_s$ .

## Introduction

Lignocellulosic biomass in the form of trees, grasses, and agricultural residues provides a realistic source for sustainable production of carbon-based fuels and chemicals.<sup>1,2</sup> Recent analysis by the U.S. Department of Agriculture estimates that annual production of lignocellulosic biomass could exceed one billion dry tons, providing sufficient energy to supplant a significant fraction of existing demand for fossil fuels.<sup>3</sup> The dominant structure in all non-food sources of biomass, lignocellulose, consists of the biopolymers cellulose, hemicellulose, and lignin in a design that provides optimal material properties to plant structures while resisting chemical degradation. These same properties also prevent the direct utilization of most conventional petroleum processing equipment thereby driving the development of new technology for handling and processing solid, carbonaceous materials.

Conversion of biopolymers to synthesis gas ( $\text{H}_2 + \text{CO}$ ) and subsequent production of synthetic fuels is a major thermochemical processing route commonly called biomass-to-liquid (BTL). The entire BTL process consists of a combination of unit operations including biomass preparation, gasification, synthesis gas cleaning, synthesis gas processing, synthetic fuel production, and synthetic fuels refining. The availability of technologies and number of process variables for each process step provides an enormous number of configurations and design

options which must be evaluated as an integrated system for optimal process development.<sup>4</sup> The overall process competes economically with existing biological processes (*e.g.* corn to ethanol) as demonstrated by a recent process design analysis of the BTL process for the production of ethanol from wood.<sup>5</sup>

The efficacy of the BTL process can be enhanced by either improving the performance of any single process step or by eliminating or combining process steps. A significant opportunity for process improvement exists with synthesis gas production and preparation. The cost of conversion to clean, conditioned synthesis gas for a synthetic fuels reactor can dominate process economics as this equipment can comprise 60–75% of the total process investment.<sup>6,7</sup> This paper demonstrates that at least three BTL process steps (gasification, tar-cleaning, and water-gas-shift) can be combined as a one-step millisecond residence time reactor for continuous operation. Each of these steps provides a necessary process function and contributes a non-negligible capital and operating cost. Conventional biomass gasifiers (updraft, downdraft, and fluidized bed) partially oxidize biomass to a gaseous syngas-rich effluent that commonly contains impurities such as tars and aromatics, unconverted oxygenated organics, nitrogen-containing species such as  $\text{NH}_3$  or HCN, and soot.<sup>8</sup> Organic impurities must be selectively removed to ppm levels by one of several technologies that can be categorized into wet scrubbing, dry scrubbing, or hot gas conditioning.<sup>9</sup> Existing techniques applicable to the integrated reactor considered here include steam reforming and partial oxidation of tars and organics using Ni, Pt, or Rh metal catalysts. Biomass-derived synthesis gas typically exhibits a  $\text{H}_2/\text{CO} \sim 1.0$ , and an additional process step must also be used to adjust the ratio of  $\text{H}_2$  to CO by the water-gas-shift reaction for synthetic fuel reactors to produce Fischer–Tropsch alkanes ( $\text{H}_2/\text{CO} \sim 2$ ), methanol for dimethyl ether ( $\text{H}_2/\text{CO} \sim 2$ ), or mixed alcohol fuel ( $\text{H}_2/\text{CO} \sim 1.2$ ).<sup>5</sup>

Department of Chemical Engineering and Materials Science, University of Minnesota, 421 Washington Ave, Minneapolis, MN, 55455, USA.  
E-mail: schmi001@umn.edu; Fax: +1 612 626 7246

† Electronic supplementary information (ESI) available: The supplementary material contains a description of the assumptions that went into the construction of Fig. 7. See DOI: 10.1039/b804691c

An extremely short residence time (milliseconds) reactor integrating at least three process steps provides the possibility for dramatic improvement in the utilization of biomass for synthetic fuels. Conventional gasifiers exhibit residence times on the order of seconds to minutes, while catalytic partial oxidation of organic compounds occurs in milliseconds permitting a reduction in biomass reactor size by at least an order of magnitude. Additionally, combined chemistries permit simpler overall processes by eliminating multiple process vessels and ancillary equipment. The capital costs of traditional BTL equipment has restricted the processes to large scales ( $\sim 400$  MW<sub>th</sub>), demanding an abundant, local supply of biomass.<sup>7</sup> Small efficient processes allow for localized processing facilities, reducing costs associated with biomass transportation.

A highly integrated, millisecond biomass reactor operates faster and with more functionality than a large number of existing catalytic gasifiers. There exist numerous experimental examples of the integration of metal catalysts such as Ni, Co, and Rh with conventional fluidized bed gasifiers to reduce the production of char and tars *in situ*.<sup>10–12</sup> Most gasification catalysts exhibit deactivation and poisoning due to the development of surface carbon (coke) and char and the condensation of inorganic ash. Rh-based catalysts with the addition of Ce have exhibited significant resistance to the formation of coke in the oxidative reforming of tars and organics.<sup>13,14</sup> Additionally, catalytic partial oxidation of highly oxygenated organic compounds such as ethylene glycol and glycerol on Rh–Ce catalysts has been selected for equilibrium concentrations of synthesis gas during steady, autothermal operation on millisecond time-scales.<sup>15</sup> The utilization of Rh–Ce fluidized catalytic beds integrated with volatilization of carbohydrate-rich solids has demonstrated reduced tar formation, but has been restricted to indirectly heated processes and residence times on the order of one second.<sup>16</sup>

The direct impingement of solid particles of carbohydrate-rich biomass with a hot ( $T > 700$  °C), catalytic surface in thermal contact with a catalytic bed provides an optimal situation for fast, integrated processing of nonvolatile feedstock material. We have recently demonstrated this technique, referred to as ‘reactive flash volatilization,’ on Rh–Ce catalytic beds for the

air-blown reforming of soy oil, cellulose, and lignocellulose.<sup>17,18</sup> Multiple zones of chemistry (volatilization, oxidation, and reforming) provide efficient chemical routes to synthesis gas. Particles contacting a hot surface volatilize to gases and volatile organic compounds (VOCs) which can flow into the catalyst bed and oxidize to synthesis gas and combustion species. The remaining gases and VOCs after  $>99\%$  oxygen conversion can then steam reform to gases and equilibrate by the water-gas-shift (WGS) reaction. Autothermal processing is realized between endothermic zones (volatilization and reforming) and the exothermic oxidation chemistry through balanced heat transfer by conduction in the alumina catalyst support and convection forward by the process gases.

The adjustment of chemistry and heat transfer by the addition of steam and removal of feed N<sub>2</sub> provides the opportunity to reduce effluent synthesis gas dilution and fully integrate the water-gas-shift step within the millisecond reactor. Rh–Ce catalysts have demonstrated strong activity for the water-gas-shift reaction on millisecond time-scales.<sup>19</sup> In this study we demonstrate the tunability of the synthesis gas ratio by adjusting the feed S/C (steam-to-carbon) ratio, the C/O (carbon-to-oxygen) ratio, the N<sub>2</sub>/O<sub>2</sub> (feed nitrogen/feed oxygen) ratio, and the total flow rate of solid material. Spatial temperature measurements were conducted along the axis of the catalyst bed to analyze system behavior and define process limitations. Additionally, system performance is analyzed through thermodynamic analysis, and the domain of operation is presented for considered feed parameters. Finally, the results lead to the development of an autothermal, steady-state operating configuration that permits integration of gasification, tar-cleaning, and water-gas-shift chemistry in the absence of nitrogen at high process feed rates and millisecond residence times.

## Experimental

### Reactor design

The autothermal steam reforming of cellulose was performed in a 20 mm I.D., 22 mm O.D. quartz tube shown in Fig. 1. A 17 mm O.D. ceramic foam monolith, used to support the 30 mm bed of

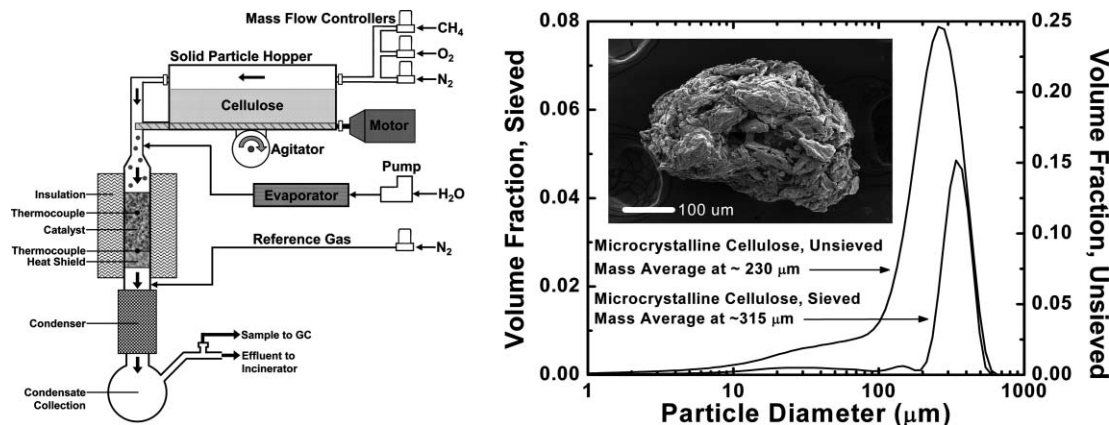


**Fig. 1** Left: the experimental apparatus consisted of an insulated quartz reactor tube supplied with N<sub>2</sub>, O<sub>2</sub>, CH<sub>4</sub>, cellulose, or steam. Particles of cellulose were metered using a servo-motor powered auger passing through a sealed hopper. Reactor effluent gases passed through a condenser and were sampled for gas chromatography. Right: particle size distribution generated by light scattering of microcrystalline cellulose samples processed by reactive flash volatilization. Inlet micrograph shows a representative cellulose reactor feed particle with high porosity.

spherical catalysts, was inserted into the quartz tube from the bottom and held in place *via* friction fit against the reactor wall with ceramic cloth.

Cellulose was fed to the top of the reactor tube with a 0.25 in. auger, which was rotated by a small volume laboratory mixer to accuracies  $\pm 1$  RPM. The auger functioned as a volumetric feeder, conveying cellulose from a gas-sealed acrylic hopper to the reactor. An unbalanced rotor vibrator was attached to the base of the hopper to ensure uniform and complete filling of the auger during operation, minimizing oscillation in fuel flow rates. Gases were fed through the hopper to the reactor using mass flow controllers operated by LabVIEW software accurate to  $\pm 0.05$  SLPM. Water was supplied by a syringe pump to a steam generator, where it was vaporized and fed  $\sim 2$  in. upstream of the catalyst bed *via* heated stainless steel tubing. Steam was fed in close proximity to the catalyst in order to avoid water condensation on the reactor walls and cellulose conglomeration prior to contact with the catalyst. The reactor effluent was directed through a laboratory condenser (maintained at 25 °C) to minimize throughput of condensable species, primarily water, to the sampling tube. Effluent was periodically sampled upstream of the condenser to verify the absence of condensable organic compounds.

### Temperature measurement

Experiments were primarily conducted with thermocouples placed at 10 mm and 30 mm from the front face of the catalyst bed. These thermocouples were inserted from the downstream side of the reactor tube during the placement of the foam monolith support. Axial temperature profile experiments were conducted using a reactor tube with 16, 0.7 mm diameter holes placed in the quartz reactor tube along the length of the catalyst bed. Through these holes 16 K-type thermocouples were fed horizontally to the center of the catalyst bed as depicted in

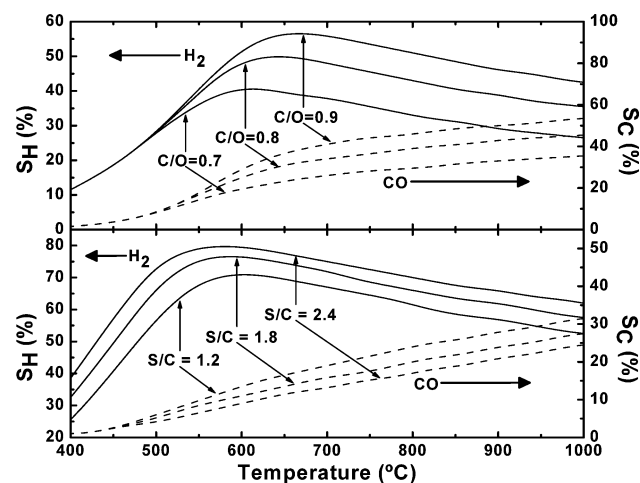


**Fig. 2** The conversion of cellulose ( $C_6H_{10}O_5$ ) to equilibrium products by dry oxidation (upper panel) at  $C/O = 0.7, 0.8$  and  $0.9$ , and steam reforming at  $C/O = 0.8$  (lower panel) at  $S/C = 1.2, 1.8$  and  $2.4$ , predicts 40–80% selectivity to  $H_2$  (solid lines) and 0–50% selectivity to CO (dashed lines) for the temperature range 400–1000 °C.  $C/O$  is defined as molar feed rate of carbon in the fuel relative to molar feed rate of oxygen atoms in the gaseous  $O_2$ .  $S/C$  is defined as molar feed rate of steam relative to the molar feed rate of carbon in the fuel.

Fig. 5D. The quartz reactor tube was sealed using ultra high temperature ceramic adhesive. This apparatus facilitated the acquisition of steady state and transient reactor bed temperature profiles.

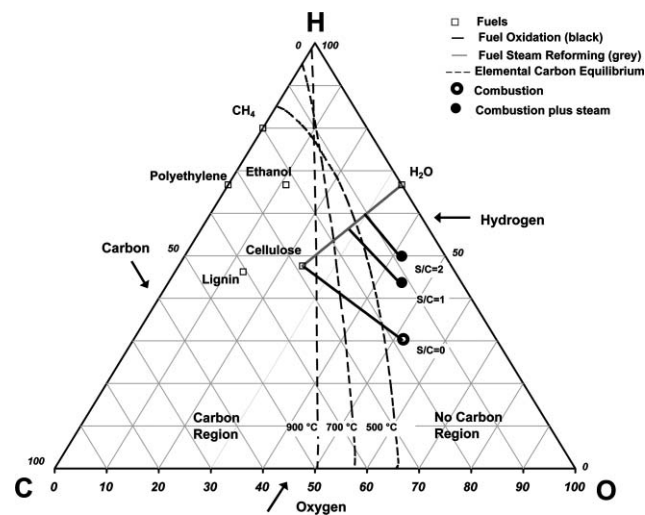


**Fig. 3** The formation of solid carbon,  $C_s$ , by processing of solid, organic feedstocks such as cellulose, lignin, polyethylene, or ethanol inhibits the use of catalysts due to surface poisoning. Dashed lines represent the interface between the region for which  $C_s$  is predicted as a thermodynamic product, and the region for which it is not, at 500, 700, and 900 °C. The stoichiometry of steam reforming (solid grey line) cellulose oxidation and autothermal steam reforming (solid black lines) demonstrate that conversion to combustion products or synthesis gas occurs near the interface of these two regions permitting autothermal carbon-free processing.

### Reactor operation

Reactor start-up involved pre-heating an isolated portion of the catalyst to  $\sim 300$  °C using an external heat source while passing methane and nitrogen gas through the reactor. Once hot, oxygen was added to the gas mixture at air stoichiometry and fuel-rich conditions necessary to avoid combustion. This procedure initiated the autothermal partial oxidation of methane in the catalyst bed, which heated the reactor bed to  $\sim 900$  °C. Cellulose was then added to the reactor at  $\sim 30$  g  $h^{-1}$ . Flow of methane was discontinued, and the oxygen flow rate was adjusted to a fuel-rich regime for experimental trials.

The reactor was insulated to minimize heat loss to the surroundings. In order to accurately determine cellulose flow rate to the reactor, the system was initially operated at low  $C/O$  in order to heavily oxidize any carbon before being exhausted from the sphere bed. The effluent was then analyzed to quantify carbon content (*i.e.* the CO and  $CO_2$  were measured with gas chromatography). Once a steady cellulose flow rate was observed, gases were adjusted to achieve the desired  $S/C$ ,  $N_2/O_2$ , and  $C/O$  ratios, and the effluent was sampled. The system was then returned to a low  $C/O$  in order to verify that the cellulose flow rate had not changed. This procedure was used for determining the cellulose flow rate upon start-up, and for data obtained at operating conditions capable of producing condensable product species. The reactor was shut down by

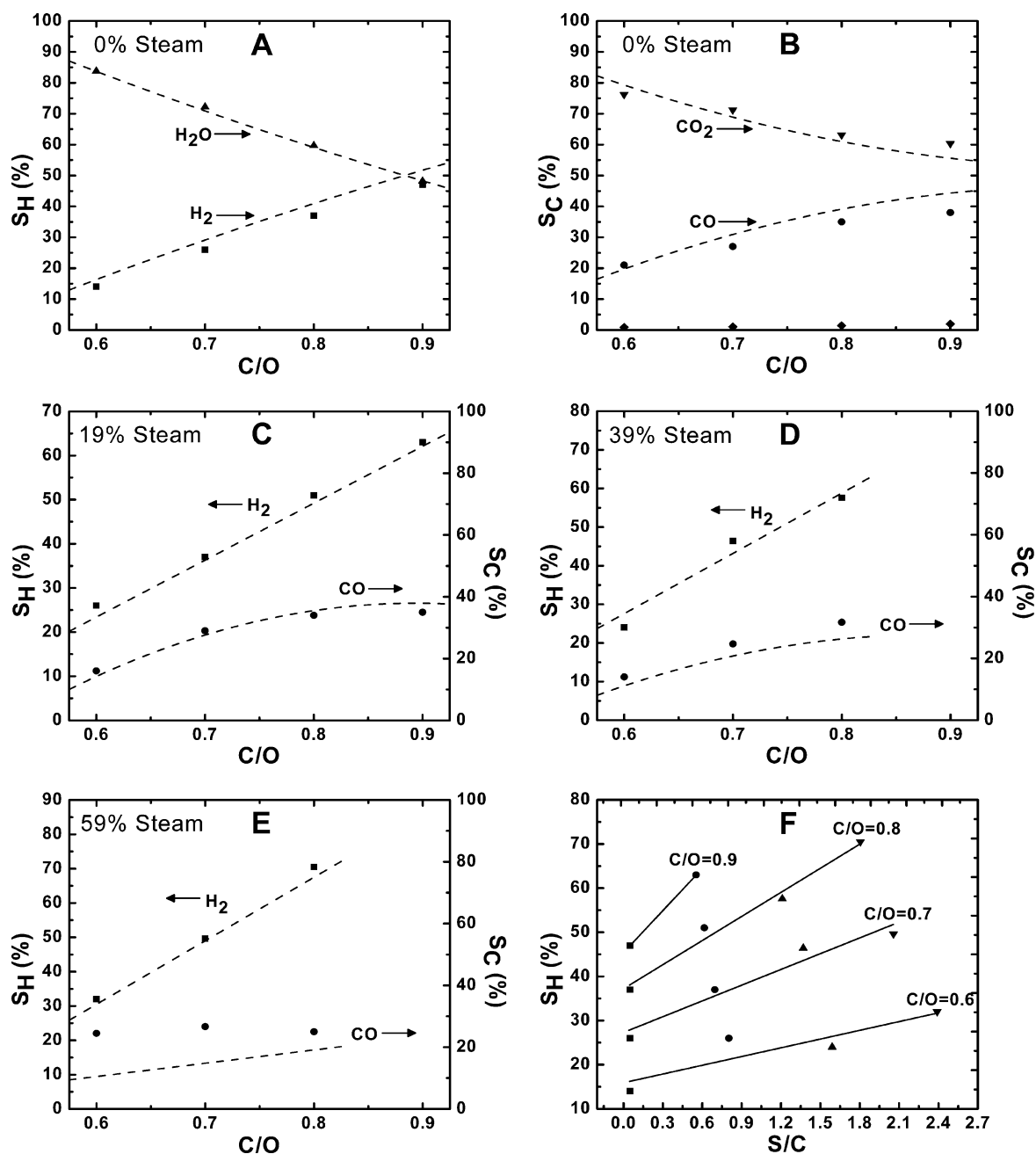


**Fig. 4** The selectivity to hydrogen (■), water (▲), carbon monoxide (●), carbon dioxide (▼) and methane (◆) achieves equilibrium in the reforming of cellulose at a flow rate  $30 \text{ g h}^{-1}$  with gaseous co-feed: (79%  $\text{N}_2$  + 21%  $\text{O}_2$ ) in Panels A and B, co-feed (60%  $\text{N}_2$  + 21%  $\text{O}_2$  + 19%  $\text{H}_2\text{O}$ ) in Panel C, co-feed (40%  $\text{N}_2$  + 21%  $\text{O}_2$  + 39%  $\text{H}_2\text{O}$ ) in Panel D, co-feed (20%  $\text{N}_2$  + 21%  $\text{O}_2$  + 59%  $\text{H}_2\text{O}$ ) in Panel E, and at  $0 \leq \text{S/C} \leq 2.4$  in Panel F. Dashed lines represent equilibrium concentrations and solid lines are fitted.

terminating cellulose, oxygen, and steam flows. Once the system was cooled, nitrogen flow was terminated.

All experiments without steam addition were operated at air stoichiometry ( $\text{N}_2/\text{O}_2 = 3.76$ ). C/O is defined to be the molar ratio of carbon in the fuel to atomic oxygen fed as air. Complete cellulose combustion to  $\text{CO}_2$  and  $\text{H}_2\text{O}$  therefore occurs at  $\text{C/O} = 0.5$ . Experiments were carried out at C/O ratios of 0.6, 0.7, 0.8, and 0.9. These experiments were run in oxygen deficient environments in order to maximize selectivity to synthesis gas

and hydrogen. Cellulose flow rates of  $25\text{--}60 \text{ g h}^{-1}$  were used for all data collection.

Steam addition experiments were performed by replacing nitrogen with steam in increments of 20% of the gaseous feed to maintain a constant gaseous co-feed flow rate. Gas feed compositions considered were (in mole percents): (1) 60%  $\text{N}_2$ , 21%  $\text{O}_2$ , 19%  $\text{H}_2\text{O}$ , (2) 40%  $\text{N}_2$ , 21%  $\text{O}_2$ , 39%  $\text{H}_2\text{O}$ , (3) 20%  $\text{N}_2$ , 21%  $\text{O}_2$ , 59%  $\text{H}_2\text{O}$ , and (4) 0%  $\text{N}_2$ , 21%  $\text{O}_2$ , 79%  $\text{H}_2\text{O}$ . S/C is defined to be the molar ratio of steam to carbon in the fuel.



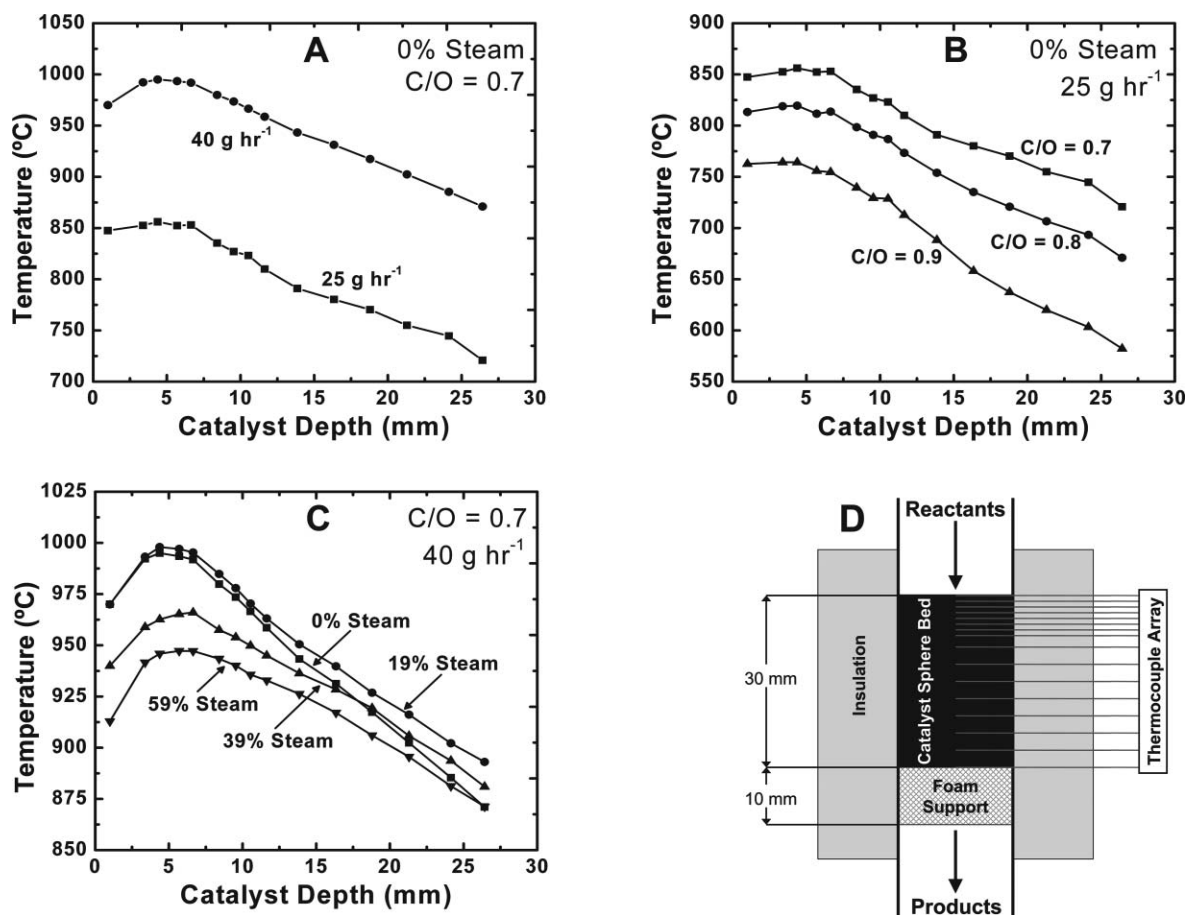


**Fig. 5** Measured axial temperature profile within the 30 mm fixed bed of Rh–Ce/ $\gamma$ -Al<sub>2</sub>O<sub>3</sub>/ $\alpha$ -Al<sub>2</sub>O<sub>3</sub> spheres was examined as a function of total solid cellulose particle flow rate (A), C/O ratio (B), and magnitude of steam substitution for nitrogen (C). In Panel A, the temperature profile was measured with C/O = 0.7, S/C = 0.05, and at cellulose flow rates of 25 g h<sup>-1</sup> (▼) and 40 g h<sup>-1</sup> (●). In Panel B, the temperature profile was measured at S/C = 0.05, cellulose flow rate of 25 g h<sup>-1</sup>, and C/O = 0.7 (■), C/O = 0.8 (●), and C/O = 0.9 (▲). In Panel C, the temperature profile was measured at a cellulose flow rate of 40 g h<sup>-1</sup>, C/O = 0.7, and steam substitution of N<sub>2</sub> with steam in the gaseous feed of 0 mol% (■), 19 mol% (●), 39 mol% (▲), and 59 mol% (▼). The temperature at each axial position (catalyst depth) was measured simultaneously by inserting and sealing multiple thermocouples radially into the reactor (D).

Experiments were run at C/O ranging from 0.6 to 0.9, depending on whether autothermal operation was sustainable.

### Catalyst preparation

All catalysts were prepared on Saint-Gobain NorPro Corporation 1.3 mm diameter  $\alpha$ -Al<sub>2</sub>O<sub>3</sub> spheres. The unmodified spheres have a surface area of 5.35 m<sup>2</sup> g<sup>-1</sup> and a packing density of 64.1 lbs ft<sup>-3</sup>. Prior to Rh–Ce deposition, a  $\gamma$ -Al<sub>2</sub>O<sub>3</sub> washcoat was added to the spheres to increase surface area *via* incipient wetness technique.<sup>20</sup> A 5 wt% slurry of  $\gamma$ -Al<sub>2</sub>O<sub>3</sub> in distilled water was added drop-wise to the spheres, which were then allowed to dry. Once dry, the spheres were calcined for 6 h at 600 °C. Rh(NO<sub>3</sub>)<sub>3</sub> and Ce(NO<sub>3</sub>)<sub>3</sub>·6H<sub>2</sub>O metal salts were then added to the spheres also using the incipient wetness technique. A 1 wt% Rh and 1 wt% Ce solution of metal salts in distilled water was added drop-wise to the spheres, which were then allowed to dry. Once dry, the spheres were calcined for 6 h at 600 °C. Catalysts were conditioned for ~1 h under representative operating conditions before conducting experiments. Experiments were repeated on catalysts with no measurable differences in activity. Catalysts

were generally used for no less than 10 h, during which there was no observable deactivation.

### Feedstock analysis

Microcrystalline cellulose used in all experiments was obtained from FMC BioPolymer. Samples of cellulose exposed to the air naturally absorbed ~5 wt% moisture (S/C~0.05). Moisture content was determined gravimetrically by drying in a vacuum oven. The particle size distribution in Fig. 1 was measured by light scattering. The raw cellulose sample was separated in a No. 50 mesh sieve to obtain a sample with fewer particles smaller than 200  $\mu$ m to increase ease of handling by reducing particle conglomeration. Steam was produced from distilled water. The high purity gases, N<sub>2</sub> and O<sub>2</sub>, were supplied separately with high pressure cylinders.

### Product analysis

Gas samples were sampled with a syringe downstream of the condenser, and injected into a gas chromatograph. The system was calibrated to measure permanent gases and higher

hydrocarbon species. Species response factors and column retention times were determined using known concentrations of premixed gases. During standard operation the carbon, oxygen, and hydrogen mass balances typically closed to within  $\pm 5\%$ .

Experiments were conducted several times, typically repeated on several identical catalysts, with no significant differences observed between experiments. Catalyst operating temperature and time ranged from 550–1100 °C and 10–30 h, respectively. Selectivity to product species was calculated on an atomic carbon basis,  $S_C(\text{species})$ , or an atomic hydrogen basis,  $S_H(\text{species})$ . The selectivity was defined as (atoms in the product species)/(atoms in the converted fuel). Co-fed steam was not considered fuel. The sum of all selectivities to product species based on the same element (C or H) should equal unity within experimental error. The residence time was calculated as the void volume of the catalyst bed divided by the volumetric flow of effluent gases at the exit temperature. Sphere beds exhibit smaller void fractions resulting in faster residence times than foams.

### Equilibrium calculations

Equilibrium calculations were performed by numerical minimization of Gibbs free energy using HSC Chemistry® software.<sup>21</sup> Calculations were performed at 1 atm pressure and the temperature of the sphere bed 10 mm downstream of the front face ( $T_{10}$ ). Back-face catalyst bed temperatures were not used due to significant temperature gradients, resulting from heat conduction to the monolith support. High (>99%) conversion of fuel to  $C_1$  products was expected at low S/C, facilitating the inclusion of the following species in the calculation:  $\text{CO}_2$ ,  $\text{CO}$ ,  $\text{CH}_4$ ,  $\text{O}_2$ ,  $\text{H}_2$ ,  $\text{H}_2\text{O}$ .

The measured reactor process efficiency in Table 1 has been examined by calculating the fuel chemical flow availability (exergy),  $a_i$ , of all non-cellulose species by eqn (1),

$$a_i = (h_i - h_i^\circ) - T^\circ(s_i - s_i^\circ) + (\mu_i^\circ - \mu_i) \quad (1)$$

where  $h_i$  is the specific enthalpy of the species  $i$ ,  $T$  is the temperature,  $s_i$  is the specific entropy of species  $i$ , and  $\mu_i$  is the chemical potential of species  $i$ .<sup>22</sup> The values of  $h_i^\circ$ ,  $s_i^\circ$ , and  $\mu_i^\circ$  were calculated at the restricted dead state defined as  $T^\circ = 298 \text{ K}$ ,  $P^\circ = 1 \text{ atm}$ , and the gaseous molar fractions  $X(\text{O}_2) = 0.20$ ,  $X(\text{N}_2) = 0.76$ ,  $X(\text{H}_2\text{O}) = 0.03$ , and  $X(\text{other}) = 0.01$ . The chemical availability of cellulose was calculated using a correlation developed by Szargut and Styrylska,

$$\beta = \frac{1.0438 + 0.1882\left(\frac{H}{C}\right) - 0.2509\left(\frac{O}{C}\right)\left(1 + 0.7256\frac{H}{C}\right)}{1 - 0.3035\frac{O}{C}} \quad (2)$$

where  $H$ ,  $C$ , and  $O$  represent atomic mass fractions of feedstock cellulose, and  $\beta$  relates the chemical availability of cellulose,  $a_{\text{cell}}$ , to the lower heating value (LHV) of cellulose by  $a_{\text{cell}} = \beta * \text{LHV}_{(\text{cellulose})}$ .<sup>23</sup> The lower heating value of cellulose, obtained from a correlation assuming  $C/H/O = 6/10/5$ , was  $15.7 \text{ kJ g}^{-1}$ .<sup>24</sup> Process efficiency in Table 1 is defined as the flow availability of all products divided by the flow availability of all feed species.

### Results and discussion

The results demonstrate that reforming of cellulose with steam addition can produce equilibrium selectivity to synthesis gas with very little selectivity to minor products. By this method, the effluent syngas stoichiometry is tunable by adjusting the S/C ratio. Sustainable processing to a clean product stream maintains a significant fraction of the cellulose fuel value without observable formation of a solid carbon byproduct.

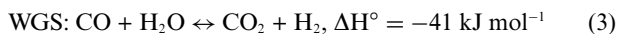
**Table 1** Selected experimental data for the millisecond reforming of microcrystalline cellulose<sup>a</sup>

Experiment	1	2	3	4	5
Catalyst bed length/mm	30	30	30	30	60
C/O ratio	0.9	0.9	0.8	0.8	0.9
H <sub>2</sub> O substitution for N <sub>2</sub>	0	19	39	59	79
S/C ratio	0.05	0.55	1.21	1.81	2.14
N <sub>2</sub> /O <sub>2</sub> ratio	3.76	2.86	1.91	0.95	0
Mass flow/g h <sup>-1</sup>	30	30	30	30	60
Residence time/ms	33	31	24	25	29
Space velocity/mol h <sup>-1</sup> L <sup>-1</sup>	118	118	118	118	118
Mass velocity/h <sup>-1</sup>	53	53	53	53	53
H selectivity (%)					
H <sub>2</sub>	48	63	58	71	79
H <sub>2</sub> O	38	34	42	21	21
C selectivity (%)					
CO	38	35	32	25	27
CO <sub>2</sub>	60	64	68	72	72
CH <sub>4</sub>	1.9	1.2	0.3	3	0.2
Temperature at 30/°C	600	730	710	625	825
H <sub>2</sub> /CO	1.1	1.4	1.5	3.0	2.3
Syngas dry mole fraction (%)	18	24	22	25	42
Process efficiency (%)	58	66	63	68	73

<sup>a</sup> All experiments were considered on a bed of 1.3 mm  $\alpha\text{-Al}_2\text{O}_3$  spheres with 5 wt%  $\gamma\text{-Al}_2\text{O}_3$  washcoat and 2 wt% loading of Rh and Ce with >99% conversion of cellulose to  $C_1$  products. The space velocity was defined as (molar flow of carbon)/(volume occupied by the catalytic spheres). The mass velocity was defined as the (mass flow of carbon)/(mass of RhCe). The process efficiency was defined in the experimental section of the text.

## Thermodynamic considerations

Fig. 2 shows representative equilibrium selectivity output data for the reaction of cellulose ( $C_6H_{10}O_5$ ) with steam and oxygen at variable C/O and S/C. As the reaction feed becomes more carbon rich (increasing C/O), the selectivity to more oxygen deficient species such as  $S_H(H_2)$  and  $S_C(CO)$  increase. Additionally, as the reaction feed contains more steam (higher S/C), the selectivity to hydrogen,  $S_H(H_2)$ , increases and  $S_C(CO)$  decreases. This behavior can be described very generally by an increased reaction of CO with steam to form hydrogen by the water-gas-shift reaction (WGS) (eqn (3)) at higher S/C.



The gaseous products predicted in Fig. 2 are achievable, provided a chemical route exists to equilibrium. The formation of a second, solid phase of carbon,  $C_s$ , has the potential to develop on catalytic surfaces, blocking surface chemistry and preventing the reactor from operating sustainably. This inhibition can likely be eliminated if solid carbon or carbon-rich solid residue is not a favored thermodynamic product. The prediction of a solid carbon equilibrium product ( $C_s$ ) is a function of the reaction feed stoichiometry (cellulose/oxygen/steam) and the reaction temperature. By calculating the stoichiometry for a set of temperatures (500, 700, and 900 °C) for which the activity of  $C_s$  goes to one, it is possible to define a boundary between a region for which  $C_s$  is unstable and not predicted by equilibrium. As shown in the ternary diagram of Fig. 3, this “no carbon region” is defined by a boundary (dashed lines) for which an increase in process temperature expands the operable “no carbon region” to nearly half of the possible reaction stoichiometry.<sup>25,26</sup>

The relevance of this calculation to the processing of feedstocks can be determined by placing the internal atomic stoichiometry (*i.e.* cellulose: C/H/O ~ 28.6/47.6/23.8 mol%) of each material on the ternary diagram (points). All considered feedstocks exist within the region for which solid carbon is a predicted thermodynamic product at  $T < 900$  °C. However, the addition of oxygen (solid black line) shifts the overall atomic stoichiometry across temperature boundaries such that no carbon is predicted at combustion stoichiometry (●). Processing at oxygen-deficient (syngas-producing) conditions occurs along the cellulose oxidation line and at lower adiabatic temperatures than combustion. The key implication for autothermal reforming is that there exists a specific oxidation feed stoichiometry around C/O = 1.1 (C/O calculated as defined in the experimental section) for the considered reaction conditions for which carbon becomes a predicted product. The addition of steam provides a processing alternative (solid grey line) to extend the overall stoichiometry across the thermodynamic boundaries. By co-feeding steam with oxygen at S/C = 1.0, nearly the entire oxidation stoichiometry exists within the no-carbon region defined at 500 °C, and higher S/C offer and even more expansive range of feed stoichiometry.

## Autothermal catalytic partial oxidation of cellulose

The production of gaseous products from the autothermal reforming of cellulose at S/C = 0.05 (due to particle moisture) is described in panels A and B of Fig. 4. Steady operation

was observed at all experimental conditions without oxygen breakthrough, and transient behavior due to a change in experimental operating conditions was resolved in 1–2 min. Carbon conversion to  $C_1$  products is >99% for all C/O presented, and carbon selectivity to methane was <3% for all C/O. Selectivity to  $H_2$  ranges from a minimum of 14% at C/O = 0.6, to a maximum of 47% at C/O = 0.9. The majority of the remaining hydrogen atoms were converted to water. Selectivity to carbon monoxide ranges from a minimum of 21% at C/O = 0.6, to a maximum of 38% at C/O = 0.9. The majority of the remaining carbon atoms were converted to  $CO_2$ . For C/O < 1.0 at S/C = 0.05, experimentally measured selectivity to gaseous products achieved equilibrium within experimental error. Complete conversion was attainable at residence times less than 40 ms.

At C/O = 1.0, production of organic species larger than  $C_1$  was observed in the chromatogram. The incomplete decomposition to equilibrium products can be attributed to slower kinetics, resulting from the decreased temperature at C/O = 1.0. For all C/O, the coldest part of the catalyst bed ( $T_{30}$ ) never dropped below 500 °C. The experimentally measured temperatures are shown in Fig. 5, and will be discussed in the next section. Overall performance with alumina spheres as a support for the Rh–Ce catalyst was very similar to that of 80 ppi alumina foams.<sup>17</sup>

Panels C–E of Fig. 4 show selectivity to hydrogen and carbon monoxide as a function of C/O for the CPO<sub>x</sub> of cellulose at varying concentrations of  $N_2$ ,  $O_2$ , and  $H_2O$  feed gases. Steady operation was observed at all experimental conditions without oxygen breakthrough, and transient behavior due to a change in experimental operating conditions was resolved in 1–2 min. Carbon conversion to  $C_1$  products is >99% for all C/O presented. Additionally, average methane selectivity with respect to carbon was <3% for all C/O. In panel C, 19% molar substitution of nitrogen with steam raised the selectivity to  $H_2$  to 63% while lowering selectivity to CO to 35% at C/O = 0.9. When the substitution for nitrogen with steam was raised to 39% in panel D, the overall operating temperature decreased (shown in Fig. 5), and the  $C_2$  organic species were observed at C/O = 0.90. However, at C/O = 0.8, selectivity to  $H_2$  was 58% and selectivity to CO was 32%. Further substitution of steam for nitrogen to 59%  $H_2O$  gaseous feed further cooled the operating temperature of the reactor (Fig. 5), but the addition of steam raised the observed selectivity of  $H_2$  to 71% and lowered the selectivity to CO to 25% at C/O = 0.8. Panel F of Fig. 4 relates the observed species to the operating S/C ratio for each of the experimental trials.

## Spatial temperature profiles

Measurements of the temperature within the fixed bed of catalyst spheres provide experimental insight to support the proposed mechanism detailed in the next section. By inserting thermocouples radially into the fixed bed of catalyst as shown in panel D of Fig. 5, the temperature at which reforming chemistry is occurring is known with millimetre resolution. Panels A, B, and C describe the effect of cellulose flow rate, process C/O ratio, and magnitude of steam substitution for nitrogen, respectively.

Panel A of Fig. 5 shows that the spatial temperature profile is a very strong function of the flow rate of cellulose. Both flow rates,

25 g h<sup>-1</sup> and 40 g h<sup>-1</sup>, exhibit a rise in temperature between the top of the catalyst bed (0 mm) and the maximum temperature (~5 mm). However, the magnitude of the temperature increase appears to be a function of the total flow rate with higher feedstock flow rates exhibiting higher thermal gradients within the oxidation zone. This can be partially explained by an increased distance between the endothermic chemistry at the catalyst front face and exothermic chemistry taking place in the oxidation zone. In contrast, both flow rates of cellulose exhibit the same rate of temperature decline after the temperature maximum (~5–30 mm). The difference in exit temperature ( $T_{30}$ ) for differing flow rates can be attributed to heat loss from the reactor.

Panel B of Fig. 5 details the effect of C/O ratio on the spatial temperature profile for a cellulose feed rate of 25 g h<sup>-1</sup> at S/C = 0. More oxygen feed (lower C/O) exhibits an overall hotter profile due to more overall exothermic chemistry. Panel C of Fig. 5 shows the effect of substituting steam for nitrogen at 0 mol%, 19 mol%, 39 mol%, and 59 mol% on the spatial temperature profile for a cellulose feed rate of 40 g h<sup>-1</sup> and C/O = 0.7. The initial substitution (0→19 mol%) has the effect of slightly raising the temperature from ~5–30 mm likely due to the temperature of steam (100 °C). However, further substitution (19→39 mol%, and 39→59 mol%) monotonically decreases the overall temperature profile 10–15 °C. A likely explanation is the increased heat capacity of steam over nitrogen.

### Process chemistry

The process by which solid particles of cellulose ~315 μm in average diameter are reduced to C<sub>1</sub> products (Fig. 6) at millisecond time scales must account for particle volatilization in the presence of oxygen integrated with the catalytic partial oxidation of volatilized products on a noble metal surface. Each

process (particle volatilization or catalytic reforming) consists of complex multi-phase chemical mechanisms and multiple modes of heat transfer for which the current understanding by computer modeling does not even extend to the individual process.<sup>27,28</sup> The chemical and heat integration of the two processes expands the complexity of the overall reaction such that mechanistic observations are currently only available through effluent data and experiments considering more simple fuel species.

The impact of the cellulosic particle with the hot catalytic surface likely initiates the process chemistry. The extent of particle conversion occurring within the gaseous region 3–10 mm above the catalytic bed is likely limited, because previous examination has measured the gas-phase temperature of this region less than 300 °C severely limiting particle conversion by pyrolysis.<sup>17,29</sup> Fig. 5 (panel B) shows that  $T = 700\text{--}800$  °C for C/O = 0.9 at the leading edge of the catalyst, providing sufficient conductive heat transfer from catalyst support to particle for volatilization.

Particle volatilization is likely a complex convolution of heat transfer and reaction chemistry. Complete particle conversion must account for at least (1) the drying of the particle (~5 wt% moisture), (2) cellulose pyrolysis to gases (*e.g.* CO, H<sub>2</sub>), volatile organics, and chars, (3) volatile organic cracking to gases, and (4) oxidation of gases, volatile organics, and chars. Multiple cellulose pyrolysis lumped kinetic models exhibit some form of competitive pathways to either gases (*e.g.* H<sub>2</sub>O) and char, volatile organics (*e.g.* acetic acid, methanol), or just gases.<sup>30–34</sup> Fluidized bed fast pyrolysis reactors maximize selectivity (~70 wt%) to volatile organics around 500 °C for ~1–2 s with millimetre-sized particles.<sup>35</sup> Lower temperatures favor char production, while higher temperatures exhibit higher selectivity to gases with the lower kinetic limit for char production of ~3 wt% at 700–800 °C.<sup>36</sup>

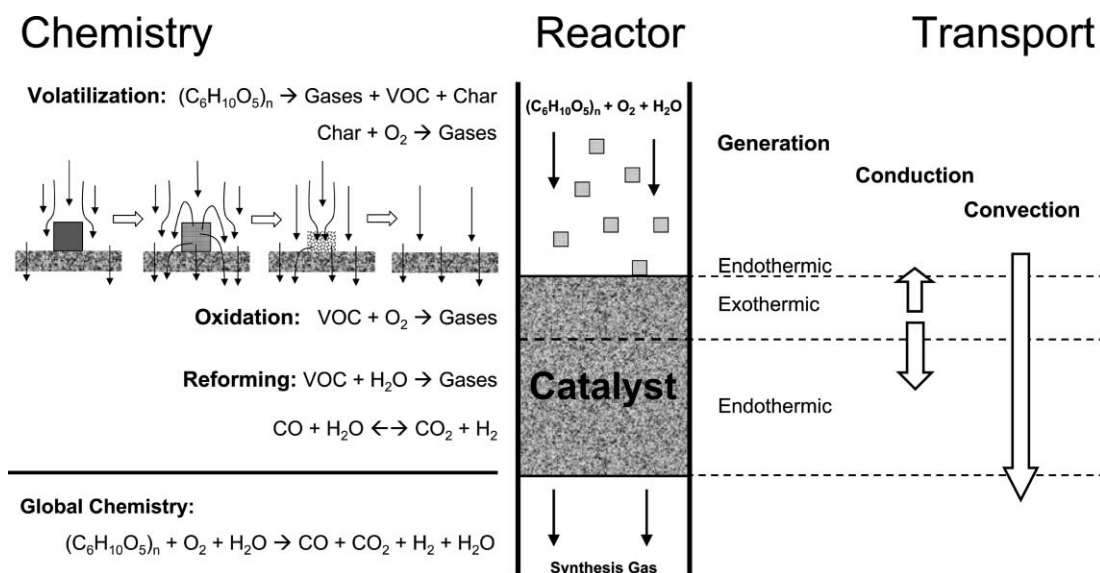


**Fig. 6** The proposed chemical and thermal integration of millisecond particle reforming on a fixed bed of noble metal catalyst permits rapid conversion of organic solid materials to synthesis gas. Particles undergo rapid endothermic volatilization upon impact with a hot, catalytic surface, producing gases (*e.g.* H<sub>2</sub> and CO) and volatile organic compounds (VOCs). Volatile species flow into the catalyst and produce gases by exothermic surface and gaseous oxidation chemistry. Thermal energy generated in the oxidation zone conducts upward to the volatilization zone, and down to the reforming zone where remaining VOCs and gases undergo steam reforming and water-gas-shift to achieve equilibrium selectivity to synthesis gas.



Application of cellulose pyrolysis kinetics to spherical geometry to account for heat and mass transport has considered particle degradation in an inert atmosphere extensively.<sup>37–39</sup> Under optimal fast pyrolysis conditions, organic particles as large as 1 mm usually exhibit heat transport control, while particles with diameters less than  $\sim 200$   $\mu\text{m}$  exhibit chemical kinetic control.<sup>37</sup> The experiment considered here examines a related situation of direct impingement of a  $\sim 315$   $\mu\text{m}$  particle with a hot surface. One-dimensional transport/kinetic models considering solid cellulose rods contacting isothermal hot surfaces has shown superior selectivity to volatile organics due to higher particle heating rates.<sup>36</sup> In an inert atmosphere with solid surface temperatures of 700–800 °C, models predict cellulose pyrolysis of particles on the order of millimetres to exhibit selectivity to volatile organics as high as  $\sim 90$  wt% and char less than 5 wt%.<sup>40</sup>

The applicability of these simulations to the particle volatilization of the considered experiment depends greatly on the magnitude of oxidation chemistry occurring within the particle by interaction with the gaseous feed. The considered microcrystalline cellulose, depicted in Fig. 1, exhibits high porosity permitting an initial internal supply of oxygen. However, the evolution of gases and volatile organics that must be transported to the particle surface due to a difference in density must significantly hinder diffusion of oxygen into the particle. Alternatively, the oxidation of evolved species at the particle surface can only be elucidated through the consideration of a flow boundary layer as has been considered for particle combustion in a methane flame.<sup>27</sup>

Evolved species from the solid particle likely mix with the bulk gas ( $\text{O}_2 + \text{N}_2 + \text{H}_2\text{O}$ ) and flow into the fixed catalyst bed of Rh–Ce/ $\gamma$ - $\text{Al}_2\text{O}_3$ / $\alpha$ - $\text{Al}_2\text{O}_3$  spheres. Likely devolatilized species include the same species observed in bio-oil samples that are derived from carbohydrate pyrolysis such as methanol, hydroxyacetaldehyde, acetic acid, or several furan-based compounds.<sup>41</sup> Highly oxygenated species such as polyols (ethylene glycol and glycerol) have exhibited continuous, steady-state processing to synthesis gas with high conversion ( $>99\%$ ) and equilibrium selectivity to synthesis gas.<sup>15</sup> Similar behavior has also been observed from the reforming of other species classes including esters and acids, ethers, and sugars.<sup>18,42,43</sup> However, the role of competition existing within mixtures for surface chemistry is unknown, and limited research exists examining the catalytic partial oxidation of mixtures of organics.<sup>44</sup>

The conversion of oxygenated species by catalytic partial oxidation is likely to occur by the general mechanism observed with methane reforming. Internal species measurements of methane have shown that conversion of fuel occurs in two distinct zones: oxidation and reforming.<sup>45</sup> In the oxidation zone, volatile fuel species premixed with bulk gases enter the fixed-bed of catalyst spheres at high velocity and undergo exothermic surface oxidation chemistry. Greater than 99% of oxygen is consumed (by definition) within this region likely producing a significant fraction of the thermodynamic species ( $\text{H}_2$ ,  $\text{H}_2\text{O}$ ,  $\text{CO}$ , and  $\text{CO}_2$ ) by surface chemistry. At low C/O ratios (more oxygen rich), the oxidation zone converts a large fraction of the fuel.

At higher C/O, a more significant fraction of fuel passes through the oxidation zone to the reforming zone. Endothermic surface chemistry between fuel and oxidation products such as  $\text{H}_2\text{O}$  (steam reforming) or  $\text{CO}_2$  (dry reforming) provide chemical

routes to equilibrium. Additionally, the gas temperature is sufficiently high to permit endothermic cracking of fuel to smaller fuel species. Both of these chemistries are likely occurring simultaneously, effectively lowering both the surface and gas phase temperature as shown in Fig. 5. The performance of the reforming zone ultimately determines the conversion of volatile fuel species. By selecting a sphere bed (small pores) with a  $\gamma$ - $\text{Al}_2\text{O}_3$  washcoat, the reactor is tuned in favor of the surface chemistries to the desired  $\text{C}_1$  species. For high conversion of fuel, this zone must remain sufficiently hot to permit chemistries at millisecond time-scales. As C/O increases, less thermal energy is generated in the oxidation zone, and the endothermic chemistry of the reforming zone critically cools denying complete conversion of volatile organics. By this mechanism, volatile organics are initially produced at  $\text{C/O} > 1.0$  for fuel flow rates of 25–40  $\text{g h}^{-1}$  on the considered fixed bed catalytic reactor ( $L = 30$  mm).

### Process limitations

The combination of solid conversion chemistry with the autothermal reforming of gaseous compounds introduces a greater number of process variables and prevents a clear definition of the limits of the process. If the objective of the process is steady long-term reforming to synthesis gas, then selected sets of process parameters which result in either incomplete conversion to  $\text{C}_1$  products, catalyst deactivation, or upstream combustion of particles are outside of the domain of sustainable parameters. The incomplete conversion of cellulose to  $\text{C}_1$  was observed when the temperature 30 mm into the catalyst bed was at or below about 500 °C. Table 1 (trials 1–4) lists a set of performance specifications that permit operation relatively close to this requirement. Catalyst deactivation can occur if the maximum in temperature observed at  $\sim 5$  mm within the catalyst bed exceeds  $\sim 1200$  °C, permitting conversion of  $\gamma$ - $\text{Al}_2\text{O}_3$  to  $\alpha$ - $\text{Al}_2\text{O}_3$  or sintering of Rh. This high temperature is accessible at any flow rate (25–60  $\text{g h}^{-1}$ ) provided the C/O is low enough to generate sufficient heat. The third major process restriction is the ignition of solid particles above the catalyst which can propagate up the feed stream in an unsafe, unsustainable manner. The minimum ignition temperature of small (1  $\mu\text{m}$ –1 mm) organic particles is a function of at least particle size and concentration, with smaller particles igniting at lower temperatures.<sup>46</sup> The precise characteristics describing the ignition of particles approaching a hot surface are unknown. However, we have demonstrated that sets of process parameters exist for which processing can occur without dilution with  $\text{N}_2$  on particles as small as 300  $\mu\text{m}$ .

### Process performance

Using the knowledge gained from the experiments described in Fig. 4 and 5, experimental trials were executed to demonstrate the conversion of solid cellulose to an optimal synthesis gas stream. By selecting a fixed sphere-bed catalyst 6 cm in length and a process flow rate of 60  $\text{g h}^{-1}$  at a C/O = 0.9 with steam addition of S/C = 2.14 and 0% nitrogen addition, it was possible to completely convert cellulose to a synthesis gas rich stream with a synthesis gas ratio of  $\text{H}_2/\text{CO} = 2.3$  comprising a dry mole fraction of 42%. Under these conditions the reactor exhibited

steady autothermal reforming with no oxygen breakthrough at a gaseous residence time less than 30 ms. Additionally,  $\sim 80\%$  of the atomic hydrogen provided by the feedstock cellulose was converted to molecular  $H_2$ .

Analysis of the conversion from a solid fuel to a gaseous fuel must account for the loss in fuel value. Using the method described in the experimental section, the maximum theoretical work that could be achieved from the feedstock cellulose (availability) was  $\sim 18 \text{ MJ kg}^{-1}$ . By millisecond reforming, nearly  $\sim 75\%$  of this potential was maintained as the gaseous effluent in the optimal experiment (trial 5 of Table 1). Most of the retained fuel availability existed within the synthesis gas (75–80%) with the remaining fraction occurring with the high temperature (600–800 °C) steam, carbon dioxide or nitrogen. The loss in  $\sim 25\%$  of the fuel value of cellulose can be attributed process irreversibilities such as the generation of a large number of moles from cellulose. The primary benefit offsetting the one quarter loss in fuel value is an improvement in ease of fuel handling. Relative to gases, the transportation of solids within a chemical process remains a demanding, energy intensive technique requiring significant maintenance.

Comparison of the autothermal steam reforming of cellulose with other catalytic gasification techniques will ultimately determine the benefit of small, fast chemistry. While a complete process design and economic analysis is ultimately the best technique for determining the optimal process, an analysis of the operation of the gasification reactor provides an alternative metric that can be realistically assessed within this report. Fig. 7 details the performance of four different biomass gasification reactors containing multiple catalysts with the goal of relating the rate of biomass processing to both the size of the reactor and

the use (mass) of the catalyst. The carbon space velocity has been defined as the ratio of the molar flow rate of biomass carbon to the volume necessary for reaction chemistry. By this definition, higher carbon space velocities result in smaller reactors. The carbon mass velocity has been defined as the ratio of the mass flow of biomass carbon to the mass of catalyst such that higher mass velocities result in lower use of catalyst. Full details of all data points and calculations are located in the electronic supplementary information.†

As shown in Fig. 7, the existing technology for the BTL process of fluidized (circulating and bubbling) bed gasifiers with downstream gas cleaning in fixed bed catalytic reactors exhibit carbon space velocities of  $\sim 0.5\text{--}8.0 \text{ mol L}^{-1} \text{ h}^{-1}$  and carbon mass velocities of  $\sim 0.8\text{--}9.0 \text{ h}^{-1}$ . By applying catalysts directly to the fluidized bed, the use of catalyst (mass velocity) remains about the same, but the volume can be reduced as the space velocity increases to  $8.0\text{--}30 \text{ mol L}^{-1} \text{ h}^{-1}$ . An alternative process to produce synthesis gas produces volatile organics (bio-oil) in fluidized bed reactors which can be steam reformed to synthesis gas. Because this process still uses a fluidized bed, the space velocity remains in the  $8.0\text{--}30 \text{ mol L}^{-1} \text{ h}^{-1}$  range, but the high throughput of bio-oil steam reformers has permitted very high utilization of the Ni and Ru catalysts corresponding to high mass velocities in the range of  $50\text{--}80 \text{ h}^{-1}$ . Millisecond reactors further improve the carbon space velocity to  $100\text{--}300 \text{ mol L}^{-1} \text{ h}^{-1}$  by carrying out the solid conversion to reformable species directly on the reforming catalyst. In general, millisecond reactors are at least an order of magnitude smaller and use less catalyst than most conventional catalytic gasification schemes.

## Conclusions

We show that three sets of chemistries necessary for the biomass-to-liquids process (volatilization of cellulose, tar-cleaning of organic compounds, and the water-gas-shift of the gaseous effluent) can be integrated into one continuous flow catalytic reactor by reactive flash volatilization. Complete conversion of microcrystalline cellulose particles ( $\sim 300 \mu\text{m}$ ) to only  $C_1$  products can occur faster than 30 milliseconds with the use of Rh–Ce/ $\gamma\text{-Al}_2\text{O}_3$  catalysts over a wide range of S/C, C/O, and  $N_2/O_2$ . Steady, autothermal reforming without the presence of a diluent such as  $N_2$  produces a more synthesis gas rich effluent. Additionally, the effluent synthesis gas ratio is tunable ( $1.0 < H_2/CO < 3.0$ ) by manipulating the S/C of the reactor feed. The process appears to occur by the thermal integration of endothermic particle volatilization driven by heat conducted from an exothermic oxidation zone within the catalyst bed. Sufficient heat transfer from the oxidation zone to the entire fixed catalytic bed is thought to maintain the temperature above that at which coke is predicted by equilibrium. By this method, optimal processing conditions permit conversion such that  $\sim 75\%$  of the fuel value of the cellulose is maintained in the synthesis gas effluent.

## Acknowledgements

This work was supported by the U.S. Department of Energy (DOE), Office of Basic Energy Sciences and the Initiative for Renewable Energy (IREE) at the University of Minnesota–Twin Cities.

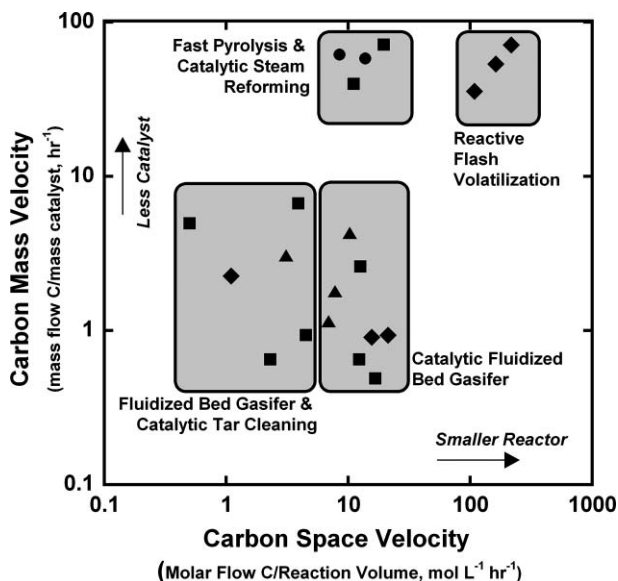


**Fig. 7** Various processes to convert organic solids to synthesis gas exhibit operational performance grouped by process type despite utilizing several different catalysts: dolomite (▲), Ni (■), Rh (◆), Ru (●). The carbon space velocity provides a measure of the reactor volume by relating the molar processing of carbon to the volume necessary for chemical conversion. The carbon mass velocity provides a measure of catalyst usage by relating the molar processing of carbon to the mass of the catalyst. Complete details and references are located in the ESI.†

## Notes and References

- 1 A. J. Ragauskas, *et al.*, The Path Forward for Biofuels and Biomaterials, *Science*, 2006, **311**, 484–489.
- 2 K. Sanderson, U.S. Biofuels: A Field in Ferment, *Nature*, 2006, **444**, 673–676.
- 3 R. D. Perlack, L. L. Wright, A. F. Turhollow, R. L. Graham, B. J. Stokes and D. C. Erbach, *Biomass as feedstock for a Bioenergy and Bioproducts Industry: The Technical Feasibility of a Billion-Ton Annual Supply*, United States Department of Energy, Oak Ridge National Laboratory, Oak ridge, Tn, USA, DOE/GO-102005-2135, 2005, pp. 1–78.
- 4 M. J. A. Tijmensen, A. P. C. Faaij, C. N. Hamelinck and M. R. M. van Hardeveld, Exploration of the possibilities for production of Fischer Tropsch liquids and power *via* biomass gasification, *Biomass Bioenergy*, 2002, **23**, 129–152.
- 5 S. Phillips, A. Aden, J. Jechura, D. Dayton and T. Eggeman, *Thermochemical Ethanol via Indirect Gasification and Mixed Alcohol Synthesis of Lignocellulosic Biomass*, U.S. Department of Energy, National Renewable Energy Laboratory, Golden, CO, USA, NREL/TP-510-41168, 2007, pp. 1–58.
- 6 J. R. Rostrup-Nielsen, Syngas in Perspective, *Catal. Today*, 2002, **71**, 243–247.
- 7 C. N. Hamelinck, A. P. C. Faaij, H. den Uil and H. Boerrigter, Production of FT transportation fuels from biomass; technical options, process analysis and optimization, and development potential, *Energy*, 2004, **29**, 1743–1771.
- 8 J. P. Ciferno, J. Marano, *Benchmarking Biomass Gasification Technologies for Fuels*, National Energy Technology Laboratory, US Department of Energy, Pittsburgh, PA, USA, 2002.
- 9 T. A. Milne, R. J. Evans, *Biomass Gasifier 'Tars': Their Nature, Formation, and Conversion*, U.S. Department of Energy, National Renewable Energy Laboratory, Golden, CO, USA, NREL/TP-570-25357, 1998, pp. 1–68.
- 10 K. Tomishige, M. Asadullah and K. Kunimori, Syngas production by biomass gasification using Rh/CeO<sub>2</sub>/SiO<sub>2</sub> catalysts and fluidized bed reactor, *Catal. Today*, 2004, **89**, 389–403.
- 11 P. Lv, Z. Yuan, C. Wu, L. Ma, Y. Chen and N. Tsubaki, Bio-syngas production from biomass catalytic gasification, *Energy Convers. Manage.*, 2007, **48**, 1132–1139.
- 12 K. Tasaka, T. Furusawa and A. Tsutsumi, Biomass gasification in fluidized bed reactor with Co catalyst, *Chem. Eng. Sci.*, 2007, **62**, 5558–5563.
- 13 M. Asadullah, S. Ito, K. Kunimori, M. Yamada and K. Tomishige, Biomass gasification to hydrogen and syngas at low temperature: Novel catalytic system using fluidized-bed reactor, *J. Catal.*, 2002, **208**, 255–259.
- 14 K. Tomishige, T. Miyazawa, M. Asadullah, S. Ito and K. Kunimori, Catalyst performance in reforming of tar derived from biomass over noble metal catalysts, *Green Chem.*, 2003, **5**, 399–403.
- 15 P. J. Dauenhauer, J. R. Salge and L. D. Schmidt, Renewable hydrogen by autothermal steam reforming of volatile carbohydrates, *J. Catal.*, 2006, **244**, 238–247.
- 16 M. Asadullah, K. Tomishige and K. Fujimoto, A novel catalytic process for cellulose gasification to synthesis gas, *Catal. Commun.*, 2001, **2**, 63–68.
- 17 P. J. Dauenhauer, B. J. Dreyer, N. J. Degenstein and L. D. Schmidt, Millisecond reforming of solid biomass for sustainable fuels, *Angew. Chem., Int. Ed.*, 2007, **46**, 5864–5867.
- 18 J. R. Salge, B. J. Dreyer, P. J. Dauenhauer and L. D. Schmidt, Renewable hydrogen from nonvolatile fuels by reactive flash volatilization, *Science*, 2006, **314**, 801–804.
- 19 C. Wheeler, A. Jhalani, E. J. Klein, S. Tummala and L. D. Schmidt, The water-gas-shift reaction at short contact times, *J. Catal.*, 2004, **223**, 191–199.
- 20 A. S. Bodke, S. S. Bharadwaj and L. D. Schmidt, The Effect of Ceramic Supports on Partial Oxidation of Hydrocarbons over Noble Metal Coated Monoliths, *J. Catal.*, 1998, **179**(1), 138–149.
- 21 A. Roine, *Outokumpu HSC Chemistry for Windows Ver. 4.0*, Outokumpu Research Oy, Pori, Finland, 2007.
- 22 M. J. Moran, *Availability Analysis: A Guide to Efficient Energy Use*, ASME Press, New York, 1989.
- 23 J. Szargut, T. Styrylska, Approximate evaluation of the exergy of fuels, *Brennst. Waerme Kraft*, **16**, 1964, pp. 589–596.
- 24 M. Dietenberger, Update for Combustion Properties of Wood Components, *Fire Mater.*, 2002, **26**, 255–267.
- 25 S. R. F. Probst and R. E. Hicks, *Synthetic Fuels*, Dover Publications Inc, Mineola N. Y., 2006.
- 26 K. J. Ptasinski, M. J. Prins and A. Pierik, Exergetic evaluation of biomass gasification, *Energy*, 2007, **32**, 568–574.
- 27 Y. B. Yang, V. N. Sharifi, J. Swithenbank, L. Ma, L. I. Darvell, J. M. Jones, M. Pourkashanian and A. Williams, Combustion of a Single Particle of Biomass, *Energy Fuels*, 2008, **22**, 306–316.
- 28 A. B. Mhadshwar and D. G. Vlachos, Hierarchical multiscale mechanism development for methane partial oxidation and reforming and for thermal decomposition of oxygenates on Rh, *J. Phys. Chem. B*, 2005, **109**, 16819–16835.
- 29 C. Di Blasi, Comparison of semi-global mechanisms for primary pyrolysis of lignocellulosic fuels, *J. Anal. Appl. Pyrolysis*, 1998, **47**, 43–64.
- 30 A. G. W. Bradbury, Y. Sakai and F. Shafizadeh, A Kinetic Model for Pyrolysis of Cellulose, *J. Appl. Polym. Sci.*, 1979, **23**, 3271–3280.
- 31 A. G. Liden, F. Berruti and D. S. Scott, A Kinetic Model for the Production of Liquids from the Flash Pyrolysis of Biomass, *Chem. Eng. Commun.*, 1988, **65**, 207–221.
- 32 J. P. Diebold, A Unified, Global Model for the Pyrolysis of Cellulose, *Biomass Bioenergy*, 1994, **7**, 75–85.
- 33 M. J. Antal, Jr. and G. Varhegyi, Cellulose Pyrolysis Kinetics: The Current State of Knowledge, *Ind. Eng. Chem. Res.*, 1995, **34**, 703–717.
- 34 J. G. Reynolds and A. K. Burnham, Pyrolysis Decomposition Kinetics of Cellulose-Based Materials by Constant Heating Rate Micropyrolysis, *Energy Fuels*, 1997, **11**, 88–97.
- 35 A. V. Bridgwater, Renewable fuels and chemicals by thermal processing of biomass, *Chem. Eng. J.*, 2003, **91**, 87–102.
- 36 C. Di Blasi, The state of the art of transport models for charring solid degradation, *Polym. Int.*, 2000, **49**, 1133–1146.
- 37 A. M. C. Janse, R. W. J. Westerhout and W. Prins, Modelling of flash pyrolysis of a single wood particle, *Chem. Eng. Process.*, 2000, **39**, 239–252.
- 38 D. R. Soravia and P. Canu, Kinetics modeling of cellulose fast pyrolysis in a flow reactor, *Ind. Eng. Chem. Res.*, 2002, **41**, 5990–6004.
- 39 L. J. Curtis and D. J. Miller, Transport model with Radiative Heat Transfer for Rapid Cellulose Pyrolysis, *Ind. Eng. Chem. Res.*, 1988, **27**, 1775–1783.
- 40 C. Di Blasi, Heat transfer mechanisms and multi-step kinetics in the ablative pyrolysis of cellulose, *Chem. Eng. Sci.*, 1996, **51**, 2211–2220.
- 41 M. Garcia-Perez, A. Chaala, H. Pakdel, D. Kretschmer and C. Roy, Characterization of bio-oils in chemical families, *Biomass Bioenergy*, 2007, **31**, 222–242.
- 42 D. C. Rennard, P. J. Dauenhauer and Sarah A. Tupy, Autothermal Catalytic Partial Oxidation of Bio-Oil Functional Groups: Esters and Acids, *Energy Fuels*, 2008, **22**, 1318–1327.
- 43 S. Wang, T. Ishihara and Y. Takita, Partial oxidation of dimethyl ether over various supported metal catalysts, *Appl. Catal., A*, 2002, **228**, 167–176.
- 44 C. Rioche, S. Kulkarni, F. C. Meunier, J.P. Breen and R. Burch, Steam reforming of model compounds and fast pyrolysis bio-oil on supported noble metal catalysts, *Appl. Catal., B*, 2005, **61**, 130–139.
- 45 R. Horn, K. A. Williams, N. J. Degenstein and L. D. Schmidt, Syngas by catalytic partial oxidation of methane on rhodium: Mechanistic conclusions from spatially resolved measurements and numerical simulations, *J. Catal.*, 2006, **242**, 92–102.
- 46 M. Mittal and B. K. Guha, Minimum Ignition Temperature of Polyethylene Dust; a Theoretical Model, *Fire Mater.*, 1997, **21**, 169–177.



# Mixture effects and predictability of combination effects of imidazolium based ionic liquids as well as imidazolium based ionic liquids and cadmium on terrestrial plants (*Triticum aestivum*) and limnic green algae (*Scenedesmus vacuolatus*)

Marianne Matzke,<sup>\*a</sup> Stefan Stolte,<sup>b</sup> Andrea Bösch<sup>b</sup> and Juliane Filser<sup>a</sup>

Received 12th February 2008, Accepted 24th April 2008

First published as an Advance Article on the web 4th June 2008

DOI: 10.1039/b802350f

Up to now the issues of mixture toxicity and combination effects were neglected within a prospective hazard assessment of ionic liquids (ILs). However when being released to the environment, mixtures of ILs or mixtures of ILs and other pollutants are likely to occur and therefore the impact of mixture toxicity should be taken into account. Thus this study investigates the effects of three differently composed mixtures containing ILs as well as ILs and the heavy metal cadmium on limnic green algae (*Scenedesmus vacuolatus*) and wheat (*Triticum aestivum*). For an evaluation of the results, two well established concepts of concentration addition (CA) and independent action (IA) were used. Both (CA and IA) underestimated the effects of the mixtures consisting exclusively of ILs leading to the assumption that interactions between the mixture components or between the mixture components and the environmental matrix occurred. The general applicability of CA and IA must be questioned. For the mixture of ILs and cadmium the deviations from the predictions were moderate (and less toxic than expected) so that CA can be recommended as a starting point for the analysis of combination effects of ILs and heavy metals. In general the presence of cadmium reduced the toxicity for both the aquatic as well as the terrestrial organisms. The green algae reacted approximately two orders of magnitude more sensitive to the mixture scenarios than wheat and proved to be a good reference test system for the evaluation of measured effects within a prospective hazard assessment of ionic liquids.

## Introduction

Ionic liquids (ILs) are a promising substance class regarding their interesting physicochemical properties. Manifold applications of certain ILs have been described in the fields of e.g. synthesis,<sup>1</sup> electrochemistry<sup>2</sup> and (bio)catalysis.<sup>3,4</sup> The main advantage of certain ILs is their improved operational safety in comparison to conventional solvents. This is based on the negligible vapour pressure of ILs, resulting in reduced air emissions and non-flammability. Nevertheless, there is a great uncertainty regarding their hazard potential and up to now studies investigating the ecotoxicological hazard potential emanating from ILs focused on single substance toxicities only.<sup>5–10</sup> However aquatic and terrestrial ecosystems are exposed to various multi-component mixtures of pollutants differing in composition and concentration. It is impossible to test all possible mixtures of chemicals and in general the problem of chemical mixtures is neglected in regulation to a large extent due to the high complexity of combination effects. To deal with this

problem there are large efforts to reliably predict combination effects of xenobiotics based on single substance toxicities. Two well established concepts, originating from pharmacological research have successfully been used in ecotoxicology for the investigation of mixture toxicities in single species tests<sup>11–16</sup> as well as in community studies.<sup>17,18</sup>

(a) Concentration addition (CA) describes similarly acting substances, first introduced by Loewe and Muischnek in 1926/1927<sup>19,20</sup> and

(b) Independent action (IA) describes dissimilarly acting compounds, first introduced by Bliss in 1939.<sup>21</sup>

Especially in aquatic toxicology the concept of concentration addition is mostly used for the prediction of combination effects.<sup>22</sup>

Because an IL itself represents a mixture (consisting of a cationic and an anionic moiety) first attempts were made in previous studies to apply the concept of CA for the prediction of the toxicity of one single ionic liquid. The applicability of concentration addition was confirmed for the prediction of ionic liquid toxicity for the mammalian cell line IPC-81.<sup>23</sup> The here presented study investigates the applicability of the concepts of CA and IA to mixtures of selected imidazolium based ILs and to mixtures of selected imidazolium based ILs in combination with the heavy metal cadmium. Cadmium was chosen because it is widespread in the aquatic and terrestrial environment due to natural occurrence and anthropogenic pollution and due to

<sup>a</sup>UFT—Centre for Environmental Research and Technology, Department 10: Ecology, University of Bremen, Leobener Straße, D-28359, Bremen, Germany. E-mail: matzke@uni-bremen.de

<sup>b</sup>UFT—Centre for Environmental Research and Technology, Department 3: Bioorganic Chemistry, University of Bremen, Leobener Straße, D-28359, Bremen, Germany



its persistence<sup>24,25</sup> If ILs are being released to the environment mixture toxicities of this heavy metal and ILs are likely to occur. For a prospective hazard assessment of substances or substance classes in general investigations on behaviour and toxicity of mixtures of those substances with well known environmental pollutants are desirable.

The major difference in the applicability of the two concepts is the distinction between similarly and dissimilarly acting substances. The criteria for similarity/dissimilarity can include similar target sites, similar mechanisms/modes of action or even similar chemical structures. Up to now no clear definition exists for similarity/dissimilarity and the criteria for a definition are controversially discussed in the literature.<sup>26</sup> For the context of this study the selected ILs are treated as similarly acting substances, based on the assumption that the mode of toxic action of ILs is mainly driven by the hydrophobicity of the compounds, which is named baseline toxicity. In contrast for a combination of the heavy metal cadmium and ILs a mixture of dissimilarly acting substances is to be expected. Several studies have found that CA fits for most chemical mixtures (even with independent modes of toxic action)<sup>27,28</sup> or overestimates the measured effects (lower EC<sub>x</sub> values), resulting in a “worst case” scenario which would be preferable from a precautionary point of view.

The concepts of concentration addition and independent action are based on the assumption that no interactions between the mixture components or the mixture components and the environmental matrix occur. Deviations from the respective predicted mixture toxicities are called synergistic (more toxic than expected) or antagonistic events (less toxic than expected). For a clear description of the observed effects it is important to refer to the used model, e.g. synergistic with respect to CA or antagonistic with respect to CA.<sup>29</sup>

The concept of concentration addition is based on similarly acting components only differing in the relative strength of their toxic effects, i.e. one substance acts like a dilution of another. CA can be mathematically expressed as follows:

$$\sum_{i=1}^n \frac{c_i}{\text{EC}_{x_i}} = 1 \quad (1)$$

with  $n$  = number of mixture compounds, EC<sub>x<sub>i</sub></sub> = concentration of the  $i$ th mixture component causing  $x$ % effect when applied

alone,  $c_i$  = the concentration of the respective compound in the mixture.<sup>22</sup>

In contrast the concept of independent action is based on the assumption that the mixture compounds affect different biological subsystems within one organism. So if the single components of a mixture are present in non-effect producing concentrations they do not contribute to mixture toxicity, which is in contrast to CA.

The mathematical formulation of the concept of IA is:

$$E(c_{\text{Mix}}) = E(c_1 + \dots + c_n) = 1 - \prod_{i=1}^n [1 - E(c_i)] \quad (2)$$

with  $E(c_{\text{Mix}})$  = predicted effect (scaled from 0–1) of an  $n$ -component mixture,  $c_i$  = concentration of the  $i$ th component,  $E(c_i)$  = effect of that component when applied alone.<sup>22</sup>

The aim of this study was the analysis of mixture toxicities of three imidazolium based ILs as well as of mixtures of ILs and the heavy metal cadmium. Fig. 1 shows the structures of the analysed compounds.

### The test compounds

Dependent on the investigated environmental compartment, different effects of the analysed mixtures can be expected. The soil matrix represents more interaction potential with the compounds and the bioavailability of the mixture can be reduced e.g. due to sorption processes. In contrast in an aquatic surrounding sorption processes are of minor importance and the organisms are exposed to the mixture in a more pronounced way. So for a prospective hazard assessment representatives from the terrestrial environment (*Triticum aestivum*, wheat) as well as from the aquatic environment (*Scenedesmus vacuolatus*, limnic green alga) were taken into account. Three different mixtures were analysed either containing three selected imidazolium based ILs alone or in combination with cadmium:

- Mixture I analyses an EC<sub>20</sub> fixed ratio mixture containing IM14 BF<sub>4</sub>, IM18 BF<sub>4</sub> and IM14 (CF<sub>3</sub>SO<sub>2</sub>)<sub>2</sub>N.
- Mixture II analyses an EC<sub>20</sub> fixed ratio mixture containing IM14 BF<sub>4</sub>, IM18 BF<sub>4</sub> and IM14 (CF<sub>3</sub>SO<sub>2</sub>)<sub>2</sub>N and cadmium chloride.
- Mixture III simulates an EC<sub>20</sub> fixed ratio ionic liquid mixture containing IM14 BF<sub>4</sub>, IM18 BF<sub>4</sub> and IM14 (CF<sub>3</sub>SO<sub>2</sub>)<sub>2</sub>N which gets in contact with a cadmium

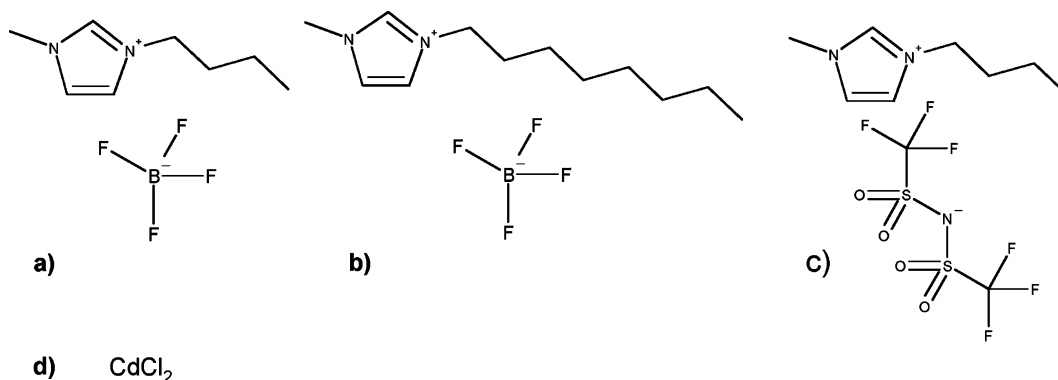


**Fig. 1** Structures of the test compounds: (a) 1-butyl-3-methyl-imidazolium tetrafluoroborate (IM14 BF<sub>4</sub>), (b) 1-octyl-3-methyl-imidazolium tetrafluoroborate (IM18 BF<sub>4</sub>), (c) 1-butyl-3-methyl-imidazolium bis[(trifluoromethyl)sulfonyl]imide (IM14 (CF<sub>3</sub>SO<sub>2</sub>)<sub>2</sub>N), (d) cadmium chloride.

contaminated environment (aquatic and terrestrial). For this mixture a constant cadmium background concentration at environmentally relevant levels was used for all tested mixture concentrations.

In general a fixed ratio design means that the ratio of the mixture components is kept constant while the overall concentration of the mixture is varied so that a complete dose response curve can be experimentally recorded.<sup>30</sup> The single compounds contribute to the mixture in relation to their individual toxicities ( $EC_{20}$ ). A detailed description of the mixture design is given in the experimental section. The  $EC_{20}$ -fixed ratio design was used because it allows an analysis at low effect levels, which is more likely to occur in the environment.

The three different mixtures were analysed according to the following hypotheses:

- For the prediction of combination effects of the ILs mixtures the concept of concentration addition fits.
- For the prediction of combination effects of the ILs mixtures and cadmium the concept of independent action is expected to fit.
- The test system with the freshwater alga will react more sensitive to the investigated mixtures than the one with wheat.
- The occurrence of cadmium within the mixture (either as an environmental relevant background concentration or as

a component of the mixture) leads to antagonistic (less toxic) effects due to interactions of the substances in comparison to the ILs mixture.

## Results

### Comparison of the obtained mixture toxicities with the predictions

The experimental data with the fits, the 95% confidence intervals and the prediction bands for all three mixtures obtained in the reproduction inhibition assay with *Scenedesmus vacuolatus* and the growth inhibition assay with *Triticum aestivum* are shown in Fig. 2 and 3.

Table 1 provides an overview on the experimentally obtained  $EC_{20}$ ,  $EC_{50}$  and  $EC_{80}$  values as well as the predictions according to CA and IA for mixture I and II in the reproduction inhibition assay with *Scenedesmus vacuolatus*. The calculated  $EC_{20}$ ,  $EC_{50}$  and  $EC_{80}$  for mixture III (containing cadmium as a fixed background concentration) are additionally given to compare all three mixtures with each other.

In the reproduction inhibition assay with *Scenedesmus vacuolatus* for mixture I CA only fits for the  $EC_{20}$  value. For the other concentrations both concepts underestimated the toxicities indicating synergistic effects. Within mixture II the

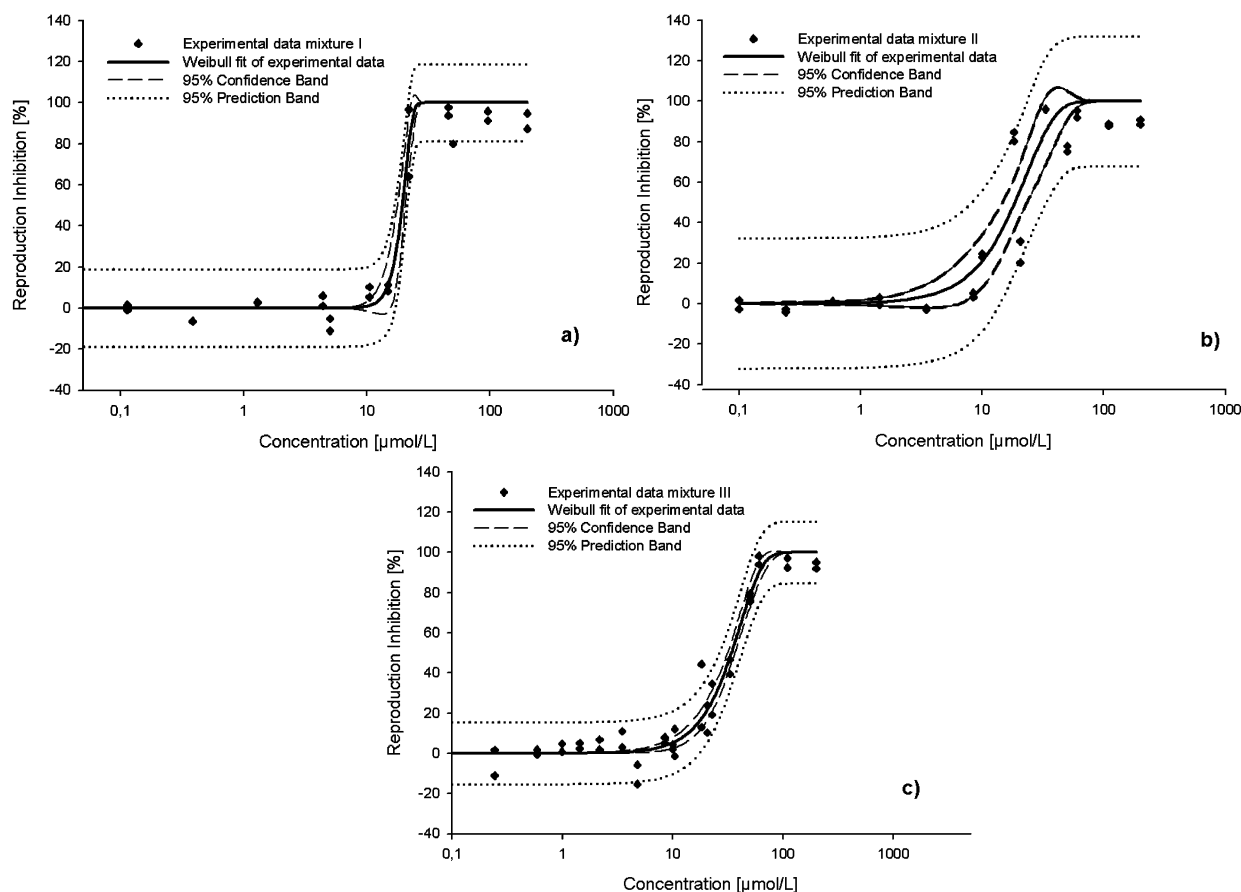


**Fig. 2** Experimental data with fit, 95% confidence intervals and prediction bands for all three mixtures in the reproduction inhibition assay with *Scenedesmus vacuolatus*. (a) mixture I =  $EC_{20}$  fixed ratio mixture with the three ILs; (b) mixture II =  $EC_{20}$  fixed ratio mixture with the three ILs and cadmium chloride; (c) mixture III = cadmium chloride background concentration and an  $EC_{20}$  fixed ratio mixture of the three ILs.

**Table 1** Overview on the obtained  $EC_{20}$ ,  $EC_{50}$  and  $EC_{80}$  values for all three mixtures as well as the calculated values for the CA and IA predictions in the reproduction inhibition assay with *Scenedesmus vacuolatus* for mixture I and II; n.d. = not determined because both concepts are not suitable to calculate the predictions with a fixed background concentration of a pollutant; squared brackets show the 95% confidence intervals of the experimental data

	$r^2$	$EC_x$	Experimental/ $\mu\text{mol L}^{-1}$	CA/ $\mu\text{mol L}^{-1}$	IA/ $\mu\text{mol L}^{-1}$
Mixture I	0.958	20	16 [15–19]	15	22
		50	20 [19–22]	30	45
		80	22 [21–23]	48	68
Mixture II	0.868	20	10 [6–14]	11	17
		50	19 [15–24]	24	39
		80	30 [24–41]	40	62
Mixture III	0.96	20	20 [17–23]	n.d.	n.d.
		50	31 [31–38]		
		80	51 [46–56]		

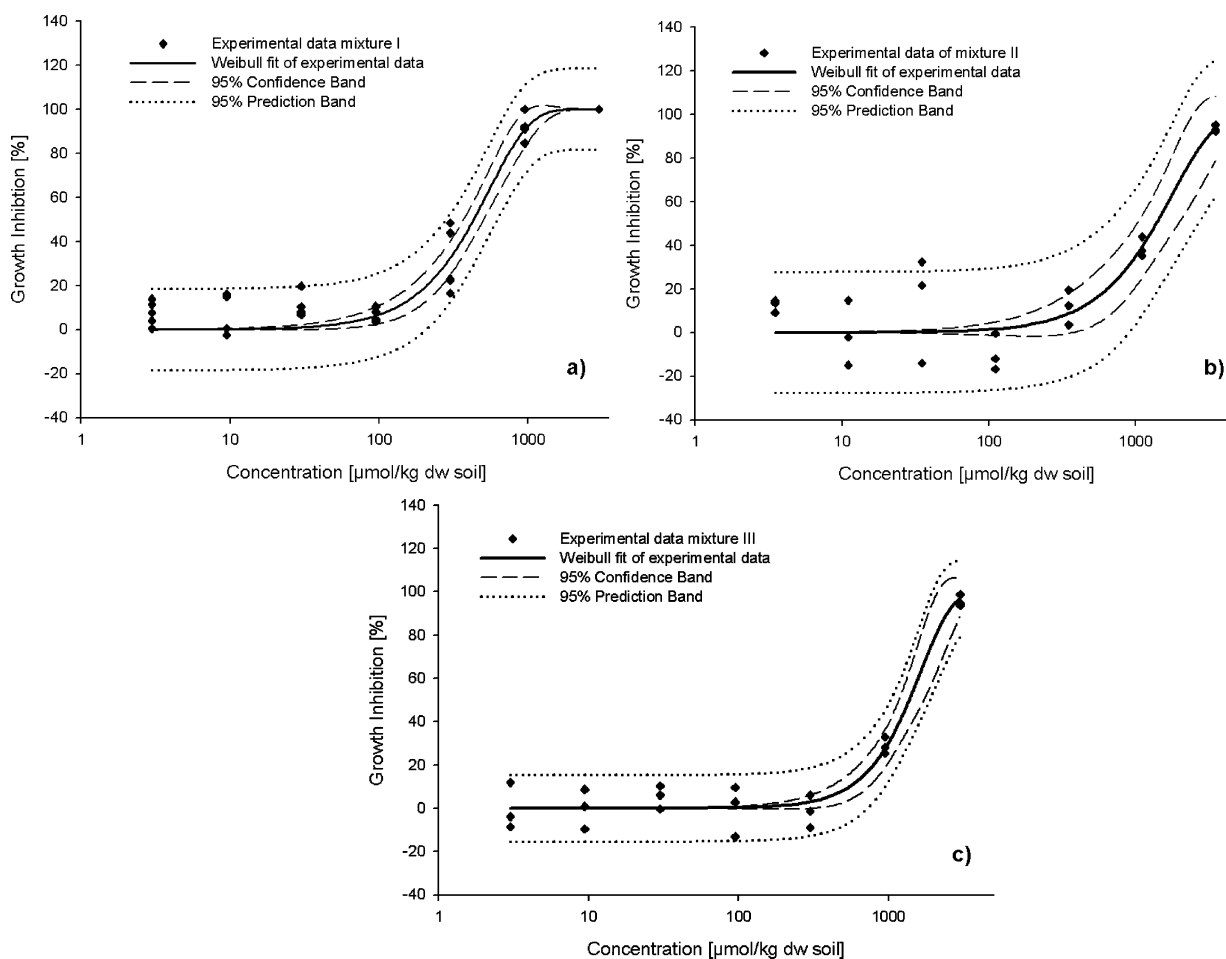


**Fig. 3** Experimental data with fit, 95% confidence intervals and prediction bands for all three mixtures in the growth inhibition assay with *Triticum aestivum*, (a) mixture I =  $EC_{20}$  fixed ratio mixture with the three ILs; (b) mixture II =  $EC_{20}$  fixed ratio mixture with the three ILs and cadmium chloride; (c) mixture III = cadmium chloride background concentration and an  $EC_{20}$  fixed ratio mixture of the three ILs.

experimentally obtained mixture toxicity data can be predicted by the concept of concentration addition. Fig. 4 and 5 show the results of the fit of the experimental data in comparison to the predictions according to CA and IA.

In Table 2 an overview on the experimental obtained  $EC_{20}$ ,  $EC_{50}$  and  $EC_{80}$  values as well as the predictions according to CA and IA is given for mixture I and II in the growth inhibition assay with *Triticum aestivum*. The calculated  $EC_{20}$ ,

$EC_{50}$  and  $EC_{80}$  for mixture III (containing cadmium as a fixed background concentration) are additionally given to compare all three mixtures with each other.

In the growth inhibition assay with *Triticum aestivum* for both mixtures the predictions of CA and IA are nearly congruent. For mixture I at the  $EC_{20}$  level CA correctly described the obtained effects, for the other concentrations both concepts clearly underestimated the observed mixture toxicities. Within

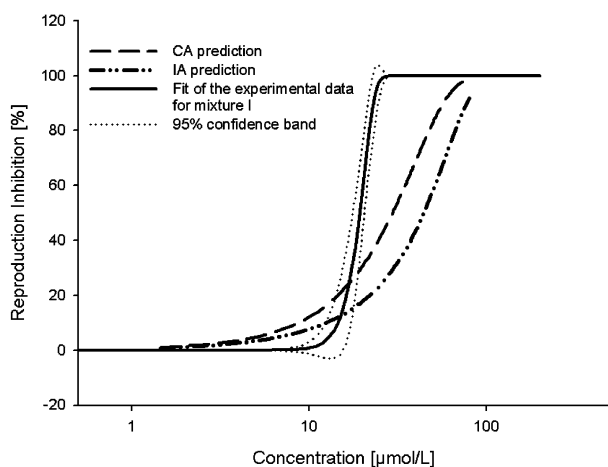


**Fig. 4** Fit of the experimental data (with 95% confidence bands) to a two-parametric Weibull model in comparison to the predictions for the reproduction inhibition assay with *Scenedesmus vacuolatus* for the EC<sub>20</sub> fixed ratio mixture containing IM14 BF<sub>4</sub>, IM18 BF<sub>4</sub> and IM14 (CF<sub>3</sub>SO<sub>2</sub>)<sub>2</sub>N (mixture I).

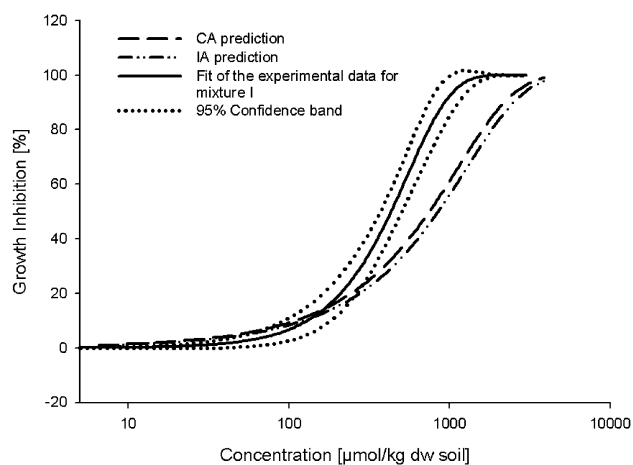


**Fig. 6** Fits of the experimental data (with 95% confidence bands) to a two-parametric Weibull model in comparison to the predictions for the growth inhibition assay with *Triticum aestivum* for the EC<sub>20</sub> fixed ratio mixture containing IM14 BF<sub>4</sub>, IM18 BF<sub>4</sub> and IM14 (CF<sub>3</sub>SO<sub>2</sub>)<sub>2</sub>N (mixture I).

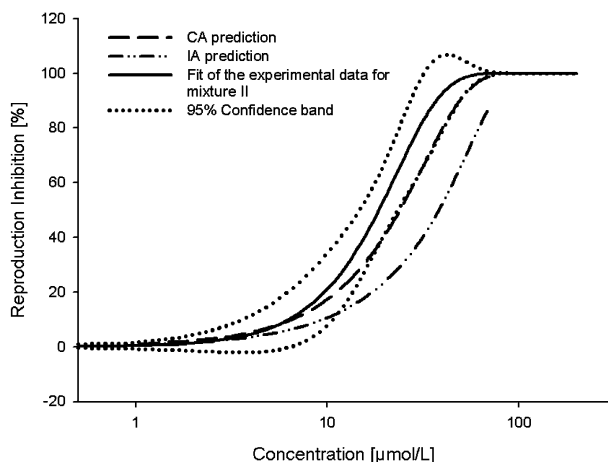


**Fig. 5** Fit of the experimental data (with 95% confidence bands) to a two-parametric Weibull model in comparison to the predictions for the reproduction inhibition assay with *Scenedesmus vacuolatus* for the EC<sub>20</sub> fixed ratio mixture containing IM14 BF<sub>4</sub>, IM18 BF<sub>4</sub>, IM14 (CF<sub>3</sub>SO<sub>2</sub>)<sub>2</sub>N and cadmium (mixture II).

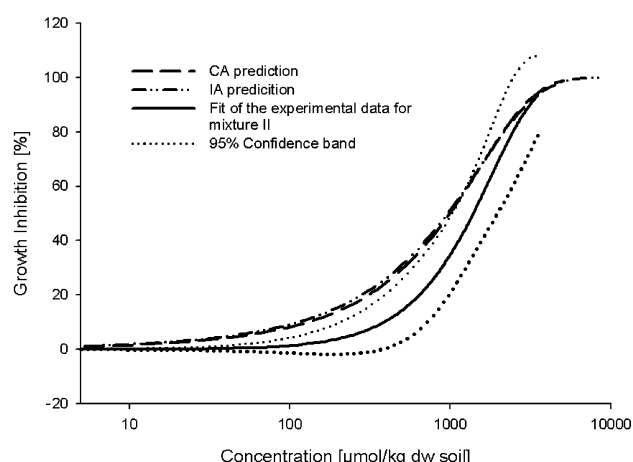


**Fig. 7** Fits of the experimental data (with 95% confidence bands) to a two-parametric Weibull model in comparison to the predictions for the growth inhibition assay with *Triticum aestivum* for the EC<sub>20</sub> fixed ratio mixture containing IM14 BF<sub>4</sub>, IM18 BF<sub>4</sub>, IM14 (CF<sub>3</sub>SO<sub>2</sub>)<sub>2</sub>N and cadmium (mixture II).

mixture II antagonistic effects occurred for the concentration response curves up to the level of the EC<sub>80</sub> values, only at these

high effect concentrations the effects were correctly described by both concepts. In Fig. 6 and 7 the results of the fit of the

**Table 2** Overview on the obtained EC<sub>20</sub>, EC<sub>50</sub> and EC<sub>80</sub> values for all three mixtures as well as the calculated values for the CA and IA predictions in the growth inhibition assay with *Triticum aestivum* for mixture I and II; n.d. = not determined because both concepts are not suitable to calculate the predictions with a fixed background concentration of a pollutant; squared brackets show the 95% confidence intervals of the experimental data

	r <sup>2</sup>	EC <sub>x</sub>	Experimental/µmol kg <sup>-1</sup>	CA/µmol kg <sup>-1</sup>	IA/µmol kg <sup>-1</sup>
Mixture I	0.949	20	214 [167–265]	244	287
		50	436 [375–505]	749	854
		80	741 [627–915]	1606	1853
Mixture II	0.857	20	645 [404–985]	309	290
		50	1396 [1039–1985]	961	964
		80	2460 [1736–3500]	2131	2189
Mixture III	0.957	20	799 [644–1002]	n.d.	n.d.
		50	1372 [1187–1738]		
		80	2075 [1663–2685]		



experimental data in comparison to the predictions according to CA and IA are given.

### Comparison of the three mixture scenarios

In general the green algae reacted approximately two orders of magnitude more sensitive to the mixture scenarios than wheat (Fig. 8).

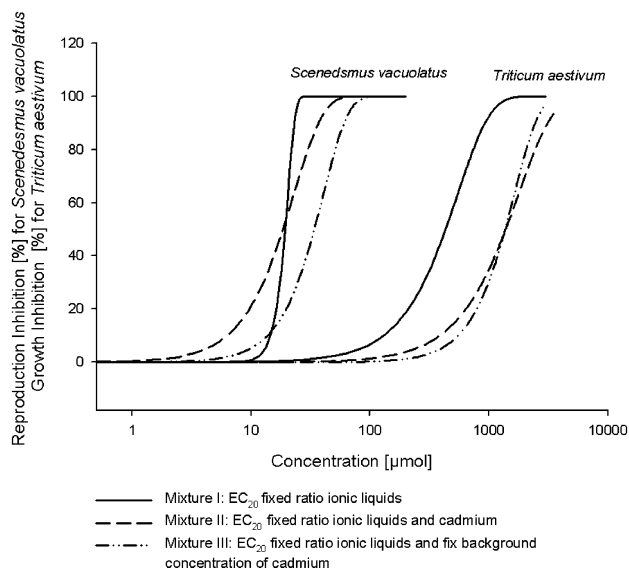


**Fig. 8** Fits of the experimental data for all three mixtures in the reproduction inhibition assay with *Scenedesmus vacuolatus* (left side) and in the growth inhibition assay with *Triticum aestivum* (right side).

Dependent on the investigated environmental compartment and organism, different results were obtained for the three mixtures. For *Scenedesmus vacuolatus* it made a clear difference whether cadmium was present as a fixed background concentration or the heavy metal was part of the fixed ratio mixture. With cadmium being a background pollutant the toxic effects were clearly reduced in comparison to the fixed ratio mixtures of the three ILs with or without the heavy metal. For the terrestrial compartment no differences were observable between the mixtures containing a fixed ratio cadmium concentration or a cadmium background concentration. Both mixtures produced less toxic effects (~factor 3) in comparison to the pure ionic liquid mixture.

### Discussion

In general the concepts of concentration addition and independent action provided no precise prediction of the observed effects with one exception. Only within mixture II (reproduction inhibition assay with *Scenedesmus vacuolatus*, mixture containing ILs and cadmium) the concept of concentration addition approximately confirmed the prediction in accordance with the observed effects.

The toxicities of the ionic liquid mixtures were underestimated by CA and IA for both organisms and clear synergistic effects could be observed. In contrast, for the ionic liquids–cadmium mixture the effects for wheat were slightly overestimated by both concepts. So both concepts did not give precise predictions

of the expected mixture toxicities. Even if the used concepts strictly exclude interactions of the mixture compounds<sup>19–21</sup> the deviations of the experimental data from the predictions lead to the assumption that interactions between the tested substances or interactions with the environmental compartment occurred. The lack of knowledge about the mode of toxic action of ILs and the various modes of toxic action caused by cadmium complicate the interpretation of the obtained results.

Since the obtained experimental data did not fit in with the predictions of CA and IA, especially for ionic substances interactions are likely and further studies are recommended to obtain more precise prediction concepts for combination effects of ILs, which would be desirable from a regulator's point of view. In particular an analysis of the modes of toxic action is needed for a better understanding of the observed deviations from the two prediction concepts.

The obtained synergistic effects (ILs mixture for both green algae and wheat) are a worst case incidence because the mixture toxicity was underestimated by both concepts. In contrast a result overestimating the toxicity (mixture with ILs and cadmium for wheat) is the more favourable case from an ecological and a regulatory point of view because the observed effects are not as drastic as expected. It is also important to analyse a complete concentration response curve of a mixture because, as shown in this study, for selected parts of the curves the experimental data and the predictions fitted quite well (e.g. mixture of ILs and cadmium in the assay with *Scenedesmus vacuolatus*).

An ionic liquid itself represents a mixture because it consists of a cationic and an anionic moiety. Previous studies proved the applicability of concentration addition for the prediction of the toxicity of single ILs in different combinations of cations and anions with the exception of the  $(CF_3SO_2)_2N^-$  anion for the mammalian cell line IPC-81 and the marine bacterium *Vibrio fischeri*.<sup>23,31</sup> This means in the presence of the  $(CF_3SO_2)_2N^-$  anion the observed mixture toxicity was synergistic in comparison to the prediction. Hence, a possible explanation for the synergistic effects of the ILs mixture on the green algae and wheat could be the presence of the  $(CF_3SO_2)_2N^-$  anion in the mixture. Therefore the question arises if concentration addition could precisely predict mixture toxicity for ILs mixtures excluding ILs containing the  $(CF_3SO_2)_2N^-$  anion, e.g. a mixture of IM14  $BF_4$ , IM16  $BF_4$  and IM18  $BF_4$ .

As expected, differences in the observed effects occurred dependent on the investigated environmental compartment and organism. In general the green algae proved to be more sensitive, probably due to the higher bioavailability of the tested pollutants. In contrast to the aquatic environment the soil matrix represents a good interaction basis for (ionic) substances to react with and thus reduces the bioavailability of the pollutant or the pollutant mixture, e.g. due to sorption processes. When cadmium was present in the mixture the toxic effects were in general lower than for the pure ILs mixtures. This could perhaps be explained by the possibility of complexation processes of the ILs with the heavy metal since all test compounds are ionic substances and show potential to interact with each other. The bioavailability and therefore toxicity of chemicals in the environment is strongly dependent on variations of the pH values as documented in a literature review by Frische *et al.*<sup>32</sup> No changes of the pH values

were recorded within the test duration, therefore influences of differing pH conditions can be excluded but should be taken into account in following studies for both the terrestrial and the aquatic environment since pH is a key factor varying with site conditions.

Both prediction concepts are limited in their explanatory power due to interactions between the substances themselves and because the influence of environmental conditions (abiotic or biotic) on mixture toxicity cannot be considered within these mathematical models due to the high complexity of environmental systems. Effects of chemical mixtures can change with environmental conditions (*e.g.* changes in pH values, in the composition of aquatic or terrestrial systems, in temperature *etc.*) or with interactions of the inhabitants of the observed compartment. All these factors influence mixture toxicity and complicate the assessment of combination effects. Additionally CA and IA do not consider mixture scenarios, which are environmentally more relevant, *e.g.* mixtures with differing ratios of the mixture compounds or pre-pollution of the environment with certain compounds with a subsequent pollution through further chemicals. The results in this study proved the importance of pre-pollution scenarios because for the aquatic test system clear differences could be noticed if either cadmium was present as a background concentration or if it was present as a “fixed” part in the mixture. Therefore further studies should deal with more complex mixture scenarios. Still, despite a number of reservations, the two concepts of concentration addition and independent action represented a starting point to investigate combination effects.

## Conclusion

None of the two used concepts precisely predicted the obtained mixture toxicities. This leads to the assumption that interactions between the analysed mixture components occurred. Nevertheless the concept of concentration addition can be used as a basis for the analysis and prediction of mixture toxicities of ILs and cadmium due to the fact that in this case the deviations from the predictions were moderate. The presence of cadmium reduced the toxicity for all tested mixtures in comparison to the pure ILs mixture. For the limnic green algae a distinction could be made for the cadmium being present in the mixtures: a fixed background concentration of the heavy metal resulted in different toxicities in comparison to cadmium as part of the mixture. This leads to the conclusion that more complex mixture scenarios should be investigated in comparison to a “classic” mixture analysis using fixed ratio designs. Subsequent studies should include *e.g.* varying ratios of the mixture components and pre-pollution scenarios as well as pulsed exposure of the mixture compounds. Differences in the observed effects occurred in dependence on the investigated compartment, and therefore it is strongly recommended to investigate always both the terrestrial and the aquatic environment. The limnic green algae *Scenedesmus vacuolatus* proved to be a sensitive reference organism for the evaluation of ionic liquid hazards. Therefore this test organism should always be included in the prospective hazard assessment strategy for ILs to allow a comparison and a classification of the measured effects.

## Material and methods

### Chemicals

All tested ILs were received by the Merck KGaA (Darmstadt, Germany). Cadmium chloride and  $\text{CaCl}_2 \cdot 2\text{H}_2\text{O}$  were purchased from the Sigma-Aldrich Cooperation (Germany). The German standard soil LUFA 2.2 was obtained from the Landwirtschaftliche Untersuchungs- und Forschungsanstalt Speyer (Germany). Wheat seeds (*Triticum aestivum*, Demeter, Donath-Mühle, D-BY-M-1-6043-B) were bought in a health food shop to ensure that the seeds were not treated with any kind of pesticides to exclude additional mixture effects during the experiments.

### Reproduction inhibition assay with limnic green algae *Scenedesmus vacuolatus*

For this assay the unicellular limnic green algae *Scenedesmus vacuolatus* (strain 211-15, SAG (Culture Collection of Algae, University of Göttingen, Germany) was used, and toxicity tests were done using a synchronised culture.<sup>33</sup> The stock culture was grown under photoautotrophical conditions at 28 °C ( $\pm 0.5$  °C) in an inorganic, sterilized medium (pH 6.4) with saturating white light (intensity of 22 to 33 klx) (Lumilux Daylight L 36 W-11 and Lumilux Interna L 36 W-41, Osram, Berlin, Germany). Cells were aerated with 1.5 vol%  $\text{CO}_2$  and synchronised by using a 14 h light and 10 h darkness cycle. The stock culture was diluted every day to a cell density of  $5 \times 10^5$  cells  $\text{mL}^{-1}$ .

This test is a modified version of the assay described in ref. 34 and its sensitivity is comparable to the standardised 72 h test according to ISO guideline.<sup>35</sup>

The toxicity tests started with autospores (young algal cells at the beginning of the growth cycle). Algae were exposed to the single substances and the mixtures for one growth cycle (24 h). The endpoint of this assay is inhibition of algal reproduction measured as inhibition of population growth. All cell numbers (stock culture and test) were determined with the Coulter Counter Z2 (Beckmann, Nürnberg, Germany). The tests were performed in sterilized glass tubes (20 mL Pyrex tubes sealed with caps containing a gas tight Teflon membrane). Algae were stirred over the whole test period of 24 h and the test conditions were the same as for the stock culture except for the  $\text{CO}_2$  source. Here 150  $\mu\text{L}$  of  $\text{NaHCO}_3$  solution was added to each test tube. The methods for stock culturing and testing are described in detail in ref. 13 and 36. Laboratory facilities allowed parallel testing of up to 60 tubes. All substances were tested at least twice: first a range finding was undertaken (4 concentrations, two replicates) and in a second test the results were verified with 8 concentrations per substance in two replicates. The obtained data (from both tests) were pooled because the test conditions were consistent which was proven by a comparable growth rate of the controls (data not shown). The growth inhibition was calculated using the cell counts of the treated samples in relation to the untreated controls (pure medium). For each assay at least 6 controls were used.

### Growth inhibition assay with *Triticum aestivum*

We used the standardised growth inhibition assay according to ISO guideline with wheat (*Triticum aestivum*).<sup>37</sup>

The measured endpoint is growth inhibition. The test duration is three weeks from sowing and the assay was conducted in plastic plant pots each containing 10 seeds. The plants were cultivated in a German standard soil (Lufa 2.2) characterised as loamy sand with a pH of  $5.6 \pm 0.2$ , a clay content of 7.5% and an organic carbon content of 2.3%. The water content was fixed at 50% of the water holding capacity (48%) with aqueous substance solutions respectively deionised water for the controls. For each test at least six controls with uncontaminated soil were grown. Within the test each plant pot contained 300 g dry weight (dw) soil and for all substance or mixture concentrations three replicates were used. The dose–response curves of the mixtures contained seven different concentrations. To minimise the waste amount of contaminated soils a toxic reference (cadmium) was used to ensure that the obtained data were valid and a constant quality of the tests was given. The water content was adjusted every second day by weighing. To exclude pH effects on plant growth, the pH values of the soil samples were checked at the beginning and the end of the test. For all tested single substances and the mixtures, the pH values ranged in the original pH band of Lufa 2.2. For measuring the pH value 5 g soil and 25 mL 0.01 M  $\text{CaCl}_2$  solution were shaken (150 rpm) for 2 h. After sedimentation of the soil samples (at least 4 h) the pH values were measured. The plants were grown in a phytotron chamber under controlled conditions (temperature 20 °C, 80% humidity) with a 16 h light and 8 h darkness cycle.

### Effect data modelling, predictions of mixture toxicity and mixture toxicity testing

To obtain the plots for all dose–response curves, the dose–response curves parameters, the 95% confidence intervals and prediction bands Sigma Plot Version 10 was used. For the analysis and prediction of mixture toxicity complete dose–response curves covering the range from 0 to 100% effect for each of the single mixture components (the three ILs and cadmium) are necessary and were obtained before analysing the different mixture scenarios (data not shown). The data were normalised to the mean of the untreated controls and expressed as fractionated effects on a scale from 0 to 1 to fit the data points using the non-symmetric two parametric regression Weibull model. The Weibull model proved to fit the data best<sup>38</sup> for all single substance dose–response curves. The prediction of the mixture toxicities according to the concepts of CA and IA were calculated on the basis of the fitted concentration response curves of the single compounds.<sup>22</sup>

### Prediction of the mixture toxicities

The predictions of the mixture toxicities were conducted on the basis of fitted concentration response curves of the single mixture compounds. A constant ratio of the mixtures is used and therefore the concentration of each substance in the mixture can be expressed as a fraction ( $p$ ) of the total concentration. For each effect level of the single substances toxic units ( $p/\text{EC}_x$ ) were calculated. The sum of the toxic units of all mixture components at each effect level are corresponding to the effect concentration by concentration addition (see eqn (3)). Eqn (3) represents the re-written form of the concept of concentration addition (eqn (1))

$$\text{EC}_{x_{\text{MIX}}} = \left( \sum_{i=1}^n \frac{p_i}{\text{EC}_{x_i}} \right)^{-1} \quad (3)$$

where  $\text{EC}_{x_{\text{MIX}}}$  is the total concentration of the mixture with  $x\%$  effect;  $p_i$  is the fraction of compound  $i$  in the mixture.<sup>22</sup>

The resulting effect concentrations were calculated in steps of 1% and the concentration–effect pairs were connected with straight lines to visualise the predicted concentration–response curve.

The prediction of the mixture toxicity according to independent action can directly be calculated from effects. Eqn (2) was used as a basis to calculate the prediction according to independent action. The 99 effect concentrations which were already used for the CA prediction were taken as a basis for the independent action model and therefore the fraction of every individual compound ( $c_i$ ) which was present in the mixture could be calculated. The concentration–response relationships  $F_i$  of the individual compounds were used to calculate the corresponding individual effects ( $E(c_i)$ ).

$$E(c_{\text{MIX}}) = 1 - \prod_{i=1}^n [1 - E(c_i)] = 1 - \prod_{i=1}^n [1 - F_i(c_i)] \quad (4)$$

As a consequence the overall effect of any given total mixture concentration can be calculated when expressing the concentrations of the individual compounds as fractions  $p_i$  of the total concentration  $c_{\text{MIX}}$ .<sup>22</sup>

$$E(c_{\text{MIX}}) = 1 - \prod_{i=1}^n [1 - F_i(c_i)] = 1 - \prod_{i=1}^n [1 - F(p_i c_{\text{MIX}})] \quad (5)$$

The experimentally determined mixture toxicities were compared to the predictions obtained by concentration addition and independent action. The mixtures were composed with the following constant molar ratios of:

Mixture I and III: 12.26% IM14  $\text{BF}_4$ , 0.007% IM18  $\text{BF}_4$  and 87.72% IM14 ( $\text{CF}_3\text{SO}_2$ )<sub>2</sub>N for *Scenedesmus vacuolatus*.

Mixture I and III: 82.59% IM14  $\text{BF}_4$ , 7.97% IM18  $\text{BF}_4$  and 9.43% IM14 ( $\text{CF}_3\text{SO}_2$ )<sub>2</sub>N for *Triticum aestivum*.

Mixture II: 11.97% IM14  $\text{BF}_4$ , 0.006% IM18  $\text{BF}_4$ , 85.64% IM14 ( $\text{CF}_3\text{SO}_2$ )<sub>2</sub>N and 2.37% cadmium for *Scenedesmus vacuolatus*.

Mixture II: 58.41% IM14  $\text{BF}_4$ , 5.64% IM18  $\text{BF}_4$ , 6.67% IM14 ( $\text{CF}_3\text{SO}_2$ )<sub>2</sub>N and 29.27% cadmium for *Triticum aestivum*.

For mixture III the environmentally relevant cadmium background concentrations were chosen according to monitoring data obtained from the Umweltbundesamt (= Federal Environmental Agency) Germany:<sup>39</sup> for the terrestrial environment a cadmium background concentration of 44  $\mu\text{mol}$  cadmium was used and for the aquatic environment a background concentration of cadmium of 22  $\mu\text{mol}$  was analysed.

### Acknowledgements

The authors thank Prof. Dr Bernd Jastorff, Enken Hassold, Tanja Juffernholz and the whole ionic liquids team in the UFT for helpful comments and discussion. Furthermore, special thanks are given to Merck KGaA for providing chemicals and for their generous support within our strategic partnership. The first author especially thanks the Hans Böckler Stiftung for funding the work with a PhD scholarship.

## References

- 1 P. Wasserscheid and T. Welton, *Ionic Liquids in Synthesis*, Wiley-VCH-Verlag, Weinheim, 2nd edn, 2007.
- 2 F. Endres, *Eur. J. Chem. Phys. Phys. Chem.*, 2002, **3**(2), 145–154.
- 3 H. Zhao, *J. Mol. Catal. B: Enzym.*, 2005, **37**, 16–25.
- 4 T. Welton, *Coord. Chem. Rev.*, 2004, **248**(21–24), 2459–2477.
- 5 R. J. Bernot, E. E. Kennedy and G. A. Lamberti, *Environ. Toxicol. Chem.*, 2005, **24**(7), 1759–1765.
- 6 R. J. Bernot, M. A. Brueseke, M. A. Evans-White and G. A. Lamberti, *Environ. Toxicol. Chem.*, 2005, **24**(1), 87–92.
- 7 K. M. Docherty and C. F. Kulpa, *Green Chem.*, 2005, **7**(4), 185–189.
- 8 A. Latala, P. Stepnowski, M. Nedzi and W. Mrozik, *Aquat. Toxicol.*, 2005, **73**(1), 91–98.
- 9 C. Pretti, C. Chiappe, D. Pieraccini, M. Gregori, F. Abramo, G. Monni and L. Intorre, *Green Chem.*, 2005, **8**(3), 238–240.
- 10 J. Ranke, K. Molter, F. Stock, U. Bottin-Weber, J. Poczobutt, J. Hoffmann, B. Ondruschka, J. Filser and B. Jastorff, *Ecotoxicol. Environ. Saf.*, 2004, **58**(3), 396–404.
- 11 T. Backhaus, A. Arrhenius and H. Blanck, *Environ. Sci. Technol.*, 2004, **38**(23), 6363–6370.
- 12 T. Backhaus, R. Altenburger, W. Boedeker, M. Faust, M. Scholze and L. H. Grimme, *Environ. Toxicol. Chem.*, 2000, **19**(9), 2348–2356.
- 13 M. Faust, R. Altenburger, T. Backhaus, H. Blanck, W. Boedeker, P. Gramatica, V. Hamer, M. Scholze, M. Vighi and L. H. Grimme, *Aquat. Toxicol.*, 2001, **56**(1), 13–32.
- 14 J. Hermens and P. Leeuwangh, *Ecotoxicol. Environ. Saf.*, 1982, **6**(3), 302–310.
- 15 J. Hermens, F. Busser, P. Leeuwangh and A. Musch, *Ecotoxicol. Environ. Saf.*, 1985, **9**(1), 17–25.
- 16 M. Junghans, T. Backhaus, M. Faust, M. Scholze and L. H. Grimme, *Pest Manage. Sci.*, 2003, **59**(10), 1101–1110.
- 17 A. Arrhenius, F. Gronvall, M. Scholze, T. Backhaus and H. Blanck, *Aquat. Toxicol.*, 2004, **68**(4), 351–367.
- 18 A. Arrhenius, T. Backhaus, F. Gronvall, M. Junghans, M. Scholze and H. Blanck, *Arch. Environ. Contam. Toxicol.*, 2006, **50**(3), 335–345.
- 19 S. Loewe and H. Muischnek, *Naunyn Schmiedebergs Arch. Exp. Pathol. Pharmacol.*, 1926, **114**, 313–326.
- 20 S. Loewe, *Klinische Wochenschr.*, 1927, **6**, 1077–1085.
- 21 C. Bliss, *Ann. Appl. Biol.*, 1939, **26**, 585–615.
- 22 T. Backhaus, M. Scholze and L. H. Grimme, *Aquat. Toxicol.*, 2000, **49**(1–2), 49–61.
- 23 S. Stolte, J. Arning, U. Bottin-Weber, M. Matzke, F. Stock, K. Thiele, M. Uerd-ingen, U. Welz-Biermann, B. Jastorff and J. Ranke, *Green Chem.*, 2006, **8**(7), 621–629.
- 24 J. Moore and S. Ramamoorthy, in *Heavy Metals in Natural Waters*, Springer-Verlag, New York, Berlin, Heidelberg, Tokyo, 1984, ch. 3, pp. 28–51.
- 25 L. Friberg, C. G. Elinder and T. Kjellström, in *Environmental Health Criteria 134—Cadmium*, World Health Organisation, Geneva, 1992, ch. 1–6, pp. 17–65.
- 26 R. Altenburger, M. Nendza and G. Schuurmann, *Environ. Toxicol. Chem.*, 2003, **22**(8), 1900–1915.
- 27 T. Backhaus and L. H. Grimme, *Chemosphere*, 1999, **38**(14), 3291–3301.
- 28 A. Arrhenius, On the ecotoxicology of chemical mixtures—The predictive power of the concepts of concentration addition and independent action in microalgal communities Göteborg, *Dissertation*, Göteborg University, Sweden, 2005.
- 29 M. C. Berenbaum, *Pharmacol. Rev.*, 1989, **41**(2), 93–141.
- 30 A. Arrhenius, T. Backhaus, F. Gronvall, M. Junghans, M. Scholze and H. Blanck, *Arch. Environ. Contam. Toxicol.*, 2006, **50**(3), 335–345.
- 31 M. Matzke, S. Stolte, K. Thiele, T. Juffernholz, J. Arning, J. Ranke, U. Welz-Biermann and B. Jastorff, *Green Chem.*, 2007, **9**(11), 1198–1207.
- 32 T. Frische, K. H. Mebes and J. Filser, *Assessing the bioavailability of contaminants in soils: a review on recent concepts*, Berlin, 2003, Research Report 201 64 214.
- 33 M. Faust, R. Altenburger, W. Boedeker and L. H. Grimme, *Schriften. Ver. Wasser Boden Lufthyg.*, 1992, **89**, 311–321.
- 34 R. Altenburger, W. Boedeker, M. Faust and L. H. Grimme, *Ecotoxicol. Environ. Saf.*, 1990, **20**(1), 98–114.
- 35 ISO Guideline 8692: Water Quality—Fresh water algal growth inhibition test with *Scenedesmus subspicatus* and *Selenastrum capricornutum*, 1989.
- 36 M. Faust, R. Altenburger, T. Backhaus, H. Blanck, W. Boedeker, P. Gramatica, V. Hamer, M. Scholze, M. Vighi and L. H. Grimme, *Aquat. Toxicol.*, 2003, **63**(1), 43–63.
- 37 ISO Guideline 11269-2: Soil quality—Determination of the effects of pollutants in soil flora—Part 2: Effects of chemicals on the emergence and growth of higher plants, 2003.
- 38 M. Scholze, W. Boedeker, M. Faust, T. Backhaus, R. Altenburger and L. H. Grimme, *Environ. Toxicol. Chem.*, 2001, **20**(2), 448–457.
- 39 Umweltbundesamt, Germany, <https://www.uba.de>; 2007.



# Mild catalytic oxidation of secondary and tertiary amines to nitrones and *N*-oxides with H<sub>2</sub>O<sub>2</sub> mediated by Pt(II) catalysts

Marco Colladon, Alessandro Scarso and Giorgio Strukul\*

Received 1st April 2008, Accepted 8th May 2008

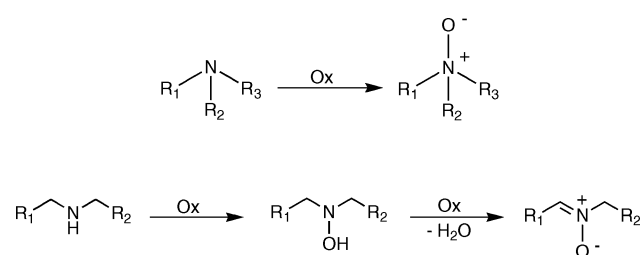
First published as an Advance Article on the web 13th June 2008

DOI: 10.1039/b805404e

Bridging hydroxo complexes of Pt(II) can be used as catalysts for the oxidation of tertiary and secondary amines under mild conditions using the environmentally benign hydrogen peroxide as the oxidant. The reaction proceeds with medium to excellent yields particularly in the case of the more electron rich tertiary amines.

## Introduction

Nitrogen containing compounds such as amines are important substrates in the field of oxidation processes. Primary amines, particularly anilines, are converted to nitrosoarenes for azobenzenes synthesis,<sup>1,2</sup> secondary amines are transformed into nitrones<sup>3</sup> while tri-substituted amines and pyridines<sup>4,5</sup> yield the corresponding *N*-oxides (Scheme 1). The use of the latter compounds in industrial chemistry spans from surfactants production to alkene synthesis *via* Cope elimination.<sup>6</sup> *N*-oxides are emerging compounds with a growing interest in many fields of chemistry, as witnessed by a rapid increase in publications in the last ten years.<sup>7</sup> Their use ranges from stoichiometric oxidants,<sup>8</sup> including in asymmetric processes,<sup>9</sup> to a more recent application as Lewis base catalysts.<sup>10</sup> They have also been employed as ligands for transition metals<sup>7,11</sup> applied as catalysts in epoxidation reactions.<sup>12</sup> Similarly, enantiopure chiral *N*-oxides are emerging as Lewis base catalysts for asymmetric transformations.<sup>7,13,14</sup>



**Scheme 1** Oxidation of tertiary amines provides *N*-oxides while oxidation of secondary amines to nitrones is generally a two step reaction, with hydroxylamine species as intermediates.

*N*-Oxides can be prepared by a wide range of methods and reagents including both organic oxidants like Bromamine-T,<sup>15,16</sup> dioxiranes<sup>17</sup> and HOF·CH<sub>3</sub>CN,<sup>18</sup> and catalytic methods under either heterogeneous (employing oxone or hydroperoxides<sup>19</sup> as oxidants) or homogeneous conditions. In the latter case, noteworthy examples are the oxidation of pyridines and tertiary

amines *via* metal catalyzed reactions with RuCl<sub>3</sub><sup>20</sup> and Re with percarbonates.<sup>21</sup>

Among the primary oxidants employed for *N*-oxides production, oxygen<sup>22</sup> and hydrogen peroxide<sup>23</sup> are the most interesting species because of their high atom efficiency,<sup>24</sup> safe handling and low cost. Moreover water is the only by-product of their reduction, and this makes their use very attractive for the development of “green” oxidation processes. Employment of O<sub>2</sub> for *N*-oxides production has been reported,<sup>25</sup> while H<sub>2</sub>O<sub>2</sub> has been investigated mainly with heterogeneous catalysts.<sup>26</sup> As far as homogeneous catalytic oxidation is concerned, the use of H<sub>2</sub>O<sub>2</sub> has been largely under-investigated. Examples are known with organic catalysts like flavin derivatives,<sup>27</sup> as well as a few cases where metal catalysts like methyl trioxorhenium (MTO),<sup>5</sup> and Mn-porphyrins were employed.<sup>28</sup> New methods and catalysts are therefore required in order to improve the experimental conditions, productivity and selectivity and to reduce the amount of oxidant consumed. As to the enantioselective version of the reaction, a few methods were reported employing proteins<sup>29</sup> or enzymes<sup>30</sup> but none involving chiral metal catalysts.

Nitrones are generally obtained *via* condensation of carbonyl compounds with *N*-monosubstituted hydroxylamines, but the direct double oxidation of secondary amines would have the advantage of being a much more straightforward synthetic pathway, albeit less favorable for secondary amines bearing different groups due to the formation of two possible isomeric products. The synthesis of nitrones is formally a two-step process involving the initial oxidation to secondary hydroxylamines followed by further oxidation and water elimination to nitrones (Scheme 1).

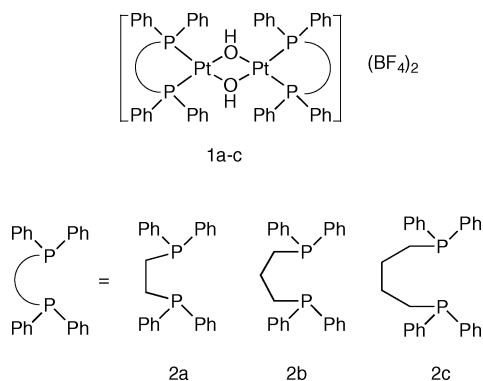
Nitrones are emerging intermediates both in the synthesis of heterocycles<sup>31</sup> and natural products<sup>32</sup> because of their use as active 1,3-dipoles in cycloaddition reactions, and as important spin trap reagents<sup>33</sup> for biological systems. Recently, chiral nitrones have attracted much interest and their synthesis, usually not performed *via* asymmetric oxidation steps, has been recently reviewed.<sup>34</sup> The development of direct asymmetric oxidation procedures is still challenging and this target spurs the discovery of new, active and selective catalytic systems.

While the direct oxidation of hydroxylamines to nitrones has been reported using hydroperoxides<sup>35</sup> or hypochlorite,<sup>36</sup> recent studies by the groups of Goti and Murahashi have considered

Dipartimento di Chimica, Università Ca' Foscari di Venezia, Dorsoduro 2137, 30123, Venezia, Italy. E-mail: strukul@unive.it; Fax: +39 041 2348517; Tel: +39 041 2348931

the more environmentally friendly  $\text{H}_2\text{O}_2$ , employing as catalysts different transition metals like Re<sup>37</sup> and W.<sup>38</sup>

Herein we present the mild and highly efficient catalytic oxidation of tertiary and secondary amines to the corresponding *N*-oxides and nitrones with hydrogen peroxide catalyzed by Pt(II) complexes of general formula  $((\text{P}-\text{P})\text{Pt}\mu\text{OH})_2^{2+}$  **1a–c**, Scheme 2) that were successfully exploited in epoxidation,<sup>39a,b</sup> sulfoxidation<sup>39c</sup> and Baeyer–Villiger<sup>39d</sup> oxidation reactions with the same oxidant.



**Scheme 2** Pt(II) complexes **1a–c** employed as catalysts for secondary and tertiary amines oxidation with hydrogen peroxide.

## Results and discussion

### Tertiary amines oxidation

Triethylamine was used as a model substrate for the oxidation to the corresponding *N*-oxide with 35% hydrogen peroxide employing different Pt(II) species **1a–c**. Reaction performed with  $\text{K}_2\text{PtCl}_4$  did not show *N*-oxide production due to extensive hydrogen peroxide decomposition *via* dismutation, while, on the contrary, dimeric diphosphine Pt(II) complexes **1a–c** showed a marked activity under mild experimental conditions and a strong ligand effect. In particular the larger the bite angle of the diphosphine ligand, the higher the activity and productivity (turnover number, TON) of the catalyst, in agreement with the results already observed for the same class of catalysts in the Baeyer–Villiger oxidation of ketones.<sup>39d</sup> In the latter case, increasing the bite angle increases the dissociation of the dimeric catalysts and, consequently, the catalytic activity. Reaction in the presence of pyridine *N*-oxide demonstrates the negligible effect of the *N*-oxide species in the organo-catalytic electrophilic activation of  $\text{H}_2\text{O}_2$  through hydrogen bonding.

Table 1 reports also the results of experiments performed with different loading of the most active catalyst **1c**. TON's up to 152 were observed, this being a positive result considering the mild experimental conditions. Autocatalysis by *N*-oxide species is negligible, as observed when the reaction was performed in the presence of both 0.4% mol of **1c** and pyridine *N*-oxide.

The substrate scope of the reaction was then investigated (Table 2) with the aim of elucidating the role played by the nucleophilic character of the nitrogen lone pair. Catalyst **1c** was generally active towards trialkylamines, in particular sterically hindered ones (entries 1 and 2) with moderate to good yields. *N*-oxide production was even higher for amino alcohols (entry

**Table 1** Triethylamine oxidation to the corresponding *N*-oxide with  $\text{H}_2\text{O}_2$  mediated by Pt(II) complexes **1a–c**: catalysts screening. *Experimental conditions*: [sub] = 2.0 mmol,  $[\text{H}_2\text{O}_2]$  = 2.0 mmol, methylene chloride (DCM, 2.0 mL), RT

Entry	Catalyst	Catalyst loading (%)	Time/h	Yield (%) <sup>a</sup>	TON
1	—	—	24	1	—
2	$\text{K}_2\text{PtCl}_4$	0.4	24	0	—
3	Pyridine <i>N</i> -oxide <sup>b</sup>	0.4	5	7	17
4	<b>1a</b>	0.8	5	9	11
5	<b>1b</b>	0.8	5	25	31
6	<b>1c</b>	1.5	5	> 99	66
7	<b>1c</b>	0.8	5	89	111
8	<b>1c</b>	0.4	5	61	152
9	<b>1c</b> + pyridine <i>N</i> -oxide <sup>b</sup>	0.4	5	62	155

<sup>a</sup> Isolated yield. <sup>b</sup> 2 mol%.

6), while aniline derivatives resulted much less reactive due to their intrinsic lower basicity and nucleophilicity. Similarly, lower activity was observed with pyridine unless aromatic substitution changes markedly the electronic properties of the heteroatom (entries 11 and 12). The presence of aromatic substituents as in entries 4, 5 also reduces the catalyst activity. It is worth noting that in the cases of tri-substituted diamines only mono-oxidation occurred when the reaction was performed with one equivalent of hydrogen peroxide (entries 7 and 10). Albeit slower, the catalytic activity of complex **1c** can be compared to other efficient homogeneous catalytic systems,<sup>27</sup> with the additional advantage of no need of excess of  $\text{H}_2\text{O}_2$  indicating that the oxidant does not undergo parallel decomposition pathways, as already observed with the same catalysts in other oxidation reactions.<sup>39</sup>

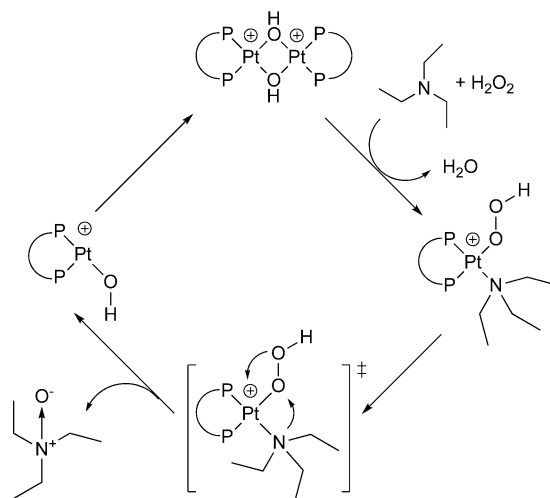
In order to shed light into the catalytic effect of complexes **1a–c**, <sup>1</sup>H and <sup>31</sup>P NMR investigation were performed under catalytic conditions. Addition of 20 eq. of triethylamine to a  $\text{CDCl}_3$  solution of **1c** left the spectrum of the free complex unchanged. Further addition of 20 eq. of  $\text{H}_2\text{O}_2$  caused the immediate formation of a new species characterized by the presence of two different <sup>31</sup>P resonances at 5.1 ppm with  $J_{\text{P-Pt}}$  2920 Hz and  $-3.9$  ppm with  $J_{\text{P-Pt}}$  4210 Hz, respectively. The presence of both  $a > 4000$  Hz and  $a \sim 3000$  Hz coupling constants supports the formation of a mononuclear, mono-cationic hydroperoxo-amino complex<sup>40,39d</sup> by dissociation of the dimeric  $\mu$ -OH structure aided by protonation and water displacement (Scheme 3). At the same time, a small peak at 30.9 ppm with no coupling constant, related to diphosphine dioxide, started increasing. Reaction progress caused the concomitant increase of the latter resonance and the gradual decrease of the mononuclear complex. A possible catalytic cycle consistent with the above observations is reported in Scheme 3. Analogous NMR investigation on complexes **1a** and **1b** showed either no or negligible formation of the new monomeric species, respectively, and formation in both cases of the diphosphine dioxide. This comparison clearly speaks of the importance of the dimeric structure dissociation in favoring high activity. In complex **1c**, a larger bite angle diphosphine ligand

**Table 2** Oxidation of tertiary amines to *N*-oxides with H<sub>2</sub>O<sub>2</sub> catalyzed by **1c**. Experimental conditions: [sub] = 2.0 mmol, [H<sub>2</sub>O<sub>2</sub>] = 2.0 mmol, methylene chloride (DCM, 2.0 mL), RT

Entry	Substrate	Catalyst loading (%)	Time/h	Product	Yield (%) <sup>a</sup>
1		5	5		80
2		5	5		70
3		2.5	5		74
4		5	24		81
5		5	24		83
6		1.5	5		94
7		1.5	5		79
8		1.5	5		68
9		5	5		28
10		1.5	3		95
11		1.5	3		> 99
12		5	5		17

<sup>a</sup> Isolated yield.

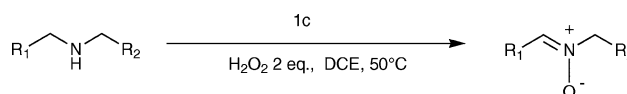
favors dissociation and formation of the hydroperoxy-amino complex where amine oxidation occurs intramolecularly. The intramolecular oxidation of the diphosphine ligand and release of an inactive Pt(II) metal species is a parallel undesired reaction (not shown).



**Scheme 3** Mechanistic hypothesis on the basis of the NMR investigations for tertiary amine oxidation mediated by Pt(II) complex **1c**.

### Secondary amines oxidation

The interesting results observed with tertiary amines as substrates, prompted us towards the investigation of secondary amines (Scheme 4 and Table 3).



**Scheme 4** Oxidation of secondary amines to the corresponding nitrones with 2 eq. hydrogen peroxide mediated by Pt(II) complex **1c**.

Secondary amines are less electron rich substrates and consequently their oxidation is more difficult, requiring higher temperature (50 °C) and with yields from medium to good. Cyclic amines like pyrrolidines and piperidines are better substrates, probably due to lower steric hindrance compared to the acyclic analogs. Interestingly, the catalytic system seems to be sensitive to steric requirements: in fact increase in the bulkiness of the *N*-alkyl groups causes a marked decrease of activity (entries 5 and 6). Benzyl secondary amines are suitable substrates, with higher yields for less sterically demanding compounds.

Worth mentioning is the unusual selectivity observed for 2-methyl-piperidine oxidation, which is opposite to that commonly observed in other metal catalyzed oxidation.<sup>36</sup> These results underline the importance of the steric hindrance at the nitrogen atom in **1c** catalyzed oxidation, rather than the relative stability of the nitronium products.

Here again, it is interesting to underline that good yields were obtained using stoichiometric amounts of H<sub>2</sub>O<sub>2</sub>, at variance with what observed in other catalytic systems.<sup>3,37</sup>

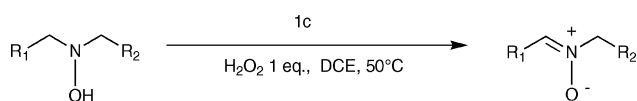
Oxidation to nitrones is a two step reaction: (i) oxidation of secondary amines to hydroxylamines and (ii) oxidation of the latter to nitrones. Therefore, in order to shed light on which of the two steps is the most difficult, we investigated the activity of catalyst **1c** in the second step employing hydroxylamines as substrates (Scheme 5). The results are reported in Table 4.

Nitronium formation from hydroxylamines is generally faster than the direct oxidation of the corresponding secondary

**Table 3** Oxidation of secondary amines to nitrones with H<sub>2</sub>O<sub>2</sub> catalyzed by **1c**. *Reaction conditions:* Catalyst **1c** 10% mol; [sub] = 2.0 mmol, [H<sub>2</sub>O<sub>2</sub>] = 2.0 mmol, methylene chloride (DCM, 2.0 mL), 50 °C

Entry	Substrate	Time/h	Product	Yield (%) <sup>a</sup>
1		24		7 <sup>b</sup>
2		24		13
3		20		57
4		20		64
5		20		73 (85 : 15)
6		4		10
7		24		28
8		24		15
9		24		55

<sup>a</sup> Isolated yield. <sup>b</sup> 25% of diethylhydroxylamine present.



**Scheme 5** Oxidation of secondary hydroxylamines to the corresponding nitrones with H<sub>2</sub>O<sub>2</sub> mediated by Pt(II) complex **1c**.

amines, in particular in the case of *N,N*-diethylhydroxylamine vs. *N,N*-diethylamine. This behavior is likely indicative of a more difficult first oxidative step which hampers the further conversion of the intermediate hydroxylamine to the corresponding nitrone.

Nitrones could also be produced from secondary amines by oxidation to imines, which usually is performed with molecular oxygen mediated by Rh catalysts<sup>41</sup> or with quinone derivatives with Ru species,<sup>42</sup> followed by subsequent oxidation of the latter intermediate species to nitrones. Such a second oxidative step was recently reported using MTO with urea-H<sub>2</sub>O<sub>2</sub> (UHP) adduct as oxidant.<sup>43</sup> Attempts to convert the imines *N*-benzylideneaniline and *N*-benzylidenemethylamine directly to

**Table 4** Oxidation of secondary hydroxylamines to nitrones with H<sub>2</sub>O<sub>2</sub> catalyzed by **1c**. *Reaction conditions:* Catalyst **1c** 10% mol; [sub] = 2.0 mmol, [H<sub>2</sub>O<sub>2</sub>] = 2.0 mmol, methylene chloride (DCM, 2.0 mL), 50 °C

Entry	Substrate	Time/h	Product	Yield (%) <sup>a</sup>
1		3 20		73 80
2		3 20		61 72
3		3 20		17 23

<sup>a</sup> Isolated yield.

the corresponding nitrones with **1c** and one equivalent of H<sub>2</sub>O<sub>2</sub> at 50 °C provided only substantial hydrolysis of the substrate and benzaldehyde release with no traces of the nitrone product. In these cases, the substrate coordinates to the Lewis acid catalyst and is nucleophilically attacked by water rather than H<sub>2</sub>O<sub>2</sub>, thus leading to hydrolysis of the imine moiety to the primary amine and aldehyde. On the other hand, during direct secondary amine oxidation to nitrones with 2 eq. H<sub>2</sub>O<sub>2</sub>, no resonances were observed in the range 10–7.5 ppm where aldehyde and imine CH signals usually appear. All this evidence, confirm that oxidation of secondary amines to nitrones mediated by **1c** proceeds *via* formation of the hydroxylamine intermediate species rather than imines.

<sup>31</sup>P NMR investigation of catalyst **1c** under the experimental conditions used for nitrone production was performed to identify possible active Pt(II) intermediate species. Addition of 10 eq. of H<sub>2</sub>O<sub>2</sub> to a solution of **1c** in CDCl<sub>3</sub> showed no change in the spectrum. Alternatively, addition of *N,N*-diethylamine caused the partial formation of a new species characterized by the presence of two different <sup>31</sup>P resonances at 4.9 ppm with *J*<sub>P-Pt</sub> 2930 Hz and –3.6 ppm with *J*<sub>P-Pt</sub> 4206 Hz. Finally, sequential addition of both 10 eq. of H<sub>2</sub>O<sub>2</sub> and diethylamine caused the complete disappearance of the resonance of the dimeric  $\mu$ -OH complex and the formation of a new main symmetric species **A** at –2.6 ppm with *J*<sub>P-Pt</sub> 3972 Hz and partial formation of diphenylphosphino butane dioxide (dppbO<sub>2</sub>) at 31.2 ppm indicative of partial catalyst decomposition due to ligand oxidation and consequent release of metal.

Addition of 10 eq. of diethylhydroxylamine to **1c** caused the complete disappearance of original resonances and the formation of a new species **B**, characterized by different P resonances at 4.8 ppm with *J*<sub>P-Pt</sub> 3898 Hz and 1.5 ppm with *J*<sub>P-Pt</sub> 3764 Hz, probably to be ascribed to displacement of one  $\mu$ -OH group by the hydroxylamino moiety. Further addition of 20 eq. of H<sub>2</sub>O<sub>2</sub> caused only partial (<25%) formation of species **A** at –2.6 ppm with *J*<sub>P-Pt</sub> 3972 Hz, which is the same observed for diethylamine oxidation, indicative of a symmetric species with weak coordinating neutral ligands. In this case, only traces of dppbO<sub>2</sub> were observed, which is clearly indicative that hydroxylamine substrates lead to Pt(II) species **B** that are more robust against degradation. Species **A** that is present in both experiments could be attributed to double coordination of



nitron product to the Pt(II) metal center, thus leading to a dead end for the catalyst. The lack of species **B** in the oxidation of diethylamine is probably due to the faster second oxidative step compared to the first one.

The same  $^{31}\text{P}$  NMR investigation performed with *N,N*-dibenzylamine and *N,N*-dibenzylhydroxylamine, showed the formation of analogous species, and the faster formation of  $\text{dppbO}_2$  for the former substrate confirms the positive effect on catalyst stability imparted by hydroxylamino substrate coordination to Pt(II).

## Conclusion

Diphosphine Pt(II) complexes **1a–c** showed good catalytic performance towards secondary and tertiary amines oxidation with highly environmentally friendly oxidant  $\text{H}_2\text{O}_2$ . The latter oxidant is highly atom economic, and in the present work it was used in stoichiometric quantities without over-consumption, while, to the best of our knowledge, all the known homogeneous and heterogeneous catalysts for *N*-oxides and nitrones production required an excess of  $\text{H}_2\text{O}_2$ . The system is characterized by the following properties: (a) a considerable catalytic effect for all substrates investigated compared to the uncatalyzed reactions; (b) short reaction times and good yields under mild experimental conditions; (c) for *N*-oxide production trialkylamines are preferentially oxidized over dialkyl-anilines or pyridines; (d) for nitrones production strong steric effects influence secondary amine oxidation and lead to unusual regioselectivity. The ultimate target in the environmentally friendly oxidation of nitrogen containing compounds is the development of asymmetric versions of such reactions, such as the enantioselective oxidation of tertiary amines and desymmetrization of secondary amines. Both issues are currently under investigation in our laboratory.

## Experimental

### Reagents and materials

The complexes **1a–c** were prepared following the procedure reported in the literature,<sup>39d</sup> hydrogen peroxide (35% Aldrich) as well as all the tertiary amines, secondary amines and secondary hydroxyl-amines employed as substrates are commercial products (Aldrich) and were used without further purification.

### General

$^1\text{H}$  NMR, and  $^{31}\text{P}\{^1\text{H}\}$  NMR spectra were recorded at 298 K, unless otherwise stated, on a Bruker AVANCE 300 spectrometer operating at 300.15 and 121.50 MHz, respectively.  $\delta$  values in ppm are relative to  $\text{Si}(\text{CH}_3)_4$  and 85%  $\text{H}_3\text{PO}_4$ . All reactions were monitored by  $^1\text{H}$  NMR. The concentration of the commercial 35%  $\text{H}_2\text{O}_2$  solution was checked iodometrically prior to use.

### Oxidation reactions

These were carried out in a 5 mL vial equipped with a screw-capped silicone septum to allow sampling. Stirring was performed by a Teflon-coated bar driven externally by a magnetic stirrer (700 rpm). Constant temperature was maintained by water circulation through an external jacket connected with a

thermostat. Typically, the proper amount of catalyst **1a–c** was placed in the vial, followed by the solvent (2.0 mL), then the vial was thermostatted. After stirring for 10 min, the substrate (2.0 mmol) was added and the mixture stirred for 10 min. To this, 35% hydrogen peroxide was added in one portion (2.0 mmol for tertiary amines and hydroxylamines, 4.0 mmol for secondary amines) and time was started. All reactions were monitored with  $^1\text{H}$  NMR by direct sampling from the reaction mixtures with a micro syringe. Quenching of the samples by adding an excess of LiCl was performed prior to NMR analysis. At the end of the reaction the solution was diluted with dichloromethane (10.0 mL) and water (10.0 mL). The organic phase was separated, dried with  $\text{Na}_2\text{SO}_4$  and concentrated. The crude product was purified by flash chromatography (hexane–ethyl acetate 80/20 to 100/0).

## Acknowledgements

The authors thank MiUR, the Università Ca' Foscari di Venezia for financial support (PRIN 2003). G.S. thanks Johnson–Matthey for the loan of platinum. Dr L. Sperti for GC–MS analysis is gratefully acknowledged.

## Notes and references

- 1 B. Priewisch and K. Rück-Braun, *J. Org. Chem.*, 2005, **70**, 2350.
- 2 Z. Zhu and J. H. Espenson, *J. Org. Chem.*, 1996, **60**, 1326.
- 3 S.-I. Murahashi, H. Mitsui, T. Shiota, T. Tsuda and S. Watanabe, *J. Org. Chem.*, 1990, **55**, 1736.
- 4 M. R. Prasad, G. Kamalakar, G. Madhavi, S. J. Kulkarni and K. V. Raghavan, *Chem. Commun.*, 2000, 1577.
- 5 R. W. Murray, K. Iyanar, J. Chen and J. T. Wearing, *Tetrahedron Lett.*, 1996, **37**, 805.
- 6 J. March, *Advanced Organic Chemistry*, Wiley, New York, 4th edn, 1992, p 1018.
- 7 G. Chelucci, G. Murineddu and G. A. Pinna, *Tetrahedron: Asymmetry*, 2004, **15**, 1373–1389.
- 8 (a) M. Schroder, *Chem. Rev.*, 1980, **80**, 187; (b) S. V. Ley, J. Norman, W. P. Griffith and S. P. Marsden, *Synthesis*, 1994, 639; (c) A. G. Godfrey and B. Ganem, *Tetrahedron Lett.*, 1990, **31**, 4825; (d) W. P. Griffith, S. V. Ley, G. P. Whitcombe and A. D. White, *J. Chem. Soc., Chem. Commun.*, 1987, 1625; (e) T. Petrowsitch and P. Eibracht, *Synlett*, 1997, 287.
- 9 T. Petrowsitch and P. Eibracht, *Synlett*, 1997, 287.
- 10 (a) F. X. Chen, H. Zhou, X. Liu, B. Qin, X. Feng, G. Zhang and Y. Jiang, *Chem.–Eur. J.*, 2004, **10**, 4790; (b) B. He, F.-X. Chen, Y. Li, X. Feng and G. Zhang, *Eur. J. Org. Chem.*, 2004, **69**, 4657; (c) Y. Shen, X. Feng, Y. Li, G. Zhang and Y. Jiang, *Eur. J. Org. Chem.*, 2004, **69**, 129; (d) F. Chen, X. Feng, B. Qin, G. Zhang and Y. Jiang, *Org. Lett.*, 2003, **5**, 949; (e) Y.-S. Lin, C.-W. Liu and T. Y. R. Tsai, *Tetrahedron Lett.*, 2005, **46**, 1859; (f) M. Nakajima, S. Yamamoto, Y. Yamaguchi, S. Nakamura and S. Hashimoto, *Tetrahedron*, 2003, **59**, 7307; (g) M. Saito, M. Nakajima and S. Hashimoto, *Tetrahedron*, 2000, **56**, 9589; (h) M. Nakajima, S. Kotani, T. Ishizuka and S. Hashimoto, *Tetrahedron Lett.*, 2005, **46**, 157; (i) M. Nakajima, M. Saito, M. Shiro and S.-I. Hashimoto, *J. Am. Chem. Soc.*, 1998, **120**, 6419; (j) M. Nakajima, T. Yokota, M. Saito and S. Hashimoto, *Tetrahedron Lett.*, 2004, **45**, 61; (k) M. Nakajima, M. Saito, M. Uemura and S. Hashimoto, *Tetrahedron Lett.*, 2002, **43**, 8827; (l) Z. Jiao, X. Feng, B. Liu, F. Chen, G. Zhang and Y. Jiang, *Eur. J. Org. Chem.*, 2003, **68**, 3818; (m) I. A. O'Neil, C. D. Turner and S. B. Kalindjian, *Synlett*, 1997, 777; (n) W. J. Kerr, G. G. Kirk and D. Middlemiss, *Synlett*, 1995, 1085.
- 11 (a) M. Carmeli and S. Rozen, *J. Org. Chem.*, 2005, **70**, 2131; (b) G. Dyker, B. Hölzer and G. Henkel, *Tetrahedron: Asymmetry*, 1999, **10**, 3297; (c) B. Gao, Y. Wen, Z. Yang, X. Huang, X. Liu and X. Feng, *Adv. Synth. Catal.*, 2008, **350**, 385.

- 12 M. Nakajima, Y. Sasaki, H. Iwamoto and S.-I. Hashimoto, *Tetrahedron Lett.*, 1998, **39**, 87.
- 13 A. V. Malkov and P. Kočovský, *Eur. J. Org. Chem.*, 2007, **72**, 29.
- 14 M. Nakajima, Y. Sasaki, M. Shiro and S.-I. Hashimoto, *Tetrahedron: Asymmetry*, 1997, **8**, 341.
- 15 C. Copéret, H. Adolfsson, J. P. Chiang, A. K. Yudin and K. B. Sharpless, *Tetrahedron Lett.*, 1998, **39**, 761.
- 16 C. Copéret, H. Adolfsson, T.-A. V. Khuong, A. K. Yudin and K. B. Sharpless, *J. Org. Chem.*, 1998, **63**, 1740.
- 17 M. Ferrer, F. Slinchez-Baeza and A. Messegueur, *Tetrahedron*, 1997, **53**, 15877.
- 18 S. Dayan, M. Kol and S. Rozen, *Synthesis*, 1999, 1427.
- 19 J. D. Fields and P. J. Kropp, *J. Org. Chem.*, 2000, **65**, 5937.
- 20 Vishal B. Sharma, S. L. Jain and B. Sain, *Tetrahedron Lett.*, 2004, **45**, 4281.
- 21 J. L. Suman, J. K. Jomy and S. Bir, *Synlett*, 2006, **16**, 2661.
- 22 S. L. Jain and B. Sain, *Chem. Commun.*, 2002, 1040.
- 23 J. M. Campos-Martin, G. Blanco-Brieva and J. L. G. Fierro, *Angew. Chem., Int. Ed.*, 2006, **45**, 6962.
- 24 B. M. Trost, *Angew. Chem., Int. Ed. Engl.*, 1995, **34**, 259.
- 25 Y. Imada, H. Iida, S. Ono, Y. Masui and S.-I. Murahashi, *Chem.–Asian J.*, 2006, **1–2**, 136.
- 26 (a) L. Rout and T. Punniyamurthy, *Adv. Synth. Catal.*, 2005, **347**, 1958; (b) B. M. Chaudary, B. Bharathi, Ch. Venkat Reddy, M. Lakshmi Kantam and K. V. Raghavan, *Chem. Commun.*, 2001, 1736; (c) M. Ramakrishna Prasad, G. Kamalakar, G. Madhavi, S. J. Kulkarni and K. V. Raghavan, *Chem. Commun.*, 2000, 1577; (d) P. Phukan, R. S. Khisti and A. Sudalai, *J. Mol. Catal. A: Chem.*, 2006, **248**, 109.
- 27 K. Bergstad and J. E. Bäckvall, *J. Org. Chem.*, 1998, **63**, 6650.
- 28 A. Thellend, P. Battioni, W. Sanderson and D. Mansuy, *Synthesis*, 1997, 1387.
- 29 (a) S. Colonna, N. Gaggero, J. Drabowicz, P. Łyżwa and M. Mikołajczyk, *Chem. Commun.*, 1999, 1787; (b) S. V. Dzyuba and A. M. Klibanov, *Tetrahedron: Asymmetry*, 2004, **15**, 2771.
- 30 G. Ottolina, S. Branchi, B. Belloni, G. Carrea and B. Danieli, *Tetrahedron Lett.*, 1999, **40**, 8483.
- 31 K. V. Gothelf and K. A. Jørgensen, *Chem. Rev.*, 1998, **98**, 863.
- 32 R. Bloch, *Chem. Rev.*, 1998, **98**, 1407.
- 33 (a) C. Frejaville, H. Karoui, B. Tuccio, F. Le Moigne, M. Culcasi, S. Pietri, R. Lauricella and P. Tordo, *J. Med. Chem.*, 1995, **38**, 258; (b) T. L. Fevig, S. M. Bowen, D. A. Janowick, B. K. Jones, H. R. Munson, D. F. Ohlweiler and C. E. Thomas, *J. Med. Chem.*, 1996, **39**, 4988.
- 34 J. Revuelta, S. Cicchi, A. Goti and A. Brandi, *Synthesis*, 2007, **4**, 485.
- 35 M. Forcato, W. A. Nugent and G. Licini, *Tetrahedron Lett.*, 2003, **44**, 49.
- 36 S. Cicchi, M. Corsi and A. Goti, *J. Org. Chem.*, 1999, **64**, 7243.
- 37 R. Saladino, V. Neri, F. Cadorna and A. Goti, *Adv. Synth. Catal.*, 2004, **346**, 639.
- 38 S.-I. Murahashi, H. Mitsui, T. Shiota, T. Tsuda and S. Watanabe, *J. Org. Chem.*, 1990, **55**, 1736.
- 39 (a) C. Baccin, A. Gusso, F. Pinna and G. Strukul, *Organometallics*, 1995, **14**, 1161; (b) R. Sinigaglia, R. A. Michelin, F. Pinna and G. Strukul, *Organometallics*, 1987, **6**, 728; (c) A. Scarso and G. Strukul, *Adv. Synth. Catal.*, 2005, **347**, 1227; (d) R. Gavagnin, M. Cataldo, F. Pinna and G. Strukul, *Organometallics*, 1998, **17**, 661.
- 40 T. G. Appleton and M. A. Bennett, *Inorg. Chem.*, 1978, **17**, 738.
- 41 J.-R. Wang, Y. Fu, B.-B. Zhang, X. Cui, L. Liu and Q.-X. Guo, *Tetrahedron Lett.*, 2006, **47**, 8293.
- 42 J. S. M. Samec, A. H. Èll and J.-E. Bäckvall, *Chem.–Eur. J.*, 2005, **11**, 2327.
- 43 G. Soldaini, F. Cadorna and A. Goti, *Org. Lett.*, 2007, **9**, 473.

# Catalytic dehydration of fructose into 5-hydroxymethylfurfural by ion-exchange resin in mixed-aqueous system by microwave heating†

Xinhua Qi,<sup>a,b</sup> Masaru Watanabe,<sup>\*a</sup> Taku M. Aida<sup>a</sup> and Richard Lee Smith, Jr.<sup>\*a</sup>

Received 30th January 2008, Accepted 24th April 2008

First published as an Advance Article on the web 13th June 2008

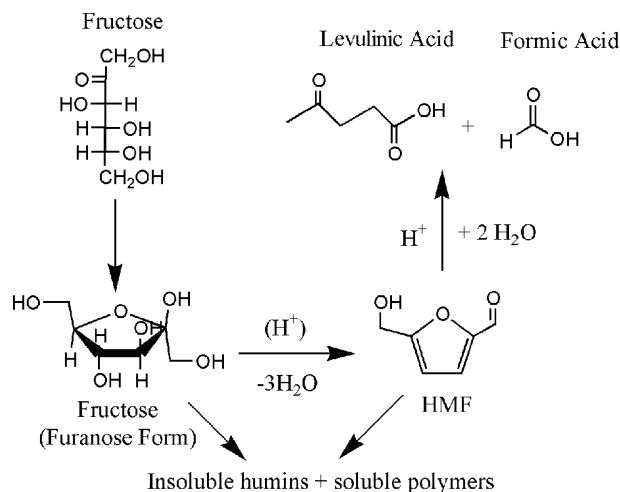
DOI: 10.1039/b801641k

Catalytic dehydration of fructose into 5-hydroxymethylfurfural by microwave heating was studied in acetone–water mixtures in the presence of a cation exchange resin catalyst. The use of acetone–water reaction media resulted in yields of 5-HMF as high as 73.4% for 94% conversion at 150 °C. It was confirmed that there was no decrease of catalytic activity and selectivity for five reuses of the resin, which was in accordance with the elemental analysis results that showed that sulfonic acid groups attached on the resin were stable at the experimental conditions. A comparison between conventional sand bath heating and microwave heating revealed that the latter had a remarkable accelerating effect not only on fructose conversion, but also on 5-HMF yield. Under the conditions (5 ml of 2 wt% fructose solution, 0.1 g of resin, 150 °C and 10 min), fructose conversion and HMF yields by microwave heating (91.7% and 70.3%, respectively) were higher than those by sand bath heating (22.1% and 13.9% respectively). Therefore, the process that we developed in this study showed that high 5-HMF yields from fructose could be achieved under mild conditions.

## 1. Introduction

Diminishing fossil fuel reserves and growing concerns about global warming indicate that renewable sources of energy and chemicals are needed in the near future. Abundant biomass resources are a promising alternative for the sustainable supply of fuel and valuable chemicals.<sup>1</sup> Among the many possible biomass-derived chemicals, 5-hydroxymethylfurfural (5-HMF) is a valuable intermediate for fine chemicals, pharmaceuticals and furane-based polymers,<sup>2</sup> and has been called a “sleeping giant” as an intermediate.<sup>3</sup> The study of acid-catalyzed dehydration of fructose or fructose-precursors into 5-HMF has received considerable attention,<sup>1,4–11</sup> and its chemistry is shown in Scheme 1. The detailed mechanism of the reaction was proposed by Antal *et al.*<sup>12</sup>

This process has been widely studied by the other authors, where many types of acid catalysts have been used, such as mineral acids (such as H<sub>2</sub>SO<sub>4</sub>, HCl, H<sub>3</sub>PO<sub>4</sub>),<sup>1,3–5,13,14</sup> organic acids (such as oxalic acid and levulinic acid),<sup>4</sup> H-form zeolites,<sup>15</sup> transition metal ions,<sup>11,16–18</sup> solid metal phosphates<sup>19–22</sup> and strong acid cation exchange resins.<sup>1,9,13,23,24</sup> Homogenous acid catalyzed processes are effective and can achieve medium 5-HMF yields (40–60%) with high fructose conversion (70–90%),<sup>4</sup>



**Scheme 1** Possible reaction products of the acid catalyzed dehydration and subsequent rehydration of fructose and related compounds.<sup>12,13</sup>

but it has serious drawbacks in terms of separation and recycling as well as equipment corrosion. Solid acid catalysts, such as H-form zeolites and metal phosphates can be recycled and have high selectivity (60–90%), but only low fructose conversion (30–60%) even at reaction times as long as 2 h.<sup>20,21</sup> An ion exchange resin could be a candidate as a green catalyst for 5-HMF formation, however, only limited studies have been performed since resins are considered to be useful below 100 °C, which can greatly limit the reaction rate.<sup>25</sup>

Solvents used as reaction media can be divided into four main groups: reactions in water,<sup>4,15,17–21,26,27</sup> reactions in organic solvents or organic–water mixtures,<sup>1,5–7,16</sup> reactions in ionic liquids,<sup>9–11,28,29</sup> and more recently, biphasic water/organic

<sup>a</sup>Research Center of Supercritical Fluid Technology, Tohoku University, 6-6-11 Aoba, Aramaki, Aoba-ku, Sendai, 980-8579, Japan.

E-mail: meijin@scf.che.tohoku.ac.jp, smith@scf.che.tohoku.ac.jp;

Fax: (+81) 022-795-5864

<sup>b</sup>College of Environmental Science and Engineering, Nankai University, Tianjin, 300071, China

† Electronic supplementary information (ESI) available: Microwave heating experimental setup (Fig. S1), typical work-up procedure and a typical heating profile (Fig. S2). See DOI: 10.1039/b801641k

systems.<sup>1,13,14,24</sup> Aqueous processes are favored in respect to ecological aspects but are unfortunately, inefficient, because 5-HMF further rehydrates into levulinic acid and formic acid in water. Roman–Leshkov *et al.*<sup>14</sup> studied acid-catalyzed fructose dehydration in a two-phase reactor system, in which fructose was dehydrated in the aqueous phase with dimethylsulfoxide (DMSO) and poly(1-vinyl-2-pyrrolidinone) (PVP) was added to suppress undesired side reactions. The 5-HMF product was continuously extracted into an organic phase (methylisobutylketone) modified with 2-butanol to enhance partitioning from the reactive aqueous solution. A maximum 5-HMF selectivity of 85% with 89% fructose conversion was obtained. Although a high 5-HMF yield could be achieved in this system, the product had to be separated from high boiling point solvents such as DMSO from both the reaction phase and extraction phase. Zhao *et al.*<sup>11</sup> studied the catalytic conversion of fructose into 5-HMF in an ionic liquid solvent (1-alkyl-3-methylimidazolium chloride) with metal halides such as chromium(II) chloride as catalysts, in which a yield of 73% of 5-HMF was achieved at a temperature of 120 °C for a reaction time of 3 h. Ionic liquids are advanced solvents in view of controllability of its properties, but many of these are too expensive to allow their use on a practical scale.

Within the past decade, green chemistry has attained the status of a major scientific discipline. Among the 12 principles of green chemistry, the need for using “safe solvents” and for “energy efficiency” can be considered as two key principles.<sup>30</sup> In this respect, it has been shown that microwave-assisted organic syntheses (MAOS) have much higher yield and selectivity for a given reaction time for many types of reactions.<sup>30</sup> A study comparing the energy efficiency between a conventional oil bath organic synthesis and a MAOS has indicated that a significant energy savings (up to 85-fold) can be expected for most chemical transformations using microwaves as an energy source on a laboratory scale.<sup>31</sup> If those data can be applied to larger scale microwave applications on a pilot or production scale, the possibility of performing reactions in a very short time period by direct interaction of microwave energy with the reaction mixture could certainly be considered “green” and highly efficient, because of the reduced energy consumption and the associated time savings.

Up to now, most studies on MAOS have been applied to organic synthesis,<sup>30,32–35</sup> and only a limited number of applications have been studied in carbohydrate conversion<sup>36–41</sup> related to non-food products. Orozco *et al.*<sup>37</sup> studied dilute acid hydrolysis of grass and cellulose with phosphoric acid in a microwave reactor system and showed that high yields (90%) of glucose could be obtained in short reaction times. Cottier and Descotes described a microwave process that produced 5-HMF with 28% yield in aqueous fructose (or sucrose) mixed with inorganic phosphates for 3 min reaction time.<sup>8</sup>

In this work, we report on microwave-assisted catalytic dehydration of fructose into 5-HMF with a strong acid cation exchange resin as catalyst in a mixed organic–aqueous solvent system. The resin is stated as being potentially dangerous at high temperatures with possible reaction products being aromatics, hydrocarbons, organic sulfonates, and sulfur oxides. We examined the applicability of the resin at high temperatures ranging between 100 °C and 180 °C under microwave irradiation.

## 2. Experimental

### 2.1 Material

Fructose (purity: 99%) and acetone were purchased from Wako Pure Chemical Company and used without further purification. Dowex 50wx8-100 ion-exchange resin was purchased from Sigma–Aldrich Corporation. Pure water (with a conductivity of 18 MΩ cm<sup>-1</sup>), which was distilled after deionization, was obtained by a water distillation apparatus (Yamato Co., Model WG-220).

### 2.2 Resin properties

The strong acid cation exchange resin Dowex 50wx8-100 (50-100 mesh beads, gel, water content: 40–70%) that is insoluble in water, consists of a sulfonated copolymer of styrene and divinyl benzene in the hydrogen form. The matrix of the resin was styrene–DVB, and total exchange capacity was 1.7 meq ml<sup>-1</sup> (H<sup>+</sup>).

### 2.3 Typical work-up procedure

The microwave reaction apparatus and experimental procedure are described in the ESI.† Briefly, a solution (5 g) of fructose and a given amount of the catalyst were loaded into a thick-wall Pyrex glass tube (volume 10 ml, id: 11.6 mm, od: 18 mm, wall thickness: 3.2 mm, and maximum supporting pressure 10 MPa). The glass tube was mounted into a polycarbonate (PC) tube that was closed with PEEK screw caps. This assembly was placed into the microwave oven. N<sub>2</sub> gas was used for purging air inside the reactor at a pressure of about 1.2 MPa, which would give calculated gas pressures of 1.73 MPa and 1.86 MPa assuming ideal gas at the given temperatures of 150 and 180 °C. The use of N<sub>2</sub> gas pressure increase the boiling point of the solvent mixtures and reduces volatilization. According to calculation with UNIFAC, the solvent mixtures will not boil below 150 °C under the given pressures, and the amount of acetone volatilizing into the vapor would cause liquid phase composition changes of 5% maximum. Boiling of the solvent mixtures was not observed during all of the experiments. When the microwave irradiation was started, the reaction mixture could be heated up to 150 °C within 30 s. In the reaction analyses, zero time was taken to be when the temperature reached 150 °C. After the desired reaction time passed, the microwave irradiation was turned off and the reactor was cooled down by loading cooling water. The reactor was taken down and the reaction solution was collected by washing the glass tube with an amount of distilled water.

For the sand bath experiments, a SS316 tube bomb reactor (inner volume: 6 cm<sup>3</sup>) as reactor was used, in which the procedures for loading and recovering the samples were similar to those used in the microwave heating experiments. Previous work<sup>27</sup> and the ESI† provides additional information.

### 2.4 Analysis

An HPLC (Jasco) with SH 1011 column (Shodex) and refractive index detector (ERC-7571A) were employed to analyze the liquid samples. Each sample was diluted with ultra pure water before analysis to prevent the overloading of the column with organic solvents.



Elemental analysis (C, H, S) of the resin before and after being used was carried out using Elementar Analysensysteme GmbH VarioEL (Germany).

The fructose conversion (mol%), the product yield (mol%) and selectivity (mol%) of each carbon compound was evaluated from carbon base as shown below:

Fructose conversion (mol%):

$$X = \left( 1 - \frac{\text{Fructose concentration in product}}{\text{Fructose concentration in the loaded sample}} \right) \times 100\% \quad (1)$$

Product yield (mol%):

$$Y = \frac{\text{Moles of carbon in product}}{\text{Moles of carbon loaded as fructose}} \times 100\% \quad (2)$$

Product selectivity (mol%):

$$S = \frac{\text{Yield of product}}{\text{Fructose conversion}} \times 100\% \quad (3)$$

The weight ratio of substrate to ion exchange resin was defined as  $R$ :

$$R = \frac{\text{Weight of substrate}}{\text{Weight of ion exchange resin}} \quad (4)$$

### 3. Results and discussion

#### 3.1 Products

In this study, the main product of the reaction of fructose was always 5-HMF regardless of the experimental conditions. The main by-products were levulinic acid (1 to 20% yield), formic acid (0.2 to 2% yield), furfural (0.5 to 2% yield) and glucose (0.2 to 0.6% yield). When the fructose initial concentration was higher than 10%, there were also some polymer products that were not characterized.

#### 3.2 Influence of the reaction media composition on fructose conversion and 5-HMF yield

The dehydration of fructose in water in the presence of the resin was initially studied. For this case, the fructose conversion reached 82.6% at a reaction time of 60 min, temperature 150 °C for  $R = 1$ , but the 5-HMF yield was only 34%. The low yield can be attributed to the rehydration of 5-HMF into levulinic acid and formic acid that occurs in aqueous and acidic solvents.<sup>2,19</sup> The corresponding levulinic acid yield was 24%. To depress the formation of levulinic acid, changing the reaction solvent was considered.

DMSO has been proven to be an effective solvent that can depress side-reactions in the fructose dehydration because the furanoid form is preferred in DMSO. The dehydration of fructose to form 5-HMF is thought to be the most selective if the carbohydrate molecule is in its furanoid form,<sup>1,12,13</sup> but DMSO has some disadvantages due to its high boiling point (189 °C). On the other hand, acetone, has a low boiling point (56 °C, 1 atm) and fructose has been shown to rearrange to the furanoid form in acetone–water mixtures.<sup>3</sup> Bicker *et al.* examined the fructose dehydration in a water–acetone mixture at subcritical

and supercritical conditions in which a maximum selectivity of 78% with 90% of fructose conversion was obtained at 180 °C and 20 MPa with H<sub>2</sub>SO<sub>4</sub> in an acetone–water mixture (90 : 10 v/v) for 2 min of reaction time.<sup>5</sup> More mild conditions would be preferable. Therefore, solvent composition was changed with acetone to replace some part of the water to study the dehydration of fructose in acetone–water mixture using resin as catalyst under microwave irradiation heating at 150 °C and at the saturation pressure. The composition of the reaction solvent was varied from 0 to 85 wt% acetone in water.

Fig. 1 shows the influence of the reaction solvent composition on the fructose conversion and 5-HMF yield. As the percentage of acetone in the mixture was increased, the conversion rate and 5-HMF yield increased, and the 5-HMF yield reached 73.4% in 70 wt% acetone mixture for a reaction time of 15 min at 150 °C. The 5-HMF selectivity was as high as 83.7% for 5 min for the 70 wt% acetone mixture, but it reduced with increasing reaction time due to the rehydration of 5-HMF into levulinic acid and formic acid for 30 wt% water. Theoretically, the 5-HMF is stable in pure acetone reaction media and the rehydration will not occur, but, because the solubility of fructose in acetone–water mixture decreases with increasing acetone content, the solubility of fructose in pure acetone is as low as 0.5 g L<sup>-1</sup>.<sup>3</sup> When acetone–water is 90 : 10 (v/v), the fructose solubility increases to 14 g L<sup>-1</sup> (25 °C).<sup>3</sup> Therefore, an acetone–water mixture of 70 : 30 (w/w) was employed as reaction media hereafter.

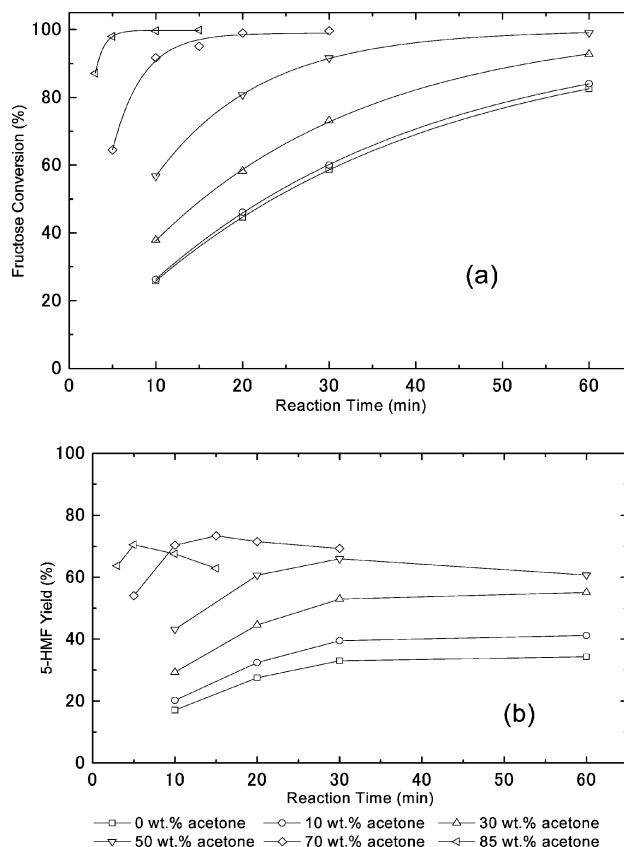
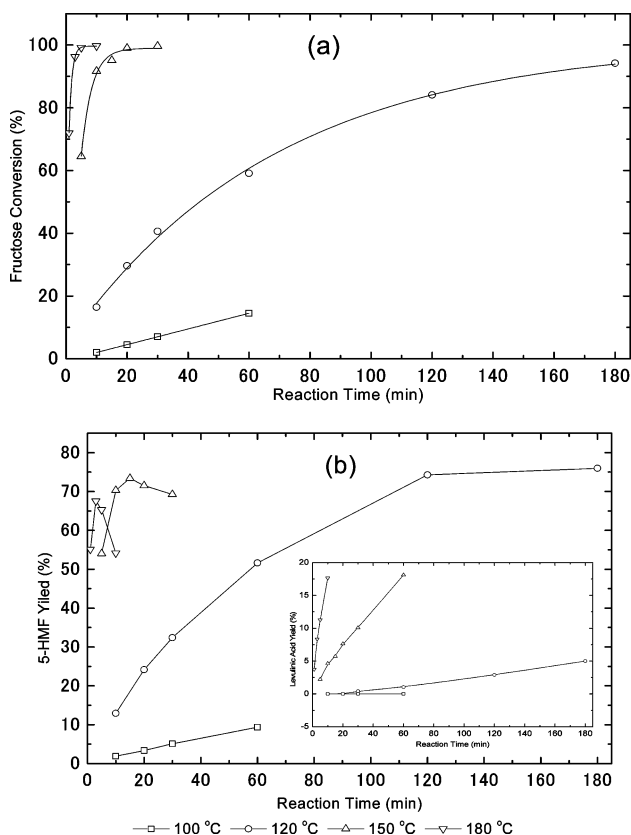


Fig. 1 Influence of the reaction media composition on the fructose conversion (a) and 5-HMF yield (b) (2 wt% fructose, 150 °C,  $R = 1$ ).

### 3.3 Influence of reaction temperature on fructose conversion and 5-HMF yield

Fig. 2 shows the influence of the temperature with respect to the fructose conversion and 5-HMF yield. Reaction temperature had a large effect on the fructose conversion and 5-HMF yield. When reaction temperature was 100 °C, the fructose conversion was only 14.5% for 60 min reaction time and when the temperature increased to 120 °C, the fructose conversion and 5-HMF yield increased to 59.1% and 51.6%, respectively, for 60 min reaction time. Conversion of fructose and yield of 5-HMF reached 94.2% and 76%, respectively, for 180 min reaction time. Levulinic acid yield was always below 5%. The fructose conversion and 5-HMF yield was 95.1% and 73.4%, respectively, at 150 °C for 15 min, and the corresponding levulinic acid yield was 5.7%. At 180 °C, the rate of fructose conversion rate was much higher, and fructose conversion reached 99.2% for 5 min, but the 5-HMF yield was only 65.3% due to the further reaction of 5-HMF and a higher yield of levulinic acid formed which reached 11.3% and 17.7% at a reaction time of 5 and 10 min, respectively. Thus, a reaction temperature of 150 °C was chosen as the best temperature since fructose conversions and 5-HMF yields were high and levulinic acid yields were low.



**Fig. 2** Influence of temperature on the (a) fructose conversion and (b) HMF yield by microwave irradiation (acetone–water 70 : 30 w/w, 2 wt% fructose,  $R = 1$ ).

### 3.4 Reaction kinetics analysis

Kuster<sup>25</sup> and Bicker *et al.*<sup>5</sup> reported that the dehydration of fructose was first-order on fructose concentration. Kinetic analysis

of the dehydration of fructose in acetone–water (70 : 30 w/w) was performed by plotting  $\ln(1 - X)$  versus reaction time ( $t$ ) to obtain the rate constants at different temperatures ( $T$ ). With those constants, an Arrhenius plot was generated, as shown in Fig. 3. Activation energy determined was 103.4 kJ mol<sup>-1</sup>. Bicker *et al.* reported an activation energy of 99 kJ mol<sup>-1</sup> for the fructose dehydration with 3 mmol L<sup>-1</sup> sulfuric acid as catalyst at a pressure of 20 MPa,<sup>5</sup> Antal *et al.* obtained 100 kJ mol<sup>-1</sup> for the dehydration of glucose under sulfuric acid concentration of 5 mmol L<sup>-1</sup>.<sup>12</sup> The value of this work ( $E_a = 103$  kJ mol<sup>-1</sup>) was comparable with previous values reported in the literature.

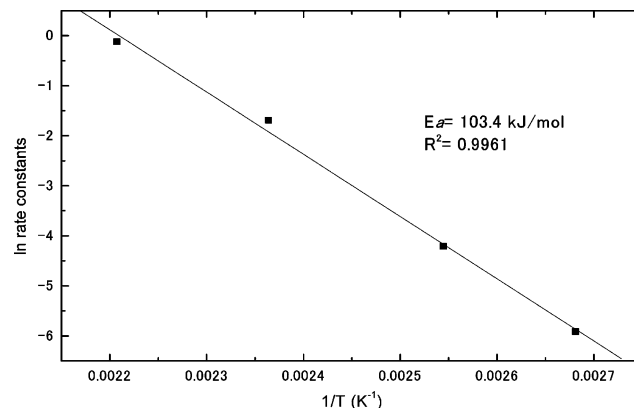


**Fig. 3** Determination of activation parameters from Arrhenius equation for the fructose dehydration.

### 3.5 Effect of the catalyst dosage on the fructose conversion and 5-HMF yield

Table 1 shows the effect of the catalyst dosage with respect to fructose conversion, 5-HMF, levulinic acid and formic acid yield. In the absence of catalyst, at a reaction temperature of 150 °C, no fructose conversion was observed for a reaction time of 20 min. On the other hand, when catalyst was used with  $R$ -values of 0.5, 1.0 and 2.0, fructose conversion remarkably increased, whereas the 5-HMF yield did not change much for  $R$ -values below 1 for a reaction time of 10 min. The reason of the small effect of  $R$  on the 5-HMF yield might be the decomposition of 5-HMF being accelerated at high  $R$ -values due to the availability of acidic sites that favour the rehydration of 5-HMF into levulinic acid, which offsets increases in the 5-HMF yield. Therefore, an  $R$  of 1 was chosen as an appropriate catalyst concentration in subsequent experiments if not otherwise indicated.

### 3.6 Influence of the fructose initial concentration on fructose conversion and 5-HMF yield

From a practical point of view, if higher concentrations of fructose can be used as feedstock, the technique can be economical. Different initial concentrations of fructose were studied. The fructose concentrations that were studied were 2 wt%, 5 wt%, 10 wt% and 20 wt%. The reaction media was acetone–water (70 : 30 w/w) and the reaction temperature was 150 °C with the resin concentrations being given in Table 2. It can be seen that the rate of fructose conversion had little effect for

**Table 1** Influence of the weight ration of fructose to resin (*R*) on the fructose conversion and primary product yield under microwave irradiation (2 wt% fructose, acetone-water 70 : 30 w/w, 150 °C)

<i>R</i> (w/w)	Reaction time/min	Fructose conversion (%)	Product yield (%)		
			Formic acid	Levulinic acid	5-HMF
0.5	3	70.5	1.6	2.7	56.5
	5	86.8	1.6	3.9	66.6
	10	97.5	2.8	7.0	72.3
	15	99.2	3.5	10.2	70.8
1.0	5	64.5	1.2	2.2	54.0
	10	91.7	2.0	4.6	70.3
	15	95.1	2.0	5.7	73.4
	20	99.0	2.8	7.6	71.5
2.0	5	44.7	1.6	1.6	37.0
	10	63.4	1.7	2.2	51.4
	15	76.4	1.5	3.0	61.3
	20	84.8	1.6	3.7	66.5

**Table 2** Different initial concentration fructose dehydration to 5-HMF carried out in acetone-water medium (70 : 30 w/w) by Dowex 50wx8 ion-exchange resin <sup>a</sup>

Fructose concentration	<i>R</i> <sup>b</sup> (w/w)	Reaction time/min	Conversion (%)	5-HMF yield (%)	TON <sup>c</sup>
2 wt%	1	5	64.5	54.0	36.0
		10	91.7	70.3	23.4
		15	95.1	73.4	16.3
		20	99.0	71.5	11.9
5 wt%	1	3	82.7	60.0	66.7
		5	93.6	68.5	45.7
		7	95.5	66.9	31.9
		10	98.6	66.6	22.2
10 wt%	1	3	91.8	61.1	67.9
		5	98.2	61.5	41.0
		10	99.6	52.7	17.6
		15	99.8	44.7	9.9
20 wt%	2	3	81.9	49.2	109.3
		5	89.3	54.3	72.4
		10	98.1	51.5	34.4
		15	99.3	44.2	19.6

<sup>a</sup> Reaction conditions: temperature: 150 °C. <sup>b</sup> Substrate to catalyst weight ratio. <sup>c</sup> Turnover number expressed as (mmol of 5-HMF per g of catalyst × h).

different initial concentration of fructose, but the 5-HMF yield reduced gradually with increasing initial fructose concentration.

The highest 5-HMF yield was 73.4% at 2 wt% of initial fructose concentration, but the value reduced to 54.3% at 20 wt% initial concentration of fructose. The losses in 5-HMF yield are thought to be due to the higher fructose concentrations, which would increase the probability that reactive compounds such as fructose and 5-HMF would collide with each other, cross-polymerize and form humins.<sup>25</sup> In aqueous systems, including aqueous mixtures, losses due to humin formation can amount up to 35% for 1 M fructose solution, and this value reduces to 20% for 0.25 M fructose solutions.<sup>25</sup> These polymers were not analyzed in this work. In certain non-aqueous systems or biphasic water/organic systems, few problems occur with polymerizations at high concentrations. Roman-Leshkov *et al.* used a two-phase reactor system (7 : 3 water : PVP + 7 : 3 MIBK : 2-butanol) and obtained a fructose conversion of 90% with 77% of 5-HMF selectivity for 50 wt% initial fructose concentration.<sup>1</sup> Some other investigations for fructose conversion and 5-HMF yield with different initial fructose concentrations using different methods by other authors are listed in Table 3. Comparing these methods, high 5-HMF yields with high fructose conversions

were obtained under milder conditions, recyclable catalyst and moderate temperatures with the present method.

### 3.7 Resin catalyst recycle

Generally, the strong acid sulfonated copolymer resin is thought to be unusable above 130 °C,<sup>25</sup> but our experimental results showed that the resin could work well above 130 °C or even 150 °C. In green engineering, the recycling of catalyst is very important in practice. Thus, the recycling of the resin was tried for 5 times to study its change in activity (Fig. 4). From Fig. 4, the catalytic activity and selectivity of the resin for the dehydration of fructose into 5-HMF did not show systematic decrease after 5 uses at 150 °C for 10 min reaction time. The fructose conversions and 5-HMF yields were always about 98% and 72%, respectively.

If the resin had been decomposed from exposure to the experimental conditions, the sulfonic acid groups attached on the resin would probably be released and dissolved into solution, and the sulfur content of the resin would decrease. To examine the decomposition of the resin after being reused 5 times, the used resin was collected, rinsed with pure water and acetone, and dried for 24 h in vacuum drying oven, and in the same manner

**Table 3** Fructose conversion ( $X$ ) and 5-HMF yield ( $Y$ ) with different initial fructose concentrations using different methods by the other researchers

Solvent system	Catalyst	Fructose concentration (wt%)	Reaction temperature/°C	Reaction time/min	$X$ (%)	$Y$ (%)	Ref.
H <sub>2</sub> O	H <sub>3</sub> PO <sub>4</sub>	0.9	240	2	98.0	65.3	4
H <sub>2</sub> O–MIBK	Zeolite	1.7	165	60	76.0	69.2	15
H <sub>2</sub> O	NbOPO <sub>4</sub>	6.0	100	120	61.4	21.6	19
H <sub>2</sub> O–DMSO/PVP	IER <sup>a</sup>	10	90	480	76.0	58.5	1
Ionic Liquid	PtCl <sub>2</sub>	10	80	180	98.0	83.0	11
H <sub>2</sub> O–salt/butanol	HCl	30	180	3	74.0	65.9	14
Acetone–water	IER	2.0	150	15	95.1	73.4	This work

<sup>a</sup> Ion exchange resin PK-216.

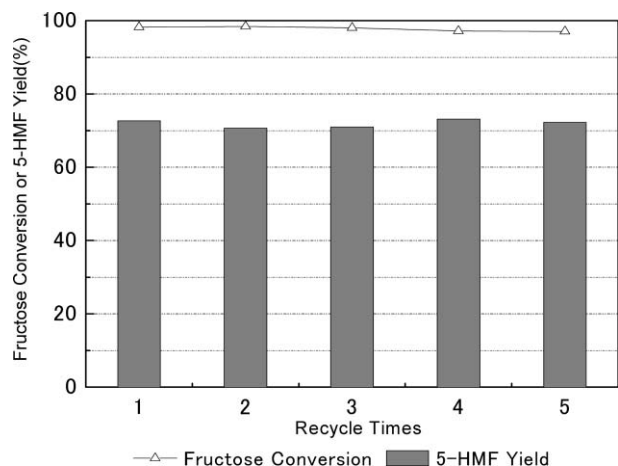


**Fig. 4** Catalyst recycle (2 wt% fructose, reaction media: acetone–water 70 : 30 w/w, reaction time: 10 min; temperature: 150 °C;  $R = 0.5$ ).

that was used for new resin. Then, elemental analysis (C, H, S) of both of these resins was carried out as shown in Table 4. It can be seen that the C and H content in the reused resin increased by about 4.6% and 0.94%, respectively over that of new resin, and S content reduced by about 1.3%. The increasing in C and H is probably due to adsorption of some reaction products such as humins on the resin, and humins did not seem to be able to be washed from the resin after reaction. It seems that the S content in the reused resin reduced by about 1.3%, but if we take into account that the humins adsorbed on the resin and increased the C and H content, the S content decreasing in the resin matrix would be lower. Therefore, it can be concluded that the resin was stable in this system and the nearly constant fructose conversions and 5-HMF yields verified this conclusion.

### 3.8 Comparison of D-fructose dehydration by sand bath and microwave heating

The dehydration of D-fructose (2 wt%) in an acetone–water mixture (70 : 30, w/w) with the resin as catalyst by convective heating (sand bath) and microwave irradiation heating was studied (Fig. 5). As shown in Fig. 5, microwave irradiation

**Table 4** Elemental analysis results (C, H, S) of resin before and after being reused for 5 times

Element	C (%)	H (%)	S (%)
New resin	42.5	5.38	13.7
Used resin	47.2	6.32	12.4

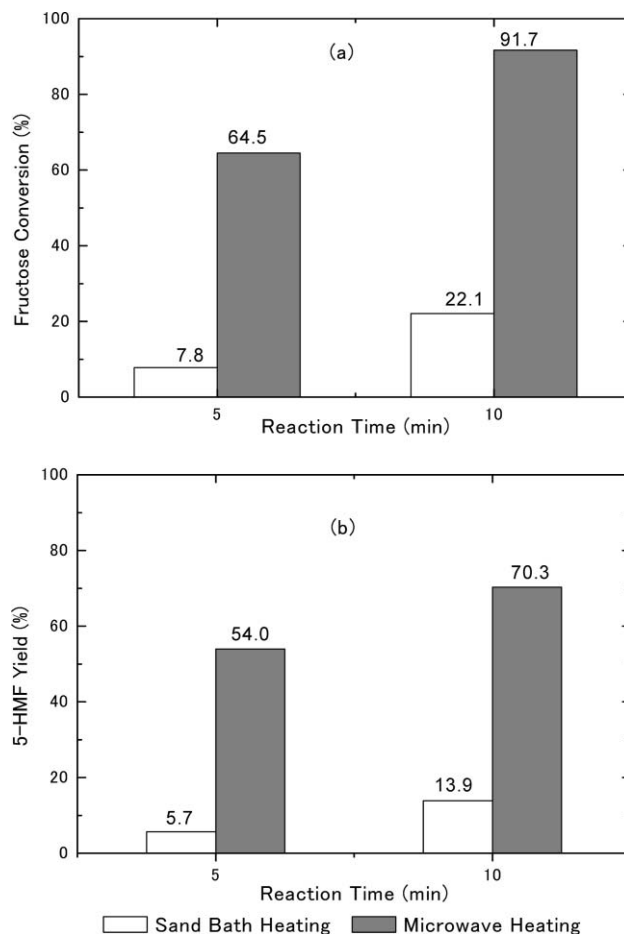


**Fig. 5** Comparison of (a) fructose conversion and (b) HMF yield by sand bath and microwave heating (reaction media: acetone–water 70 : 30 w/w, 2 wt% fructose solution, 150 °C,  $R = 1$ ).

was remarkably more efficient not only for fructose conversion, but also in achieving high 5-HMF yields. When the reaction mixture was heated by sand bath, the fructose conversion and 5-HMF yield was 22.1% and 13.7%, respectively, at a reaction time of 10 min, while the corresponding value for microwave heating was 91.7% and 70.3%, respectively. These kind of difficult-to-rationalize effects have been referred to as “specific” or “nonthermal” microwave effects.<sup>35</sup> Generally, this specific microwave effect has been proposed to be the result from a direct interaction of the electric field with specific molecules in the reaction medium. It has been argued that there is a decrease in activation energy or an increase in the



pre-exponential factor in the Arrhenius law due to orientation effect of polar species in an electromagnetic field.<sup>34,42</sup> Some researchers have proposed that the effective collision among reactant molecules under microwave irradiation is enhanced and result in the pre-exponential factor in the Arrhenius law increases.<sup>34</sup> Furthermore, a similar effect should be observed for reaction mechanisms where reactants contain polar groups, where the rotation of polar species increases and leads to molecules going from the ground state to the transition state under the microwave irradiation, thus enhance the reactivity by lowering the activation energy.<sup>35</sup> Currently microwave effects are still the subjects of investigation in many fields of research.

#### 4. Conclusions

Microwave-assisted dehydration of fructose into 5-HMF using a strong acid cation exchange resin as catalyst in aqueous-acetone mixtures was investigated. The fructose conversion rate improved with an increase in acetone concentration in the acetone–water mixtures, and an increase in the 5-HMF yield was also obtained due to the suppression of 5-HMF dehydration. At 20 wt% initial concentration of fructose, the 5-HMF yield was 54.3% with 89.3% fructose conversion due to the soluble polymer formation. The resin could work well at temperatures up to 150 °C, and there was no catalytic activity decrease after 5 times reuse. Compared with conventional sand bath heating, microwave irradiation heating had a remarkable accelerating effect, not only on the fructose conversion, but also on the 5-HMF yield. In conclusion, fructose can be converted to 5-HMF in high yields at mild conditions with microwave heating in acetone–water mixtures in the presence of a strong acid ion exchange resin. An examination on how to avoid polymer formation and how to improve 5-HMF yield for high initial concentrations (>10 wt%) of fructose is being carried out.

#### References

- 1 Y. Roman-Leshkov, J. N. Chheda and J. A. Dumesic, *Science*, 2006, **312**, 1933–1937.
- 2 J. Lewkowski, *Arkivoc*, 2001, **2**, 17–54.
- 3 M. Bicker, D. Kaiser, L. Ott and H. Vogel, *J. Supercrit. Fluids*, 2005, **36**, 118–126.
- 4 F. S. Asghari and H. Yoshida, *Ind. Eng. Chem. Res.*, 2006, **45**, 2163–2173.
- 5 M. Bicker, J. Hirth and H. Vogel, *Green Chem.*, 2003, **5**, 280–284.
- 6 M. Bicker, S. Endres, L. Ott and H. Vogel, *J. Mol. Catal. A: Chem.*, 2005, **239**, 151–157.
- 7 G. W. Huber, J. N. Chheda, C. J. Barrett and J. A. Dumesic, *Science*, 2005, **308**, 1446–1450.
- 8 L. Cottier and G. Descotes, *Trends Heterocyclic Chem.*, 1991, 233–248.
- 9 C. Lansalot-Matras and C. Moreau, *Catal. Commun.*, 2003, **4**, 517–520.
- 10 C. Moreau, R. Durand, A. Roux and D. Tichit, *Appl. Catal., A*, 2000, **193**, 257–264.
- 11 H. B. Zhao, J. E. Holladay, H. Brown and Z. C. Zhang, *Science*, 2007, **316**, 1597–1600.
- 12 M. J. Antal, W. S. L. Mok and G. N. Richards, *Carbohydr. Res.*, 1990, **199**, 91–109.
- 13 J. N. Chheda, Y. Roman-Leshkov and J. A. Dumesic, *Green Chem.*, 2007, **9**, 342–350.
- 14 Y. Roman-Leshkov, C. J. Barrett, Z. Y. Liu and J. A. Dumesic, *Nature*, 2007, **447**, 982–U985.
- 15 C. Moreau, R. Durand, S. Razigade, J. Duhamet, P. Faugeras, P. Rivalier, P. Ros and G. Avignon, *Appl. Catal., A*, 1996, **145**, 211–224.
- 16 K. Seri, Y. Inoue and H. Ishida, *Chem. Lett.*, 2000, 22–23.
- 17 K. Seri, Y. Inoue and H. Ishida, *Bull. Chem. Soc. Jpn.*, 2001, **74**, 1145–1150.
- 18 H. Ishida and K. Seri, *J. Mol. Catal. A: Chem.*, 1996, **112**, L163–L165.
- 19 T. Armaroli, G. Busca, C. Carlini, M. Giuttari, A. M. R. Galletti and G. Sbrana, *J. Mol. Catal. A: Chem.*, 2000, **151**, 233–243.
- 20 C. Carlini, M. Giuttari, A. M. R. Galletti, G. Sbrana, T. Armaroli and G. Busca, *Appl. Catal., A*, 1999, **183**, 295–302.
- 21 C. Carlini, P. Patrono, A. M. R. Galletti and G. Sbrana, *Appl. Catal., A*, 2004, **275**, 111–118.
- 22 F. Bavenuti, C. Carlini, P. Patrono, A. M. R. Galletti, G. Sbrana, M. A. Massucci and P. Galli, *Appl. Catal., A*, 2000, **193**, 147–153.
- 23 Y. Nakamura and S. Morikawa, *Bull. Chem. Soc. Jpn.*, 1980, **53**, 3705–3706.
- 24 L. Rigal, A. Gaset and J. P. Gorrichon, *Ind. Eng. Chem. Prod. Res. Dev.*, 1981, **20**, 719–721.
- 25 B. F. M. Kuster, *Starch*, 1990, **42**, 314–321.
- 26 M. Watanabe, Y. Aizawa, T. Iida, T. M. Aida, C. Levy, K. Sue and H. Inomata, *Carbohydr. Res.*, 2005, **340**, 1925–1930.
- 27 M. Watanabe, Y. Aizawa, T. Iida, R. Nishimura and H. Inomata, *Appl. Catal., A*, 2005, **295**, 150–156.
- 28 C. Moreau, A. Finiels and L. Vanoye, *J. Mol. Catal. A: Chem.*, 2006, **253**, 165–169.
- 29 S. K. Tyrlik, D. Szerszen, M. Olejnik and W. Danikiewicz, *Carbohydr. Res.*, 1999, **315**, 268–272.
- 30 D. Dallinger and C. O. Kappe, *Chem. Rev.*, 2007, **107**, 2563–2591.
- 31 M. J. Gronnow, R. J. White, J. H. Clark and D. J. Macquarrie, *Org. Process Res. Dev.*, 2005, **9**, 516–518.
- 32 E. Comer and M. G. Organ, *J. Am. Chem. Soc.*, 2005, **127**, 8160–8167.
- 33 T. N. Glasnov and C. O. Kappe, *Macromol. Rapid Commun.*, 2007, **28**, 395–410.
- 34 M. Hosseini, N. Stiasni, V. Barbieri and C. O. Kappe, *J. Org. Chem.*, 2007, **72**, 1417–1424.
- 35 C. O. Kappe, *Angew. Chem., Int. Ed.*, 2004, **43**, 6250–6284.
- 36 C. Limousin, J. Cleophax, A. Petit, A. Loupy and G. Lukacs, *J. Carbohydr. Chem.*, 1997, **16**, 327–342.
- 37 A. Orozco, M. Ahmad, D. Rooney and G. Walker, *Process Safety Environ.*, 2007, **85**, 446–449.
- 38 A. M. Sarotti, R. A. Spanevello and A. G. Suarez, *Green Chem.*, 2007, **9**, 1137–1140.
- 39 A. Corsaro, U. Chiacchio, V. Pistara and G. Romeo, *Curr. Org. Chem.*, 2004, **8**, 511–538.
- 40 M. R. Couri, I. Luduvico, L. Santos, R. Alves, M. A. Prado and R. F. Gil, *Carbohydr. Res.*, 2007, **342**, 1096–1100.
- 41 M. M. Andrade, M. T. Barros and P. Rodrigues, *Eur. J. Org. Chem.*, 2007, 3655–3668.
- 42 C. O. Kappe and A. Stadler, *Microwaves in Organic and Medicinal Chemistry*, Wiley-VCH, Weinheim, Germany, 2005.

# Catalytic activity of laccases in aqueous solutions of ionic liquids

Stepan Shipovskov,<sup>a</sup> H. Q. Nimal Gunaratne,<sup>b</sup> Kenneth R. Seddon<sup>b</sup> and Gill Stephens<sup>\*a</sup>

Received 24th October 2007, Accepted 7th May 2008

First published as an Advance Article on the web 13th June 2008

DOI: 10.1039/b716369j

The ionic liquids, [bmim]Br and [bmim][N(CN)<sub>2</sub>] (where [bmim] = 1-butyl-3-methylimidazolium), stimulated laccase-catalysed oxidation of catechol when provided at concentrations between 10–20% and 50–60% (v/v) in water, respectively. However, activity was inhibited at higher and lower concentrations. [bmim][BF<sub>4</sub>] was inhibitory at all concentrations tested, but residual activity was still retained in [bmim][BF<sub>4</sub>] with ≤ 20% water.

Laccases have attracted a great deal of attention as potential biocatalysts for manufacturing pharmaceutical intermediates and speciality chemicals, and for bioremediation.<sup>1–3</sup> Their catalytic versatility is a consequence of the unusual reaction mechanism in which the substrate (or *mediator*) is oxidised to a free radical intermediate using dioxygen as the electron acceptor.<sup>4</sup> This reactive intermediate can then undergo a wide range of reactions with other chemicals, and, most importantly, its mobility overcomes the requirement for close contact between the enzyme and its substrate. This means that laccases exhibit excellent catalytic activity even with water-insoluble substrates (e.g. lignin).<sup>5</sup> Further improvements in mass transport can be achieved by operating the reactions in conventional organic solvents,<sup>6–8</sup> but the range of solvents suitable for use with enzymes is extremely restricted, and there are serious problems with safety and environmental acceptability. For these reasons, we wished to explore the use of ionic liquids as alternative solvents. There are literally millions of ionic liquids,<sup>9–11</sup> offering new solvents with an unprecedented variety of chemical and physical properties. This offers a realistic prospect of tailoring the solvent to match the requirements of both the enzyme and the bioprocess with exquisite precision. Furthermore, most ionic liquids have no detectable vapour pressure at room temperature, which can provide new approaches to product work-up and separation (for example<sup>12,13</sup>), and allows operation in non-flameproof areas. It is also possible to *design* environmentally benign, non-toxic ionic liquids,<sup>9,14</sup> and some can even be produced from renewable feedstocks.<sup>15</sup> In addition, ionic liquids are electrically conducting (unlike conventional solvents),<sup>16</sup> and this may be beneficial for exploitation of laccases in biosensors and biofuel cells.<sup>17</sup>

There is already some evidence that ionic liquids can be used with laccases, but the activity in 4-methyl-1-butylpyridinium tetrafluoroborate ([<sup>+</sup>mbpy][BF<sub>4</sub>]) or 1-butyl-3-methylimidazolium hexafluorophosphate, [bmim][PF<sub>6</sub>], mixed

with water was generally much lower than in water.<sup>18</sup> Better activity was obtained only with substrates that are so insoluble in water that exploiting the residual activity in the ionic liquid/water mixture provided the only means of obtaining reasonable reactivity. Therefore, we wished to identify better ionic liquids for laccase-catalysed biotransformations. To ensure that the ionic liquids would be generally applicable to laccase biocatalysis, we studied catechol oxidation, using commercially available laccases from *Agaricus bisporus* (LAB) and *Trametes versicolor* (LTV). Catechol is oxidised efficiently in water in any case, and our aim was to identify ionic liquid/water mixtures that did not inhibit reactivity. In fact, we were fortunate enough to identify reaction mixtures that actually stimulated the biotransformation.

## Experimental

LAB and LTV were obtained from Sigma-Aldrich (UK). Catechol oxidation was measured in aqueous sodium phosphate–citrate buffer solutions (25 mM) containing laccase (25 mg l<sup>-1</sup>) in the presence or absence of ionic liquid, premixed at pH 6.0 for LAB and 4.5 for LTV.<sup>19,20</sup> The pH was checked by diluting the final reaction mixture in deionised water and measuring the pH using a pH-meter. The ionic liquids had no effect on pH during the kinetic measurements (up to 10 min). The rate of 1,2-quinone formation was measured at 405 nm and 22 °C using an Agilent spectrophotometer (USA), based on a molar extinction coefficient of 760 M<sup>-1</sup> cm<sup>-1</sup>.<sup>21</sup> The ionic liquids did not alter the initial absorbance of the reaction mixture and did not affect the extinction coefficient of the product. The kinetic parameters were determined over a range of substrate concentrations (4.5 to 13 mM) using Eadie Hofstee plots. For routine determinations, 3 replicate data sets were used, since the standard deviations were small, but when the laccases were very strongly inhibited, 5 replicate datasets were used to improve accuracy. Errors were calculated as standard deviations. The activity was measured over a range of ionic liquid concentrations from 0 to 99.4%, since the laccases were not soluble in the pure ionic liquids, but could be dissolved when the ionic liquids were mixed with 0.6% of buffer solution containing enzyme. The ionic liquids, [bmim][N(CN)<sub>2</sub>], [bmim][BF<sub>4</sub>] and [bmim]Br were synthesised using the established procedures.<sup>22–25</sup> Although the melting point

<sup>a</sup>Manchester Interdisciplinary Biocentre, University of Manchester, 131 Princess Street, M1 7DN, Manchester, UK.

E-mail: gill.stephens@manchester.ac.uk; Fax: +44 161 3068918; Tel: +44 161 3064377

<sup>b</sup>Queen's University Ionic Liquid Laboratories (QUILL), The Queen's University of Belfast, David Keir Building, Stranmillis Road, BT9 5AG, Belfast, UK. E-mail: k.seddon@qub.ac.uk; Fax: +44 28 90665297; Tel: +44 28 90975420

of pure [bmim]Br is above room temperature,<sup>26</sup> it is extremely difficult to exclude water from the preparation. Therefore it is a viscous liquid at room temperature.<sup>27,28</sup>

## Results

When laccase from *Agaricus bisporus* (LAB) was used to oxidise catechol in [bmim]Br–water mixtures, it was surprising to find that the maximum reaction velocity ( $V_m^{\text{app}}$ ) was stimulated by 1.5-fold as the volume fraction of the ionic liquid was increased from 0 to 20% (0–0.91 M; Fig. 1). In contrast, the ratio  $V_m^{\text{app}}/K_M^{\text{app}}$  decreased by 1 order of magnitude, due to a 16-fold increase in the  $K_M^{\text{app}}$ . This suggested that the affinity of the enzyme for its substrate had decreased significantly. When the [bmim]Br concentration was increased further, LAB activity was inhibited, and the ratio of  $V_m^{\text{app}}/K_M^{\text{app}}$  continued to decrease. The activity was barely detectable when the [bmim]Br concentration reached 60% (2.74 M). When the [bmim]Br concentration was above 40%, the  $K_M^{\text{app}}$  values were higher than the maximum substrate concentration used in the assays due to the increasing inhibition, and, therefore, should be regarded as estimates.

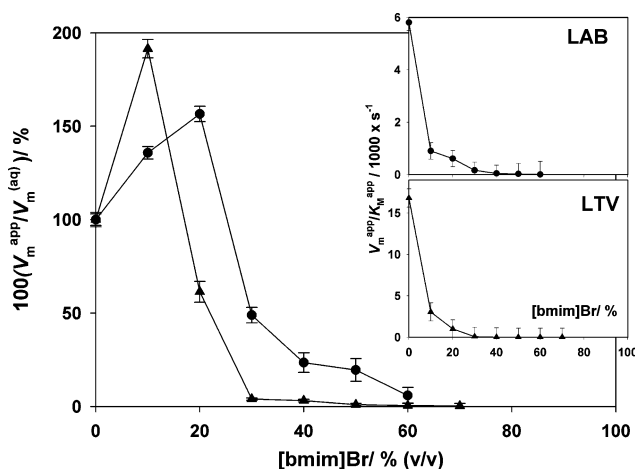


**Fig. 1** The dependence of the relative catalytic activity ( $100(V_m^{\text{app}}/V_m^{\text{aq}})/\%$ ) of LAB (circles) and LTV (triangles) on the volume fraction of [bmim]Br mixed with water. The maximum velocity,  $V_m^{\text{aq}}$ , of LAB and LTV in buffer was 5.11 and 15.30  $\mu\text{M s}^{-1}$ , respectively. Inset: the dependence of ratio  $V_m^{\text{app}}/K_M^{\text{app}}$ , of LAB and LTV on % (v/v) [bmim]Br.

A similar activity profile was obtained for laccase from *Trametes versicolor* (LTV) in [bmim]Br (Fig. 1). In this case, the activity in 10% [bmim]Br (0.46 M) was approximately twice the activity in the aqueous medium, and then the activity decreased as the [bmim]Br concentration was increased further. LTV was completely inactive when the [bmim]Br concentration was higher than 70% (3.20 M). The trend in  $V_m^{\text{app}}/K_M^{\text{app}}$  was similar to LAB, but it should be noted that the  $K_M^{\text{app}}$  values were even higher than for LAB above 50% [bmim]Br (> 50 mM) and must also be regarded as estimates. However, the enzyme was so strongly inhibited at these high ionic liquid concentrations that the  $K_M^{\text{app}}$  values have very little practical significance.

The catalytic performance of LAB in the [bmim][N(CN)<sub>2</sub>]-water system exhibited very unusual behaviour (Fig. 2). The enzyme was inhibited progressively as the concentration of

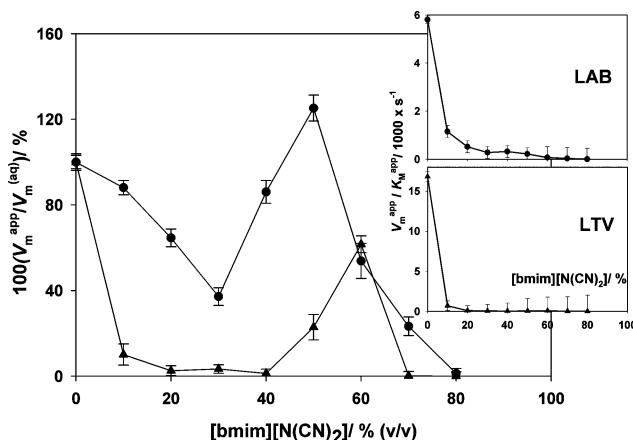


**Fig. 2** The dependence of the relative catalytic activity ( $100(V_m^{\text{app}}/V_m^{\text{aq}})/\%$ ) of LAB (circles) and LTV (triangles) on the volume fraction of [bmim][N(CN)<sub>2</sub>] mixed with water. The  $V_m^{\text{aq}}$  of LAB and LTV in buffer was 5.11 and 15.30  $\mu\text{M s}^{-1}$ , respectively. Inset: the dependence of ratio  $V_m^{\text{app}}/K_M^{\text{app}}$  of LAB and LTV on % (v/v) [bmim][N(CN)<sub>2</sub>].

[bmim][N(CN)<sub>2</sub>] was increased to 30% (1.55 M), but the activity increased thereafter, reaching a maximum  $V_m^{\text{app}}$  at 50% [bmim][N(CN)<sub>2</sub>] (2.59 M). This was 1.25-fold higher than in buffer alone. The activity then decreased as the [bmim][N(CN)<sub>2</sub>] concentration was increased further, and LAB was completely inactive when the [bmim][N(CN)<sub>2</sub>] concentration was above 80% (4.14 M). At the same time, the ratio  $V_m^{\text{app}}/K_M^{\text{app}}$  decreased rapidly up to 10% ionic liquid and then decreased more gradually up to 60% [bmim][N(CN)<sub>2</sub>]. Thus, the estimated  $K_M^{\text{app}}$  with 50% [bmim][N(CN)<sub>2</sub>] was approximately  $29 \pm 6$  mM compared with  $0.88 \pm 0.02$  mM in the aqueous control. Therefore, the ionic liquid decreased the affinity for the substrate even though activity was stimulated.

LTV was more sensitive to [bmim][N(CN)<sub>2</sub>] inhibition than LAB (Fig. 2). Thus, the catalytic activity of LTV was inhibited severely over the concentration range 10–40% [bmim][N(CN)<sub>2</sub>]. However, the activity increased as the concentration was increased further, reaching 70% of the original aqueous activity at 60% [bmim][N(CN)<sub>2</sub>] (3.10 M). The activity decreased again as the [bmim][N(CN)<sub>2</sub>] concentration was increased further, and LTV was completely inactive when the [bmim][N(CN)<sub>2</sub>] concentration was above 80%. The dependence of the ratio  $V_m^{\text{app}}/K_M^{\text{app}}$  on [bmim][N(CN)<sub>2</sub>] concentration for LTV followed a similar trend to LAB, although the values were lower. However, the estimated  $K_M^{\text{app}}$  with 60% [bmim][N(CN)<sub>2</sub>] was approximately  $160 \pm 20$  mM compared with  $0.91 \pm 0.03$  mM in the aqueous control. Although the accuracy of the  $K_M^{\text{app}}$  value is questionable since it is so high, it is evident that the ionic liquid decreased the affinity for the substrate very dramatically. This is surprising, because the reaction rate had increased again at 60% [bmim][N(CN)<sub>2</sub>] compared with the activities at lower ionic liquid concentrations.

LAB activity was retained in [bmim][BF<sub>4</sub>] when the ionic liquid concentration was  $\leq 30\%$  (v/v), with slight stimulation at 10% [bmim][BF<sub>4</sub>] (0.54 M; Fig. 3). The activity then decreased in two “steps” as the [bmim][BF<sub>4</sub>] concentration was increased further. It should be noted that LAB retained 0.5% of the activity even at 90% [bmim][BF<sub>4</sub>] (4.82 M), unlike the other ionic liquids. The trend in  $V_m^{\text{app}}/K_M^{\text{app}}$  did not match the trends in  $V_m^{\text{app}}$ , since

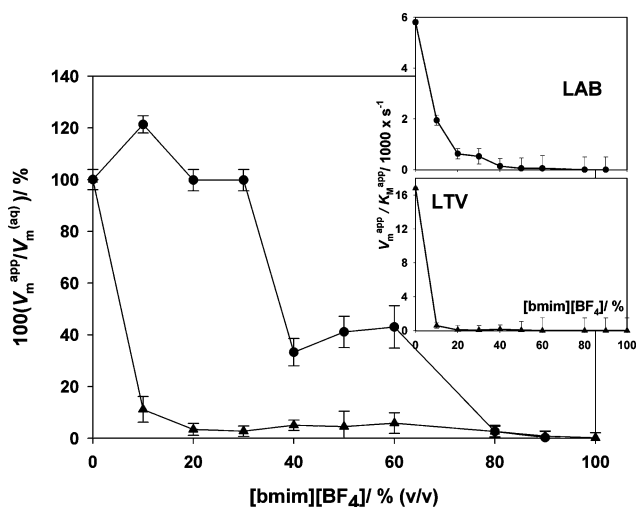


**Fig. 3** The dependence of the relative catalytic activity ( $100(V_m^{app}/V_m^{(aq)})/\%$ ) of LAB (circles) and LTV (triangles) on the volume fraction of [bmim][BF<sub>4</sub>] mixed with water. Catalytic activity of LAB and LTV in buffer was 5.11 and 15.30  $\mu\text{M s}^{-1}$ , respectively. Inset: the dependence of ratio  $V_m^{app}/K_M^{app}$  of LAB and LTV on % (v/v) [bmim][BF<sub>4</sub>].

the  $V_m^{app}/K_M^{app}$  decreased continuously up to 50% [bmim][BF<sub>4</sub>]. Thus, activity was retained at low ionic liquid concentrations despite an increase in the  $K_M^{app}$ .

LTV was much more sensitive to [bmim][BF<sub>4</sub>] inhibition than LAB, and lost *ca.* 85% activity even in 10% [bmim][BF<sub>4</sub>] (Fig. 3). Nevertheless, LTV retained 0.25% of the activity even in 99.4% [bmim][BF<sub>4</sub>] (5.32 M). The trend in  $V_m^{app}/K_M^{app}$  matched the trend in  $V_m^{app}$ , unlike LAB. It should be noted that these enzyme assays were completed in <10 min, making it unlikely that there was significant hydrolysis of the BF<sub>4</sub><sup>-</sup> anion to form HF.<sup>29,30</sup> Nevertheless, F<sup>-</sup> is a potent inhibitor of laccases,<sup>1</sup> and we cannot exclude the possibility that sufficient F<sup>-</sup> was formed to account for some of the inhibition observed.

## Discussion

In this study, we have demonstrated that catalytic activity of laccases can be stimulated in mixtures of water with ionic liquids based on the [bmim]<sup>+</sup> cation. The optimum ionic liquid concentration depends very strongly on the anion, and there are significant differences between the behaviour of LAB and LTV.

The behaviour of laccases in ionic liquids is analogous to solvent activation of certain enzymes in conventional, polar solvents mixed with water. Most enzymes lose their catalytic activity in the presence of polar organic solvents,<sup>31,32</sup> but tyrosinase and chymotrypsin are stimulated by low concentrations of ethanol.<sup>33–36</sup> At higher concentrations, the enzymes are inhibited progressively. The resulting bell-shaped curves of activity *versus* solvent concentration are remarkably similar to the trends of laccase activity in ionic liquids.

A number of mechanisms have been proposed to account for activation of tyrosinase and chymotrypsin by ethanol, including interactions of the solvent with water, the enzyme, the substrate and impurities in the enzyme preparation.<sup>33–36</sup> Similar mechanisms could apply equally well to laccases in solutions of

ionic liquids, with the notable exception that ionic liquids are salts rather than neutral molecules.

Water-miscible ionic liquids dissolve fully in water. This means that the component anion and cation are present as the free ions in water, just like any other salt solution. In general, ions interact strongly with water, according to the nature of the ion and its concentration. The behaviour of proteins in salt solutions can be predicted with some degree of accuracy according to the position of the ions in the Hofmeister series, which describes the strength of the interactions of ions with water.<sup>37–44</sup> Kosmotropic ions interact strongly with water, and, therefore, tend to produce ordered water structures at low concentrations,<sup>38,39,41,43–45</sup> although the nature of the interactions between the ions, water, and proteins is far more complex than originally suspected.<sup>46</sup> The combination of water structuring and direct interactions between the ions and the protein tends to stabilise the protein structure. In contrast, chaotropic ions are less hydrophilic, and interact less strongly with water than water does itself. Chaotropes tend to denature enzymes. The balance of kosmotropicity and chaotropicity between all the anions and cations in a system determines the fate of the protein.<sup>44,47,48</sup> These concepts have been applied very successfully to explain salt activation of lyophilised enzymes in organic solvents.<sup>42,47</sup> There is now considerable interest in applying the same concepts to explain the behaviour of enzymes in dilute solutions of ionic liquids. There have been some successes, but there are also some anomalies.<sup>43,44,48</sup> Our study also represents an anomaly, because laccase activity does not seem to correlate with the Hofmeister series.

In fact, there is very little correlation between kosmotropicity<sup>44</sup> and the laccase activation/inhibition phenomena observed in this study. Only [bmim]Br seems to behave as expected. Thus, [bmim]Br activates the laccases at 10–20% (0.46–0.91 M). This is a relatively dilute solution and is within the range where the enzyme may be stabilised by a combination of water structuring and direct interaction between the ionic liquid with the enzyme.<sup>38,42</sup> The inactivation when the concentration is increased would also be expected, given the relatively weak kosmotropicity of the ionic liquid.<sup>44</sup> Possible mechanisms for inactivation include unfavourable Hofmeister interactions between the ions and the enzyme,<sup>38,42,44</sup> formation of unnatural H-bonds between the enzyme and the ions,<sup>49–52</sup> or interaction of the butyl substituent of the cation with non-polar amino acid side chains.<sup>53</sup> However, it should also be noted that Br<sup>-</sup> is a specific inhibitor of laccases,<sup>54</sup> and this may provide an alternative explanation for the inhibition.

Unlike [bmim]Br, the effects of [bmim][N(CN)<sub>2</sub>] on the enzyme are extremely difficult to explain. Both laccases were inhibited by low concentrations of [bmim][N(CN)<sub>2</sub>], but were activated at intermediate concentrations (50–60%), and then completely inhibited at higher concentrations of this ionic liquid. None of these phenomena can be explained simply by Hofmeister interactions. Thus, the dilute solutions inhibited the enzyme rather than stabilising it. It was only at relatively high concentrations that the enzyme was activated (2.95 M and 3.10 M for LAB and LTV, respectively). This suggests that activation of laccases by [bmim][N(CN)<sub>2</sub>] is the result of specific interactions between the ionic liquid and the enzyme that are, as yet, uncharacterised.



The effects of [bmim][BF<sub>4</sub>] are even harder to explain. Here, the ionic liquid stimulated LAB activity at low concentrations, as expected for a kosmotropic system. However, this is at odds with the behaviour of [bmim][N(CN)<sub>2</sub>], which is more kosmotropic than [bmim][BF<sub>4</sub>]. Furthermore, [bmim][BF<sub>4</sub>] inhibited LTV even at very low concentrations. The latter observation, in particular, demonstrates that there must be enzyme-specific interactions between the laccases and the ions, and these seem to overwhelm the underlying Hofmeister effects.

We would like to note that residual LTV activity was retained in very high concentrations of [bmim][BF<sub>4</sub>] (99.4%), unlike the more polar [bmim][N(CN)<sub>2</sub>] and [bim]Br. Here, the condition is much more similar to a conventional solvent system, with water (0.33 M, assuming anhydrous ionic liquid) dissolved in the ionic liquid (5.32 M) rather than *vice versa*. This suggests that [bmim][BF<sub>4</sub>] was sufficiently non-polar to maintain the enzyme structure without stripping away the tightly bound shell of essential water.<sup>55</sup> On the other hand, LAB only retained activity up to 90% [bmim][BF<sub>4</sub>]. This system contains 4.82 M [bmim][BF<sub>4</sub>] and 5.56 M water. This suggests either that the water shell was more easily removed from this enzyme, or that other factors were more important in the inactivation process. Indeed, water stripping seems unlikely to be involved in the inactivation of laccases in [bmim]Br and [bmim][N(CN)<sub>2</sub>], which occurred between 60–80% ionic liquid in water. Here, the water concentration was very high (between 11 and 22 M) and the enzyme should be fully hydrated.

Overall, laccase activation and inhibition in ionic liquids must be the result of numerous, complex interactions between the enzyme, the ionic liquid, water, substrate, product, and buffer system. Attempts to find simple correlations between the physical properties of the ionic liquid solutions and the behaviour of laccases seem to be unsuccessful, even though there has been some success with other enzymes.<sup>43,44,48,53</sup> This suggests that the behaviour of enzymes in ionic liquids needs to be approached on a case by case basis. In the case of laccases, detailed structural and mechanistic studies are needed to understand the behaviour of the enzymes in ionic liquids. Such studies are currently in progress in our laboratory.

## Conclusions

Whatever the physical and chemical mechanisms underlying stimulation of laccase activity, there are clear practical benefits for industrial biocatalysis. The ability to stimulate laccase activity in ionic liquid/water mixtures could be extremely useful in biotransformations involving poorly water soluble substrates. We have demonstrated that the peak of activity can be “tuned” to specific ionic liquid/water concentrations by manipulating the ionic liquid structure. In cases when the substrate can be dissolved efficiently in water/solvent mixtures, this would offer a practical route to maximise enzyme activity whilst also minimising solvent usage.

## Acknowledgements

We thank the UK Department of Trade and Industry, Enviroways Ltd, QUILL, and CoEBio3 for financial support.

## Notes and references

- P. Baldrian, *FEMS Microbiol. Rev.*, 2006, **30**, 215–242.
- S. Couto and J. Herrera, *Biotechnol. Adv.*, 2006, **24**, 500–513.
- A. Wells, M. Teria and T. Eve, *Biochem. Soc. Trans.*, 2006, **34**, 304–308.
- E. I. Solomon, P. Chen, M. Metz, S. K. Lee and A. E. Palmer, *Angew. Chem., Int. Ed.*, 2001, **40**, 4570–4590.
- A. Leonowicz, N. S. Cho, J. Luterek, A. Wilkolazka, M. Wojtas-Wasilewska, A. Matuszewska, M. Hofrichter, D. Wesenberg and J. Rogalski, *J. Basic Microbiol.*, 2001, **41**, 185–227.
- V. V. Mozhaev, Y. L. Khmelnskiy, M. V. Sergeeva, A. B. Belova, N. L. Klyachko, A. V. Levashov and K. Martinek, *Eur. J. Biochem.*, 1989, **184**, 597–602.
- A. V. Pshchetskiy, S. Merker, G. S. Pepanyan, N. L. Klyachko, K. Martinek and A. V. Levashov, *Biochemistry (Moscow)*, 1988, **53**, 1013–1016.
- J. Rodakiewicz-Novak, *Top. Catal.*, 2000, **11/12**, 419–434.
- P. Wasserscheid and T. Welton, *Ionic liquids in synthesis*, Wiley-VCH, Weinheim, 2003.
- K. R. Seddon, in *The International George Papatheodorou Symposium*, ed. S. Boghosian, V. Dracopoulos, C. G. Kontoyannis and G. A. Voyiatzis, Institute of Chemical Engineering and High Temperature Chemical Processes, Patras, 1999, pp. 131–135.
- A. Stark, and K. R. Seddon, in *Kirk-Othmer Encyclopaedia of Chemical Technology*, ed. A. Seidel, John Wiley & Sons, Inc., Hoboken, New Jersey, 2007, pp. 836–920.
- M. C. Kroon, J. van Spronsen, C. J. Peters, R. A. Sheldon and G.-J. Witkamp, *Green Chem.*, 2006, **8**, 246–249.
- M. T. Reetz, W. Wiesenhoefer, G. Francio and W. Leitner, *Chem. Commun.*, 2002, 992–993.
- M. Deetlefs and K. R. Seddon, *Chim. Oggi.*, 2006, **24**, 16–23.
- S. T. Handy, M. Okello and G. Dickinson, *Org. Lett.*, 2003, **5**, 2513–2515.
- C. M. DiCarlo, D. L. Compton, K. O. Evans and J. A. Laszlo, *Bioelectrochemistry*, 2006, **68**, 134–143.
- R. F. Service, *Science*, 2002, **296**, 1223.
- G. Hinckley, V. Mozhaev, C. Budde and Y. L. Khmelnskiy, *Biotechnol. Lett.*, 2002, **24**, 2083–2087.
- J. Rogalski, A. L. Dawidowicz and A. Leonowicz, *Acta Biotechnol.*, 1990, **10**, 261–269.
- C. R. Perry, S. E. Matcham, D. A. Wood and C. F. Thurston, *J. Gen. Microbiol.*, 1993, **139**, 171–178.
- S. Shipovskov and A. Levashov, *Biocatal. Biotransform.*, 2004, **22**, 57–60.
- J. M. Crosthwaite, S. N. V. K. Aki, E. J. Maginn and J. F. Brennecke, *J. Phys. Chem. B*, 2004, **108**, 5113–5119.
- J. D. Holbrey and K. R. Seddon, *J. Chem. Soc., Dalton Trans.*, 1999, 2133–2139.
- N. L. Lancaster, P. A. Salter, T. Welton and G. B. Young, *J. Org. Chem.*, 2002, 8855–8861.
- D. R. MacFarlane, S. A. Forsyth, J. Golding and G. B. Deacon, *Green Chem.*, 2002, **4**, 444–448.
- R. A. Ando, L. J. A. Siqueira, F. C. Bazito, R. M. Torresi and P. S. Santos, *J. Phys. Chem. B*, 2007, **111**, 8717–8719.
- K. D. Collins, *Methods*, 2004, **34**, 300–311.
- S. G. Cull, J. D. Holbrey, V. Vargas-Mora, K. R. Seddon and G. J. Lye, *Biotechnol. Bioeng.*, 2000, **69**, 227–233.
- M.-D. Bermudez, A.-E. Jimenez and G. Martinez-Nicolas, *Appl. Surf. Sci.*, 2007, **253**, 7295–7302.
- C. Villagran, M. Deetlefs, W. R. Pitner and C. Hardacre, *Anal. Chem.*, 2004, **76**, 2118–2123.
- A. M. Klivanov, *Nature*, 2001, **409**, 241–246.
- A. Zaks and A. M. Klivanov, *J. Biol. Chem.*, 1988, **263**, 3194–3201.
- G. R. Castro, *Enzyme Microb. Technol.*, 1999, **25**, 689–694.
- E. V. Kudryashova, A. K. Gladilin, A. V. Vakurov, F. Heitz, A. V. Levashov and V. V. Mozhaev, *Biotechnol. Bioeng.*, 1997, **55**, 267–277.
- S. Shipovskov and A. Levashov, *Biotechnol. Bioeng.*, 2003, **84**, 258–263.
- S. Torres and G. R. Castro, *Food Technol. Biotechnol.*, 2004, **42**, 271–277.
- T. Arakawa and S. N. Timasheff, *Methods Enzymol.*, 1985, **114**, 49–77.
- R. L. Baldwin, *Biophys. J.*, 1996, **71**, 2056–2063.

- 39 K. D. Collins and M. W. Washabaugh, *Q. Rev. Biophys.*, 1985, **18**, 323–422.
- 40 W. Melander and C. Horvath, *Arch. Biochem. Biophys.*, 1977, **183**, 200–215.
- 41 V. A. Parsegian, *Nature*, 1995, **378**, 335–336.
- 42 M. T. Ru, S. Y. Hirokane, A. S. Lo, J. S. Dordick, J. A. Reimer and D. S. Clark, *J. Am. Chem. Soc.*, 2000, **122**, 1565–1571.
- 43 H. Zhao, *J. Mol. Catal. B: Enzym.*, 2005, **37**, 16–25.
- 44 H. Zhao, *J. Chem. Technol. Biotechnol.*, 2006, **81**, 877–891.
- 45 R. Leberman and A. K. Soper, *Nature*, 1995, **378**, 364–366.
- 46 X. Chen, T. Yang, S. Kataoka and P. S. Cremer, *J. Am. Chem. Soc.*, 2007, **129**, 12272–12279.
- 47 J. P. Lindsay, D. S. Clark and J. S. Dordick, *Biotechnol. Bioeng.*, 2004, **85**, 553–560.
- 48 H. Zhao, S. M. Campbell, L. Jackson, Z. Song and O. Olubajo, *Tetrahedron: Asymmetry*, 2006, **17**, 377–383.
- 49 F. Van Rantwijk, F. Secundo and R. A. Sheldon, *Green Chem.*, 2006, **8**, 282–286.
- 50 D. A. Sate, M. H. A. Janssen, G. Stephens, R. A. Sheldon, K. R. Seddon and J. R. Lu, *Green Chem.*, 2007, **9**, 859–867.
- 51 R. M. Lau, M. J. Sorgedraeger, G. Carrea, F. Van Rantwijk, F. Secundo and R. A. Sheldon, *Green Chem.*, 2004, **6**, 483–487.
- 52 R. M. Lau, F. Van Rantwijk, K. Seddon and R. A. Sheldon, *Org. Lett.*, 2000, **2**, 4189–4191.
- 53 C. A. Summers and R. A. Flowers II, *Protein Sci.*, 2000, **9**, 2001–2008.
- 54 S. R. Couto and J. L. Toca, *Curr. Enzyme Inhib.*, 2006, **2**, 343–352.
- 55 A. M. Klivanov, *Trends Biotechnol.*, 1997, **15**, 97–101.

The biannual conference series "Green Solvents" has been established as an important international forum for the discussion of modern approaches to sustainable solution phase processes. With previous editions focusing on "Catalysis", "Synthesis" and "Processes", the 2008 edition aims at a broad evaluation and critical discussion of the current state of the art for alternative media in chemistry and chemical engineering, biotechnology, materials sciences, and related areas.

# Green Solvents Conference

Progress in Science and Application

Lake Constance · Friedrichshafen · Germany  
28 September – 1 October 2008



## KEYNOTE LECTURES:

- T. Adschiri**, Tohoku University/J
- C. Chiappe**, University of Pisa/I
- D.J. Cole-Hamilton**, University of St. Andrews/UK
- I.T. Horvath**, Eötvös University, Budapest/HU
- A. Copper**, University of Liverpool/UK
- M.G. Finn**, The Scripps Research Institute, La Jolla, CA/USA
- J. Karthäuser**, SIOX Machines AB, Sollentua/S
- S. Mecking**, University of Constance/D
- R.D. Rogers**, QUILL, Belfast/UK
- B. Subramaniam**, University of Kansas, KS/USA
- N.R. Thomas**, University of Nottingham/UK
- U. Vagt**, BASF SE, Ludwigshafen/D
- A. Wells**, AstraZeneca R&D Charnwood, Loughborough/UK

For the programme and the registration form please look at:

[www.dechema.de/gpsa](http://www.dechema.de/gpsa)

# RSC Database and Current Awareness Products



- Abstracted from high quality sources
- Easy to use search functions
- Clearly displayed results
- Spanning the chemical sciences

for quick and easy searching

## Graphical Databases

present search results in both text and graphical form. Titles include *Catalysts & Catalysed Reactions*, *Methods in Organic Synthesis* and *Natural Product Updates*.

## Specialist Databases

review both academic and industrial literature on a wide range of hard to reach and unique information. Titles include *Chemical Hazards in Industry* and *Laboratory Hazards Bulletin*.

## Analytical Abstracts

is the first stop for analytical scientists. Offering coverage on all areas of analytical and bioanalytical science. With a fresh new look, including improved search and results features, *Analytical Abstracts* offers an excellent online service.

Find out more at

RSC Publishing

[www.rsc.org/databases](http://www.rsc.org/databases)

Registered Charity Number 207890